Histological atlas of freshwater mussels (Bivalvia: Unionidae) with comparison of Alabama rainbow (*Villosa nebulosa*), Gulf pigtoe (*Fusconaia cerina*), and Alabama creekmussel (*Strophitus connasaugaensis*), from the Mobile River Basin, Alabama

by

Andrew McElwain

A dissertation submitted to the Graduate Faculty of
Auburn University
in partial fulfillment of the
requirements for the Degree of
Doctor of Philosophy

Auburn, Alabama
December 8 2012

Keywords: Unionidae, *Villosa*, *Fusconaia*, *Strophitus*, Mobile River Basin

Approved by

Stephen A. Bullard, Chair, Assistant Professor of Fisheries and Allied Aquacultures
Covadonga R. Arias, Associate Professor of Fisheries and Allied Aquacultures
James A. Stoeckel, Assistant Professor of Fisheries and Allied Aquacultures
Paul D. Johnson, Program Supervisor of the Alabama Aquatic Biodiversity Center, Alabama Department of Conservation and Natural Resources

Abstract

The “freshwater mussels” (Mollusca: Bivalvia: Unionoida) are a species rich group of parasitic bivalves comprising an estimated 898 species in 6 families, 2 subfamilies, and 29 genera worldwide. Renown for its biodiversity, Alabama has a large proportion of this total number of species, with 180 species of Unionidae and 2 of Margaritiferidae. The total number of unionid species in Alabama also includes 24 extinct, 26 extirpated, and 74 imperiled unionids, and, because of that, the conservation status of these invertebrates is of interest to the Alabama Department of Conservation and Natural Resources. Historically, our understanding of unionid systematics was based on shell morphology and larval (glochidia) characteristics. More recently, phylogentic relationships of mussels are being revealed following the sequencing of highly conserved genes. However, scant information is available on the soft tissues of these invertebrates, and no comprehensive histological treatment of any species has been published to date. This lack of foundational information is a barrier to advancing our knowledge of mussel biology.

This dissertation is a systematic, comparative anatomical study that treats morphological diversity of cells and tissues across three primary lineages (subfamilies) of unionids. I test the hypothesis that freshwater mussel lineages exhibit few morphological differences in their “soft tissues,” which contrasts to the level of morphological diversity exhibited by their shells and larvae. Representative mussel species subjected to anatomical study were selected based upon the taxonomic arrangement of Ortmann (1910) and the combined phylogenetic analysis of Graf

and Cummings (2006). The Alabama rainbow (*Villosa nebulosa*) was selected as the representative of Lampsilinae, Unioninae was represented by the Gulf pigtoe (*Fusconaia cerina*), and the Alabama creekmussel (*Strophitus connasaugaensis*) was selected as the representative of Anodontinae. Alabama rainbows were collected from the South Fork of Terrapin Creek during May 2010 (n=36), August 2010 (n=39), and August 2011 (n=5) plus Shoal Creek in May 2011 (n=5). Gulf pigtoes were collected from the Cahaba River in May 2011 (n=10), August 2011 (n=28), and June 2012 (n=7). Alabama creekmussels were collected from Shoal Creek in May 2011 (n=5), January 2012 (n=3), and May 2012 (n=8) as well as from the South Fork of Terrapin Creek in August 2011 (n=7). Select specimens of *V. nebulosa* (n=45) and *S. connasaugaensis* (n=10) were sourced from pond and recirculating culture systems of the Alabama Aquatic Biodiversity Center (Marion, Alabama). Mussels were digitally photographed to document gross features and routinely processed for histology following standard protocols before being photographed with a digital camera mounted to a compound microscope.

Herein, the null hypothesis that the level of morphological diversity in cells and tissues was qualitatively low across the studied mussel species is accepted. Major and minor anatomical differences between the studied mussels are reported in tables provided herein (totaling 12 distinctive histological features). Some of these differences are relevant to assessing mussel health and propagation efficacy. For example, I speculate that a robust, branched mantle edge with a high surface area may be linked to shell thickness, and, if not fully formed, may cause shell deformities. Workers monitoring mussel health or stream health by studying soft tissue structure should focus on structurally conserved tissues whereas histopathological changes to unionid tissues that exhibit interspecific variation may be less easily comparable.

Acknowledgments

I thank my major professor, Dr. Stephen Bullard, and Dissertation Committee Co-Chair, Dr. Covadonga Arias, for providing me with guidance throughout my doctoral program. Dr. Bullard has supported me, and invested alot of time nuturing my professional growth by encouraging me to present at conferences, participate on projects for publication, and encouraging me to teach. Thank you to my committee members, Drs. Stephen Bullard, Covadonga Arias, James Stoeckel, and Paul Johnson for reviewing my dissertation and providing valuable comments. I would also like to thank Dr. Michael Miller (Department of Biological Sciences, AU) for serving as an outside reader of my dissertation and providing insightful feedback. I thank Dr. Bullard, and my labmates, Andrew Austin, Carlos Ruiz, Triet Truong, my friend, Stanton Belford (Auburn University, Department of Curriculum and Teaching), and Dr. Paul Johnson, and Mr. Thomas Tarpley (Alabama Department of Conservation and Natural Resources) for assistance with mussel collections. Thank you to Ms. Raquel Patella de Azambuja for assistance with microtomy of some *Strophitus connasaugaensis* specimens. Thanks to Ms. Pambanisha Whaley of the Ralph Brown Draughn Library, Document Delivery Department for assistance with interlibrary loan requests, Dr. Werner Bergen (Department of Animal Science, AU) for providing a translation for the title page of Margo, (1860), Dr. David Campbell (Paleontological Research Institute) for reprints of Campbell and Lydeard, (2012a), (2012b), and my friend, Zhen Tao (Department of Fisheries and Allied Aquacultures, AU) for assistance with locating the useful reference on water mites by Haobin et al., (2008). I especially

thank my family members Susan, John, and Penny McElwain for their strong encouragement throughout my graduate program. A pilot study that lead to the development of this dissertation was funded by ADCNR.

Table of Contents

List of Tables

List of Plates

Chapter 1

INTRODUCTION

1.1. Introduction to the freshwater mussels (Bivalvia: Unionoida)
1.2. Cultural importance of freshwater mussels in the United States
1.3. Environmental importance and ecosystem services provided by freshwater mussels
1.4. Biodiversity and imperilment of freshwater mussels in the United States
1.5. Physical changes to stream habitat as a threat to freshwater mussels
1.6. Freshwater mussels as biological indicators of toxic contaminants
1.7. Histopathology of metazoan parasite infections as a proxy for infectious disease
1.8. Epizootics of freshwater mussels
1.9. Objective and hypothesis
1.10. Introduction to anatomy and physiology of freshwater mussels

1.1. Introduction to the freshwater mussels (Bivalvia: Unionoida)

Unionoida is a diverse and geographically widespread group of bivalve mollusks commonly known as freshwater mussels or naiads. Presently, Unionoida comprises six families (Unionidae, Margaritiferidae, Hyriidae, Etheriidae, Mycetopodidae, and Iridinidae) and 898 species, 2 subfamilies, and 29 genera, with representatives distributed across all continents except Antarctica. Unionidae is the largest family with approximately 674 species while there are fewer than 100 species in each of the other mussel families (Graf and Cummings, 2006). Freshwater mussels are notable for several reasons. Unionoida is a relict group dating back to the Triassic Period, making mussel shells useful towards understanding continental drift and historic climate changes. Unionidae is one of the most specious bivalve families second to Veneridae (ca. 800 species). Gravid females exhibit parental care by withholding their developing larvae within the gills for several weeks or months before their release. Most notably however, freshwater mussels have a unique lifecycle characterized by a parasitic larval stage that must attach to skin or gill of an aquatic vertebrate (typically a fish) (Graf and Cummings, 2007). Complimenting this unique lifecycle, some unionid species have elaborate luring mechanisms to ensure the delivery of their larvae on the proper host species (Barnhart et al., 2008).

1.2. Cultural significance of freshwater mussels in the United States

The significance of the diverse North American freshwater mussel fauna transcends their value to scientists. Naiads have historically had a large impact on Native American cultures as well as European settlers seeking to make a living on the American continent. Piles of mussel shells, or middens, located at known or suspected Native American settlements may be an indication of the use of mussels as a food resource (Ortmann, 1909a, Baker, 1930). Mussel shells were crafted into jewelry including ear, neck, wrist and ankle ornaments. Native

Americans crafted tools from shells including spoons, scoopers, and hoes (Baker, 1923, Baker, 1930). Furthermore, effigies of human and animal heads were carved from mussel shells (Baker, 1930, Parmalee and Bogan, 1998).

Notably, European explorers reported widespread usage of pearl jewelry among Native Americans. The Spanish explorer, DeSoto documented the usage pearl jewelry from indigenous people during his 1540-1541 expedition from Florida to the Mississippi River (Kunz, 1897). Rafinesque, (1820) reported how many Ohio River unionid species produce pearls and that pearls may be appreciated for personal adornment. Such reports did not receive much attention initially, possibly in part because freshwater pearls were uncommon in Europe given its comparatively depauperate mussel fauna. However, the finding of a 93-gram pearl during 1857 in New Jersey, dubbed "queen pearl," would later lead to zealous search for pearls throughout the eastern United States (Kunz, 1897). Concomitantly, mussel shells formed the basis for a large pearl button industry in the United States (Alexander, 2007). Despite what the name may imply, pearl buttons are derived from discoid cutouts of mussel shells, and typically, a large, heavy, circular to ovular shell with a white nacre and smooth periostracum was commercially valued for buttons (Smith, 1898). More recently, North American mussels have become commercially valued for "mother of pearl," a lustrous seed material derived from the nacre, used in the production of cultured pearls in Asia (Parmalee and Bogan, 1998, Williams et al., 2008).

1.3. Environmental importance and ecosystem services provided by freshwater mussels

Freshwater mussels are important components of a watershed as they provide a variety of ecosystem services. As stationary suspension feeders, mussels cycle large quantities of water, and ingest phytoplankton, bacteria, and particulates, thus playing an important role in nutrient cycling and help maintain water clarity (Vaughn and Hakenkamp, 2001, Atkinson et al., 2011).

Mussel valves largely contain calcium carbonate and thus, the construction, eventual dissolution of shells or their incorporation into the lithosphere as fossils signifies their role in mineral cycles (Radley and Barker, 1998, Ravera et al., 2003, Gutiérrez et al., 2004). Furthermore, minerals and organic compounds may be recycled by means of the extension and retraction of the muscular, blade-like foot during pedal feeding or when burrowing (Trueman, 1966, 1968, McCall et al., 1986, Yeager et al., 1994). Mussels are a prey item for a wide variety of animals including crayfish, salamanders, turtles, fish, birds, and mammals (Fuller, 1974, Cosgrove et al., 2007). Therefore, mussel-derived biomass may be distributed throughout a stream by serving as a prey item for aquatic animals, while terrestrial predators may distribute mussel derived biomass throughout a watershed. Mussels may be thought of as "ecosystem engineers" because they are sedentary burrowers and when embedded, mussels may provide added stability to surrounding riverine sediments (McCall et al., 1986, Gutiérrez et al., 2004). Additionally, mussels are a "landscape" to many organisms. The calcareous valves serve as a substrate for algae (Wilson and Clark, 1912a), and epizoic invertebrates such as snails, and insects (Beckett et al., 1996) and can provide a refuge for small stream fishes (Grabarkiewicz and Davis, 2008). Parasitic animals depend on mussel tissues as part of their lifecycle. For instance, water mites may colonize the gill and mantle (Gordon et al., 1979, Haobin et al., 2008), and the viscera may represent a milieu for parasitic trematodes (Fredericksen, 1972, Chittick et al., 2001). Parasites represent another means to disperse unionid-derived biomass during their dispersal stages.

1.4. Biodiversity and imperilment of freshwater mussels in United States

The greatest concentration of mussel species is located in the inland waters of North America with a total of 302 species comprising Unionidae (297 spp.) and Margaritiferidae (5 spp.) (Graf and Cummings, 2007). The richest North American mussel assemblages have historically been

located between the Mississippi River, east to southern coast of the Atlantic Ocean, and within interior basin drainages from the Great Lakes to the coastal drainages of the Gulf of Mexico (van der Schalie, 1938). Especially the southeastern United States comprising Alabama, Arkansas, Florida, Georgia, Louisiana, Mississippi, Kentucky, South Carolina, Tennessee, North Carolina, Virginia, and West Virginia, is a biodiversity focus and Alabama has the richest mussel fauna in the region with 182 species (Neves et al., 1997, Gangloff et al., 2006, Williams et al., 2008, 2009, Jones and Neves, 2010). Unfortunately, freshwater mussels are imperiled, and the number of extant species in Alabama, and other states, is dwindling. Garner et al. (2004) provides lists of extinct and imperiled mussels in Alabama, however there are presently 24 extinct unionid species, 26 extirpated species, 74 species with priority conservation status (P. Johnson, personal communication).

1.5. Physical changes to stream habitat as a threat to freshwater mussels

Awareness of mussel imperilments dates back to the late 1800's during a period of prodigious population growth and economic development in the United States. Mussels were widely collected during the late 1800's by people seeking wealth through freshwater pearls (Kunz, 1897). Secondly, the pearl button industry was associated with intense collections of large mussels in the Mississippi River (Alexander, 2007). However, there are early observations suggesting unionids are vulnerable to environmental disturbances. Simpson, (1898) noted that deforestation can significantly alter the hydrology of a river and unionids are vulnerable to subsequent damage to their habitat. Mussels are burrowing animals that require specific substrate and hydrological stability, and physical damage to riverbeds, and to the surrounding landscapes, are associated with the loss of substrate and hydrological stability. For example Clark and Wilson (1912) noted that a river bottom loses stability when sediments such as cobble,

gravel and sandy are removed during dredging and channelization activities. Damage to the benthos can also occur when extreme erosion events or headcutting causes riparian habitats to collapse (Hartfield, 1993). Erosion may also be associated with increased deposition of fine sediments to cover important substrata. Österling et al., (2010) for example, found a correlation between turbidity and low recruitment of *M. margaritifera* and suggested that deposition of fine sediment had a clogging effect that might obfuscate movements or respiration of recently transformed juveniles.

1.6. Freshwater mussels as biological indicators of toxic contaminants

Mussel die-offs have long been linked to water pollution such as wastewater releases from industrial facilities and sewage discharges from municipalities (Simpson, 1898). Ortmann, (1909b) suggested that mussels are vulnerable to toxic contaminants because of their sessile nature and complex life cycle. Ortmann's observations represent early recognition of the utility of freshwater mussels as biological indicators. An indicator species has specific characteristics that are useful towards measuring the presence or absence of environmental conditions that cannot be feasibly measured from other taxa or from the environment. Unionids are good indicator organisms considering their sedentary lifestyle as suspension feeders and burrowers. Additionally, mussels are large enough animals to provide ample tissue for histological or chemical analysis, and empty shells can provide a long-lasting record of species composition, and traces of contaminants may become incorporated into the shell (Grabarkiewicz and Davis, 2008). While species composition of can indirectly reflect environmental health (McGregor and Garner, 2004, Haag and Warren, 2010), mussels can directly signal water quality by accumulating trace amounts of toxic contaminants such as metals (Naimo, 1995) or polyaromatic hydrocarbons (Bedford et al., 1968). Biomarkers, particularly biotransformation or

detoxification enzymes, have been used to show that a specific stress response has occurred in response to a toxin (Newton and Cope, 2007). Although toxicity of contaminants has been verified though laboratory tests, criticisms focus on how laboratory exposures are not realistic simulations of contaminant releases. Hydrology, water chemistry, and substrate can affect the speciation and distribution of toxins (Salazar and Salazar, 2007). Therefore it may be difficult to predict whether a contaminant release would cause acute mortality or chronic health problems to mussels.

1.7. Histopathology of metazoan parasite infections as a proxy for infectious disease

Whilst there is good evidence linking contaminants to mussel health, the possibility that infectious disease is associated with mussel kills warrants further study. A recent review of parasites and diseases of freshwater mussels indicates a limited range of metazoan parasites have been reported from freshwater mussels while viral, bacterial, protozoan, and fungal agents are largely unknown from unionids (Grizzle and Brunner, 2009). There are limited histological observations regarding tissue damage or host responses to an infection. For example, viruses are potential etiological agents of freshwater pearl mussels (*Hyriopsis cumingii*) in pond aquaculture and are associated with hydropic degeneration of digestive gland tubules (Zhong et al., 2001). *Aspidogaster conchicola* is a trematode (Aspidogastrea) that typically infects pericardial cavity and nephridium. Compression of digestive gland tubules has been reported from infections in which *A. conchicola* invaded the viscera, and some hosts exhibited an encapsulation response to the worms (Pauley and Becker, 1968). Digenetic trematodes may infect mantle, foot, and kidney, and may reduce reproductive output when sporocyst and cercarial stages infect gonad (Taskinen et al., 1997). Water mites (Unionicola) are cosmopolitan parasites of freshwater mussels, and adult mites are often located on the gill. Mites may lance gill tissue with their mouthparts during

feeding or with their spinous appendages or tarsal claws when mites attach to tissue (Baker, 1976). However, it is difficult to determine if there is local tissue damage surrounding an attached mite considering that mites are vagile. Additionally, ovigerous female mites may oviposit into tissue and histological sections of deposited eggs may reveal cellular injury (Haobin et al., 2008). Although metazoan parasites are not likely to be associated with unionid declines, it is uncertain whether there are natural epizootics involving freshwater mussels. Furthermore, it is also unclear whether non-endemic pathogens have been introduced with zebra mussels (*Dressinia polypmorpha*) or Asian clams (*Corbicula fluminea*). Zebra mussels and Asian clams are invasive freshwater bivalves and they are generally viewed as spatial or trophic competitors (McGregor and Garner, 2004), *Dressinia* spp. notably affect mussel health by encrusting on unionid valves (van Appledorn and Bach, 2007).

1.8. Epizootics of freshwater mussels

Considering the above, disease may represent an important factor associated with mussel declines. Observations of disease or "kill events" have sometimes reported high mortalities, exceeding 100 individuals, and are typically characterized by floating mussels with remnants of soft tissue that have totally or partially become detached from the shell (Ahlstedt and Jenkinson, 1986, Blodgett and Sparks, 1986, Havlik, 1986). The full extent of a mussel-kill can be difficult to assess considering a potentially long time course of days or weeks from when health problems are manifested to the time when floating mussels are observed. Additionally, survey data from affected streams prior to a die-off may be lacking (Buchanan, 1986). Regarding signs of distress, investigators have typically reported gaping, characterized by an expansion of the valves with or without extension of the foot, and individuals are typically lethargic or unresponsive to handling (Pauley, 1968, Ahlstedt and Jenkinson, 1986, Zale and Sutters, 1986). There are limited details

regarding tissue discolorations or colored residues on the surface of gill or mantle. Ahlstedt and Jenkinson (1986) reported a black oil-like substance on dead mussels. Spots or masses of a pearly or iridescent, pink material were observed by Jenkinson and Ahlstedt, (1986). Tissue discoloration may be an indication of microscopic damage that could be evaluated histologically for cellular changes. However, there are scant details regarding tissue damage or wound repair following a disease event (Pauley, 1968). A possible explanation for this may be that the body of a freshwater mussel consists of delicate tissues that degrade rapidly after death (P. Johnson, personal communication, also see Neves, 1987)

1.9. Objective and hypothesis

Freshwater mussels are a diverse and marquee group of aquatic invertebrates. Considering that many unionid species in Alabama are extinct or imperiled, the conservation status of mussels is of interest to the Alabama Department of Conservation and Natural Resources. Enhancement of stream-dwelling mussel stocks with hatchery-reared individuals is viewed as a necessary conservation strategy to maintain a specious fauna in Alabama, and there is a need to understand health of wild and cultured mussels. However, there is limited descriptive information about the morphology of soft tissues at the cellular level, and no comprehensive reference of all unionid tissues exists in peer-reviewed literature. The histological atlas of *Pleurobema cordatum* by Yokley, (1968) is a non-circulating dissertation, the reproduction available from ProQuest Dissertations and Theses A&I database contains blackened photographs of described tissues, and the descriptions contain limited details of cell structure. Therefore, this lack of foundational information is a barrier to advancing our knowledge of mussel biology.

This dissertation is a systematic and comparative anatomical study that treats morphological diversity of cells and tissues across three primary lineages (subfamilies) of unionids. I test the

hypothesis that freshwater mussel lineages exhibit few morphological differences in their "soft tissues," which contrasts to the level of morphological diversity exhibited by their shells and larvae (Williams et al., 2008). The representative species subjected to anatomical study were selected based upon the taxonomic arrangement of Ortmann (1910a) and the combined morphological and molecular (28S rDNA, mitochondrial COI DNA) phylogenetic analysis of Graf and Cummings, (2006). The Alabama rainbow (*Villosa nebulosa*) was selected as the representative of Lampsilinae, the Gulf pigtoe (*Fusconaia cerina*) was the representative of Unioninae, and the Alabama creekmussel (*Strophitus connasauagaensis*) was selected as the representative of Anodontinae. The focus of the phylogenetic analysis by Graf and Cummings (2006) was to test the hypothesis that Unionoida is monophyletic and the authors indicated that there is a need to understand interrelationships between unionid lineages.

1.10. Introduction to anatomy and physiology of freshwater mussels

This dissertation describes twenty-five major tissues of *Villosa nebulosa*, *Fusconaia cerina*, and *Strophitus connasaugaensis* (Table 1). The body of a freshwater mussel consists of the mantle, gill, and visceral mass (Figs. 1.8, 22.8, 45.8). The mantle is a skin-like organ between the calcareous valves, gill, and viscera, and is sometimes referred to as the pallium, given its resemblance to a white cloak (Beedham, 1958). Mantle consists of the edge, middle mantle, and isthmus, and its main purpose is to secrete the calcium-based shell and dorsally placed median ligament. Mussels have paired inner and outer gills extending into the mantle cavity (Figs. 1.6, 1.7, 22.6, 22.7, 45.6, 45.7). A whole gill may be considered a demibranch, consisting of a series of cylindrical, ciliated structural units that are referred to as filaments. The filaments extend along the length of each demibranch and each inner and outer lamina or face, is united in such a way as to form interbranchial septa. Additionally, ctenidia have a series of vertically oriented

water tubes that relay water as it passess through the mantle cavity (Posner, 1875, Ridewood, 1903). Water enters these compartments by means of laterally oriented pores or ostia. The gills of a freshwater mussel are important for respiration, feeding, brooding, and the liberation of waste products (Williams et al., 2008).

The main body of a mussel is referred to as the visceral mass (Williams et al., 2008). The visceral mass consists of the coelom, located dorsally, at the base of the visceral mass, and the muscular, blade-like foot that extends ventrally into the mantle cavity (Figs. 1.8, 22.8, 45.8). The visceral mass contains many of the tissues associated with the digestive, cardiovascular, reproductive, nervous, and renal systems (Williams et al., 2008, also see Appendix 1). Mussels are typically embedded in a riverbed with their foot inserted into the sediment while the posterior aspect of the body is extended obliquely into the water to expose the siphons (Simpson, 1899, also see Figs. 1.5, 22.5, 45.5).

The adductors, pedal protractor and retractors are bundles of somatic musculature associated with the shell and foot. Adductors are large cylindrical muscles that unite the left, right valves and control the opening and closing of the shell (e.g., Figs. 1.8, 22.8, 45.8). Pedal protractors and retractors are inserted into the shell, medially to the adductor, and extend obliquely, and ventrally into the foot (Brück, 1914, Appendix 1). The pedal muscles are associated with the expansion and contraction of the foot (Trueman, 1968, Williams et al., 2008).

Mussels feed by capturing particles along the gill, and foot and deliver them to the labial palps (Tankersley and Dimock, 1992b, Yeager et al., 1994). The palps are transluscent, triangular, lip-like structures located anteriorly within the mantle cavity. Labial palps have cilia, and produce mucus enabling them to trap particulate matter. Additionally, the palps have muscle fibers and can open wide to receive particulate matter, and can also purse the free distal tips and

expel particulate matter (e.g., algae, bacteria, sediment particles) back into the mantle cavity. Thus, the labial palps may "accept" or "reject" particulate matter (Allen, 1914).

Particulate matter accepted by the palps may be transported along a tubular structure known as the oral groove. The oral groove delivers particulate matter to the esophagus located at the anterior-dorsal margin of the visceral mass. The esophagus is a short tubular structure that carries particulate matter posteriorly towards the digestive diverticulum and stomach. The digestive diverticulum constitutes a network of small, blind-ended tubules located within the anterior-half of the coelom. Literature regarding the function of the digestive diverticulum suggests tubules secrete lytic enzymes into the lumen or perhaps engulf or absorb ingested matter for intracellular digestion (Mansour and Zaki, 1946, Eble, 1966). The stomach is a large, bag-like chamber located medially within the anterior visceral mass. The stomach features folds or grooves along the gastric walls possibly to enable mixing of particulate matter with digestive secretions and or sorting of sediment particles from algae or bacteria (Dinamani, 1967). Following the stomach is the crystalline style sac and intestine. Food may be delivered to the intestine by means of the crystalline style. The style is a gelatinous rod that rotates along the length of the style sac possibly capturing loose particles circulating in the stomach (Nelson, 1918). The intestine is coiled within the coelom and it extends along the base of the visceral mass parallel to the hinge.

The nervous system consists of three pairs of ganglia, nerves and a pair of accessory structures called the statocysts (Splittstoβer, 1913). Cerebral ganglia are located anteriorly, associated with the sinistral, dextral labial palps. Pedal ganglion consists of fused lobes of nerve tissue located medially and dorsally within the coelom. Statocysts are spherical to ovular capsules located laterally to the pedal ganglion, and are associated with equilibrium (Kraemer,

1978). The visceral ganglion consists of a pair of fused lobes located posteriorly around the posterior visceral mass (Smith, 1988).

The nephridium, heart, and pericardial gland are located between the coelom and hinge (Myers and Franzen, 1970, Andrews and Jennings, 1993). Nephridium consists of a sinistral and dextral pair of tubular chambers between the digestive diverticulum and posterior adductor. The heart is located dorsally with respect to the nephridium and is situated within a thin, fluid-filled pericardial sac. The heart receives blood from the dorsal aspect of the coelom and pumps blood anteriorly and posteriorly, and ventrally within the coelom (Motley, 1932, Brand, 1972, Andrews and Jennings, 1993). The pericardial gland is a spongy region of tissue surrounding the nephridium and pericardial cavity. There is scant information regarding the function of the pericardial gland, but possibly it delivers fluid into the nephridium (White, 1942, Andrews and Jennings, 1993).

The reproductive system consists of a large number of spherical to ovular acini containing ova, spermatozoa and associated germinal cells, and a series of ciliated ducts that extend throughout the viscera to the dorsal end of the coelom (Zale and Neves, 1982, Smith et al., 2003). Ciliated gonadal ducts communicate with the exterior at the sinistral and dextral gonopores. Gonopores are situated at the dorsal end of the visceral mass, just ventral to the nephridium (Henley et al., 2007).

Table 1. Major tissue types of Alabama rainbow (*Villsoa nebulosa*), Gulf pigtoe (*Fusconaia cerina*), and Alabama creekmussel (*Strophitus connasaugaensis*).

Mantle edge	Statocyst
Middle mantle	Nerve
Mantle isthmus	Heart
Non-marsupial gill	Blood vessel
Marsupial gill	Pericardial gland
Foot	Nephridium
Pedal protractor/retractor	Ovarian acinus
Adductor	Testicular acinus
Labial palp	
Esophagus	
Digestive diverticulum	
Stomach	
Crystalline style sac	
Intestine	
Cerebral ganglion	
Pedal ganglion	
Visceral ganglion	

Chapter 2

REVIEW OF DESCRIPTIVE ANATOMICAL WORKS ON FRESHWATER MUSSELS (BIVALVIA: UNIONOIDA)

2.1. Overview of anatomical literature regarding freshwater mussels

Freshwater mussels have subject to numerous anatomical investigations over the years. Anatomical literature regarding freshwater mussels ranges in scope from texts or atlases portraying major organs and tissues (Howes, 1885, Simpson, 1884, Gutheil, 1912, Yokley, 1968), to investigations characterizing specific organ systems and tissues (e.g., Splittstöβer, 1913, Motley, 1932, Beedham, 1958, Purcheon, 1958). The subject of anatomical inquires is typically an adult mussel, while some authors have explored embryological development (Lillie, 1895, 1897, 1898), or larval (Lefevre and Curtis, 1912, Fryer, 1961, Schwartz and Dimock, 2001) or juvenile form (Lefevre and Curtis, 1912, Lasee, 1991). Investigators typically seek an understanding of specific physiological processes associated with described features (Motley, 1932, Andrews and Jennings, 1993, Smith, 2000), while other anatomical works use soft tissue structure as a taxonomic tool (Ridewood, 1903, Ortmann, 1911a, Purcheon, 1958, Smith, 1988).

2.2. Anatomical texts and atlases

There are several anatomical texts that have described morphological features of mantle cavity tissues including gill, foot, mantle, and adductor muscle and provided a schematic of visceral organs such as intestine, nephridia, ganglia, and associated nerves (Brooks, 1882, Howes, 1885, Girod, 1889). An extensive molluscan biology text by Cooke (1895) provided concise descriptions of gill, foot, mantle, crystalline style, heart, nephridium and gonad of bivalves, and provided some comparison between members of *Anodonta* and various marine bivalve taxa such as *Mytilus*. Considering the enormous task of describing virturally all aspects of molluscan biology, and its comparative approach, illustrations of bivalve tissues were much reduced and emphasized major morphological differences between taxa (Cooke, 1895). The more detailed works by Brooks (1882), Howes (1885), and Girod (1889) considered major organs of *Anodonta*

cellensis and *A. anatina*. Coronal sections were used to explain the orientation and morphology of dorsal tissues such as nephridia, intestine, and adductor muscles. Transverse sections of the visceral mass were used to reveal paired nephridia, pericardial cavity, the position of each limb of the intestine, and the gill-mantle junction. However, the transverse views of visceral mass in Brooks (1882) and Howes (1885) provided more details of morphological differences in tissue structure anterior to posterior. Howes (1885) also included some illustrations of developing ova, epithelial cells, and a hooked glochidium. The anatomical atlas of *A. fluviatilus* by Simpson (1884) differed from Howes (1885) and Girod (1889) by illustrating myofibers of pedal protractors and retractors fanning into the foot. Additionally, Simpson (1884) provided a schematic of the nervous system that showed how ganglia form a neural circuit while some nerve fibers were depicted as extending away from each ganglion. In a later histological reference of *A. cellensis*, Gutheil (1912) described the morphological and cellular features of visceral organs with an emphasis on the digestive system. Gutheil (1912) provides insight into variation in the shape and size of the intestinal lumen and how organs have a limited serosa surrounded by adipose tissue. The detailed renderings of cell types of *A. cellensis* are the focal point of the atlas, and are indicative of the complexity of unionid tissues (Gutheil, 1912). *Pleurobema cordatum* was the subject of a detailed histological atlas for Unionidae (Yokley, 1968). All tissues of *P. cordatum* were described from illustrations and photomicrographs of sections stained with either, Harris' Hematoxylin and Eosin for general differentiation, van Gieson's, and Mallory-Azan methods for connective tissue, and Bielschowsky's silver nitrate method for axons and ganglia (Yokley, 1968). The atlas of *P. cordatum* provides the reader with a comprehensive map of all mussel tissues of unionids, but discussion of the physiological function of specific tissues or organ systems is limited (Yokley, 1968). The anatomical work by Smith (1988) provided short

descriptions of selected tissues of *Margaritifera hembeli.* Gill septa, mantle edge, testes, and ovaries were histologically described while only gross morphological characteristics were described from the visceral ganglion and stomach (Smith, 1988). Based upon a literature survey there are 19 unionid organs including mantle, adductor muscle, pedal protractor, pedal retractor, gill, foot, labial palp, esophagus, digestive diverticulum, stomach, crystalline style sac, intestine, heart, nephridium, cerebro-pleural ganglia, pedal ganglia, visceral ganglia, ovaries, and testes.

2.3. Mantle

Early work on the mantle edge includes information regarding *Anodonta cellensis* from the meticulous treatises of Raβbach (1912) and Siebert (1913). Raβbach (1912) provided a detailed description of the mantle edge including lobe morphology, cellular constituents of the epithelium and connective tissue, and periostracum secretion. Additionally, there was a strong emphasis on shell structure including external and internal morphology, mineral layers, regeneration following mechanical damage, and morphology of mineral crystals. The dorsal aspect of the valves including hinge structure, umbo morphology, and layers of the ligament were also characterized (Raβbach, 1912). Siebert (1913) characterized morphology of incurrent, and excurrent apertures, and foot, and described some details of the fine structure of mantle edge, foot, and labial palp, and illustrated several cell types including ciliated and non-ciliated columnar cells, mucus cells, granular secretory cells, and sensilla. Siebert (1913) also rendered water currents in the mantle cavity.

The layout of mantle edge musculature of *A. cellensis* was described in a monograph about unionid musculature (Brück, 1914). Myofibers extend into the mantle edge from the pallial line and when viewed in a coronal plane, the tissue has a triangular array of muscle fibers. In a transverse orientation, myofibers from the pallial line extend medially towards the mantle lobes

where fascicles separate into smaller filamentous units. Branches of muscle fibers extend into each of the three mantle lobes. Additionally, there is a second set of myofibers oriented perpendicularly to the longitudinal myofibers in a horizontal plane (Brück, 1914).

The cellular composition of the mantle lobes of *A. cygnea* was described to provide more specifics about shell formation (Beedham, 1958). Variation between dorsal and ventral mantle edge was described in relation to shell and ligament secretion, respectively. The ventral aspect of the mantle edge has three lobes while the dorsal mantle edge has only two lobes. The photomicrographs of mantle lobes in Beedham (1958) depict a rugose epithelium along the surface of each lobe, and dark-staining columnar cells located along the inner and outer surface of the outer mantle lobe. Argentaffin stain and mercuric bromphenol blue were independently used to verify that the darkened columnar cells are responsible for protein synthesis. Additionally, the periostracum ribbon was determined to be protein-based following a positive Argentaffin staining reaction. Additionally, Beedham (1958) proposed that mucus cells along the outer and inner surfaces of the outer lobe are different, mucus may represent a vehicle for transport of calcium salts, and mucus may function as a lubricant, when the mantle edge is extended or retracted. Yokley (1968) described the mantle edge of *Pleurobema cordatum* and his description emphasized the columnar epithelium surrounding the three mantle lobes. Although the description of mantle lobe cell types was similar to the description provided by Beedham (1958), there was no discussion of overall mantle lobe morphology and no insight into how mante lobe structure and function of *P. cordatum* was different from what had been documented from *Anodonta* species.

Scanning electron microscopy was used to characterize mantle edge, middle mantle, isthmus, siphon, and periostracum of *Amblema plicata* (Petit et al., 1978). The inner surface of the mantle,

facing the ctenidia, is lined with rows of cilia, short microvilli, and mucus pores with mucus droplets. Epithelial cells facing the shell resemble cobblestones, lack cilia, with little or no mucus present. Periostracum resembled a fibrous sheet with a mucus coating possibly serving as a lubricant. Isthmus epithelium was similar in appearance to outer middle mantle surface, but with more mucus pores and with fibers extending from epithelium to ligament (Petit et al., 1978). In a follow up publication, Petit et al. (1979) used osmium pyroantimonate to stain the mantle edge to demonstrate the presence of inorganic ions, such as calcium. Periostracum was resting upon the microvillar surface of the periostracal groove. Pyroantimonate postivie granules were observed in the periostracum ribbon, and on surface of epithelium of the periostracal groove indicating calcium delivery to the ribbon as it is secreted. Periostracal groove may also secrete a protein-based glycocalyx that covers the periostracum ribbon. Transmission electron microscopy was used to describe shell formation as a series of five stages. In general, as periostracum is extruded ventrally around the outer lobe, the ribbon becomes folded, adjacent folds are linked together, packed with layers of protein fibers, and the combined action of folding and packing seemingly enables dense mineral deposition (Petit, 1977, Petit et al., 1979).

The mantle edge at the junction between the incurrent and excurrent apertures was described from *M. hebeli* (Smith, 1988). The photomicrograph of mantle depicts a reduced diaphragm septum that appears to be rich in fibrous tissue. Scant details were provided on the cellular composition of mantle tissue (Smith, 1988).

The cellular features of the mantle edge and middle mantle were described from *Velesunio ambiguous* and *Hyridella depressa* (Hyriidae) using thin and ultrathin sections of tissue embedded in Spurr's resin (Colville and Lim, 2003). The mantle of *V. ambiguous* and *H. depressa* had similar histological features. The epithelium around the outer, middle, and inner

lobe was marked by distinctive folds that could clearly be observed at low magnification while the base of the mantle edge consisted of muscle fibers, vesicular cells, and nerve fibers. Glandular cells were located in the epithelium of the inner and middle lobe, but not around the outer lobe. The middle mantle consisted of an inner epithelium of non-ciliated, microvillar cells, ciliated cells with apical microvilli, and glandular cells. In contrast, the outer epithelium of the middle mantle had a cuboidal epithelium, lacking cilia, and with sparsely distributed glandular cells. The subepithelium of the middle mantle consisted of vesicular cells, and hemolymph sinuses. Muscle tissue of the mantle edge consisted of thin and thick filaments, but cross striations were not observed.

2.4. Gill

2.4.1. Non-marsupial gill

Posner (1875) described histological features of *Anodonta anatina* and *Unio pictorum* gill, and rendered the structural components of gill tissue including, filaments, water tubes, ostia, septa, and the free distal tips of outer gill and inner gill. Peck (1877) described cellular structure of gill tissue of a species of *Anodonta* and the description is similar to the work of Posner (1875). Ridewood (1903) reviewed literature regarding descriptions of morphological and cellular structure of bivalve gills with comparison of species of *Anodonta*, *Unio*, and two species representing Etheriidae. Basic components of unionid gill include flat, homorhabdic lamellae, numerous interlamellar septa, occurring at intervals of 5-7 filaments. Additionally, branchial septa are more regular in the inner gill than in the outer gill. Interlamellar septa are broad, tending to fuse into masses of loose lacunar tissue. Water pores between filaments are ellipsoid and filaments contain structural rods of chitin incorporated with calcium phosphate deposits. Cilia are arranged in frontal and lateral tracts around filaments (Ridewood, 1903).

Ortmann (1911a) compared general structural differences between inner and outer gills, and differences between marsupial and non-marsupial gills. Although structural variation in the morphology of water tubes and interbranchial septa was evident, the supporting figures were reduced so much that it is difficult to comment on specific details. Gill morphology of freshwater mussels was addressed by Ortmann (1911b) to provide insight into variation between families of Unionoida, subfamilies of Unionidae, and differences between unionid species in North America and Asia. Based on a comparison of histological sections of gill from museum specimens, Ortmann (1911b) revealed that one of the principal anatomical differences between different mussel families is variation in water tube structure. The emphasis of the paper was general placement of water tubes, organization of water tubes, and interbranchial septa. *Margaritana margaritifera* (Margaritiferidae) have indistinct water tubes formed by irregularly distributed subcylindrical septa. Based upon an examination of unspecified representatives of *Unio* and *Quadrula* from North America, as well as *Parreysia wynegungaensis* and *Lamellidens consobrinus* from Asia, members of Unionidae have well-defined water tubes formed by regular septa between inner and outer laminae. Additionally, Ortmann (1911b) noted that *Lamellidens consobrinus* has incomplete septa in the marsupiua. *Spatha kamerunensis* (Iridinidae) from Africa has well developed water tubes, but with widely separated septa that create an expansive space between the inner and outer laminae. *Hyria corrugata* (Hyriidae) is characterized by indistinct water tubes in the outer gill with cylindrical projections spanning the interlamellar cavity but not united in the center. Gill morphology of representatives of each unionid subfamily was examined to address differences between inner and outer ctenidia, and differences between males and females (Ortmann, 1911b).

Allen (1914) described the general morphological composition of the gill and explained how the inner and outer gills can work together to capture particles. Ciliary currents along inner and outer gills of Unionidae were described in the investigations of Allen (1914) and Atkins (1937). There are descending currents along the surface of the outer ctenidium, and ascending ciliary currents along the inner ctenidium. Overall, ciliary currents direct particles to the ventral margin of inner ctenidium where an anteriorly directed current sends particulates towards the labial palps (Allen, 1914, Kellogg, 1915, Atkins, 1937). Stasek (1963) also illustrated ctenidial currents of *A. californensis* and explained how the inner ctenidia are closely positioned to the labial palps such that particles could quickly be dispelled into the palps.

Limited details regarding the cellular structure of *P. cordatum* were provided in the dissertation of Yokley (1968). Male and female *P. cordatum* may differ in terms of the number of water tubes present in gill, water tube shape, and number of interbranchial septa (Yokley, 1968). In the histological description of *M. hembeli*, only the fibrous composition of gill septa was detailed (Smith, 1988). Septa have a squamous epithelium and a dense core of fibers consisting of a mixture of loose connective tissue and myofibers. Furthermore, there was no discussion of branchial filaments, blood vesssels, or ostia (Smith, 1988).

The histological composition of gill musculature was explored to determine whether muscular contractions change the diameter of ostium pores and water tubes (Gardiner et al., 1991). Gill tissue from unrelaxed mussels and mussels relaxed with serotonin were compared with histology, SEM, and TEM. Anterior-posterior muscles directly underneath the filaments control the diameter of the ostia while vertically oriented muscles have the ability to constrict the central water tube, thus indicating that water tube apertures may be opened and closed (Gardiner et al., 1991). Gill ultrastructure may provide insights into the ability of mussels to capture

particles (Galbraith et al., 2009). Ctenidial surface area and organization of latero-frontal cirri was examined from four co-occurring species, *Actinonaias ligamentina*, *Amblema plicata*, *Fusconaia flava*, and *Obliquaria reflexa*, to determine whether all members of a multi-species mussel bed specialize in feeding on different particle sizes. Cilia and cirri were described with scanning electron microscopy. Cirri appear to be filamentous structures with numerous small branches. Gill surface area was significantly different between all four species except between *F. flava*, and *O. reflexa*. *Amblema plicata* had more cirri per cm than *O. reflexa*. Number of cilia per cirrus ranged from 13-23 in *A. ligamentina*, 6-16 in *A. plicata*, 21-26 in *O. reflexa*, and 15-21 in *F. flava*.

2.4.2. Marsupial gill

Lea (1828) described the helical water tubes comprising the marsupium of *Unio irroratus* and noted how females have an expanded posterior shell margin to accommodate enlarged gill. The fine structure of marsupial gill water tubes of *A. cataracta*, *Alasmidonta truncata*, and *Symphynota complanata* was described by Lefevre and Curtis (1910). Illustrations of the marsupia of *A. cataracta* and *S. complanata* indicate the presence of a set of three water tubes. Glochidia are held within in an enlarged, median, water tube referred to as the primary water tube. The smaller secondary water tubes are located lateral to the median primary water tube. Triplicate water tube structure is best seen in Lefevre and Curtis (1910) Figure 1. In contrast, only a single water tube was apparent in the marsupium of *A. truncata.* The authors rejected the idea that members of Anodontinae exhibit tripartite water tubes during the period of gravidity, but Ortmann (1910) stated that secondary water tubes were present in figure 1. The work of Lefevre and Curtis (1910) also provides other insights into overall ctenidial structure. Specifically, septum thickness, septum length, and the amount of tissue surrounding the water

tubes differed between each species. However, it was not clear how such structural configurations are related to marsupium contents.

Morphological differences in ctenidial structure between males and females, and non-gravid and gravid females were compared in Ortmann (1911). Vertical and horizontal cross sections were used to compare spacing of water tubes and thickness of non-marsupial and marsupial gill. Key observations include a furrowed ventral margin of the inner gill, and a rounded ventral margin of the outer ctenidium. In species that utilize inner gill for brooding, the distension caused by embryo packing does not cause a corresponding change in size to the ventral margin and may therefore not affect the volume of particulate matter that could be contained within the ventral groove. Additionally, females have fewer intralamellar septa and septa are strengthened to provide structural support to marsupial gill when it expands. Additionally there is considerable variation in marsupial gill structure (Ortmann, 1911). There were not details provided regarding how marsupial gill structure is related to the filling of water tubes.

The topic of tripartite marsupial gill was later revisited by Heard (1975). Triplicate water tubes were observed in female *Anodonta californiensis*, *A. couperiana, A. hallenbeckii*, *A. imbecillus*, *A. peggyae*, and *A. wahlamatensis*. Photomicrographs of marsupial gills were used to present examples of tripartite and non-tripartite gill. Secondary water tubes appeared during the ovigerous period and subsequently disappeared before glochidia were released. However, the before and after images used for comparison were from two different species, the tripartite animal was a female hermaphrodite of *A. imbecillis*, while and example of ruptured septa were displayed from a visceral female *A. peggyae*. A micrograph of marsupial gill of *A. peggyae* shows secondary water tubes, but the structure labeled as a secondary water tube resembles a septum with displacement of the dorsal and ventral epithelium (Heard, 1975). Additionally,

Heard (1975) mentioned that some members of Anodontinae packaging their glochidia within a membrane-bound sac, referred to as a placenta. However, species of *Alasmidonta*, *Anodonta*, *Anodontoides*, and *Lasmigona* do not produce placentae.

Silverman et al. (1983) described calcium distribution in gill tissue of *Ligumia subrostrata* stained with Alizarin red S. Several transverse and longitudinal sections of gill stained with Alizarin red S revealed that calcium is widely distributed in gill tissue. Specifically, the supporting rods beneath the branchial filaments and connective tissue comprising the walls of the water tubes and interbranchial septa contained diffusely distributed, globules of calcium. Blood calcium concentrations increased following experimental hypoxia via a jar of water saturated with N2. However, the physiological significance of this observation was not immediately clear.

Calcium distribution in gill tissues of *Ligumia subrostrata*, *Anodonta grandis*, *Carunculina texasensis*, and *Elliptio crassidens* were examined by Silverman et al. (1985) by means of freeze-dried histology methods and x-ray radiographs of whole gill demibranchs. Dense concretions of calcium consisting of numerous, fine, spherical bodies underlying the gill filaments were observed in histology sections. Calcium was specifically observed around axons. Analysis of whole demibranchs with x-rays indicated that there is an increasing calcium gradient from the free ventral margin to the dorsal base of the gill. Possibly, the most significant observation was the conspicuously, darkened appearance of marsupial gill prior to being filled with glochidia, and the much more pale appearance of marsupia when filled with embryos as seen from radiographs. This suggests that ctenidia of female unionids, stores and releases calcium. Calcium occurs sometime between the spawning period and during the brooding period. This suggests calcium is mobilized during the brooding period and, and since blood calcium did not increase, calcium may be transported across the epithelium to form a glochidial shell. However, the calcium

content in the gill tissue is represented by calcium phosphate, and not calcium carbonate. Calcium carbonate is delivered to developing embryos in land snails. Calcium phosphate may be more difficult to mobilize, and the exact mechanism is not known.

Silverman et al. (1987) performed experiments with *A. grandis* and *L. subrostrata* to determine calcium distributions to tissues following ^{45}Ca injections or immersion radiolabeled water bath. Radiolabeled calcium was traced to blood, gill, gonad, kidney, mantle, shell and glochidia. Large quantities of calcium were delivered to gill and some calcium was incorporated into glochidia. "Soft tissues," glcohidia, and shell can become incorporated with calcium within four hours of bath or injection-based delivery to a mussel. Based on histology of outer gill of non-reproductive mussels, calcium deposits are located in connective tissue between the free distal tip of the gill filaments and the lining of the water tubes. Calcium does not appear to be evenly distributed amongst the connective tissue sinuses seen in the micrographs. However, this could be biased considering that the gill is ventrally convex, and the filaments and the underlying connective tissue sinuses exhibit some distortion. The histological details derived from marsupial gill suggest calcium concrements are initially present in the connective tissues surrounding water tubes that enclose developing larvae. Later, calcium decreases from connective tissue sinuses and coincides with shell formation around glochidia. Gill histology of *A. grandis* corroborates the observations of previous observations of the development of secondary water tubes in marsupial gills of species of *Anodonta* (Lefevre and Curtis, 1910, Ortmann, 1910, Heard, 1975). Considering that glochidial chamber of a marsupial gill appears to be sealed off from an external water supply, the secondary water tubes may represent a conduit for gaseous exchange without bathing developing glochidia in an exogenous fluid (water).

The formation of calcium concretions in gill tissue has been described at the ultrastructure level (Silverman et al., 1989). Membrane bound granules are produced by cells containing an enlarged rough endoplasmic reticulum and Golgi apparatus. The Golgi possessed saccules containing an amorphous, electron-dense material. The amorphous intracellular granules appear to be preliminary bodies that later become extracellular calcium deposits that would appear in histology sections of gill. Following experimental injections with India ink, dark ink bodies were observed within the connective tissue of gill, but not in the epithelium. Cells associated with the formation of calcium concretions engulfed colloidal gold particles by means of phagocytosis.

Marsupial and non-marsupial gill structure of *Ligumia subrostrata* were compared by Kays et al. (1990). Intracellular calcium deposits were present in non-reproductive gill of female *L. subrostrata* and lack of calcium deposits in reproductive female gill. Non-ciliated cells contained carbonic anhydrase near the apical surface, while ciliated mucus cells had little carbonic anhydrase activity. Cytochrome oxidase was present in ciliated cells, but lacking in non-ciliated cells (Kays et al., 1990). Marsupial and non-marsupial gill structure was compared with SEM between representatives of Anodontinae (*A. grandis*) and Lampsilinae (*Lampsilis subrostrata*, *C. parva texasensis*). The gill tissue of *A. grandis* expands when filled with larvae and ventral margin becomes flattened, and the tissue stretches overall. Glochidial development precedes rupturing of ventral margin of lateral (outer) gill and gentle mechanical stimulation of gravid gill can cause glochidia to be discharged and glochidial release may be assisted by muscular contractions. Following glochidial release, marsupial gill becomes flaccid, and subsequently contracts to its normal shape over several weeks. Filaments that were creased or folded when gill was filled with glochidia became more regular with fewer creases as a result of

tissue repair. In the lampsiline representatives, anterior portion of outer gill is similar in structure to inner gill. However, there is a thickened posterior portion of outer gill serving as a marsupium. Marsupial gill expands and thickens during breeding season. Marsupia of *Anodonta* and *Lampsilis* differ in how they are filled, *Anodonta* embryos packed singly or in doublets, maintaining a close association with epithelium while *Lampsilis* gills can accommodate many more embryos in a water channel and are not closely associated with the epithelium (Kays et al., 1991).

Richard et al. (1991) compared the marsupial gill, and non-marsupial gill of *Anodonta grandis*, *Ligumia subrostrata*, and *Caruncula parva texasensis* with SEM to explain brooding differences between Anodontinae, and Lampsilinae. The authors noted that there are major morphological changes to gravid gill in Anodontinae and Lampsilinae. The outer gill of *A. grandis* expands when filled with larvae and ventral margin becomes flattened, uniformly ciliated and looses organization to the filaments as the gill expands. Glochidial development precedes rupturing of ventral margin of lateral (outer) gill and gentle mechanical stimulation of gravid gill can cause glochidia to be discharged. Glochidia may be released from the ventral margin by means of muscular contractions. The authors described structural changes associated with repair process to gill following glochidial release. Marsupial gill gradually deflates and returns to its normal shape over several weeks. Filaments that were creased or folded became more regular with fewer creases as a result of tissue repair.

The marsupial gills of *L.subrostrata*, and *C. parva texasensis*, had certain morphological features in common. The anterior end of the outer gill is structurally similar to inner gill. However, members of Lampsilinae have a thickened posterior portion of outer gill that serves to incubate developing glochidia. The marsupial gill expands, and thickens during breeding season,

and the ventral margin becomes intermittently scalloped because of underlying water tubes. The surface of the gill is ciliated, and looses filament organization. As the marsupium fills with embryos, the entire gill greatly distends and becomes thin such that glochidia may be observed within the transluscent water tubes. Glochidia of *L. subrostrata*, and *C. parva texasensis* are released from the ventral margin of the marsupium (Richard et al., 1991).

Water tubes of unionid gills have characteristic spacing. Interbranchial septa contain hemolymph sisnuses and typically converge with dorso-ventral blood vessels that run parallel with gill filaments. Spacing of septa was somewhat different between *A. grandis*, and *L. parva*. The inner gill water tubes of female *A. grandis* were separated by septa every 1000-1250 μm and at intervals of 15-20 filaments. A similar spacing pattern was observed in male *A. grandis*. Similarly the inner gill of *L. parva* had septa spaced at intervals of approximately 10-15 or intervals of 580-720 μm. Marsupial gill of each species exhibited a markedly different pattern. Outer gills of *A. grandis* featured smaller and more numerous water tubes separated by septa at intervals of approximately 2-5 filaments, but the interval between gill folds remained approximately the same (1000-1250 μm). Water tubes of *L. subrostrata* are smaller in the marsupial gill than in the inner gill and septa are 125-250 μm apart. Folds along the surface of the gill occur between intervals of four to seven branchial filaments. Additionally, the marsupial septa of *L. subrostrata* are 5-10x higher than in the non-marsupial portion of the outer gill. Likewise, the septa dividing the marsupial gill of *A. grandis* become thickened and increase in height during the reproductive period (Richard et al., 1991).

During the spawning period the marsupial gills undergo a transformation to accommodate an influx of embryos. The lateral and medial faces separate as the marsupium expands, and the septa can maintain the tensile strength necessary to support the distension. During this perod of

expansion, the base of the gill near the suprabranchial cavity expands. Interestingly, the marsupium of *A. grandis* and *L. subrostrata* appears to prevent or minimize water entry into the median water tubes where embryos are incubated. When embryos are not present in the marsupium, the tissue normally conducts water. There was a difference in embryo packing between *A. grandis* and *L. subrostrata*. The embryos of *A. grandis* were typically densely packed into doublets and closely associated with interbranchial septa. Embryos of *L. subrostrata* were restricted to the posterior portion of the outer gill and enclosed within a sac. Although embryos were not associated with a septum, the embryonic sac was united with a septum (Richard et al., 1991).

Tankersley and Dimock (1992a) compared ctenidia of male and female *A. cataracta* with SEM and emphasized general differences between marsupial and non-marsupial gill. The main observation was the development of a horizontal, ovular chamber housing glochidia in the median aspect of the water channel. The central chamber represents the primary water tube, and is flanked on either side by secondary water tubes.

Tankersley and Dimock (1992b) described the ciliary currents of the gill of *Pyganodon cataracta*. The authors described such currents by observing the pathways of fluorescent dye-labeled latex particles through an endoscope. The observations provide new insights into ciliary currents as it relates to feeding and the function of marsupial gill during brooding and glochidial discharge. The most significant conclusion of the observations reported were ventrally directed ciliary currents of both the inner and outer gills. The authors reject the hypothesis that particles are transported dorsally along the surface of the outer gill such that they would be collected by the outer cilia of the inner gill filaments. Alternatively, particles traveled ventrally along the outer gill and were pulled towards the inner gills by means of a suction current derived from

ciliary action located at the ventral margin of the inner gill. Marsupial gill, although distended maintained active ciliary currents to perform particle-delivery tasks similar to what would occur in non-brooding mussels. Interestingly, glochidia were discharged dorsally and not ventrally, through a tear or slit along the free margin, as had been reported from *Pyganodon* (=*Anodonta*) grandis. Water tubes were emptied from a posterior to anterior direction, and water filtration activity reoccurred in emptied marsupial water tubes. However, a low number of fluorescent particles were observed traveling through the marsupial water tube containing glochidia suggesting that glochidia are not completely sealed off from external water. Direct endoscopic observations of marsupia showed revealed glochidial release into the dorsally located suprabranchial cavity by means of muscular contractions. Glochidia gaping, larval threads were extended, and glochidia were bound together within packets of mucus. Water travelling dorsally through the secondary water tubes may serve to flush glochidia out of the suprabranchial cavity. Additionally, in regard to previous histological observations of the embodiment of horizontal and vertical myofibers, the authors observed rhythmic muscular contractions of gill consisting of a cadence of approximately 6-8 beats/min (not associated with glochidial discharge). Possibly, these muscular contractions correspond to blood circulation and cardiac function.

The cellular structure of marsupial and non-marsupial gills of *Utterbackia imbecillus*, and *Pyganodon cataracta* was evaluated to provide insight into whether brooding mussels transfer nutrients to developing glochidia (Schwartz and Dimock, 2001). The authors reported that the interbranchial septa are rich in multinucleated cells with abundant mitochondria, lysosomes and glycogen deposits, and these cells have apical microvilli and cilia. When filled with glochidia, marsupial gills are rich in glycogen deposits and these deposits shrank following the release of glochidia. In contrast, the non-marsupial gill did not contain glycogen deposits. Scanning

electron microscopy of glochidia revealed that there are numerous pores along the inner surface of the valves and possibly these structures would receive nutrients from the parent (Schwartz and Dimock, 2001).

Lima et al. (2006) generally described glochidia in gravid gill of *Anodonta cygnea*, and described the primary water tube as being the main glochidium chamber with a set of laterally oriented secondary water tubes.

2.5. Foot

Pedal musculature of *A. cellensis* was described in detail in Brück (1914). Myofibers from the anterior pedal protractors, anterior pedal retractors, and posterior pedal retractors begin as a cylindrical unit and gradually fan laterally and ventrally into the foot. When viewed in a transverse orientation, the foot consists of layers of musculature in distinct horizontal and vertical planes. Furthermore, the sinistral and dextral halves of the foot are symmetrical with a median, triangular cavity. Pedal epithelium is rugose and irregular, but specific cell types were not described.

The foot of *P. cordatum* is rugose with numerous epithelial folds, and the subepithelium contains numerous basophilic cells, which may form a viscous mucus coating on the pedal surface. The foot is rich with bundles of musculature threaded in different orentations. The foot is generally bilaterally symmetrical and at a low magnification the histological sections revealed that the foot consists of a sinistral and dextral layer derived from fusion of two buds. There is a central hemolymph sinus that can be filled from the anterior aorta in order to expand (Yokley, 1968).

Araujo et al. (2002) described the foot of a juvenile *Margaritifera auricularia* using SEM and showed a dense mat of cilia covering the pedal integument. Lasee (1991) and Lima et al.

(2006) characterized transformation of mussels with SEM and light microscopy. The foot developed from two symmetrical, curved lobes that eventually fuse and form a bifurcated structure. When completely joined the foot is covered by long cilia and a median pedal groove is located on the ventral margin of the foot.

2.6. Byssal gland

Juvenile unionids produce a filamentous anchor or byssus from the foot, and the byssus allows juveniles to secure themselves to substrate (Smith, 2000). Byssal gland structure, and byssus formation from juvenile (≤20 mm shell length) *E. complanata*, *Lampsilis radiata*, *Leptodea ochracea* and *Alasmidonta undulate* was investigated by Smith (2000). Byssal gland was present in *E. complanata*, and *L. radiata*, but not *A. undulata*, and only the pedal groove was evident in *L. ochracea*. The byssal gland is spherical, located posteriorly to the pedal ganglion and suspended in the visceral mass by muscular capsule. The byssal gland features branched secretory canals bordered by acidophilic cells and cell processes. Secretory canals unite to form a single canal or stem canal. The stem canal is composed of ciliated columnar cells, and extends posteriorly from the byssal gland to the ventral margin of the foot. The stem canal is lined with a series of additional glandular units. A short, anteriorly directed furrow referred to as the pedal groove is located adjacent to the external orifice of the byssal canal. A single, protein-based filament is formed from smaller fibrous components produced in branched mid-gland region. The byssus is elastic and consists of two distinct regions. At the proximal end of the thread, there is an outer layer of continuously overlapping rings while the inside contains longitudinal lamellae, possibly representing the small, filamentous components produced in the branched byssal gland tubules. In contrast, the distal end of the byssus appears solid and fractures smoothly (Smith, 2000).

2.7. Anterior and posterior adductors

One of the earliest descriptions of unionid musculature was published by Margo (1860) who illustrated fascicles and striated myofibers of *Anodonta* sp. In a treatise on muscle tissue of foot, mantle and adductor, Brück (1914) portrayed adductors as a series of twisted myofibers. Brück (1914) illustrated myocytes, periomysium and nodes of a motor endplate. Myocytes are filamentous with an elliptical nucleus and a distinct nucleolus while cellular constituents of perimysium are spindle-shaped to triangular with a compressed to circular nucleus (Brück, 1914).

2.8. Digestive system

The most comprehensive works on the digestive system of unionids are Gutheil (1912) and Yokley (1968). Gutheil (1912) described all organs and cell types of the digestive tract of *Anodonta cellensis*, and although the reference is useful towards understanding general morphological features, the illustrations of observed cell types may be inaccurate considering how much intracellular detail is depicted. For example, Figures 22–24 show cilia embedded deep into the cytoplasm, a series of distinct, and well-separated granules, and patches of chromatin that are linked together within the nucleus (Gutheil, 1912). Yokley (1968) described all digestive organs of *P. cordatum*, but the organs were described out of sequence.

2.8.1. Labial palps and esophagus

Labial palps of were diagrammatically described in Kellog (1915). Palps have cylindrical folds of ciliated tissue along the inner surface of each lip. Ciliary currents in the mantle cavity of *Anodonta* and *Unio* were depicted in illustraitons. Particles delivered to the palps may travel across the pleated surface into a canal that bends around the antero-medial margin of the foot. Some particles may not enter the interior of the palps and may be deflected off the face of the palps to be carried away by cilia currents of the mantle.

Yokley (1968) described the palps and esophagus of *P. cordatum*. The outer surface of palps is lattened with simple cuboidal cells and the inner palp surface is lined with epithelial folds featuring ciliated columnar cells. Subepitheial layers consist of musculature, a lattice of connective tissue fibers and hemolymph sinuses. The connective tissue would give the palps flexibility and musculature would achieve movement of each lip. Esophagus is flattened, ovular, with numerous folds or ridges in the lumen. The folds have ciliated columnar cells and may represent food grooves. The esophagus spirals upward and directly communicates with the stomach (Yokley, 1968).

The labial palps were described from *Velesunio ambiguous*, and *Hyridella depressa* with light microscopy using tissue embedded in Spurr's resin, and scanning electron microscopy by Colville and Lim (2003). Labial palps have a series of transverse folds along the inner surface of each palp, and folds terminate before the base of the palps to create a furrow, referred to as the oral groove. Scanning electron microscopy revealed that there are ciliated cells, non ciliated with microvilli, and irregular protrusions on the surface of the palps. The density of cilia varied from a continuous mat of ciliated cells to isolated tufts of cilia. Based on the micrographs, the ciliated cells were most abundant along the inner surface of the palps, and appeared to be absent along the outer surface.

2.8.2. Digestive diverticulum

Mansour and Zaki (1946) used feeding experiments with *Unio prasidens* to show that the vesiculated cells of the digestive diverticulum are absorptive and that the large network of digestive tubules employs intracellular digestion. The authors observed yellow and green intracellular granules in frozen sections of digestive gland cells of recently collected mussels. Following a period of six days, the colored granules disappeared. After the period of starvation,

mussels were fed a colorless mixture of starch and egg albumin and frozen sections of digestive gland revealed colorless cells. Mussels were injected with chlorophyll derived from boiled spinach, and following a period of days, brown, yellow, and green intracellular granules appeared in the digestive gland cells. However, the authors did not provide specific details regarding the location of the injection site.

Yokley (1968) described two lobes of digestive tubules, there is a right lobe located along the dextral and ventral sides of the stomach while the left lobe is located along the ventral, lateral, and dorsal faces of the stomach. Each digestive tubule consists of three distinct regions, referred to as excretory, secretory, and intercalary. Excretory ducts communicate with the stomach, excretory tubules feature ciliated cells arranged along irregularly shaped folds. Secretory ducts are more abundant and link the stomach with the lobules of the digestive gland. Secretory duct cells consist of non-ciliated columnar dells with a basophilic nucleus and cytoplasm, and goblet cells. Intercalary tubules comprise the largest portion of the digestive gland and comprise a network of secretory ducts. Intercalary tubules consist of mucus cells and wedge-shaped serous cells. According to Yokley (1968) particulate matter is swept up into the digestive tubules from the stomach where they are processed by means of extracellular and intracellular digestion. The remaining material is cast back into the stomach where it may be broken down further by the crystalline style.

2.8.3. Stomach

Purcheon (1958) reviewed major morphological characteristics of four bivalve stomach types from representatives of 21 families in Eulamellibranchia (including Unionidae). Unionids have a type four stomach, and the description was based on *A. cygnea* (Purcheon, 1958). The criteria used by Purcheon includes morphology of stomach walls and how the stomach joins associated

structures including the esophagus, digestive diverticulum, style sac, and mid-gut. Additionally, Purcheon notes that the stomach features sorting areas, major typhlosole, and a minor typhlosole. Purcheon's descriptions are accompanied by illustrations with small arrows portraying the direction of cilia currents. Type four stomachs are characterized by the anterior placement of the esophageal entrance and posterior placement of the style sac and midgut. The crystalline style has a clockwise rotation, extends anteriorly into the stomach to the mouth of the dorsal hood. Stomach contains a relatively large dorsal hood with a well-developed anterior sorting area and is covering by a gelatinous material referred to as the gastric shield. The minor and major typhlosole is associated with the midgut. The minor typhlosole terminates on right wall near the opening of the mid-gut and the major typhlosole projects forward from mid-gut and features a dextral groove. Additionally, Purcheon notes that there is a left, anterior stomach pouch, and the posterior wall features a gastric shield, and a well-developed sorting area is located on the right side and receives digestive diverticulum ducts.

Reid (1965) studied the gross anatomical features of the stomach of eight bivalve species including A. cygnea. The stomach of *A. cygnea* was portrayed with detailed illustrations indicating a series of coarse-to-fine transverse grooves along the stomach walls. The lumen has a prominent bend and a transverse fold that may represent a channel for particles to travel towards the style sac. Dinamani (1967) described major morphological features of *Lamellidens corrianus*. Short, dorsoventrally compressed esophagus opens obliquely to stomach. Ridges along the wall are thought to represent a sorting area. Major typhlosole emerges from common opening of midgut, style sac, and adjacent to minor typhlosole.

Reid (1965) suggested that there are alternating ciliary currents, which allow particulates to be circulated. Yokley (1968) illustrated the stomach *of P. cordatum* and described folded walls

with ciliated columnar cells. Kat (1983) described morphological features of the stomach from *Lampsilis radiata*, *L. splendida*, *L. ochracea*, and a fourth, unnamed *Lampsilis* species. The stomach consists of a short esophageal entrance opening into the primary sorting area characterized by grooved walls and a platform. Openings to the digestive diverticulum are located to the left and right of the sorting platform. The posterior stomach chamber is folded inward and a broad, featureless shelf would be located above the style sac. Additionally, the stomach contains a major typhlosole, minor typhlosole, and a second sorting area (Kat, 1983).

Smith (1988) described morphological features of the stomach of *M. hembeli*. Illustrations of the anterior and posterior stomach indicate that the walls consist of numerous ridges that possibly play a role in sorting particles (Smith, 1988).

2.8.4. Crystalline style sac

The crystalline style sac of *Anodonta* has been described as a tubular structure extending three quarters of the length of the body (Mitra, 1901). Despite its moniker, the style colloidal and resembles a transparent, flexible rod upon gross examination. Additionally, the style may contain concentric layers of ingested material (Mitra, 1901).

The crystalline style sac of *A. grandis* was described in Nelson (1918). The crystalline style was illustrated and its morphological characteristics were portrayed in a transverse and longitudinal plane. The style sac is generally spherical with ciliated columnar cells and contains a centrally located, and layered rod. Based on the illustration there may be three different cell types between the style sac and midgut. The style sac is separated from the midgut by a dorsal and a ventral typhlosole. Nelson (1918) notes that the style is water soluble, but coagulates when placed into boiling water or alcohol. The author reviews several historical ideas concerning the purpose of the style, but specifically for digestion, one idea suggests the style grindings food

matter like a radula by extending into the stomach and impinging on the plate-like gastric shield along the gastric wall. The second hypothesis concerning function of the style is that is may bind loose food matter as it travels from the stomach to the intestine.

There are a series of other observations regarding the style that are worth mentioning. Nelson (1925) inferred that the crystalline style rotates by tracing the path of ingested carmine particles in *Lampsilis luteola*. Yokley (1968) indicated that the style is the anterior aspect of the intestine and the rotating style rod sends digested matter into the intestine. However, Yokley (1968) did not describe cell types of the style sac. Lomte and Jadhav (1980) described the crystalline style from *Parreysia corrugata* as a soft, flexible, rod-shaped structure composed of glycoproteins. The style was positive for amylase, but negative for lactase, maltase, cellulose, protease, and lipase.

2.8.5. Intestine

Scant information regarding intestinal cell types and lumen morphology are provided in Yokley (1968). At best we know that there are tall basophilic cells, and mucus secreting cells within the anterior aspect of the intestine. Furthermore, Yokley (1968) simply states that the intestine is a long tube that is folded numerous times. The rectum was described as a large tube with a single typhlosole, but minimal details were provided.

Although the fifth intestinal limb or rectum passes through the lumen of the ventricle there is some experimental evidence to suggest that nutrients traveling through the intestine are not delivered directly into ventricular blood. However, waste products in the form of iron sulphate, when injected into the ventricle, were delivered into the rectum a short time later (Narain and Singh, 1974).

2.9. Cardiovascular system

2.9.1. Heart

The cellular structure of the heart of *Tritogonia verrucosa*, *Amblema peruviana*, *Lasmagonia complanata*, *Elliptio crassidens*, *Fusconaia ebena*, *Actinonaias carinata*, *Lampsilis purpurata*, and *Megalonaias gigantean* was compared in Motley (1932). The heart consists of a median ventricle flanked by a pair of pyramidal, thin-walled auricles. The heart is situated within a thin pericardial sac consisting of two compact cell layers. Auricles are thin-walled, and distensible blood receiving chambers while the ventricle is muscular, pump. Blood-flow is regulated by a pair of valves referred to as the auriculo-ventricular valves. After the ventricle is filled, blood travels through the ventricle to anterior and posterior aorta. Cardiac muscle of unionids is non-striated, and resembles smooth muscle since the myofibers are not branched. Cardiac myocytes are granular, possessing an ovular nucleus centrally located in the cell, and contain irregular masses of chromatin. The ventrcle surrounds the intestine along the hingeline and becomes continuous with intestinal wall at its anterior and posterior ends. A thin epicardium surrounds the ventricle and auricles, but no endocardium was evident. Motley, (1932) observed how blood cells have a stronger eosinophilic cytoplasm than muscle cells, and contain a dark monochromatic nucleus. Additionally, no conduction system of nerves or ganglia was present in cardiac tissue (Motley, 1932). The description of the heart of *P. cordatum* is similar to the description by Motley, (1932).

Chaudhry and Narain, (1972) described the structure of the heart and intestine of *Lamellidans corrianus*, but limited details were provided about cell structure. A muscular wrapping known as the posterior aortic bulb was described from *L. corrianus* (Narain, 1972). Cellular structure of the heart of *L. corrianus* was described by Narain, (1973) and generally reflected the description by Motley, (1934).

2.9.2. Blood circulation

Heart rates from 1,012 mussels representing 45 species was reported in Motley (1943). Motley's work revealed that the pericardium is necessary for maintaining a regular cardiac rhythm. The heart optimally functions between 15 and 30°C, heart rate gradually decreases with age and larger species have a slower rhythm than small unionid species (Motley, 1943).

The pathways of blood flow throughout the viscera, gill and mantle of *Anodonta anatina* were described by Brand (1972). However, there was no description of cellular structure of arteries. The main objective was to determine if body movements assist with blood circulation. Hydrostatic pressure was recorded from the heart and pericardial cavity and from within the in pedal hemocoel. The pathways of arterial and veins blood were traced after injecting rubber latex through the heart. Blood circulation is as follows; ventricular blood travels through anterior and posterior aorta. From the anterior aorta, blood travels to the visceral artery where it bifurcates to the mantle and anterior adductor. Anterior aortic flow is also delivered to intestine, foot, and palps. The pedal artery takes blood to all regions of the foot and there are many smaller branches leading to hemocoelic sinuses. Meanwhile, the posterior aorta sends blood to the posterior adductor, mantle. Returning blood is collected in a triangular cavity between sinistral and dextral foot muscles. Blood gathers in the median pedal sinus and is released by Keber's valve and travels dorsally where it travels along the median, through the nephridium, and collected by afferent branchial vessels, before retuning to the auricles. Regarding blood pressure, the pressure readings taken from the ventricle, auricles, and pericardium indicate that the heart of a freshwater mussel functions similarly to a mammalian heart. Overall, blood pressure recordings suggest muscular contractions may assist with movement of blood through parts of peripheral circulation, but do not generate high venous return pressure (Brand, 1972).

Many of the above points were summarized in a more recent synthesis about the heart and cardiac circulation in Narain (1976). However, Narain mentions that pericardial fluid may help keep a regular rhythm of cardiac contractions since severing pericardial cavity causes an arythmea. Draining of pericardial cavity may impair the ability of the heart to refill. Secondly, the blood receiving auricles have thin walls because they need to stretch to accommodate incoming blood supply easily and quickly upon the slightest amount of suction generated by ventricular contraction. Thick walled ventricle requires a preponderance of muscle fibers for the purpose of pumping and a heart with walls of a uniform thickness would not be capable of carrying out both functions. Also, some bivalve species have a posteriorly placed contractile tissue called the aortic bulb, but this structure has not been observed from unionids. An anterior aortic bulb has been observed from many bivalve species including *Anodonta* sp., *Elliptio dilata*, *Lampsilis siliquoidea*. The function of the anterior and posterior aortic bulbs is not yet understood (Narain, 1976).

2.9.3. Blood cells and immune function

Dundee (1953) described blood cells from smears freshly extracted blood with the aid of Wright's stain from *Amblema costata, Quadrula quadrula*, *Uniomerus tetralasmus*, *Tritogonia verrucosa*, *Proptera alata*, *Carunculina parva*, *Ligumia subrostrata*, *Lasmigona complanata*, *Lampsilis fallaciosa*, *Anodonta grandis*. Freshly drawn blood is white and opalescent and shortly after it is drawn, blood cells begin to coagulate. Illustrations of hemocytes indicate that there are two morphological types, a spherical cell and a spherical cell with long, sharply triangular cytoplasmic extensions. Staining characteristics suggest at least three different types of blood cells. The first type of cell is an eosinophilic amoebocyte with a single nucleus approximately one-third the diameter of the cell. Type one amoebocytes vary widely in size, 8-

20 μm, and may be round to polygonal. The nucleus of type one cells may appear granular with a nucleolus, and the cytoplasm consists of eosinophilic granules. The second cell type is a granular basophilic amoebocyte and is less common than eosinophilic amoebocytes and is between 7-12 μm. Nuclei of type two cells have heavy granules and no apparent nuclear membrane, and eosinophilic granules may be located within the periphery of the cell in contrast to its largely basophilic character. Type three cells are referred to as macronucleocytes and range in size from 10-20 μm, the nucleus is large, comprising one half to two thirds of the cell volume. Nuclei of type three cells are coarsely granular, and red granules are typically present within the cytoplasm. Although phagocytosis experiments were conducted, it was not clear whether each cell type is capable of phagocytosis or not (Dundee, 1953).

Pauley (1968) documented a significant disease event affecting *M. margaritifera* in the Ozette River, WA. Lesions were evident in 75 of 123 mussels and characterized as ulcers, watery cysts or scarred wounds. Lesioned foot exhibited significant damage to the myofibers and basophilic cells. Regarding immune responses, loose connective tissue near edematous lesions exhibited hemocytic and fibroblastic infiltration. Granulation tissue was evident in scarified wounds and described as a more robustly fibrous region where collagen fibers, leukocytes, and fibroblasts were abundant. Healed tissue was more pliable than the rigid, hydropic masses. Extensive tissue changes characterized by hydropic degeneration and granulation tissue seemed to preclude the normal function such that the digging ability was lost. Additionally, amoeboid cells containing cytoplasmic inclusions were observed in damaged stroma and were presumed to be etiological agents (Pauley, 1968).

Bakker and Davids (1973) observed encapsulation response to *A. conchicola* in six unionid species including *A. marginata*, *A. grandis*, *Lampsilis siliquidea*, *L. ventricosa*, *L. complanata*,

and *Quadrula carianata*. Encapsulation surrounded live and moribund adult worms, juveniles, viable eggs, or empty eggs with detached opercula. Capsules consisted of distinct inner and outer layers with the inner layer represented by elongate, fusiform fibroblast with agranular basophilic cytoplasm. Outer capsule constituents resembled cellular components of the inner layer, but outer layer cells were defined by an eosinophilic cytoplasm. Additionally, nuclei of outer layer cells were spaced farther apart than inner layer cells. Notably, a unique type of leukocyte, referred to as a brown cell, was located within the interior of capsules or between the inner and outer layers. Brown cells were large, irregularly shaped, containing a dark, brown cytoplasm and a peripheral, fusiform nucleus. Brown cells were positive for diastase-fast PAS, alcian blue, and luxol fast blue (Huehner and Etges, 1981).

Blood cells of an unspecified species of Quadrula were recently surveyed using standard cytological techniques (Burkhead et al., 2009). The authors indicated that there may be as many as four types of hemocytes based on staining characteristics, and cell size. Specifically, there are eosinophilic granulocytes, basophilic granulocytes, large agranulocytes and small agranulocytes. However, the function of each cell type was not immediately known.

2.10. Renal system

Nephridium, and pericardial structure were described from *Quadrula nodulata* in Myers and Franzen (1970). The nephridium is generally C-shaped with separate dorsal and ventral limbs. Ventral nephridium was described as glandular with several involuting diverticula while dorsal portion lacks extensive branches and is therefore thought to function as a bladder. Ventral nephridium consists of simple columnar cells while dorsal portion maintains a cuboidal epithelium. Three types of nephridial cells (designated A, B, C) were observed by Myers and Franzen (1970). Cell type A is simple, and ciliated with a large, granular and centrally located

nucleus and one or two nucleoli. The type-A cell is the most common nephridial cell and exhibits a random distribution. Since type-A cells are ciliated, it seems that they are responsible for transport of substances from the pericardial cavity to the ventral nephridium and fluid is directed from the pericardial cavity to the nephridum through the renal-pericardial canal or nephrostome. Additionally, type-A cells are responsible for creating ciliary currents at the urethra or nephridopore, which dispels waste products ventrally into the suprabranchial cavity. Type-B cells are columnar with a large non-granular vacuole that displaces the nucleus laterally and basally. Type-B cells are located in the posterior portion of the nephridium. Myers and Frazen (1970) suggest type-B cells release stored waste products via exocytosis. B-cells exhibited a differential staining reaction by Heindehein's hematoxylin that indicated the presence of an alkaline substance. Type-C cells are non-ciliated columnar cells in nephridium and pericardium.

The location and distribution of the nephridium and pericardial glands of representative species of Unionidae and Etheriidae were illustrated in White (1942). General morphological features were described and no emphasis was placed on cellular anatomy. Nephridium was portrayed as bilobed, U-shaped, with the proximal lobe opening into the pericardium anteriorly through a ciliated aperture or reno-pericardial opening, and the distal lobe opening into the suprabranchial cavity. The pericardial gland was described from eight unionid species and one etheriid species. The location of pericardial gland tissue varies, but it is either located between mantle tissue and the pericardial cavity or along the lateral margins of pericardium near the auricles. Coloration of pericardial gland varies from yellow-brown in *Anodonta* sp. Pericardial gland is a thin walled sac surrounding the pericardial cavity, along the midline of the body. The tissue has a spongy texture, consisting of coiled tubes, which open into the Nebenhöhle through a

series of 3 to 8 apertures. Apertures vary in size and are associated with muscle. The Nebenhöhle is a specialized tissue at the anterior end of pericardial cavity and is thought to secrete waste products into the renal-pericardial opening. Comparison of pericardial gland tissue of freshwater mussels indicated that pericardial tissues are similar across genera (White, 1942).

The structure and function of the pericardial region including the auricles, ventricle, pericardial sac, pericardial glands, and renal-pericardial canal of *A. cygnea* was described in Andrews and Jennings (1993). The investigation was aimed at describing how urine is formed and a variety of methods were employed including vital staining, tracers, corrosion casting, histology, SEM, TEM. *Anodonta cygnea* have extensive pericardial glands in the body wall dorsal to the ctenidia. Auricles have a wide mouth, but narrow medially at the junction of the ventricle. Auricles are thin-walled containing longitudinal and transverse myofibers. Auricles receive blood from efferent renal veins and efferent ctenidial veins. Latex and fluid injections indicated that fluid may leak out of the auricles and travel into the pericardial gland, but also some fluids traveling through the nephridial sinuses may bypass the auricles and travel directly to the pericardial gland. The ventricle of *A. cygnea* is bilaterally symmetrical with a conical anterior end and a concave posterior surface. Blood flows into the ventricle and travels anteriorly and posteriorly through aortic vessels and the posterior aorta is bulbous (Andrews and Jennings, 1993).

Fluid from the pericardial cavity enters the renal-pericardial openings located anteriorly to the ventricle. The canals are positioned forward of the heart possibly to minimize exposure of cardiac tissue to a waste stream. The renal-pericardial canal opens into the nephridium located directly ventral to the pericardial cavity. The pericardium consists of a simple squamous

epithelium and does not appear to be a site of fluid transport into the pericardial sac (Andrews and Jennings, 1993).

Anterior to the pericardial cavity is a region of tissue known as the Nebenhöhle. At the Nebenhöhle, there is a pair of medial pericardial gland branches, encircling the anterior aorta. The Nebenhöhle is isolated from the pericardial cavity by a constriction or sphincter. Fluid from the pericardial glands appears to drain into the Nebenhöhle where it travels into the renal-pericardial canals through a series of pores or tubules. Fluid is transported through currents generated by cilia in the Nebenhöhle and renal-pericardial canal. Longitudinal muscle fibers of the renal-pericardial canal may shorten and lengthen the canal to assist with fluid transport. The lining of the Nebenhöhle consists of a squamous epithelium, and podocytes located at the junction of the pericardial gland (Andrews and Jennings, 1993).

Podocytes are involved in resorption of solutes, and feature pits or pinocytotic vesicles, an extensive endocytotic canal system and lysosomes. The authors suggest podocytes have features similar to subcellular structures of digestive diverticulum cells. When ferritin is injected into blood, it is mostly absorbed by podocytes where it may be captured by lysosomes. However, lyosomes of *Anodonta* have a crystalline core, which makes it difficult to confirm the uptake of ferritin. Furthermore, many blood cells observed in histological sections contained ferritin following injections and possibly hemocytes play a role in extracting chemicals from blood than in marine bivalves. Pellicles located at the basal margin of podocytes, form filtration slits 12-25 nm in diameter (Andrews and Jennings, 1993).

2.11. Nervous system

Splittstoβer (1913) mapped the nervous system of *A. cellensis.* Gross morphological features of cerebral ganglia, pedal ganglia, visceral ganglia and statocysts were presented. Additionally

Splittstoβer (1913) described how extend throughout the body from ganglia. In an effort to understand how the nervous system regulates heartbeat, Motley (1943) stimulated the heart with electrical impulses and discerned that cardiac tissue is responsive to such stimulation. Stimulation of cerebral and visceral ganglia did not depress heart rate, but instead caused contractions in the pedal musculature (Motley, 1943).

Kraemer (1967) observed of mantle flapping of *Lampsilis ventricosa* and explained how flapping was positively associated with light intensity. Well-developed nerve tissue between the mantle flaps and visceral ganglion may help control flapping. Additionally, nerves near the mantle lure are more developed than in the siphonal area. The most significant finding was a small ganglion located at the base of the tail region of the mantle lure, the ganglion was present in males, and it is linked to visceral ganglion. Histological structure of statocysts of *Lampsilis ventricosa* and *Corbicula fluminea* were compared in Kraemer (1978). Statocysts are spherical sacs with either a columnar (*Lampsilis*) or cuboidal epithelium (*Corbicula*). *Corbicula* sectioned were 4 mm long and a pore was observed. Statocysts of *Lampsilis* are enclosed within a connective tissue capsule, but *Corbicula* does not have conspicuous capsule (Kraemer, 1978).

The cerebro-pleural, pedal and visceral ganglia were described from *P. cordatum* (Yokley, 1968). Cerebral-pleural ganglia are located laterally to the esophagus and are separated from each other by a large commurssure. Yokley (1968) provided a general description of the ganglion, and described the pathways of nerves from the erebral-pleural ganglion. The most notable cell type of the anterior ganglion was the multipolar neuron. The pedal ganglion was described has two hemispheres with a cortex and medulla. There was no specific detail given about the components of the cortex and medulla. The visceral ganglion are elongated, fused lobes located near thr posterior adductor and controls and there are branchial extensions of the

visceral ganglia that extend anteriorly. The statocysts are spherical capsules dorsal and lateral to the pedal ganglia in the ventral part of the coelom. Statocysts have a cuboidal epithelium and there is a spherical, basophilic mass or statolyth in the lumen, but cilia were not observed (Yokley, 1968).

Smith (1988) described gross morphological features of the visceral ganglion of *M. hembeli.* The visceral ganglion is depicted as a cube with a series of nerves extending away from the ganglion anteriorly, posteriorly, ventrally, and dorsally (Smith, 1988).

2.12. Reproductive system

Reproductive tissue consists of ovarian and testicular acini, ciliated ducts that transfer ova and sperm dorsally to gonadal pores (van der Schalie and Locke, 1941, van der Schalie and van der Schalie, 1963, Yokley, 1972, Heard, 1975, Zale and Neves, 1982, Smith, 1988, Gordon and Smith, 1990, Woody and Holland-Bartels, 1993, Heinricher and Layzer, 1999, Smith et al., 2003, Henley et al., 2007). In histological sections of testicular acini, the cellular constituents are small with condensed chromatin, and a minimal volume of surrounding cytoplasm. Spermatids and spermatozoa are so small that only the general shape of the cell body with its flagellum can be observed. Ovarian acini contain larger oocytes by comparison, with a distinct vitelline mass, and centrally located nucleus is typically seen in published micrographs.

Considering the small size of spermatocytes, spermatids and spermatozoa, it is not possible to identify and describe potential structural differences between sperm cells of different unionid species based on routine histological sections. Many details concerning overall cell morphology, as well as structural features of nuceli, and cytoplasmic organelles of spermatocytes, spermatids, and spermatozoa have been rendered from transmission electron microscopy studies (Healy, 1989, Rocha and Azevedo, 1990). Spermiogenesis and spermatozoa were primarily described from *Neotrigonia bednalli*, and limited details regarding cell morphology and organelle structure

were reported from *N. gemma* (Trigoniidae), and *Velesunio ambiguus* (Hyriidae) (Healy, 1989). Spermatocytes and early-stage spermatids of *N. bednalli* were characterized by a large, ovular nucleus, scattered, elongated mitochondria and a compact cytoplasm. The nucleus initially consists of electron dense and electron lucent areas, but electron lucent regions of the nucelus become darkened as a spermatid develops from a spermatocyte. The acrosome develops from a series of diminutive, electron dense bodies that are initially scattered throughout the cytoplasm, and become condensed near the apex of a spermatid during a later developmental stage. Spermatids contain a pair of centrioles that are oriented at a 90 angle to each other during an early stage of development. The distal centriole produces a flagellum and a complement of satellite fibers that presumably provide structural support to the centriole. The proximal centriole is located within a shallow depression that forms at the base of the nucleus. Depressions in the nucelus also allow mitochondria to become properly positioned in the basal region of the cell body. Mature spermatozoa have a reduced nucleus and a thin acrosomal complex, five mitochondria, two centrioles, and a single flagellum. The acrosomal complex is a convex group of minute, discoid, electron-dense bodies. Spermiogenesis was not described from *N. gemma* and *V. ambiguus* (Hyriidae), however the morphology of spermatozoa of *N. gemma* and *V. ambiguous* was similar to spermatozoan morphology of *N. bednalli* and suggests a close phylogenetic relationship between Trigonioida and Unionoida (Healy, 1989).

Detailed ultrastructure-level observations of spermiogenesis in *Anodonta cygnea* were presented in Rocha and Azevedo (1990). Primary and secondary spermatocytes were described but secondary spermatocytes were infrequently observed possibly reflecting rapid meiotic changes that were occurring. Spermatids are initially ovular with ovular to spherical cyotplasm, and a cluster of developing spermatids may be united by neighboring cytoplasm. During sperm

cell development, mitochondria may be abundant and located in different places surrounding the nucleus. In later developmental stages, mitochondria become enlarged, decrease in abundance, and migrate to the basal pole. Following the mitochondrial changes, an axonome leaves the cytoplasm and forms a flagellum. The volume of the spermatid nucleus decreases, and chromatin becomes condensed. During transformation from spermatid to spermatozoa, the nucleus continues to contract and becomes conical, and the acrosome forms from a series of electron dense bodies (Rocha and Azevedo, 1990).

Intespecific morphological differences to spermatocytes and spermatozoa are not evident from histological micrographs due to their small size. Oocytes are considerably larger than sperm cells and interspecific variation in oocyte structure could be more apparent. However, potential variation in oocyte structure is indeterminant because either published micrographs are at a low magnification or image resolution was low. However, some published micrographs have revealed distinct differences in vitelline structure across different unionid genera (Yokley, 1972, Zale and Neves, 1982, Woody and Holland-Bartels, 1993) or between unionids (Zale and Neves, 1982) and margaritiferids (Gordon and Smith, 1990, Grande et al., 2001). Histological sections of *Villosa nebulosa* reveal an irregular fluidic mass surrounding the vitelline, filling the lumen of the acini (Zale and Neves, 1982) while an irregular, linear membrane surrounded mature oocytes of *Cumberlandia monodonta* (Gordon and Smith, 1990), *Margaritifera auricularia* (Margaritiferidae) (Grande et al., 2001), and, *Megalonais nervosa* (Woody and Holland-Bartels, 1993), *Pleurobema cordatum* (Unionidae) (Yokley, 1972).

van der Schalie and Locke (1941) presented a detailed description of ova and was one of the first publications to specifically describe formation of sperm and ova with photomicrographs. Ova may have an irregular shape initially and maintain a connection to the acinus wall by means

of a pellicle. When ova reach maturity they are appreciably enlarged and contain a double nucleus. Sperm cells develop from small clusters of spherical cells called sperm morula. *Anodonta grandis* can be hermaphroditic, but hermaphrodites represent a small proportion of the population. Hermaphroditic individuals appeared to have an equal composition of testicular and ovarian tissue (van der Schalie and Locke, 1941).

Male mussels disperse spermatozoa by packaging them into spherical masses resembling *Volvox*. Spermatozuguemata were described from *Anodontoides ferussacianus* using light microscopy. Spermatozoa are spherical such that the acrosome was facing the median and the tail extended distally, allowing the entire mass to be propelled and steered by different groups of cells (Edgar, 1965). Ultrastructure-level observations of spermatozoa and spermatozeugmata of *Truncilla truncata* were similar to the observations of Edgar (1965) and a single spermatozeugmata was estimated to contain 8,000-9,000 spermatozoa (Waller and Lasee, 1997).

Yokley (1972) made detailed observations of the cellular structure of acini and gametogenic cycles of *Pleurobema cordatum*. Regarding cell structure of acini, the epithelium consists of single layer of spermatogonia or oogonia, recognized by large vesicular nuclei. Closer to the lumen are many primary spermatocytes distinguished by round, more chromatic nuclei and are a little smaller than the spermatogonia. Sertoli cells are yellow or pink in the lumen of acini in hematoxylin and eosin stained tissue. Spermatozoa have a cylindrical head with a long flagellum, and remain in the lumen attached to sertoli cells until shed. Descriptions of the specific attributes of oocytes were limited in comparison to testicular acini. However, the micrograph of mature ovarian acini show oocytes with a large homogenous vitelline, a nuclear center characterized by a dark, spherical nucleus and a membrane surrounding the cell (Yokley, 1972)

Seasonal differences in the composition of testes and ovaries were documented. Males and females exhibited peak gametogenesis during the spring. During the spring, testicular acini were greatly enlarged and closely positioned to each other. Mature spermatozoa were located within the lumen while the periphery was filled with secondary spermatocytes undergoing meiosis. Additionally, spermatozoa may be observed in ciliated tubules. Following spawning, the summer represented a recovery period. Acini were reduced in size and filled with spermatogonia and primary spermatocytes, spermatozoa were rarely observed. Nutrient matter derived from Sertoli cells began to accumulate in testicular acini. The fall was characterized by a noticeably increase in sperm cell production. Acini became more enlarged, and spermatozoa were more abundant. Spermatogenesis was more conspicuous with division of primary spermatocytes into secondary spermatocytes and formation of spermatids (Yokley, 1972).

The spring was characterized by prodigious oocyte production. Acini were thin walled, oocytes contain one or more nuclei and oocytes crowded the lumen. Acini contracted during the summer, leaving a large space between each unit with visible threads of connective tissue fibers between acini. The acinus wall begins to build-up with oogonia, and the remaining oocytes and ootids present in the lumen are reduced. During the fall, alveolar walls were restored in thickness as a result of numerous rounds of cell division. Small, early-stage oocytes were more numerous and meiotic figures were present. Atretic material, consisting of oocyte remnants, was present in the lumen (Yokley, 1972).

Heard (1975) provided key insights into spermatogenesis. Formation of spermatozoa from sperm morula had previously been reported from several other mussel species. Heard (1975) specifically indicated that there are two forms of spermiogenesis. Typical spermiogenesis occurs during the breeding period and is characterized by spermatozoa forming from spherical single-

celled spermatocytes. In contrast, atypical spermatogenesis leads to spermatozoa by means of multicellular sperm morula. Furthermore, sperm morula are only present during times of the year when testicular acini are not producing large quantities of spermatozoa and spermatozoa produced by typical or atypical processes are morphologically identical in histological sections (Heard, 1975).

The gametogenic cycle of *Villosa nebulosa*, *Medionidus conradicus*, and *V. vanuxemi* were compared by Zale and Neves (1982). Descriptions of gonadal cell structure were similar to the descriptive information provided by Yokley (1972), furthermore testicular and ovarian acini of *M. conradicus* and *V. vanuxemi* were identical to acini of *V. nebulosa*.

Heinricher and Layzer (1999) provided evidence that low temperature suppresses gametogenesis and hypolimnetic releases can impair normal reproduction cycles. Gonadal tissue from *Megalonaias nervosa* was compared between a population located downstream of a dam on the Cumberland River and from animals located in Kentucky Lake, which exhibited more natural seasonal temperatures. The dam group was characterized by a preponderance of emaciated and shrunken acini, while similar sized animals from Kentucky Lake exhibited normal gametogenesis. Mussels transplanted from the dam site to a natural site regained histologically normal features of gonadal tissue following a three-year period. Whereas after one year, mussels exhibited type-one maturity status, and type three maturity status was predominant during the second year. In their third year, mussels reached stage four and 49% of mussels carried glochidia in the gill.

The ciliated reproductive tracts of dioecious *V. iris* and monoecious *Utterbackia imbecillis* described to determine if captivity affects reproductive tissue and compared descriptions to gonoduts of *V. vanuxemensis*, *Elliptio complanata*, *L. fasciloa*, *Lexingtonia dolabelloides*, *P.*

oviforme, and *Amblema plicata* (Henley et al., 2007). Ciliated ducts begin as small primary gonoducts and become progressively larger at the confluence of secondary ducts. Ciliated ducts unite at a large gonosinus at the anterior, dorsal part of the body. Gonoducts feature ciliated, columnar epithelium with heterochromatic nuclei. Gonoducts and gonosinuses of *U. imbecillis* differed in having PAS-positive secretory granules (mucigen granules). The authors proposed that PAS-positive substances in the reproductive tract of *U. imbecillus* may prevent self-fertilization. Smooth muscle around gonosinuses may represent a sphincter for controlled release of gametes. Microvilli in the reproductive tract may regulate ionic composition and or glucose of fluid within the lumen or provide substances necessary for maturation of sperm.

Hermaphroditism

Heard (1975) investigated hermaphroditism, marsupial gill structure, reproductive cycles and larval development in *Anodonta californiensis*, *A. couperiana*, *A. hallenbeckii*, *A. imbecillis*, *A. peggyae* with histology. Based on qualitative ratio of testicular to ovarian acini, mussels were either male hermaphrodites (having more testicular acini than ovarian acini) or female hermaphrodites (having more ovarian acini than testicular acini). Hermaphroditism was observed in *A. californiensis*, *A. couperiana*, *A. hallenbeckii*, *A. imbecillis*, *A. peggyae*, only females and female hermaphrodites were gravid. A*nodonta couperiana* was the only species that exhibited male hermaphroditism and female hermaphroditism.

Heard (1975) mentions sperm-morula and how sperm morula are primarily observed during times of the year when gonads are not actively producing a large quantitity of spermatozoa. Spermatogenesis involving a preponderance of sperm morula is characterized by the presence of a small quantity of spermatozoa in the lumen of a testicular acinus and is referred to as atypical spermatogenesis. Typical spermatogenesis is defined as the production of a large quantity of

spermatozoa and a small number of sperm morula. Spermatozoa derived from typical spermatogenesis are indistinguishable from spermatozoa produced during typical spermatogenesis in histological sections (Heard, 1975).

While the above may indicate that there is a large body of descriptive literature on unionid tissues, and while complexity of tissue is sometimes well described, there is a need to better understand how specific tissue components contribute to overall organ function. For example, Beedham (1958) described periostracum secretion and mantle lobes, how branched mantle lobes depicted in photomicrographs might affect the morphology or chemical composition of periostracum ribbon was not addressed. It is sometimes difficult to make such determinations or to develop physiological hypotheses based on anatomical literature considering that supporting figures are typically small or have a low resolution (e.g. Ortmann, 1911a, Beedham, 1958, Smith et al., 2003).

Chapter 3

MATERIALS AND METHODS

Alabama rainbows were collected from the South Fork of Terrapin Creek near the Cleburne County Road 55 crossing (N33°51'36.56" W85°31'28.15") in May 2010 (n=36), August 2010 (n=39), and August 2011 (n=5) plus Shoal Creek near the Talladega National Forest Road 500 crossing (N33°43'30.46" W85°36'05.05"). Gulf pigtoes were collected from the Cahaba River, in shoals, upstream and downstream of a canoe launch (N33°10'10.04" W87°01'12.73") located on Slab Road (Shelby County). Gulf pigtoes were collected in May 2011 (n=10), August 2011 (n=28), and June 2012 (n=7). Alabama creekmussels were collected from Shoal Creek near the Talladega National Forest Road 500 crossing, in May 2011 (n=5), January 2012 (n=3), and from Shoal Creek near the Cleburne County Road 61 crossing (N33°46'14.57" W85°33'20.59"), as well as from the South Fork of Terrapin Creek near the Cleburne County Road 55 crossing in August 2011. A separate sample of Alabama rainbows were collected from pond and recirculating culture systems of the Alabama Aquatic Biodiversity Center in July 2010 (n=20), March 2011 (n=10), and October 2011 (n=5). Hatchery-reared Alabama creekmussels were also collected from a pond culture system at the Alabama Aquatic Biodiversity Center in March 2011 (n=10).

Mussels were collected by hand while snorkeling, transported to Auburn University in aerated cooler filled with stream water from the collection site. In the laboratory, mussels were allowed to purge to themselves of sand and particulate matter for 24 hr to minmimize the possibility of

damaging the microtome knife blade and tissue specimen with attached sand particles. The shell of each mussel was propped open with wooden dowels to enable good fixative penetration. Mussels were fixed whole in a Qt-sized mason jar filled with 10% neutral buffered formalin for 48 hr. After fixation, each animal was rinsed with tap water, to remove buffer salts from tissue and immersed in a graded series of ethanols to 70%. Mussels were removed from the shell by gently scraping the mantle and musculature away from the nacre using a scalpel blade. Whole mussels were divided into pieces by gently cutting through the visceral mass with a grossing knife.

The mussels sampled for histology consisted of 13 wild and 4 cultured *V. nebulosa* (Table 1), 37 *F. cerina* (Table 2), and 12 *S. connasaugaensis* (Table 3). The histological sample comprised a total of 57 blocks and 416 slides from *V. nebulosa*, 111 blocks and 397 slides from *F. cerina*, and 49 blocks and 376 slides from *S. connasaugaensis*. Typically, a mussel having a shell length of 40-50 mm would render 4-6 pieces of viscera from anterior to posterior. Each sample was placed into a labeled mega tissue cassette and processed for paraffin embedding from 70% ethanol inside of an automated tissue processor. Following tissue processing, pieces of visceral mass were embedded in a mega base mold to ideally obtain a whole dorsal to ventral profile of the body. Sections of mussel tissues were cut from paraffin blocks at 4µm thickness. However, paraffin blocks of unionid visceral mass would not cut smoothly at room temperature. The visceral mass of unionids has a wrapping of musculature and causes sections from paraffin blocks to wrinkle. Secondly, delicate adipose tissue surrounding coelomic organs tends to break apart causing the medial portion of the viscera to fall out of sections. To remedy this problem, paraffin blocks were immersed, for 1-2 minutes, in water chilled to approximately 5°C with ice packs prior to sectioning. Smooth (although an unavoidable rippling of muscle tissue sometimes

occurred) intact paraffin sections of visceral mass were obtained in this way. Paraffin blocks were serially sectioned and sections were laid out upon a water floatation bath pre-mixed with histobond histology adhesive, and heated to 43°C, before mounting on glass slides. To facilitate good penetration of histological staining reagents into tissue, slides with mounted paraffin sections were heated in an oven to 63°C for 45 min to remove excess paraffin. Slides were stained in an automated slide stainer using the Harris's Hematoxylin and Eosin protocol from Luna, (1968). Hematoxylin and eosin stain is a widely used to show general features of cells and tissue. Hematoxylin is a violet dye that is a nuclear stain because it has properties similar to a basic dye and carries a net positive charge. Eosin is a pink dye that stains cytoplasm and it is an acidic dye that carries a net negative charge. The function of cells and tissues may be inferred based upon its staining characteristics considering the chemical composition of organelles (Stevens, 1982, Ross et al., 2003). Stained slides were photographed using a digital camera mounted on a comound microscope. Color photomicrographs of tissues were imported into Adobe® Illustrator® to create high quality plates portraying examples of all tissues for each organ system. Photographs were resized to fit one or two column widths and optimized to a resolution of 600 DPI. Illustrator documents representing individual plates were compiled into an optimized Adobe® PDF file

Table 2. Size, site, and collection dates of Alabama rainbow (*Villosa nebulosa*) specimens used for histology.

Specimen code	Shell size			Sex	Collection site	Collection date
	Length (mm)	Width (mm)	Height (mm)			
TC-VN-5	46	26	17	♀†	Terrapin Creek	May 8 2010
TC-VN-6	48	28	15	♀	Terrapin Creek	May 8 2010
TC-VN-8	51	30	16	♀	Terrapin Creek	May 8 2010
TC-VN-9	48	26	17	♀†	Terrapin Creek	May 8 2010
TC-VN-10	51	29	14	♀	Terrapin Creek	May 8 2010
TC-VN-11	41	24	12	♂	Terrapin Creek	May 8 2010
TC-VN-12	51	28	14	♂	Terrapin Creek	May 8 2010
TC-VN-13	47	28	13	♂	Terrapin Creek	May 8 2010
TC-VN-14	45	27	11	♂	Terrapin Creek	May 8 2010
TC-VN-15	45	24	14	♂	Terrapin Creek	May 8 2010
ABC-VN-9	28	14	11	♀	Alabama Aquatic Biodiversity Center	March 10 2011
ABC-VN-13	28	9	10	*	Alabama Aquatic Biodiversity Center	March 10 2011
TC-VN-19	54	32	79	♂	Terrapin Creek	August 3 2011
TC-VN-20	63	38	20	♂♂	Terrapin Creek	August 3 2011
ABC-VN-16	41	23	14	♀†	Alabama Aquatic Biodiversity Center	October 25 2011
ABC-VN-17	38	22	15	♀†	Alabama Aquatic Biodiversity Center	October 25 2011
TC-VN-21	41	26	17	♀♀	Terrapin Creek	August 3 2011

* Dorsum sectioned in a coronal plane, gonad not sectioned
† Embryos and/or glochidia present in marsupia

Table 3. Size, site, and collection dates of Gulf pigtoe (*Fusconaia cerina*) specimens used for histology.

Specimen code	Shell size			Sex	Collection site	Collection date
	Length (mm)	Width (mm)	Height (mm)			
CR-FC-28	39	37	22	♀♀†	Cahaba River	May 28 2011
CR-FC-29	47	45	29	♂♂	Cahaba River	May 28 2011
CR-FC-30	43	39	25	♂♂	Cahaba River	May 28 2011
CR-FC-31	46	41	26	♀♀†	Cahaba River	May 28 2011
CR-FC-32	51	46	30	♂♂	Cahaba River	May 28 2011
CR-FC-33	62	54	35	♂♂	Cahaba River	May 28 2011
CR-FC-22	53	48	23	♂♂	Cahaba River	May 28 2011
CR-FC-8	66	56	32	♀♀†	Cahaba River	May 28 2011
CR-FC-11	66	53	54	♂♂	Cahaba River	May 28 2011
CR-FC-31	49	42	23	♀♀†	Cahaba River	May 28 2011
CR-FC-27	76	57	35	♀♀†	Cahaba River	August 15 2011
CR-FC-22	52	43	24	♂♂	Cahaba River	August 15 2011
CR-FC-34	58	48	30	♀	Cahaba River	August 15 2011
CR-FC-35	48	43	27	♀	Cahaba River	August 15 2011
CR-FC-36	49	46	25	♂	Cahaba River	August 15 2011
CR-FC-37	50	43	25	♂	Cahaba River	August 15 2011
CR-FC-6*	54	46	30	♂	Cahaba River	August 15 2011
CR-FC-10*	41	36	22	♀	Cahaba River	August 15 2011
CR-FC-12*	70	51	38	♀	Cahaba River	August 25 2011
CR-FC-15*	55	44	30	♀‡	Cahaba River	August 25 2011
CR-FC-17*	48	43	29	♀‡	Cahaba River	August 25 2011
CR-FC-18*	45	41	28	♀	Cahaba River	August 25 2011
CR-FC-20*	58	53	20	♀	Cahaba River	August 25 2011
CR-FC-21*	65	55	38	♀	Cahaba River	August 30 2011
CR-FC-22*	51	42	25	♀	Cahaba River	August 30 2011
CR-FC-24*	45	38	24	♀‡	Cahaba River	August 30 2011
CR-FC-26*	72	56	41	♀	Cahaba River	August 30 2011

* Only a small sample of gonad sectioned

† Embryos and/or glochidia present in marsupia

‡ Acini contained a mixture of small, immature ova, and larger degenerative ova

Table 4. Size, site, and collection dates of Alabama creekmussel (*Strophitus connasauagaensis*) specimens used for histology.

Specimen code	Shell size			Sex	Collection site	Collection date
	Length (mm)	Width (mm)	Height (mm)			
SC-SC-2	69	39	19	♂	Shoal Creek	May 19 2011
SC-SC-3	73	42	23	♀	Shoal Creek	May 19 2011
TC-SC-1	31	18	15	♂	Terrapin Creek	August 3 2011
TC-SC-2	57	30	18	♂	Terrapin Creek	August 3 2011
TC-SC-4	50	28	14	♀	Terrapin Creek	August 3 2011
TC-SC-5	31	19	9	♂♂	Terrapin Creek	August 3 2011
TC-SC-6	56	31	21	♀♀	Terrapin Creek	August 3 2011
TC-SC-7	31	19	9	♂♂	Terrapin Creek	August 3 2011
SC-SC-5	48	28	15	♀*	Shoal Creek	February 1 2012
SC-SC-16	55	30	15	♂	Shoal Creek	May 19 2011
TC-SC-8	41	25	18	♂	Terrapin Creek	May 8 2010
TC-SC-9	40	23	15	♀	Terrapin Creek	May 8 2010

* Glochidia present in marsupia

Chapter 4

SHELL MORPHOLOGY, GROSS ANATOMICAL FEATURES OF THE MANTLE CAVITY, AND CELLULAR STRUCTURE OF MANTLE, GILL, FOOT, AND VISCERAL MASS OF THE ALABAMA RAINBOW, *Villosa nebulosa* (CONRAD, 1834)

4.1. Shell morphology

Valves of *Villosa nebulosa* are elliptical, moderately thin and slightly compressed. The epidermis is yellow to light brown with thick, green to black interrupted rays. The anterior margin is narrow, rounded and the posterior margin is bluntly pointed to trapezoidal. Dorsal margin is somewhat convex and the ventral shell margin is straight to slightly convex. The umbo is low directly slightly anteriorly. Posterior ridge is low, not deeply furrowed and the posterior slope is flat to concave (Figs. 1.1, 1.2).

The nacre is silver to white with an elliptical pallial line. The anterior adductor scar is deeply inset, perpendicular to the long axis of the shell. The posterior adductor scar is flat and obliquely oriented to the long axis of the shell. The pseudocardinal teeth are triangular with two slightly divergent teeth on the left valve and one tooth on the right valve. Lateral teeth are long, convex in relation to the dorsal margin with two teeth on the left valve and one tooth on the right valve (Figs 1.3, 1.4).

4.2. Gross anatomical features of the mantle cavity

An incomplete siphon is formed when the sinistral and dextral mantle edges are cupped and slightly overlap. The incurrent aperture of *V. nebulosa* is papillose with uniramous, fine papillae and the excurrent aperture has shorter papillae. Species of *Villosa* have a mottled mantle edge with brown and black transverse bars and the mottling is most pronounced along the siphonal apertures. Incurrent and excurrent apertures are partitioned by when the mantle edge is slightly curled and forms trapezoidal flaps (Fig. 1.5).

The mantle edge is pale, orange and mottled with black transverse bars that become conspicuous along the siphonal apertures. The middle mantle extends from the pallial line to the umbo cavity and it is transluscent with fine white spots. Mantle isthmus is translucent and

trapezoidal, extending dorsally into a cleft between the left, right valves. The gills are translucent, and consisting of elongated, paired inner and outer gills arching over the posterior adductor and the inner gill is higher than the outer gill (Fig. 1.6). Outer gills and inner gills resemble each other in males, but females have an enlarged group of water tubes located along the posterior third of the outer gill. Marsupia have a blackened ventral marign and the marsupium becomes distended when filled with glochidia (Fig. 1.7). The siphonal mantle edge of males and females are distinctive, the siphon is flattened in males except for a series of fine branchial papillae. Females however, have enlarged, brown papillae along the siphon (Fig. 1.7). The foot of *V. nebulosa* is orange and there is a black spot located at the posterior margin. The visceral mass is white and extends dorsally to the base of the gills. Labial palps are transluscent, triangular lips located antero-laterally between the foot and visceral mass. The anterior adductor is pale, white, ovular in outline, and oriented vertically between the anterior shell margin and foot. Posterior adductor is grossly identical to the anterior adductor, but is parallel with the posterior shell margin. The gill is supported by a thickened white line of connective tissue representing the abdomen, and the abdomen is transluscent and triangular between the visceral mass and posterior adductor (Fig. 1.8).

4.3. Cellular structure of mantle

4.3.1. Anterior mantle edge

The free distal margin of the mantle edge is lobular with three epithelial folds, or mantle lobes, extending medially into the mantle cavity (Fig. 2.1). From ventral to dorsal, there is an outer lobe, a middle lobe, and an inner lobe. Mantle lobe morphology varies throughout the length of the mantle edge, but only a representative area from the anterior and posterior end will be described for simplicity. A conspicuous component of the mantle edge is a ribbon of

periostracum secreted by a group of cells called the basal bulb located at the base of the outer lobe (Fig. 2.1–4). Periostracum bends around a semicircular groove called the periostracal groove and extends medially towards the mantle cavity (Figs. 2.3–5). Outer lobe is characterized by a flattened ventral margin of columnar cells, and the epithelium becomes pleated along the dorsal surface for approximately half the length of the outer lobe. Columnar epithelial cells of the outer lobe are characterized by a basophilic cytoplasm, and an ovular, monochromatic (Fig. 2.3). The simple columnar epithelium terminates at the basal bulb where it abruptly transitions to a simple, squamous epithelium (Fig. 2.2). The middle lobe is ventrally flattened with a simple squamous epithelium, transitioning to columnar epithelium from the distal margin where the slope begins to decline dorsally. Like the outer lobe epithelium, cells lining the middle lobe have monochromatic nuclei, but the cytoplasm is eosinophilic (Figs. 2.4). The base of the middle lobe is plicate, with several short, broadly rounded epithelial folds. Plicae span the length of the dorsal mantle edge surface from the inner lobe to the pallial line, where the dorsal surface of the mantle edge meets the nacre. However, plicae are irregularly spaced and the shape and size of each fold is variable. (Fig. 2.5) Columnar cells continue throughout the length of the mantle edge to the pallial line. In contrast to the columnar epithelium of the outer lobe, cells representing the inner lobe have brown granular inclusions (Fig. 2.6).

Muscle tissue comprises the main histological constituent of mantle edge. Fibers are organized into dense bands in the straightened, proximal portion of the mantle edge (Figs. 2.1-7) and become less regular between each lobe. Small groups of fascicles are scattered throughout a region of adipose tissue in the proximal portion of the mantle edge (Figs. 2.6). Muscle fibers in the outer and middle mantle lobes are wavy, but generally regular (Fig. 2.3). However, muscle tissue in the inner lobe consists of branched and overlapping fibers (Fig. 2.5). Additionally there

are spheroid cells, with a basophilic, granular cytoplasm located directly beneath the epithelium of the middle and inner lobes (Fig. 2.5).

4.3.2. Posterior mantle edge, middle mantle, and mantle isthmus

The mantle edge becomes blackened near the posterior terminus of the visceral mass (Fig 3.1). Epithelial cells in this region contain brown or black granules, which may be melanin or a related substance. The concentration of granules in a cell may be so great that the nucleus and cytoplasm may be occluded (Figs. 3.1–3). Mantle lobe morphology near the posterior adductor muscle is considerably different from the morphological features characterizing the lobes near the labial palps. In the posterior region of the mantle edge, the outer and middle lobes are a forked extension of mantle tissue with each fork appearing equally long. Plications of the outer lobe are restricted to the distal tip while occasional plications along the dorsal surface of the inner lobe give the epithelium a wavy appearance. Epithelial folds around the inner lobe may be single lamellae to forked or branched papillae, giving the inner lobe a high surface area (Fig. 3.1). Branchial papillae are thin, conical extensions of the mantle located near the narrow, posterior shell margin. Papillae consist of an irregular matrix of muscle and connective tissue fibers surrounding an irregularly shaped hemolymph sinus. Papillae have a highly pleated surface with obliquely oriented epithelial folds directed towards the mantle cavity (Figs 3.2–3).

As the mantle tissue separates from the visceral mass it is composed of simple, cuboidal epithelium along the shell side, and simple, squamous epithelium along the visceral side (Fig. 3.4). Middle mantle subepithelium consists of loose connective tissue and hemolymph.

The isthmus is a tear drop-shaped extension of the mantle at the base of the visceral mass. It originates near the esophageal-digestive gland junction and terminates posterior to the posterior adductor. The isthmus has an irregular surface with simple columnar epithelium and a fibrous

subepithelium consisting of muscle and connective tissue. Columnar cells of the isthmus are basophilic with a monochromatic, elliptical nucleus (Fig. 3.5–6).

4.4. Cellular structure of gill

4.4.1. Non-marsupial gill

Gills or ctenidia of *V. nebulosa* are non-plicate, with the main functional aspect of a ctenidium consisting of horizontally oriented, cylindrical filaments. Filaments are organized into groups of two or more and occasionally separated by pores called ostia. The inner and outer faces of each gill are generally separated from each other along the anterior-posterior axis and only joined by a small number of septa (Fig. 4.1). The space between each lamina accommodates water entering through ostia and is referred to as a water tube (Fig. 3.2). Therefore, water tubes are vertical sinuses that flush the tissue with oxygenated water and correspondingly allow carbon dioxide removal. The suprabranchial cavity at the base of each gill is a conduit for vertical water currents, and the posterior confluence of the sinistral and dextral suprabranchial cavities serves to accommodate the increasing volume of water traveling from anterior to posterior. Each gill is supported by large fascicles of muscle located dorsal and lateral to each suprabranchial cavity.

Branchial filaments are cylindrical, bearing cilia organized into three groups (lateral, latero-frontal, and frontal) along the lateral and distal surfaces. A single layer of squamous cells extends along the lateral and medial portions of each filament. Each filament is supported by a set of basophilic skeletal rods located directly under the squamous epithelium, and a pale eosinophilic matrix may be observed throughout the long axis of each filament. The medial portion of each filament contains a hemolymph sinus, or lacuna, where a preponderance of hemocytes are typically observed (Fig. 4.2). The inner and outer gills appear to be functionally

identical (except for marsupial gills, see below) until the free distal tip. Outer gill have a rounded ventral margin (Fig. 4.3) while the inner gill has a furrow along the ventral surface (Fig. 4.4).

The inner lamina of the inner gill is united with the base of the visceral mass until the posterior margin of the visceral mass where both the sinistral and dextral inner gills are united across the mantle cavity. Outer lamina of inner gill is united with the abdomen until the posterior margin of the visceral mass (Fig. 4.5). The outer lamina of inner gill, and inner lamina of outer gill are supported by muscular fascicles spanning the length of the body and unite with abdominal connective tissues (Fig. 4.6). Outer lamina of outer gill joins the abdominal connective tissues medial to the middle mantle and lateral to the insertion point of the outer gill inner lamina (Fig. 4.7).

4.4.2. Marsupial gill

Female *V. nebulosa* may be distinguished from males in having a localized enlargement of the outer gill known as a marsupium (Fig. 5.1). When gravid, the posterior-most quarter of the ctenidia becomes distended and comprises the distal half of its vertical length. A marsupial ctenidium structurally differs from both the anteriorly located non-marsupial outer ctenidium, and inner ctenidium in many respects. The most obvious characteristic of marsupial gill are the greatly expanded water tubes, which become progressively larger dorsal to ventral. In one individual collected in May 2010, gills were asymmetrically filled allowing a comparison between filled and empty marsupia. Filled marsupium was appeared turgid and symmetrical (Fig. 5.2), while the empty marsupium was flaccid from partially collapsed water tubes (Fig. 5.1). Glochidia within a filled marsupium appear to be held together by strands of fibrous tissue, possibly representing a binding substance of a conglutinate of embryos (Fig. 5.2). Branchial

septa at the base of the marsupium consists of a series of ciliated papillae oriented dorso-ventrally (Fig. 5.3). In contrast, branchial septa of the ventral marsupial chambers have a fibrous composition with a lattice of connective tissue (Fig. 5.4). The epithelium representing the lateral surface of a marsupium appears to be less porous than non-marsupial gill tissue. The subepithelial tissue supporting the branchial filaments is thickened with connective tissue fibers and a ground substance (Fig. 5.6). The luminal surface of the water tubes is lined with teardrop-shaped, ciliated columnar cells. Ciliated cells lining the lumen marsupial water tubes contain brown intracellular granules, which may explain why the ventral margin of marsupium is blackened.

Marsupia may contain a mixture of glochidia and spherical to ovular masses of cells representing embryos in various stages of development. Early stage embryos consisted of clusters of eosinophilic, spherical cells within a shapeless, eosinophilic mass. Each cell contains a spherical nucleated mass, surrounded by a heterochromatic, eosinophilic matrix (Fig. 5.6). Later stage embryos were more differentiated than the largely eosinophilic cellular masses just described. Later stage embryos were ovular, possessing a spherical mass of myocytes, and distinct dorsal and ventral end characterized by basophilic cells. Glochidia were semi-circular with a centrally located adductor muscle flanked by falcate lines of eosinophilic to basophilic tissue presumably representing the mantle (Fig. 5.7).

4.5. Cellular structure of foot and associated tissues

4.5.1. Pedal musculature and byssal gland

The ventral margin of the foot consists of irregular, overlapping muscle fibers, subepithelial granulocytes, and a highly plicated integument (Fig. 6.1). Violet staining granulocytes are located directly beneath the pedal epithelium, while pale, blue-staining granulocytes are medial

in respect to violet cells (Fig. 6.2). Foot muscle is composed of regions of irregular and regular muscle fibers. Musculature in the ventral region of the foot has a woven appearance with bundles of fibers arranged into sagittal and transverse planes, giving the tissue a woven appearance (Fig. 6.3). In contrast, musculature of the base of the foot is more organized with distinct layers of transverse and sagittal fibers (Fig. 6.4). Additionally, there is a triangular, byssal gland located medially at the ventral margin of the coelom, just posterior to the pedal ganglion. The byssal gland has a wide, triangular dorsal chamber and a smaller, ovoid ventral chamber (Fig. 6.5). The luminal surface of the byssal gland features a simple, ciliated columnar epithelium and these cells have an eosinophilic cytoplasm and a monochromatic, ovular nucleus. The lumen of the dorsal chamber contains a heterochromatic, eosinophilic mass, possibly representing the remnants of the byssal thread (Fig. 6.6). The byssal gland of adult *V. nebulosa* is blind-ended, not connected to a vertical, byssal canal and although serial sections of foot revealed vertical ducts, including one near the byssal gland, it was not clear whether one of these represented the byssal canal. Reasons for this ambiguity include the presence of hemocytes within the duct most closely positioned to the byssal gland, and secondly, histologically similar ducts are located in the anterior portion of the foot (Fig. 6.7).

4.5.2. Pedal integument and mesentery

The integument of the foot and visceral mass is pleated and there are six different epithelial regions. In the first two regions, the epithelium appears to be folded and each fold is rounded with some resembling a "Y." The first region possesses ciliated, columnar cells with a subepithelium consisting of irregular muscle fibers and violet granulocytes (Fig. 7.1). Ciliated cells have an eosinophilic cytoplasm, similar to the coloration of the underlying muscle tissue, and cilia are short and nearly straight. Epithelial cells in the second region have similar

cytological characteristics as region one, however ciliated cells are sparsely distributed. Additionally, muscle tissue beneath the epithelium is generally more regular than in region one, and with fewer violet chromatocytes (Fig. 7.2). Region three possesses shorter epithelial folds, sparsely distributed ciliated cells, and mucus cells. Unlike epithelia of the first two regions, the basal portion of region three epithelial cells is parallel to the underlying musculature. Muscle underlying type-three epithelium consists an outer, thin, transverse layer and a deeper, thicker, sagitally oriented layer (Fig. 7.3). The fourth and fifth regions are dorsally located dorsally along the oblate portion of the visceral mass. The fourth type of integument surrounding the foot is similar to the third region, but is more irregular and a dark hemolymph sinus is located between the epithelium and muscle (Fig. 7.4). Region five is located near the junction between visceral mass and inner gill, and has the shortest epithelium of all five regions. Cells representing region five vary in height from a flattened, squamous type to slightly taller, domed to tear drop shaped. Mucus secreting cells also vary in morphology from dome-shaped to tear drop cells (Fig. 7.5). The sixth region is restricted to a black spot along the posterior, ventral margin of the foot. Histologically, wavy rays of tissue stem obliquely from the foot with columnar cells containing brown intracellular granules, and a subepithelial lamina consisting of basophilic chromatocytes and fibrous tissue (Fig. 7.6).

The sinistral and dextral halves of the visceral mass are united by bundles of mesentery and mesentery fascicles are distributed throughout the coelom (Fig. 7.7). Each fascicle has a heterogenous composition in terms of the staining characteristics and geometry of its fibrils. Fibrils are eosinophilic, but staining intensity varies from a pale, almost white, to dark red. Each filament is quadrangular, but varies in shape from square, to a triangular. Furthermore, there does not appear to be an obvious pattern of fibril arrangement within a fascicle (Fig. 7.8).

4.6. Anterior adductor and anterior pedal protractors

The anterior pedal retractors are located beneath the labial palps and may be observed in histological sections of palp. Retractor muscle is dark staining and eosinophilic, with distinct fascicles and fasciculi. Furthermore, fibrils are quadrangular and separated by endomysium, however perimysium appears to be more delicate since there are pale, eosinophilic wisps adjacent to fascicles and fasciculi (Fig. 8.5). Adductor muscle is organized into large fascicles containing dark, red eosinophilic fibers. Adductor myocytes are filamentous with a pale, granular, basophilic nucleus (Fig. 8.6).

4.7. Cellular structure of digestive system tissues

4.7.1. Labial palps, oral groove, and esophagus

Labial palps of *V. nebulosa* have an inner palp surface lined with a series of ciliated, rectangular plicae while the outer surface is generally smooth (Fig. 8.1). Plicae have a flattened posterior margin and a pleated anterior surface (Fig. 8.2). Ciliated columnar cells represent the main constituent of the inner palp epithelium and extend along the palp interior until the distal margin of each lip. Ciliated cells of the inner palp surface are characterized by a pale, basophilic cytoplasm and an ovular, monochromatic nucleus. The surface of the free distal palp tip transitions from a ciliated epithelium to a non-ciliated mucosa characterized by basophilic, granular mucus cells (Fig. 8.3). Although the outer surface of each palp is generally flattened, the integument is composed of teardrop-shaped columnar cells. Teardrop cells of the outer palp surface possess an ovular monochromatic nucleus, an eosinophilic cytoplasm, and a transparent, apical vescicle (Fig. 8.4). Subepithelial tissue of the palps consists a somewhat dense matrix of pale, eosinophilic fibers within a membranous ground substance, especially the supporting tissue directly beneath the epithelium. However, the medial layers of each palp have a more loose

consistency. Additionally, there are a series of well-defined hemolymph sinuses, and wandering hemocytes are widely distributed throughout the subepithelium.

In cross sections of the anterior visceral mass, oral groove resembles a U-shaped canal, travelling dorsally from the labial palps. Oral groove epithelium consists of transversely pleated, ciliated tracts. In a sagittal plane, oral groove appears multinucleated since the walls of the oral groove are curved. Oral groove epithelium is mucociliary with a preponderance of transparent vesicles, especially along the folds (Fig. 9.1). Additionally, there are wandering hemocytes nestled between columnar cells of the ventral oral groove wall (Fig. 9.2). Subepithelial tissue of the oral groove consists of a loose meshwork of thin connective tissue fibers and hemocytes. A single layer of cuboidal epithelial cells appears ventrally in sections of oral groove, and represents a short stretch of integument between the oral groove and foot (Fig. 9.3).

The esophagus is essentially a posterior continuation of the oral groove, a short tube connecting the oral groove with the stomach and digestive gland. The esophagus is located at the base of the visceral mass, and is generally between digestive gland tubules and the mantle isthmus (Fig. 9.4). Ciliated, rectangular folds extend from the dorsal and ventral esophageal walls. Epithelial cells are pseudostratified and ciliated, with an eosinophilic cytoplasm and an elliptical, monochromatic nucleus. Cilia along the apical surface of esophageal cells are short and generally straight. The lumen of the esophagus may contain a shapeless, eosinophilic mass, which may represent mucus and ingested substances. Additionally, the esophageal epithelium is supported by concentric layers pink and red eosinophilic fibers, creating a heterogenous lamina propria (Fig. 9.5).

4.7.2. Digestive diverticulum

The esophagus expands laterally into a vestibular chamber at the dorsal base of the visceral mass. Particulate matter is transported, by means of ciliary action, through small tubules located on the sinistral and dextral sides of the body (Fig. 10.1). There are three types of tubules distinguished by variations in the diverticulum lining. Ciliated primary tubules have folds of epithelial tissue that give tubule walls a wavy or serrated appearance. Primary tubules consist of eosinophilic, columnar cells with cilia that generally appear to be straight in histological sections (Fig. 10.2). Ciliated epithelium transitions into a microvillar lining in the secondary tubules. Secondary tubules connect to tertiary tubules, which are the most widely distributed diverticulum tubules (Fig. 10.3). Microvillar cells of secondary tubules are characterized by a red, vesiculated cytoplasm, and a pale, basophilic nucleus with a distinct nucleolus. Tertiary tubules are vesiculated, but have a pale eosinophilic appearance as compared to the darker staining secondary tubules. The most distinctive feature of tertiary tubules is the dark-staining nucleus, located within a basophilic triangular region of each cell. The nucleus contains a distinct nucleolus and the violet, triangular portion of the cell extends to the lumen of the tubule. The apical surface of tertiary tubules may appear to be bubbling, suggesting that it is a source of digestive secretions (Fig. 10.4).

4.7.3. Stomach

The stomach is a large bag-like chamber located between the digestive diverticulum and style sac. The dextral portion extends anteriorly slightly and has a curved surface. The dorsal, sinistral, and ventral walls are flattened. The primary constituent of stomach epithelium comprises rounded plicae containing ciliated columnar cells (Fig. 10.3). There is a ventrally located, ovular chamber located near the style sac. The walls have an irregular composition and

there is a large, median plica along the ventral wall. Thin columnar cells are located along the ventral and dorsal walls and the most distinguishing characteristic of ventral stomach epithelium is an eosinophilic cuticle (Fig. 10.7). Close inspection of the margin of the cuticle indicates that it is a gelatinous mass attached to cilia (Fig. 10.8).

4.7.4. Crystalline style sac

The crystalline style is generally a cylindrical tube spanning the visceral mass from the stomach to the posterior margin of the visceral mass. The diagnostic character of the style sac is a pale, eosinophilic rod, the style, within a circular chamber on the sinistral side (Fig. 11.1). The style may be closely associated or attached to ciliated cells along the ventral sac wall. However, eosinophilic material comprising the style appears to enter the sac from the stomach (Fig. 11.2). Although the style appears homogenous, there is a thin, semicircular layer of black particulate mater near the ventral margin of the style. Therefore, the style may be a secretion that forms in the stomach and becomes harder as it enters the style sac. Additionally, the circular shape and semicircular line of debris within the style may be an indication that ciliary action causes the style to rotate within the sac (Fig. 11.3).

There are three different types of epithelia throughout the style sac (Fig. 11.1). Type one epithelium is located within the circular portion of the sac and consists of ciliated columnar cells distinguished by a red cytoplasm and a heterochromatic, elliptical nucleus with a distinct nucleolus. The cell membrane along the apical surface of these cells is a thick line and cilia of type one cells are straight and thickened in comparison to cilia of type two epithelia (Fig. 11.4). Type-two epithelium originates along the right side of the median ventral fold and terminates near the fork. Ciliated cells characterizing this region have a basophilic cytoplasm, an elliptical, heterochromatic nucleus with a distinct nucleolus. The apical portion of the cell membrane is

noticeably thinner than the apical membrane of type one cells, and cilia appear to be more flexible than type-one cilia. The ventral fork of the style sac also has a series of ellipsoid, basophilic mucocytes interspersed among ciliated epithelial cells (Fig. 11.5). The dorsal wall of the style sac, dextral to the median fold, is characterized by a basophilic, pseudostratified, ciliated columnar epithelium. Cells in type-three epithelium appear to be densely packed, supporting thin, flexible cilia similar to cilia featured in type-two epithelium (Fig. 11.6). The crystalline style sac has a lamina propria, and it varies from a thickened connective tissue support underneath the epithelial folds of the style sac, to a thin line of connective tissue surrounding the style sac.

4.7.5. Intestine

The crystalline style represents the first limb of the intestine as it curves dorsally along the posterior margin of the visceral mass. The epithelium of the first intestinal limb maintains the same cell types characterizing the horizontal portion of the style sac (Figs. 12.1–2). The posterior wall of the first intestinal limb is representative of the ventral style sac wall and likewise, the anterior wall is a reflection of the dorsal style sac wall. However, the posterior and anterior walls of the first intestinal limb form tall epithelial folds. Anterior folds are shorter and wider than posterior plicae (Figs. 12.2–3). The lumen of the descending intestine contains an eosinophilic material likely representing chyme. Within crypts of adjacent folds, and around the distal tips of plicae, chyme appears broken up or shaped according to the contours of the tissue (Fig. 12.3). At high magnification, there is evidence of secretory activity as there are transparent vesicles around the epithelium, possibly representing mucoid releases from goblet cells. Further down the length of the initial limb, villi are replaced by shorter epithelial extensions that are generally plateau-shaped. The lower portion of the first intestinal limb appears to be an area of

active secretion and mixing. Plateaus along the anterior and posterior walls are vesiculated and releasing transparent bubbles into the lumen. The center of the lumen has a large mass of fused bubbles surrounded by series of crescent-shaped bubbles (Fig. 12.4).

In sagittal sections of the viscera, the second intestinal limb is posterior to the first limb. The lining of the second intestinal limb consists of short plicae that are generally Y-shaped. Between each Y-shaped structure, there may be a triangular cusp creating a set of oblique crypts between each Y-shaped unit (Fig. 12.5). Ciliated columnar cells are narrow, eosinophilic with a distinct nucleolus within each nucleus. Additionally, wandering hemocytes are present within the epithelium of the second intestinal limb and typically resemble a spherical mass of eosinophilic vesicles (Fig. 12.6).

The ascending second intestinal limb and descending third intestinal limb, appear to consist of the same tissue types. Transverse sections of the posterior visceral mass show that the second and third limbs are mirror images of each other (Figs. 11.7, 13.1). The second and third intestinal limbs are L-shaped with a ventral-lateral plication and a series of small pleats along the dorsal wall.

The junction between the third and fourth intestinal regions is represented by a sinuous epithelium consisting of ciliated columnar cells. Epithelial folds are short with a relatively flattened peak and simple, shallow crypts. Ciliated cells have an elliptical nucleus with pale, basophilic chromatin and a distinct nucleolus (Fig. 13.2).

The most distinctive feature of the fourth intestinal limb is the centrally located, ventrally directed major typhlosole (Fig. 13.3). Surrounding the typhlosole, the ventral lining of the intestine is pleated with a series of flattened epithelial folds. The height of each fold, and the length, width of the crypts increases from the base of the typhlosole to the ventral-lateral region

(Fig. 13.4). Epithelial tissue surrounding the lumen consists of ciliated columnar cells with short bristle-like cilia. In general, the cells lining the ventral and dorsal surfaces have similar characteristics. However, the ventral epithelium has a preponderance of red, elliptical granulocytes. The granular component of the columnar cell is tear drop-shaped to elliptical, and apically positioned within the cell. Granulocytes do not appear to be wandering hemocytes because the granular structure seems to be continuous with the cytoplasm and there is usually a slight gap surrounding a hemocyte. Furthermore, hemocytes are typically circular, with a distinct, circular nucleus and the cytoplasm may contain prominent vesicles. Cells along the circumference of the typhlosole have are well organized, with short bristle-like cilia along the apical surface (Fig. 13.5). Connective tissue of the fourth intestinal region is represented by a well-defined lamina propria supporting the typhlosole, and a thin wrapping around the lateral and ventral walls. Fibers within the major typhlosole are loosely aggregated and the tissue has a pale, eosinophilic quality in comparison to the connective tissue surrounding the lateral and ventral walls (Figs. 13.3–5). The lamina propria is supplied with blood from a series of small sinuses throughout the tissue that are just large enough for a small number of hemocytes to fit within the lumen.

The fifth limb of the intestine is a reflection of intestinal region four in terms of morphological and cytological features (Fig. 13.6). Morphologically speaking, the intestine is circular along the hinge line, but becomes flattened as it nears the posterior adductor. The ventral epithelium is a continuation of the typhlosole of the fourth intestinal limb, but there seem to be more goblet cells in the fifth limb (Fig. 13.7). The lateral and dorsal portions of the intestinal wall are pleated, but the dorsal wall has more plications than the fourth intestinal limb (Fig. 13.8). Nuclei of the ciliated columnar cells, along the dorsal and ventral walls, are more

regular, clearly revealing the presence of a single layer of cells within the ventral and dorsal walls. Unlike region four, granulocytes are absent from the outer wall of the fifth intestinal region. The connective tissue lamina of the typhlosole consists of loose connective tissue and fibroblasts as in region four, but the connective tissue wrapping around the outer wall supports taller epithelial folds than in region four.

4.8. Cellular structure of cardiovascular system tissues

4.8.1. Heart

The heart and nephridium are located dorsally in relation to the visceral mass, and cardiac muscle encircles the fifth limb of the intestine from the posterior margin of the visceral mass to the visceral mass midpoint (Fig. 14.1). Bivalves have a three-chambered heart consisting of a laterally positioned pair of auricles and a large median ventricle (Fig. 14.5). The ventricle of *V. nebulosa* is conical and contains a distinct epicardium and myocardium (Fig. 14.2). The epicardium is a sinuous layer of squamous cells and the myocardium consists of two layers of cardiac muscle. There is a thickened outer region, located directly underneath the epicardium, and characterized by a compact network of branched muscle fibers while the medial portion of the ventricle contains widely separated cardiac myofibers. The heart is situated within a pericardial cavity with a delicate pericardial sac lined with squamous cells (Fig. 14.3). Ventricle contains branched cardiac myocytes having a fibrous consistency and a pale, basophilic nucleus with a distinct nucleolus (Fig. 14.4). Auricles are generally delicate cylindrical tubes of cardiac muscle and squamous epithelium linking the ventricle to the pericardial sac (Fig. 14.5). Blood flow between the auricles and ventricle appear to be regulated by auriculoventricular valves. Valves are long, flaps extending into the lumen of the ventricle consisting of a compact layer of irregular muscle fibers surrounded by endothelium (Figs. 14.5–6).

4.8.2. Arteries, veins, capillaries, and pericardial gland

Bivalves have an open circulatory system and hemolymph is distributed throughout the body among interstitial spaces, hemolymph sinuses, and blood vessels. Hemolymph has a distinct cellular and non-cellular component consisting of spherical, eosinophilic hemocytes (e.g., Fig. 15.3) and black, ink-like granules of hemolymph (e.g., Fig. 15.1). Hemolymph sinuses are distinct cavities within tissue that are not lined by endothelial cells (e.g., Figs. 15.3, 15.4). Blood vessels resemble veins, arteries or capillaries and are lined with squamous cells. There are spindle shaped tubes with thin walls of fibrous tissue possibly representing veins (Figs. 15.1–2). Potential arteries are triangular tubules with concentric layers of muscle fibers surrounding the lumen (Figs. 15.3–4). Capillaries are simple, circular structures lined with squamous cells (Fig. 14.5).

In addition to the heart, there are three other tissues that seemingly regulate hemolymph flow in the dorsal region of the body. At the anterior end of the visceral mass, there is a U-shaped structure consisting of layers of musculature. The ventral portion of this tissue resembles a socket for a convex muscular structure located on the dorsal side of the body. Although it is not clear whether this U-shaped tissue is contractile, serial sections of the visceral mass reveal a series of sinuses at the base of the visceral mass that may represent a conduit for hemolymph passage between the visceral mass and the nephridium (Fig. 15.6).

Blood flows dorsally into auricles from the mantle and ctenidia. At the dorsal origin of the ctenidia, there is a distended chamber between the muscular supporting rods of the gill, and the auricles. There is a preponderance of hemolymph granules contained within a thin-walled chamber composed of connective tissue and muscle, seemingly representing an afferent blood-receiving chamber (Fig. 15.7).

The pericardial gland is a large network of connective tissue fibers in the dorsal region of the body bordered by gill, mantle isthmus, heart and nephridia. Fibrous connective tissue is located in the dorsal region of the body, anterior to posterior, and is similar to the composition of the middle mantle. The most distinctive feature of this tissue is the preponderance of discolored hemocytes. Eosinophilic hemocytes are present in the sinuses between connective tissue fibers, but many of the hemocytes have a brown or yellow cytoplasm. Discolored hemocytes seemingly have a cytoplasm with a low affinity for eosin given their subtle red coloration, and additionally, some discolored hemocytes seemingly lack a nucleus or the nucleus appears to be emarginated or slightly separated from the cytoplasm (Fig. 15.8). Given the above, the discolored hemocytes in the pericardial gland may represent blood cell production.

4.9. Cellular structure of renal system tissues

4.9.1. Anterior nephridium

The nephridium is a large tubular organ located dorsally to the left and right of the visceral mass. Nephridial tissue spans the length of the body from the anterior-medial point of the visceral mass to the posterior adductor. Additionally, there are distinct morphological features characterizing the anterior and posterior regions of the nephridia. Anterior nephridia have distinct ventral and dorsal limbs while the posterior nephridia lacks distinct dorsal and ventral regions (Fig. 16.1). The ventral nephridial limb is characterized by large plications of the dorsal and ventral walls while the walls of the dorsal nephridia have fewer plications (Figs. 16.1–2). Epithelial folds of the ventral limb are composed of columnar cells with an eosinophilic, granular cytoplasm, and a dark-staining, monochromatic nucleus (Fig. 16.3). The nucleus of a columnar cell is located in the basal portion of the cell, and the apical region may contain a large vacuole. Some columnar cells have a transparent or a pale eosinophilic vacuole while other cells in the

ventral nephridial limb contain a brown vacuole. Subepithelium of the ventral limb consists of connective tissue supporting the epithelium and a hemolymph sinus. The lining of the dorsal nephridium is generally flattened, but there are localized regions within the dorsal nephridium is plicated or features teardrop-shaped cells. For example, the ventral wall of the dorsal nephridium has a small number of plicae and the surface of these structures is irregular (Fig. 16.4). Plicae of the dorsal nephridium are sparsely distributed anterior to posterior. Secondly, the dorsal nephridium contains patches of teardrop-shaped cells with an apical vesicle (Fig. 16.5). Teardrop cells are typically located at the dorso-lateral corners of the dorsal nephridium.

While the above-mentioned features of the walls of the ventral and dorsal limbs of the nephridium are representative of the anterior nephridial region, there are two structures that are unique to the anterior region. The urethra is a communication between the dorsal nephridium and suprabranchial cavity, and located in the anterior end of the nephridium. Additionally, there is a ciliated tubule, the nephrostome, located in the lateral portion of the ventral nephridial limb, adjacent to the urethra (Fig. 16.6). Squamous epithelial cells lining the dorsal nephridial limb change to a ciliated, columnar epithelium at the ventral end of the urethra (Fig. 16.7). The nephrostome is the ciliated tubule at the lateral end of the ventral nephridial limb and transfers fluid from the pericardial cavity to the lumen of the ventral nephridium. The reno-pericardial canal is composed of conical epithelial folds that extend far into the lumen and these epithelial folds feature ciliated columnar cells, and conspicuous goblet cells. Surrounding the canal is a well-defined lamina propria consisting of concentric layers of fibrous tissue (Fig. 16.8).

4.9.2. Posterior nephridium

The nephridium is enlarged between the posterior margin of the visceral mass and posterior adductor. Nephridial epithelium is convoluted, consisting of rounded, and irregular epithelial

folds (Fig. 17.1). Additionally, epithelial folds of the posterior nephridium are typically spaced farther apart from each other than in the anterior nephridium. Regarding the fine structure of posterior nephridial epithelium, cells are columnar, with an eosinophilic, vesicular cytoplasm and a pale, basophilic nucleus typically lacking a well-defined nucleolus. Additionally, the lumen between the branches has expanded and is significantly larger than the lumen in the anterior region. Nephridial branches have a noticeably different composition from branches within the ventral limb of the anterior nephridium. Epithelial cells characterizing the posterior nephridial branches are columnar and vesiculated and appear to be bubbling at the apical surface. Additionally, the subepithelium of posterior nephridial branches consists of a simple squamous epithelium, and hemolymph (Fig. 17.2). Posterior nephridium has sinistral and dextral limbs divided by a septum of loose connective tissue fibers and a pair of nerves (Fig. 17.3). The posterior nephridial septum also contains a large, artery located ventrally in relation to the pedal retractors. The artery is composed of wavy muscle fibers and runs along the hinge line towards the posterior end of the mantle (Fig. 17.4).

4.10. Posterior adductor and posterior pedal retractors

Posterior pedal retractors are located within the nephridial septum, between the posterior adductor and visceral mass. Pedal retractors have a thin epimysium of squamous cells, and an endomysium consisting of pale, eosinophilic connective tissue between the myofibers. Myofibers of the retractors are quadrangular in cross section, and possess a monochromatic, ovular nucleus (Fig. 16.6).

Posterior nephridial branches encircle the posterior pedal retractors (Fig. 17.5). In transverse sections of the viscera posterior retractors represent large fascicles. The musculature has a distinct perimysium and endomysium and myofibers are polygonal in outline (Fig. 17.6). The

posterior adductor is located posterior to the retractors and oriented perpendicularly in relation to the retractor muscles. Adductor myofibers are organized into large fascicles with a simple, squamous epimysium and a delicate, fibrous perimysium. Myofibers of the posterior adductor are long, eosinophilic filaments with elliptical, heterochromatic nuclei and a distinct nucleolus (Fig. 16.7).

4.11. Cellular structure of nervous system tissues

4.11.1. Pedal ganglion, cerebral ganglia, and visceral ganglion

The nervous system of *V. nebulosa* consists of four ganglia, each with a series of nerve fibers that extend throughout the body. There is a pair of ganglia at the anterior end of the visceral mass, each located in the lateral portion of the body between the anterior adductor and labial palp. The third ganglion is the pedal ganglion located in the ventral portion of the coelom between the digestive diverticulum and gonad, dorsal to the base of the foot. Finally, the posterior ganglion is situated along the ventral surface of the posterior adductor. Each ganglion has a well-defined outer neural cortex of neuron cell bodies, and a fibrous inner medulla. Furthermore, there is not an obvious difference between the cellular characteristics of all ganglia and therefore the foregoing description of the neural cortex and medulla of the pedal ganglion is representative of the anterior and posterior ganglia.

Pedal ganglion is a bilobed group of neurons at the base of the foot between the gonad and digestive diverticula. Each hemisphere is surrounded by well-defined epinuria, and separated by a median fissure. A series of central commissures communicate horizontally with each hemisphere at the vertical midpoint (Fig. 18.1). The cortex of the pedal ganglion consists of conical to polygonal cell bodies of unipolar neurons. Neuron cell bodies have a pale, basophilic cytoplasm and a spherical heterochromatic nucleus and a distinct nucleolus. Additionally,

neurons have small, brown, granular inclusions located around the nucleus (Fig. 18.2). Fissures are composed of fibrous connective tissue with a thickened, homogenous appearance. The medulla has is distinguished by its web-like appearance formed by overlapping bundles of axons. Glial cells of the medulla have a spherical to spindle shaped nucleus with only a small amount of cytoplasm surrounding the nucleus (Fig. 18.3). Commissures represent a continuation of the medulla serving to link each half of the ganglion by means of horizontal tracts of axons (Fig. 18.4). Axons leave the hemispheres via fibrous, lateral extensions of the medulla at the lateral, dorsal and ventral margins of the tissue. Roots along the lateral margins of the pedal ganglion are circular to sinuous bundles of axons and supporting cells (Fig. 18.5). Histological sections of the visceral mass have revealed ventral pedal nerves threaded through the foot musculature and dorsal pedal nerves extending along the lateral portions of the visceral mass.

The anterior ganglia may be observed in sections of the anterior muscle group and palp. Anterior ganglia appear to control the adductor and retractor muscles since there are nerves inserted into the fascicles of each muscle (Fig. 19.1). Additional nerves from the anterior ganglia travel through the foot, and mantle edge. Sinistral and dextral nerve centers are also linked to one another by means of a nerve spanning the length of the anterior adductor.

The posterior ganglion is a cylindrical structure along the anterior, ventral side of the posterior adductor (Fig. 19.2). Nervous tissue also extends up into the base of the gill where the outer face of the inner gill and inner face of outer gill unite (Fig. 19.3). A thin, but dense stratum of fibrous connective tissue surrounds the posterior ganglion and on the ventral surface there is a simple epithelium of brown, granular cuboidal cells and goblet cells (Fig. 19.4). Regarding nerves of the posterior ganglion, the pair of nerves seen in histological sections of the nephridia

originate at the anterior end of the ganglion, and the sinistral and dextral posterior pallial nerves are rooted in the posterior ganglion

4.11.2. Nerves and statocysts

Nerves are located throughout the body and can be traced from their origin by serial sectioning the body. In a longitudinal orientation, nerves are ribbons of fine, eosinophilic filaments that have a slightly wavy appearance. Nerves may be distinguished from connective tissue by observing spindle-shaped gaps between fibers. Additionally, there are small, spindle-shaped nuclei throughout the ribbon of axons and nuclei have short, brown granular extensions, suggesting these cells are bipolar neurons. (Figs. 20.1–2). Cross sections of nerves, such as the nephridial nerves, reveal a thick, homogenous, eosinophilic band surrounding the tracts. It appears that this connective tissue wrapping may be myelin or a similar substance and emarginated nuclei are present within this wrapping (Fig. 20.3). The pallial nerve typically appears as a straight band of axons intermingled among mantle edge musculature. Histological sections of the posterior mantle edge papillae reveal pallial nerve branches directed towards the mantle papillae (Fig. 20.4). Branches of the pallial nerve, threaded through papillae, likely transmit neural impulses derived from sensory stumili to ganglia.

Statocysts are small sacs located near the lateral margin of the coelom and linked to the pedal ganglion via a horizontal band of eosinophilic tissue (Fig. 20.5). Each statocyst is an ovular chamber formed by a ciliated, columnar epithelium. Epithelial cells lining the sac have a pale, basophilic cytoplasm, and a dark-staining, ovular nucleus. Statocyst epithelium has a stratified appearance and there are dark-staining, spherical nuclei located in the basal layer of the epithelium. The lumen of the statocyst contains the statolith, a basophilic ring of fluid with a smooth inner surface and a rough outer surface, possibly from ciliary action (Fig. 20.6).

4.12. Cellular structure of reproductive system tissues

Gonadal tissue of *V. nebulosa* is organized into a series of spherical to ovular acini and ciliated gonadal ducts (Fig. 21.1). Gametogenesis occurred in males and females collected in May 2010 but production was limited in terms of the number of oocytes and spermatozoa produced as compared to sexually mature individuals collected in August 2010. In females collected in May, ova appeared to develop and arrest at an early stage. Oocytes of immature ovarian acini are basophilic with a distinct, spherical nucleus, and a series of transparent cytoplasmic vesicles. Furthermore, oocytes were typically attached to the inner wall of the acinus and the lumen contained an abundance of spherical, eosinophilic granules. Upon closer inspection, the eosinophilic granules appeared to be apoptotic oocytes given that they were usually enclosed within a membrane, with a small, polygonal nucleus (Fig. 21.2). Mature females sampled in August possessed a mixture of early stage and late stage oocytes. Oocytes begin as a small basophilic cell with a distinct nucleus and nucleolus. As oocytes mature, they become larger and eosinophilic cytoplasm becomes more prominent. Mature oocytes however, occupied the majority of the acinar volume as they were significantly enlarged. Mature oocytes are enclosed within a membrane that is indistinct and separated from the main part of the oocyte by an expansive fluidic mass. Specifically, the cytoplasm of a mature oocyte is eosinophilic, granular, and contains a pale basophilic nucleus. The nucleus of some oocytes seemingly contained a loose mass of basophilic chromatin, while other oocytes possessed a distinct nucleolus (Fig. 21.3).

The most distinctive feature of immature testicular acini is a preponderance of sperm morula (Fig. 21.4). Spermatozoa develop from single-celled spermatocytes and then proceed to divide multiple times and produce a cluster of spherical cells resembling a morula stage embryo.

Spermatocytes of sperm morula each differentiate into a pair of ovular spermatozoa. Spermatocytes of a sperm morula are housed within a thin, eosinophilic cytoplasm that is nearly obscured by the strongly basophilic heterochromatin. Furthermore, spermatocytes and sperm morula have such a strong staining quality that individual chromosomes and stages of meiosis are not visible with hematoxylin and eosin preparations. Like the immature ovarian acini, testicular acini in males collected in May contained numerous eosinophilic granules, possibly representing apoptotic spermatocytes (Fig. 21.5). Acini of males collected in August were significantly enlarged and contained a large, central mass of spermatozoa. Additionally, spermatogenesis appeared to be different than in immature individuals. Spermatocytes in mature individuals possessed a pale, basophilic nucleus containing a blend of euchromatin and heterochromatin. Spermatozoa in the lumen of the acini are small, basophilic, and cylindrical, with an eosinophilic flagellum (Fig. 21.6).

Female and male gonadal tissue contained circular to ovular, ciliated ducts. Gonadal ducts consist of pale, eosinophilic columnar cells with a densely ciliated apical surface (Figs. 20.1, 21.5). Ciliated gonadal ducts of mature male *V. nebulosa* contained a condensed mass of spermatozoa traveling towards the dorsal gonadal pore (Fig. 21.7). The sinistral and dextral gonadal pores are ciliated tubules located at the dorso-lateral margin of the visceral mass between nephridium and inner lamina of the inner gill (Fig. 21.8).

PLATE 1. Shell morphology, and gross anatomical features of the mantle cavity of *Villosa nebulosa*. 1. Lateral view of right valve showing the rounded anterior margin (AM), compressed umbo (UM), dorsally located ligament (LI), and posterior slope (PS). 2. Lateral view of left valve showing the rounded anterior margin (AM), compressed umbo (UM), dorsally located ligament (LI), and posterior slope (PS). 3. Medial view of the left valve showing the pallial line (PL), anterior adductor scar (AS), posterior adductor scar (PS), pseudocardinal tooth (PT), interdentum (ID), umbo cavity (UC), lateral tooth (LT), and ligament (LI). 4. Medial view of the left valve showing the pallial line (PL), anterior adductor scar (AS), posterior adductor scar (PS), pseudocardinal teeth (PT), interdentum (ID), umbo cavity (UC), lateral teeth (LT), and ligament (LI). 5. Ventrolateral view of *Villosa nebulosa* (ca. 50 mm shell length) buried in gravel at Shoal Creek with its mantle cupped forming an incurrent aperture (IA) and excurrent aperture (EA). 6. Medial view of the mantle cavity with the right valve and right mantle removed to show the position of the mantle edge (ME), middle mantle (MM), foot (FO), anterior adductor (AA), labial palp (LP), inner gill (IG), outer gill (OG), posterior adductor (PA), mantle isthmus (MI), and supra-anal aperture (SA). 7. Medial view of the mantle cavity with the right valve and right mantle removed emphasizing the papillose mantle edge (ME), middle mantle (MM), foot (FO), anterior adductor (AA), inner gill (IG), outer gill (OG), marsupium (MA), glochidia (GL), posterior adductor (PA), mantle isthmus (MI), and supra-anal aperture (SA). 8. Medial view of the mantle cavity with the right valve, right mantle, and right gills removed revealing the mantle edge (ME), foot (FO), labial palp (LP), visceral mass (VM), anterior adductor (AA), left inner gill (IG), posterior adductor (PA), mantle isthmus (MI), and supra-anal aperture (SA).

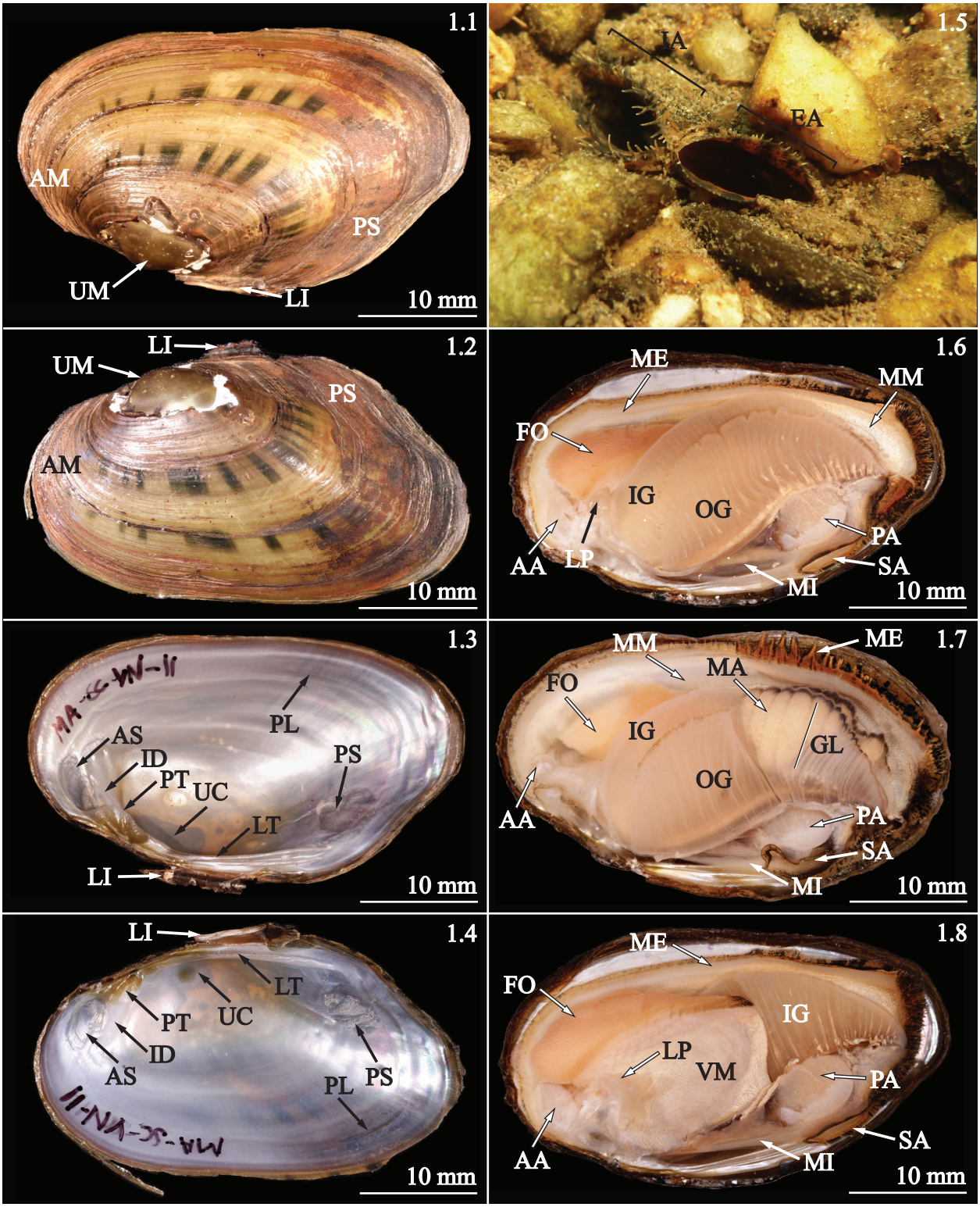
1.1
AM
PS
UM
LI
10 mm
1.5
IA
EA
1.2
LI
UM
PS
AM
10 mm
1.6
ME
MM
FO
IG
OG
PA
AA
LP
SA
MI
10 mm
1.3
PL
AS
ID
PS
PT
UC
LT
LI
10 mm
1.7
MM
ME
MA
FO
IG
GL
OG
AA
PA
SA
MI
10 mm
1.4
LI
LT
PT
UC
ID
AS
PL
PS
10 mm
1.8
ME
FO
IG
LP
VM
PA
SA
AA
MI
10 mm

PLATE 2. Anterior mantle edge of *Villosa nebulosa*. 1. Transverse section of the anterior portion of the mantle edge showing the position of the outer lobe (OL), periostracal ribbon (PE), middle lobe (ML), and inner lobe (IL). 2. Transverse section of the mantle edge emphasizing columnar epithelium (CE) of the outer lobe, basal bulb (BB), periostracal groove (PG), squamous epithelium (SE) of the middle lobe, and periostracum (PE). 3. Transverse section of the distal end of outer and middle mantle lobes where obliquely oriented plicae (PL) line the outer lobe and a periostracal ribbon (PE) leaves the interlobular space. 4. Transverse section of the middle lobe showing plciae (PL), periostracum (PE), squamous epithelium (SE), violet granulocyte (VC), columnar epithelium of the dorsal surface (CE), and brown intracellular granules (BG). 5. Transverse section of inner lobe featuring plicae (PL), violet cells (VC), and myofibers (MF). 6. Transverse section of the dorsal part of the inner mantle edge emphasizing plicae (PL), ciliated columnar cells (CC), goblet cells (GC), and adipocytes (AC). 7. Transverse section of ventral epithelium of the base of the mantle edge showing columnar epithelum (CE), myocytes (MC), and adipocytes (AC).

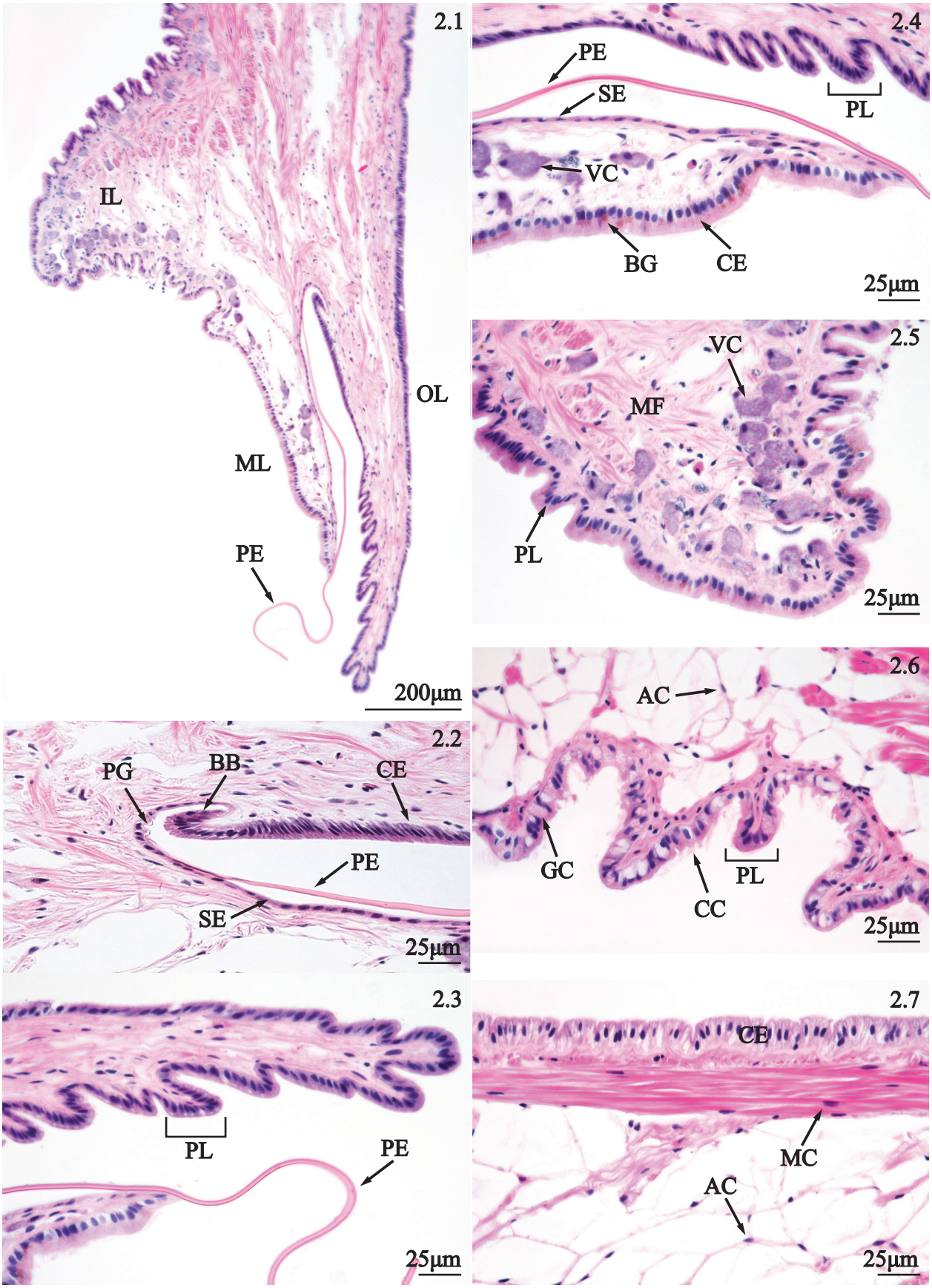
2.1
IL
OL
ML
PE
200µm
2.4
PE
SE
PL
VC
BG
CE
25µm
2.5
VC
MF
PL
25µm
2.6
AC
GC
CC
PL
25µm
2.2
PG
BB
CE
PE
SE
25µm
2.3
PL
PE
25µm
2.7
CE
MC
AC
25µm

PLATE 3. Posterior mantle edge, middle mantle, and mantle isthmus of *Villosa nebulosa*. 1. Sagittal section of posterior mantle edge showing a thin outer lobe (OL) and middle lobe (ML) and a bulbous inner lobe (IL) featuring conspicuous plications (PL). 2. Sagittal section of posterior mantle edge characterized by conical papillae (PA) with deep, obliquely oriented plications (PL) along the surface. 3. Sagittal section of a papilla emphasizing a columnar epithelium containing brown intracellular granules (BG) as well as an irregular composition of connective tissue fibers (CT) and hemolymph sinuses (HS) within the subepithelium. 4. Transverse section of middle mantle displaying a outer epithelium (OE) of columnar cells, inner epithelium (IE) of squamous cells, cilia (CI), subepithelial connective tissue (CT), and hemocytes (HC). 5. Transverse section of mantle isthmus (MI) portraying a thin dorsal extension of tissue from the visceral mass (VM) and a terminal, dorsally located bulb (BU). 6. Transverse section of mantle isthmus bulb is emphasizing a basophilic columnar epithelium (BE) with occasional goblet cells (GC) and a subepithelium consisting of irregular muscle fibers (MU).

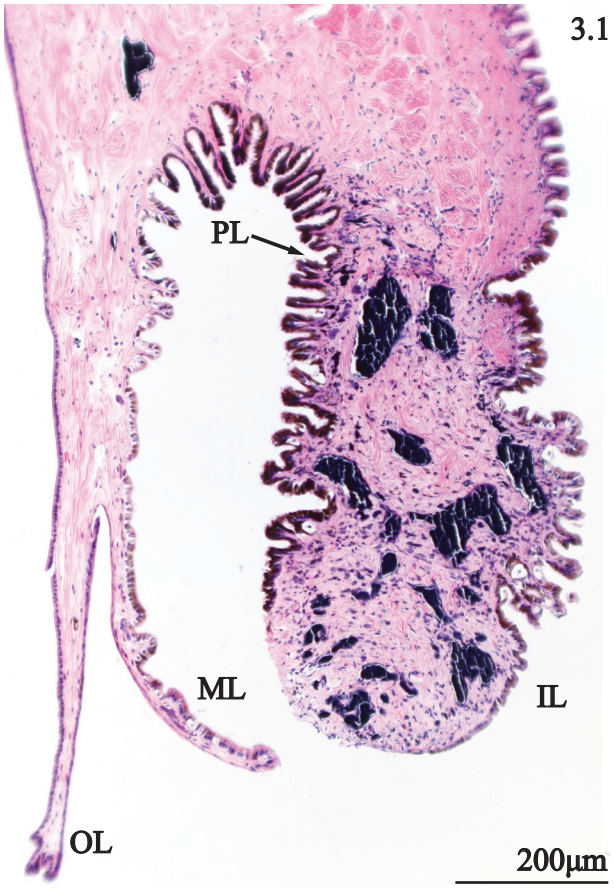
3.1
PL
ML
IL
OL
200µm

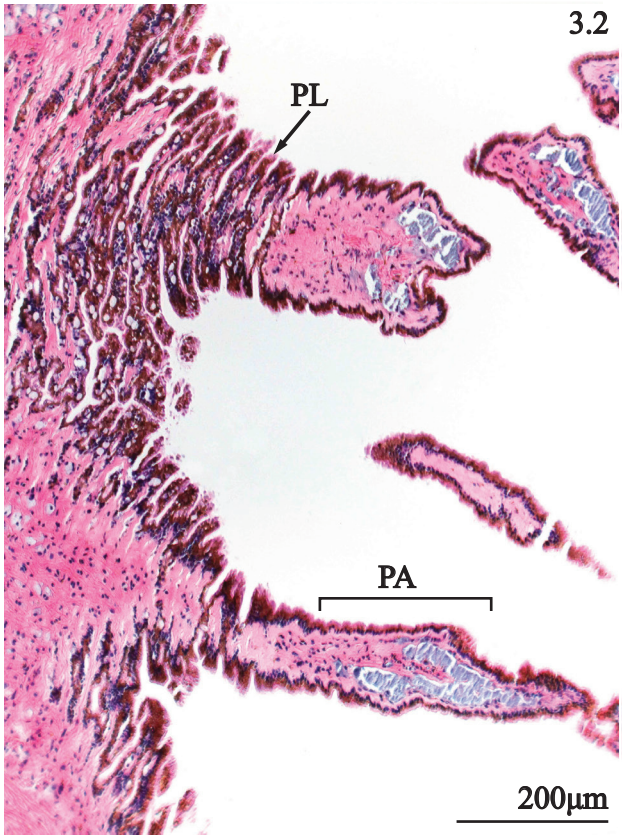
3.2
PL
PA
200µm

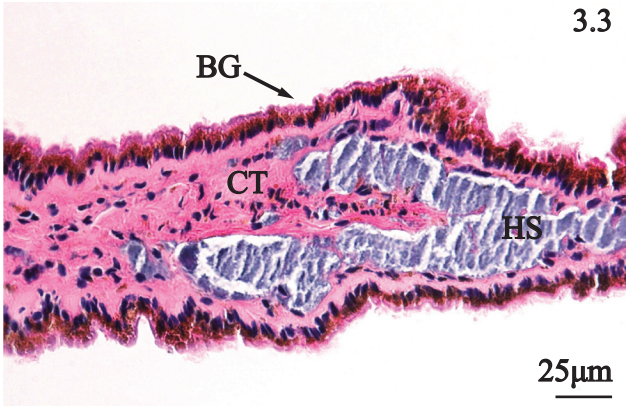
3.3
BG
CT
HS
25µm

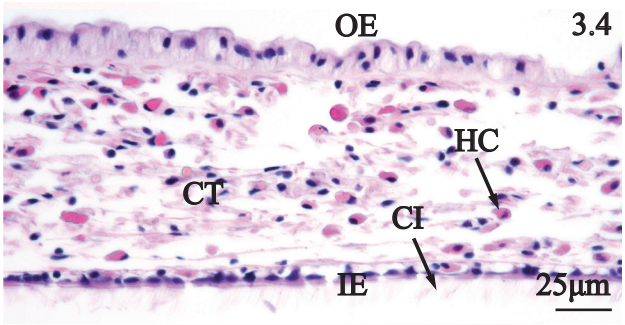
OE
3.4
HC
CT
CI
IE
25µm

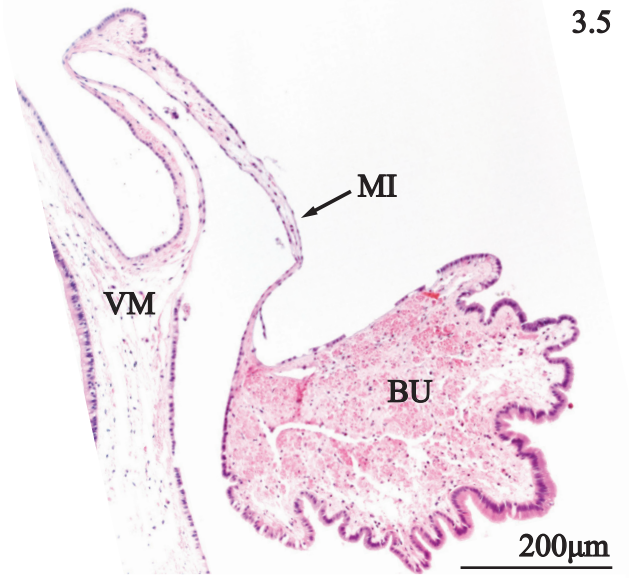
3.5
MI
VM
BU
200µm

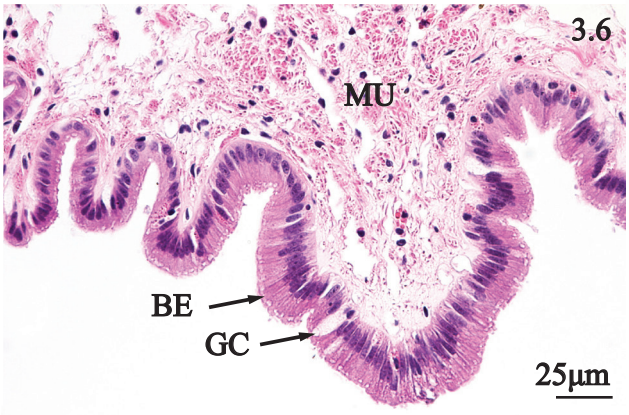
3.6
MU
BE
GC
25µm

PLATE 4. Outer gill, and inner gill of *Villosa nebulosa*. 1. Transverse section of inner gill displaying transversely oriented filaments (FI), a septum (SE) linking the inner and outer lamina, and a water tube (WT). 2. Transverse section of the inner lamina of inner ctenidia showing the main tissue components including lateral cilia (LC), frontal lateral cilia (FL), frontal cilia (FC), skeletal rods (SR), and hemolymph sinuses (HS), in addition to ostium pores (OS), and corresponding water tube (WT). 3. Transverse section of the distal tip of outer gill characterized by a rounded distal margin (DM), resembling the merger of two or more filaments (FI). 4. Transverse section of the free distal inner gill tip characterized by a bending layer of filaments (FI) around the distal margin (DM) creating a pleated surface. 5. Transverse section of the inner lamina (IL) and outer lamina (OL) of the inner ctenidia joined separately at the base of the visceral mass (VM). 6. Transverse section of ctenidia where muscle fascicles (MU) are aligned anterior to posterior where the inner lamina (IL) of inner gill and outer lamina (OL) of outer gill unite with the abdomen (AB). 7. Transverse section of gill revealing the outer lamina (OL) and outer lamina (OL) of outer gill, and mantle (MA) each uniting separately to the abdomen (AB).

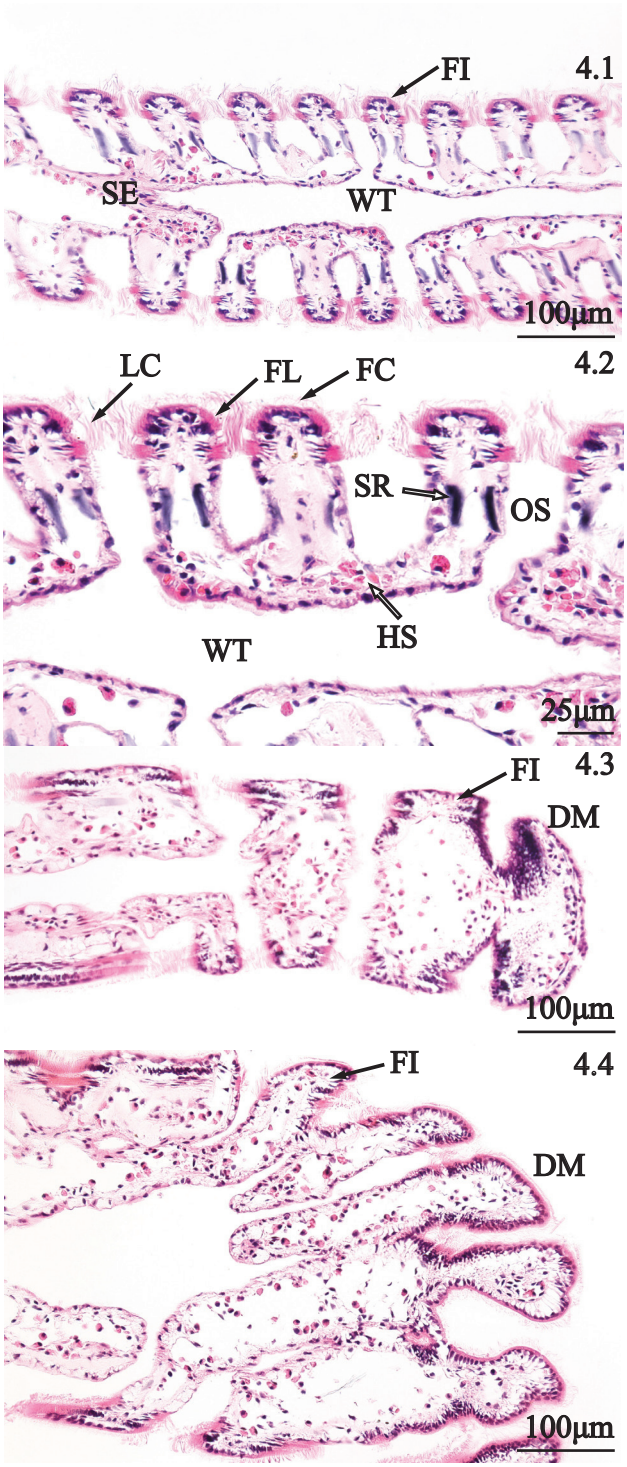
FI
4.1
SE
WT
100µm
LC
FL
FC
4.2
SR
OS
HS
WT
25µm
FI
4.3
DM
100µm
FI
4.4
DM
100µm

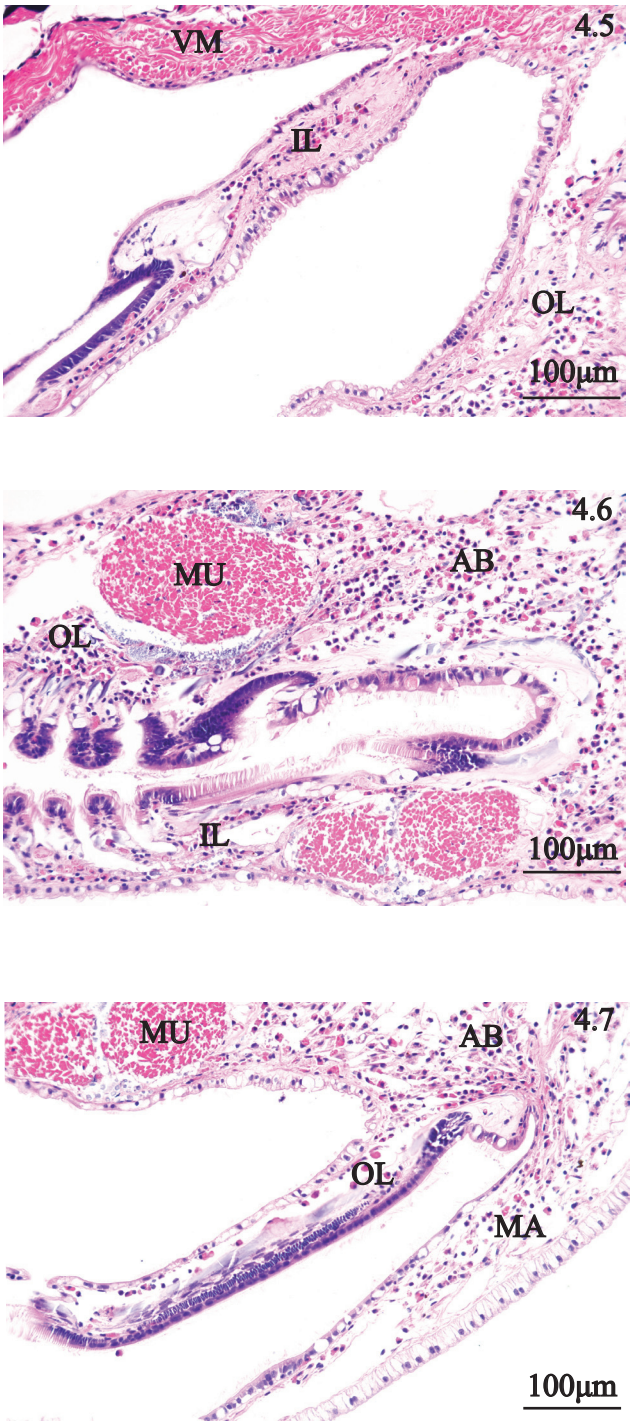
VM
4.5
IL
OL
100µm
4.6
MU
AB
OL
IL
100µm
MU
AB
4.7
OL
MA
100µm

PLATE 5. Marsupium, and embryonic development of glochidia of *Villosa nebulosa*. 1. Transverse section of an empty marsupium revealing distended water tubes (WT), thickened septa (SE), and reduced filaments (FI) along the distal margin. 2. Transverse section of a marsupium portraying a wall of concentric musculature (MU), and brown-pigmented columnar cells (BC), and a central mass of fragmented to intact glochidia (GL) enclosed by gray, wispy fibers (WF), possibly representing a substance that binds glochidia together within the conglutinate. 3. Transverse section of the marsupium at its dorsum, characterized by a thickened base of fibrous connective tissue (CT) and a series of ciliated papillae (CP) extending into the lumen. 4. Transverse section of a marsupial water tube septum emphasizing a lattice of connective tissue fibers (CT), occasional fibroblasts (FB), and brown-pigmented, ciliated cells (BC). 5. Transverse section of marsupium showing ctenidial filaments (FI) supported by a continuous subepithelium of connective tissue (CT). 6. Transverse section of a marsupium containing a mixture of early stage embryos (EE) resembling a mass of spherical cells, and late stage embryos (LE) bearing a resemblance to glochidia. 7. Transverse section of a marsupium portraying an intact glochidium with well-defined, semicircular valves (VA) and a median adductor muscle (AM).

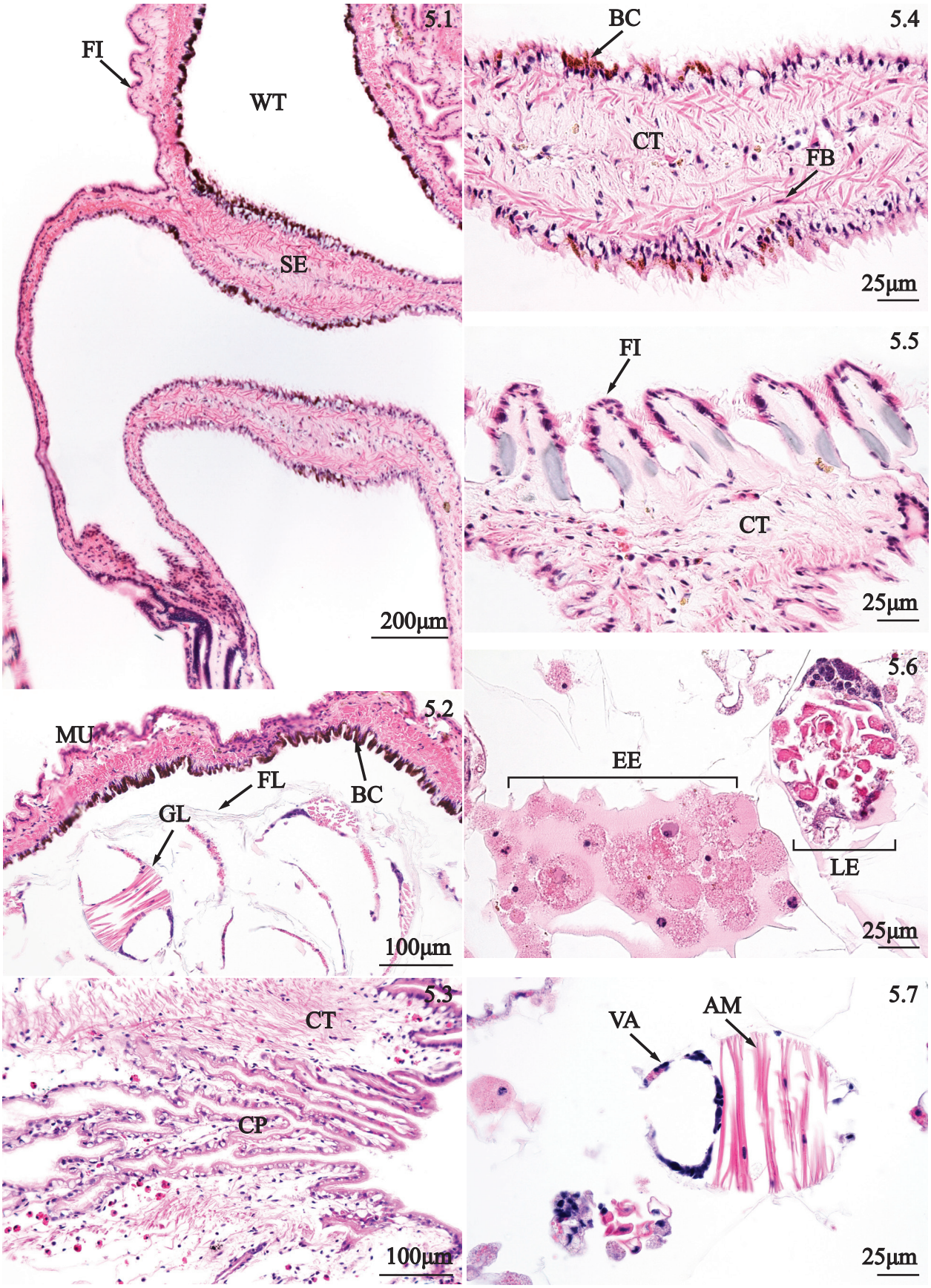
5.1
FI
WT
SE
200µm
5.2
MU
FL
BC
GL
100µm
5.3
CT
CP
100µm
5.4
BC
CT
FB
25µm
5.5
FI
CT
25µm
5.6
EE
LE
25µm
5.7
VA
AM
25µm

PLATE 6. Pedal musculature, and byssal gland of *Villosa nebulosa*. 1. Transverse section of the ventral tip of the foot characterized by somatic musculature (SM), granulocytes (GC), and a plicated integument (PI). 2. Transverse section of foot subepithelium characterized by muscle fibers (MF) pale, blue granulocytes (BC) in the median, and violet cells (VC) between the blue cells and the epithelium. 3. Transverse section of ventral foot musculature featuring an irregular meshwork (IM) of fibrous tissue. 4. Transverse section of dorso-lateral foot musculature characterized by vertically oriented myofibers (VF), and horizontally oriented myofibers (HF), and a pedal nerve branch (NE). 5. Transverse section of the byssal gland featuring a distinct dorsal chamber (DC) and a ventral chamber (VC), surrounded by lamina propria (LP). 6. Transverse section of the byssal gland displaying ciliated walls (CI) and byssal remnants (BY) within the lumen. 7. Transverse section of the base of the foot portraying irregular myofibers (IM) a vertical duct located in the median of the foot possibly representing the vestigial byssal canal (BC).

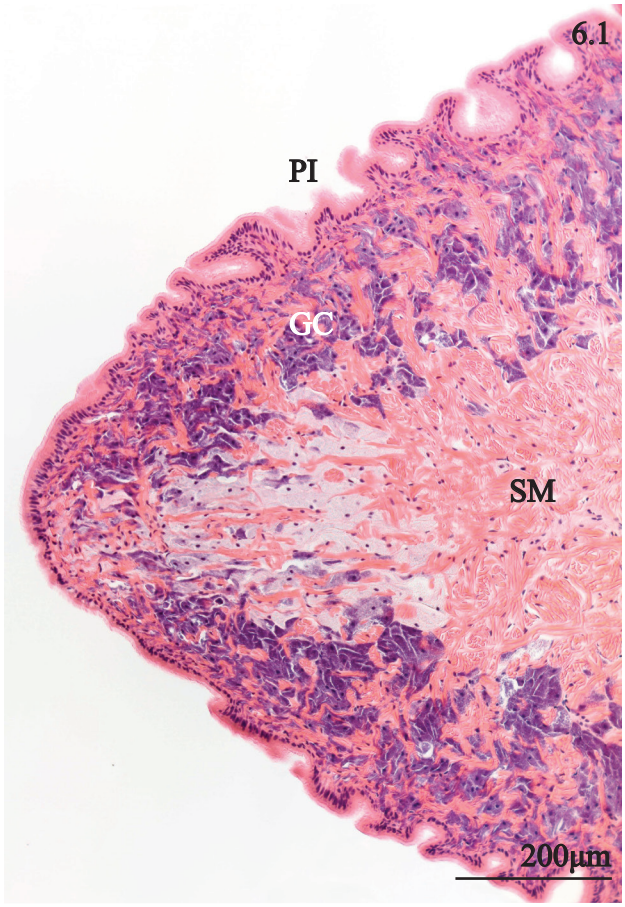
6.1
PI
GC
SM
200μm

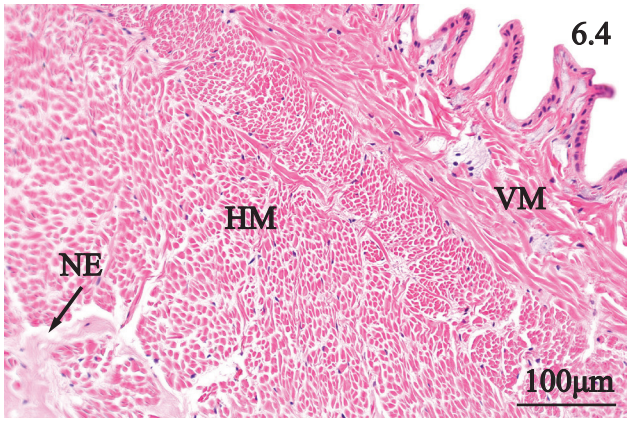
6.4
HM
VM
NE
100μm

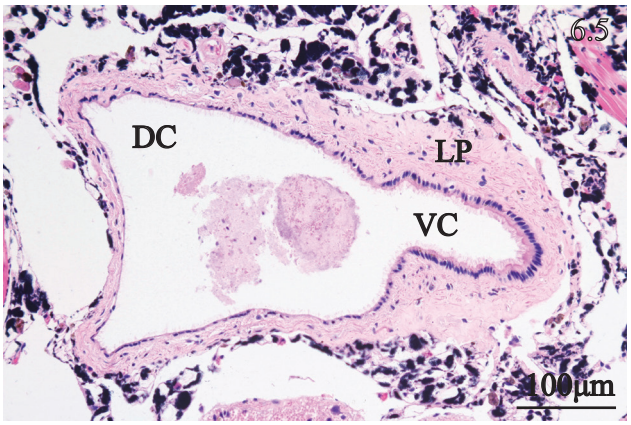
6.5
DC
LP
VC
100μm

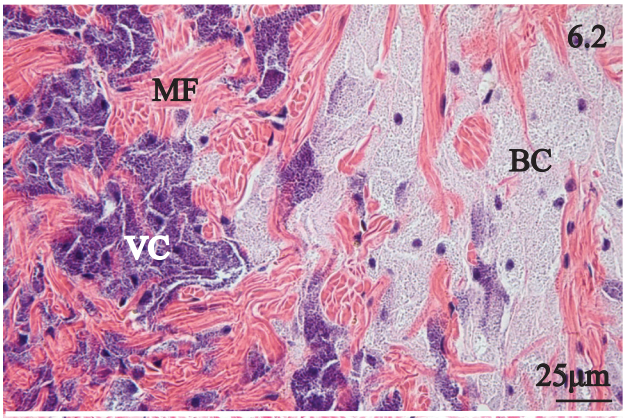
6.2
MF
BC
VC
25μm

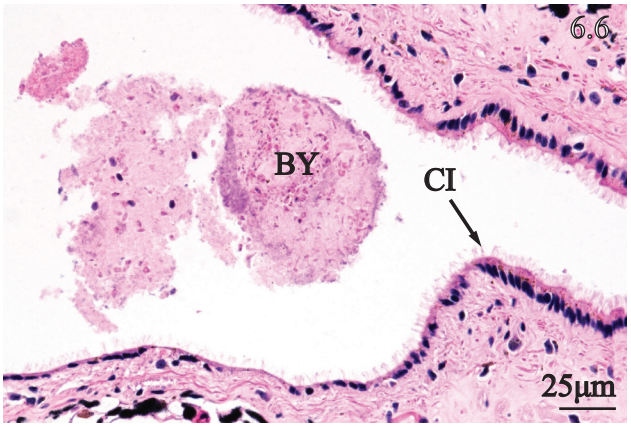
6.6
BY
CI
25μm

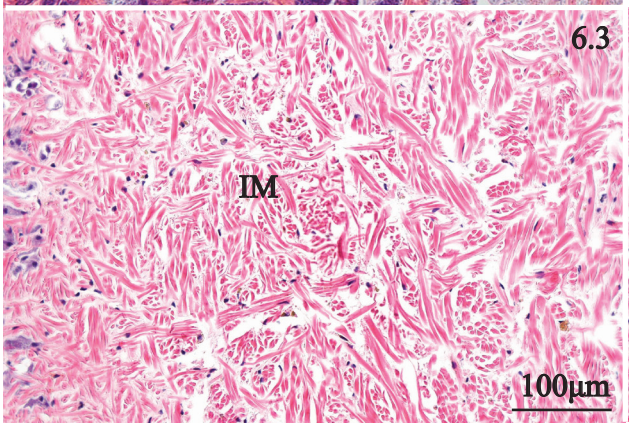
6.3
IM
100μm

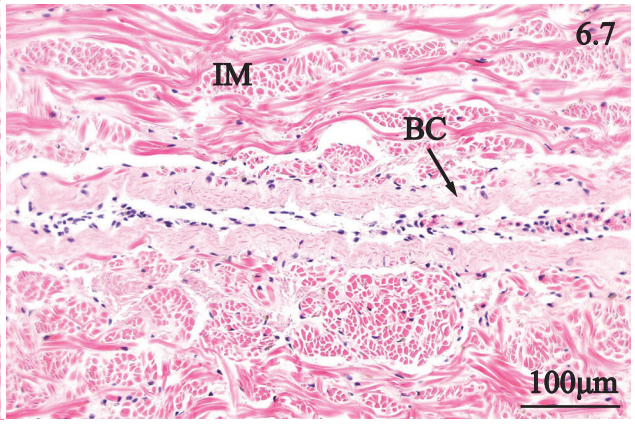
6.7
IM
BC
100μm

PLATE 7. Pedal integument, and mesentery of *Villosa nebulosa*. 1. Transverse section of pedal integument type 1, emphasizing broad, Y-shaped plicae (PL) with densely packed cilia (CI) overlying a subepithelium of irregular fibers (IF), and violet cells (VC). 2. Transverse section of pedal integument type 2 represented by Y-shaped plicae (PL), violet cells (VC), sparse cilia (CI), and supported by an organized layer of vertical musculature (SM). 3. Transverse section of pedal integument type 3, characterized by short, teardrop-shaped plicae (PL), ciliated (CI), goblet cells (GC), horiztonal musculature (HM), and vertical musculature (VM). 4. Transverse section of pedal integument type 4, characterized by short plicae (PL) with cilia (CI), and goblet cells (GC), and a hemolymph sinus (HS) between the epithelium and horizontal musculature (HM). 5. Transverse section of pedal integument type 5, featuring epithelial cells with a convex apical surface, cilia (CI), and goblet cells (GC), overlying a hemolymph sinus (HS), and horizontal musculature (HM). 6. Sagittal section of pedal integument at the black spot along the posterior margin of the foot, emphasizing plicae (PL), with columnar cells containing brown intracellular granules (BG) and a subepithelium of violet cells (VC). 7. Transverse section of the dorso-lateral aspect of the coelom, portraying fibrous mesentery (ME) extending medially from foot muscle (FM), testicular acini (TA), and ciliated gonadal ducts (CD). 8. Sagittal section through a fascicle (FA) of mesentery fibers surrounded by adipocytes (AC).

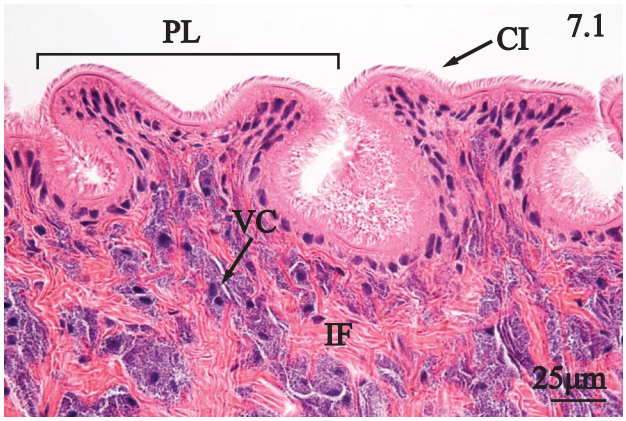
7.1
PL
CI
VC
IF
25µm

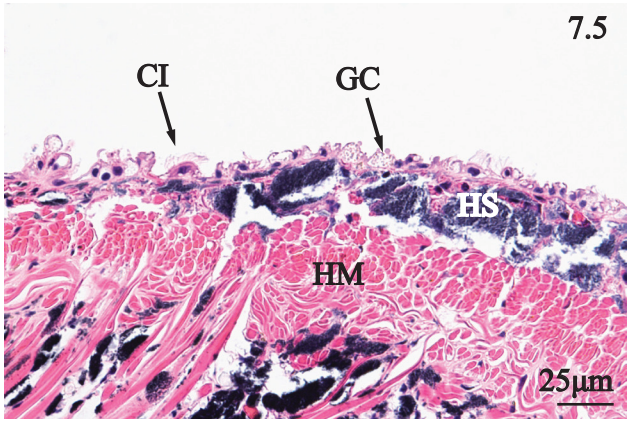
7.5
CI
GC
HS
HM
25µm

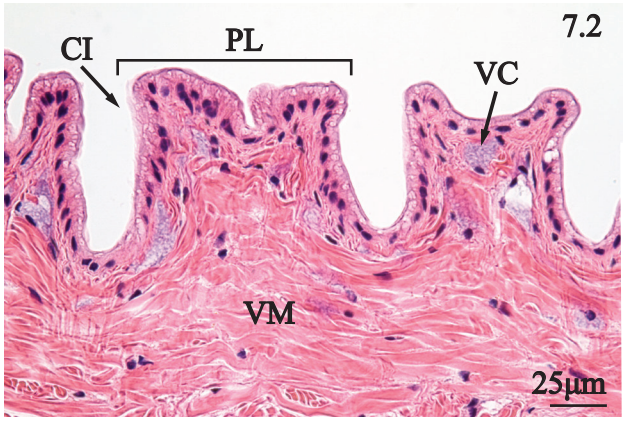
7.2
CI
PL
VC
VM
25µm

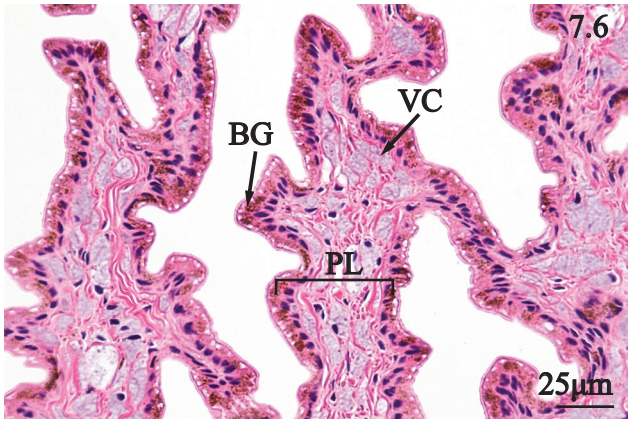
7.6
VC
BG
PL
25µm

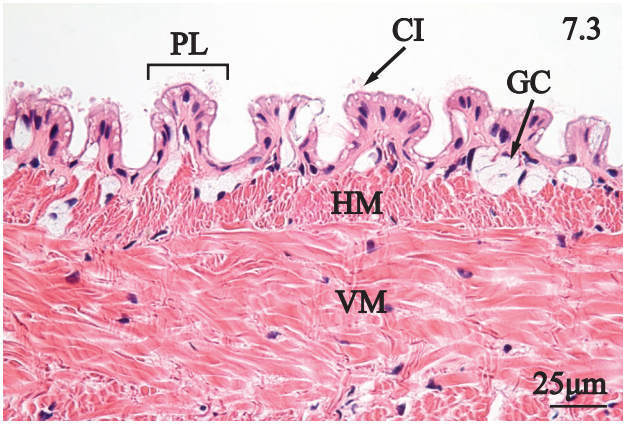
7.3
PL
CI
GC
HM
VM
25µm

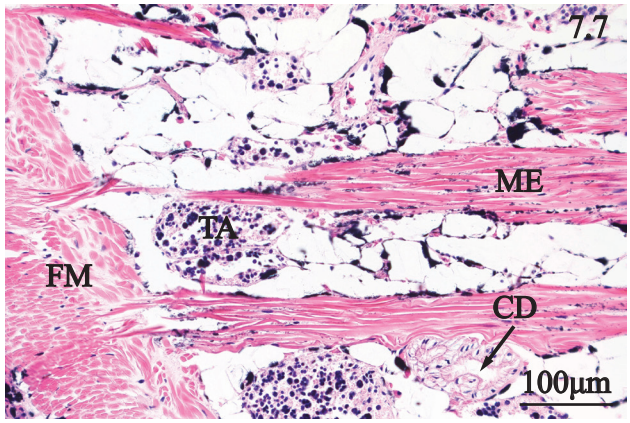
7.7
ME
TA
FM
CD
100µm

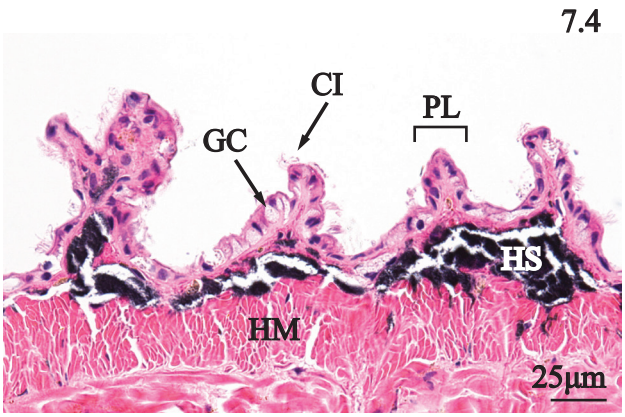
7.4
CI
GC
PL
HS
HM
25µm

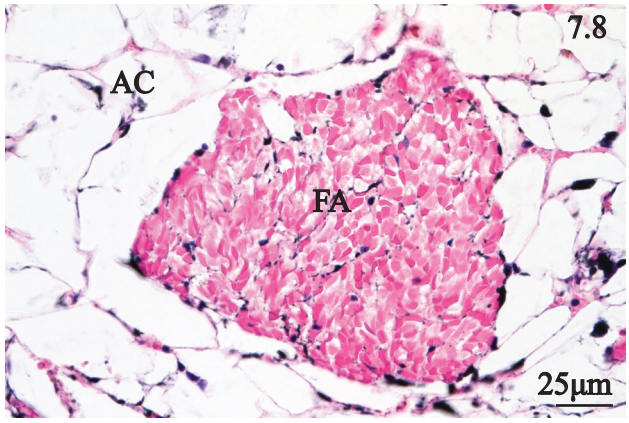
7.8
AC
FA
25µm

PLATE 8. Labial palps, anterior pedal retractor, and anterior adductor of *Villosa nebulosa*. 1. Sagittal section of labial palps revealing inner plicated surface (IS), distal palp margin (DM), outer palp surface (OS), anterior pedal retractor (AR). 2. Sagittal section of the inner palp surface featuring plicae (PL), cilia (CI), and hemocytes (HC) in the subepithelium. 3. Sagittal section of distal labial palp margin portraying cilia (CI), goblet cells (GC), and connective tissue (CT), hemolymph (HL), and hemocytes (HC) of the subepithelium. 4. Sagittal section of outer palp surface highlighting tear drop-shaped columnar cells (TC), and subepithelial connective tissue (CT), and hemolymph sinuses (HS). 5. Transverse section of anterior pedal retractor showing a fascicle (FA), with a thin perimysium (PM), and dark-staining myocyte nuclei (MN). 6. Sagittal section of anterior adductor showing the thin myofibers (MF), and ovular myocyte nuclei (MN).


8.1
DM
OS
IS
PR
200µm

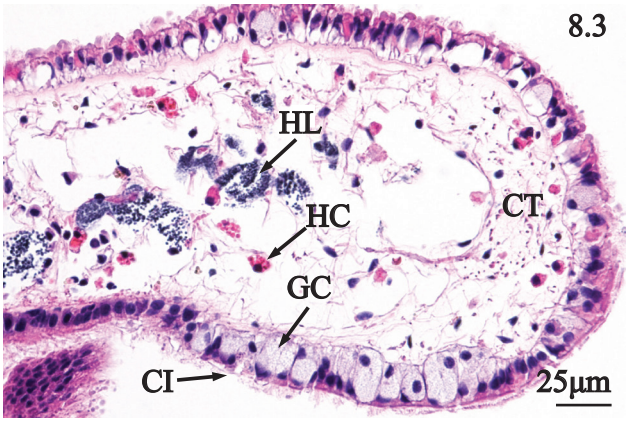
8.3
HL
HC
CT
GC
CI
25µm

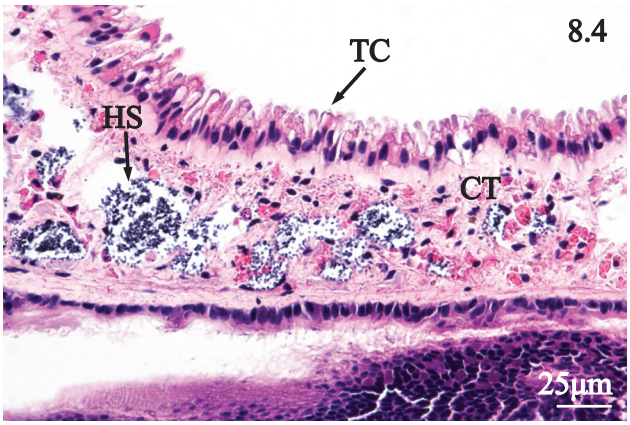
8.4
TC
HS
CT
25µm

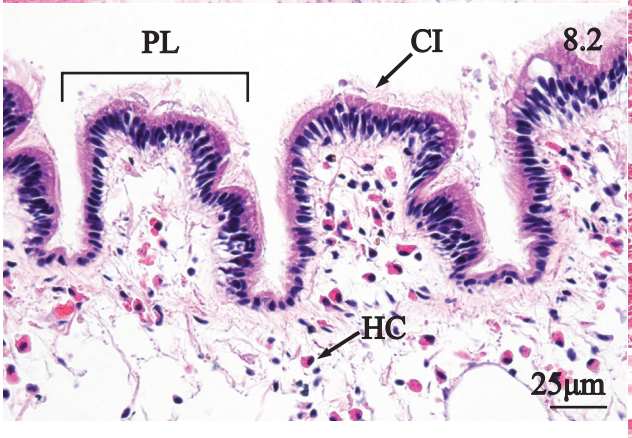
PL
CI
8.2
HC
25µm

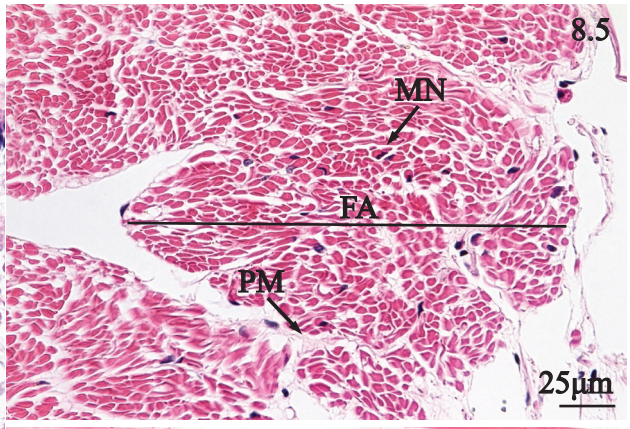
8.5
MN
FA
PM
25µm

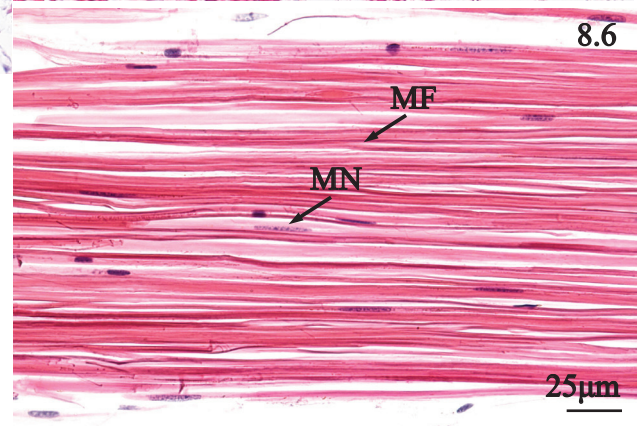
8.6
MF
MN
25µm

PLATE 9. Oral groove, and esophagus of *Villosa nebulosa*. 1. Sagittal section of oral groove showing ciliated folds (CF) along the wall. 2. Sagittal section of the ventral oral groove wall displaying ciliated columnar cells (CC) and hemocytes (HC) within the subepithelium and nestled between epithelial cells of the ventral oral groove wall. 3. Sagittal section of the ventral oral groove wall displaying a composition of loose connective tissue fibers (CT) and hemocytes (HC) between the ventral epithelium of the oral groove (VE) and the externally located dorsal epithelium (DE). 4. Transverse section through dorsal aspect of visceral mass revealing the esophagus (ES) encircled by lamina propria (LP), tubules of the digestive diverticulum (DD), and mantle isthmus (MI). 5. Transverse section of esophagus portraying plicae (PL) with densely packed cilia (CI) and the supporting lamina propria (LP).

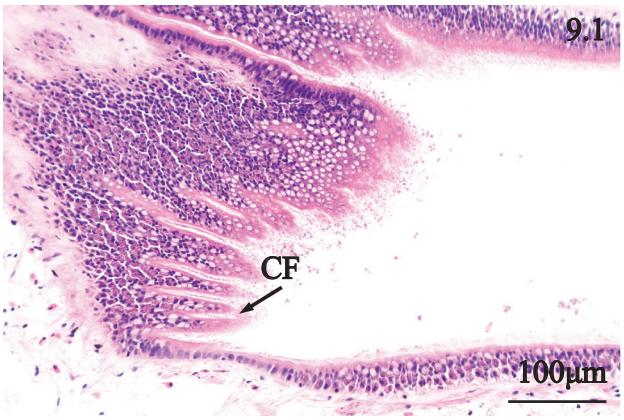
9.1
CF
100µm

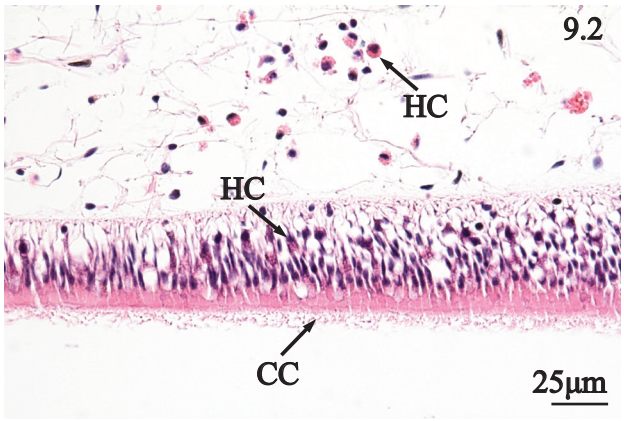
9.2
HC
HC
CC
25µm

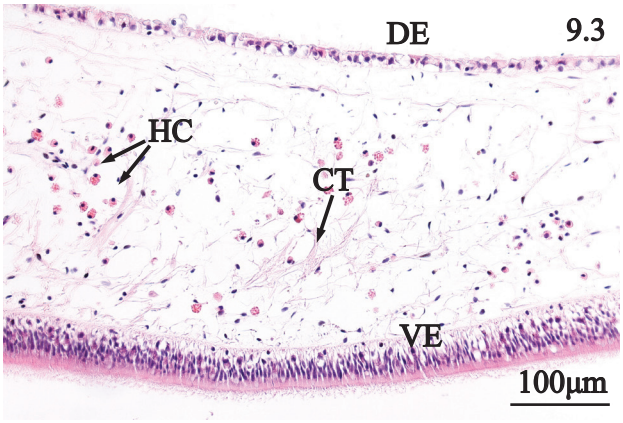
DE
9.3
HC
CT
VE
100µm


9.4
MI
ES
LP
DD
200µm

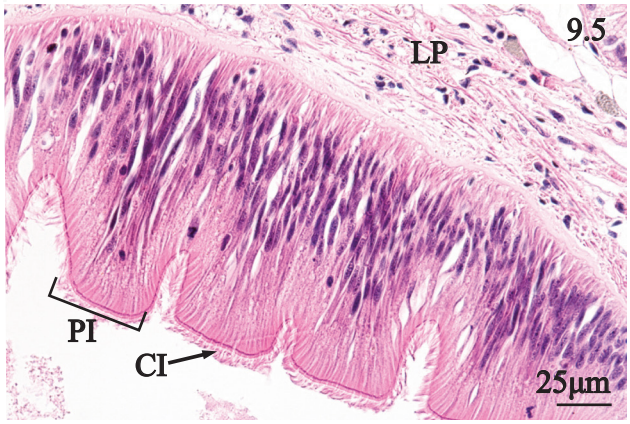
LP
9.5
PI
CI
25µm

PLATE 10. Digestive diverticulum, and stomach of *Villosa nebulosa*. 1. Transverse section of the junction between the esophagus (ES) and digestive diverticula highlighting ciliated tubules (CT) leading toward digestive tubules (DT). 2. Transverse section of digestive diverticulum emphasizing a transition from ciliated primary tubules (PT), to vesiculated secondary tubules (ST). 3. Transverse section of digestive diverticulum revealing the transition between a secondary tubules (ST) and tertiary tubules (TT). 4. Transverse section of digestive diverticulum portraying fine structure of tubules including cilia (CI) of a primary tubule (PT), microvilli (MV) of secondary tubules (ST), basophilic nuclear region (BN) of tertiary tubules (TT). 5. Transverse section of the ventral stomach wall detailing cilia (CI) along plicae (PL), and lamina propria (LP) between the stomach and digestive diverticulum (DD). 6. Transverse section of the ventral stomach wall demarcated by a large plication (PL) featuring cilia (CI), and a well-defined lamina propria (LP). 7. Transverse section of the dorsal stomach wall featuring cuticularized epithelium (CU), and lamina propria (LP). 8. Transverse section of dorsal stomach wall showing a cuticle (CU), cilia (CI) and lamina propria (LP).

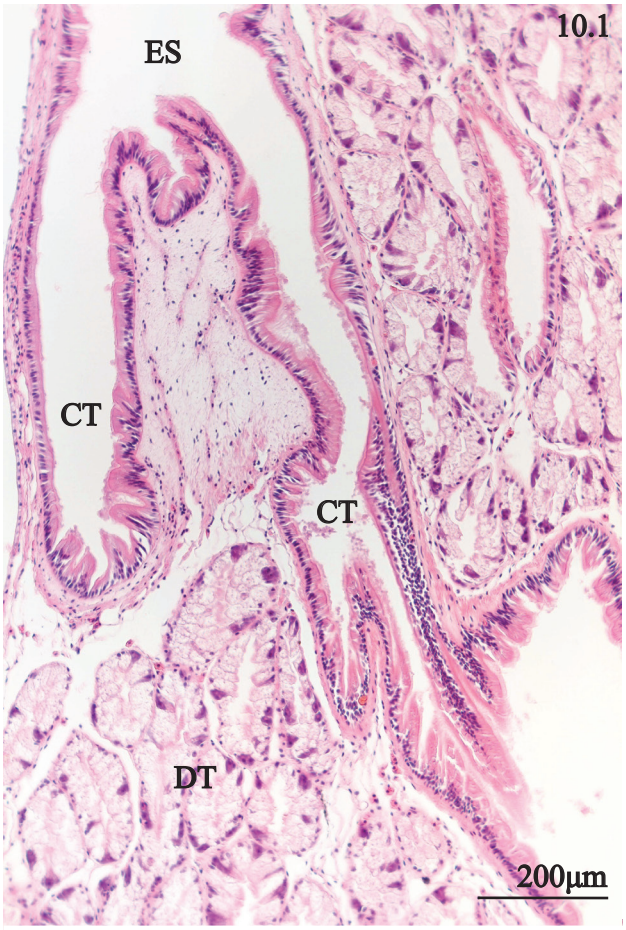
10.1
ES
CT
CT
DT
200μm

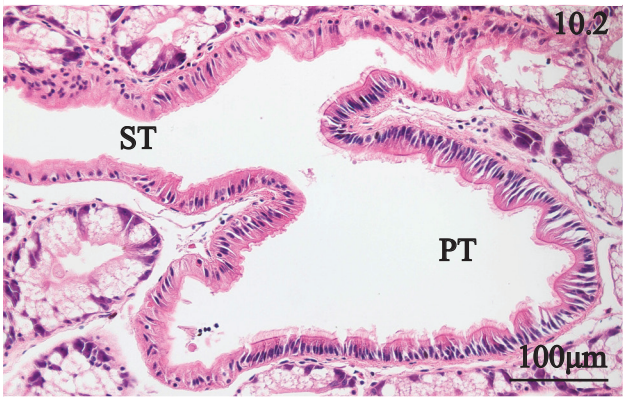
10.2
ST
PT
100μm

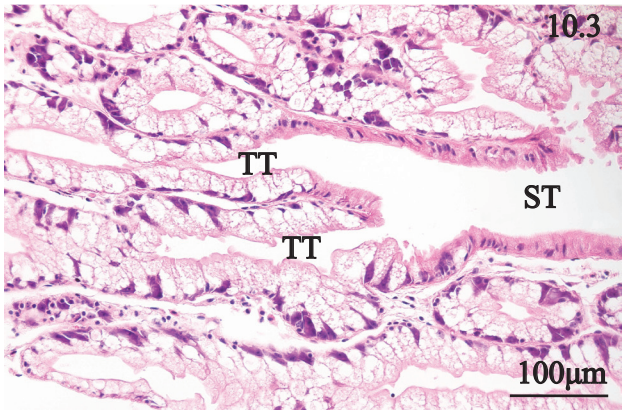
10.3
TT
ST
TT
100μm

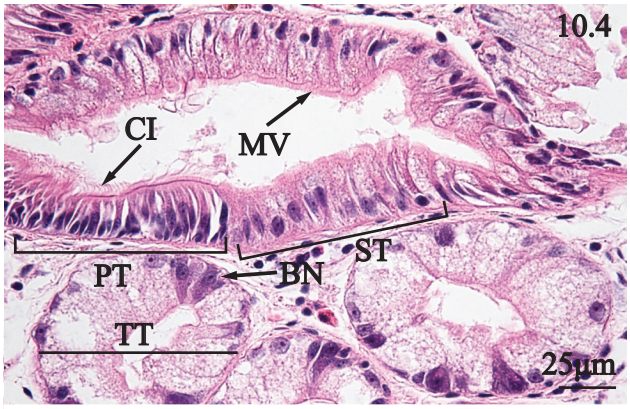
10.4
CI
MV
ST
PT
BN
TT
25μm

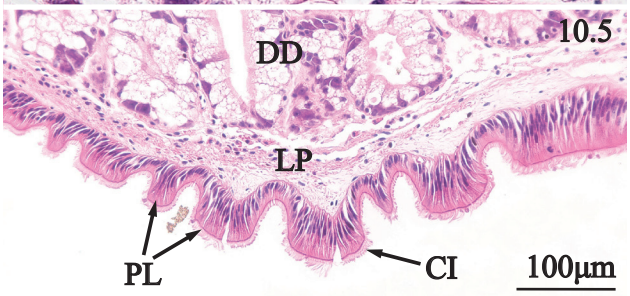
10.5
DD
LP
PL
CI
100μm

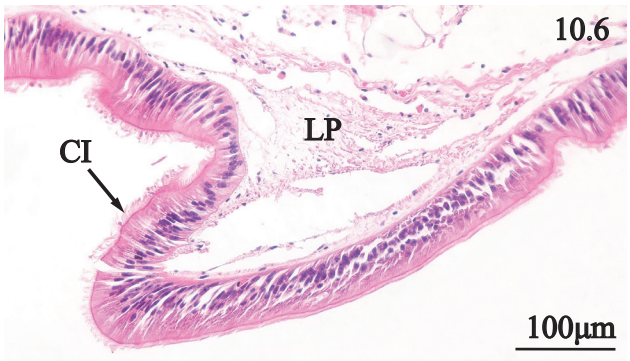
10.6
LP
CI
100μm

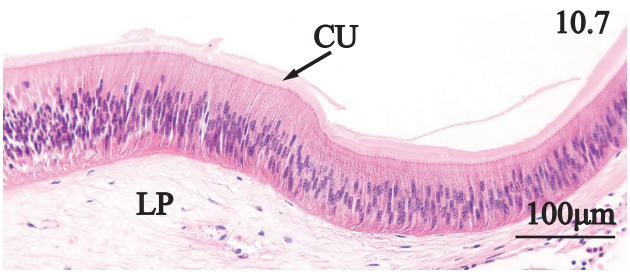
10.7
CU
LP
100μm

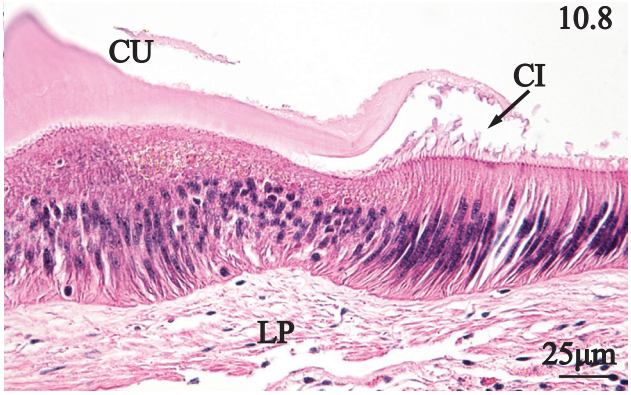
10.8
CU
CI
LP
25μm

PLATE 11. Crystalline style sac, and ascending second intestinal limb of *Villosa nebulosa*. 1. Transverse section through visceral mass portraying the overall structure of the style sac (SS), including the crystalline style (SY), lamina propria (LP), and style sac epithelium type 1 (E1), epithelium type 2 (E2), and epithelium type 3 (E3). 2. Transverse section of stomach-style sac junction showing an eosinophilic cuticle (CU) ventrally extending from the stomach (ST) into the lumen of the style sac (SS). 3. Transverse section of the rod-shaped crystalline style (SY), showing particles (PA) trapped between layers of the style. 4. Transverse section of style sac displaying a median fold along the ventral wall marking the junction between type 1 epithelium (E1), and type 2 epithelium (E2). 5. Transverse section of a lateral branch of the style sac featuring cilia (CI), type 2 epithelium (E2), goblet cells (GC), and lamina propria (LP). 6. Transverse section of the style sac featuring the junction between type 1 epithelium (E1), and type 3 epithelium (E3), and cilia (CI), along the dorsal style sac wall. 7. Transverse section of the second intestinal limb located ventrally to the style sac, and featuring cilia (CI) and plicated walls (PL).

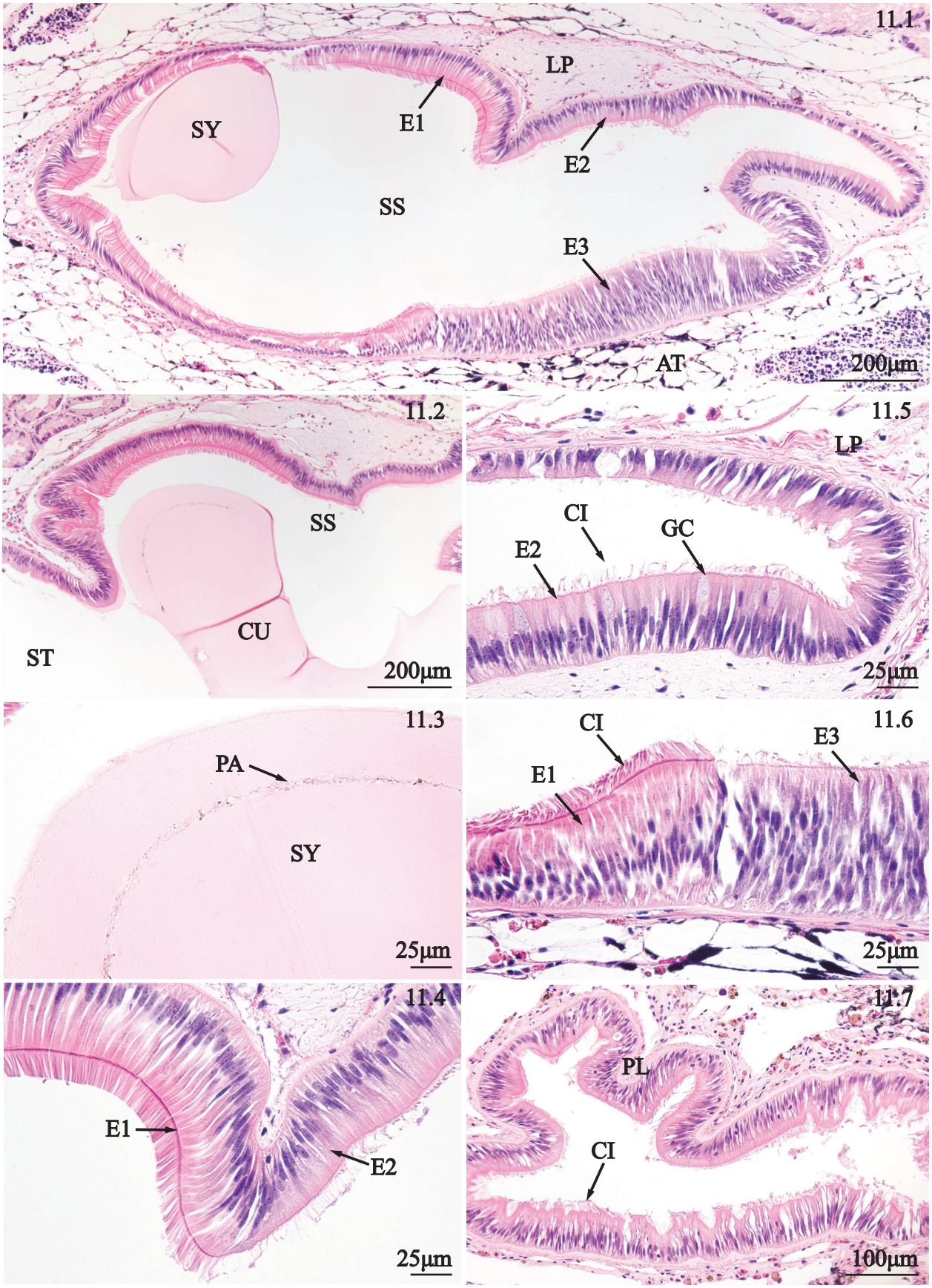
11.1
LP
E1
SY
E2
SS
E3
AT
200µm
11.2
SS
CU
ST
200µm
11.5
LP
CI
GC
E2
25µm
11.3
PA
SY
25µm
11.6
CI
E3
E1
25µm
11.4
E1
E2
25µm
11.7
PL
CI
100µm

PLATE 12. First intestinal limb, and second intestinal limb of *Villosa nebulosa*. 1. Sagittal section through the first intestinal limb portraying tall plicae (PL) and chyme (CH) in the intestinal lumen. 2. Sagittal section of posterior wall of the first intestinal limb emphasizing the tall plicae (PL), with densely ciliated surfaces (CI). 3. Sagittal section of the anterior intestinal wall showing a broad plication featuring cilia (CI), goblet cells (GC), and a distinct lamina propria (LP). 4. Sagittal section through the lower portion of the first intestinal limb revealing shorter plicae lined with cilia (CI), active mucous secretion (MS), and chyme (CH). 5. Sagittal section through the initial portion of the second intestinal limb representing a region of short plicae (PL), and chyme (CH). 6. Sagittal section of second intestinal limb portraying cilia (CI), and hemocytes (HC) between epithelial cells in the intestinal wall.

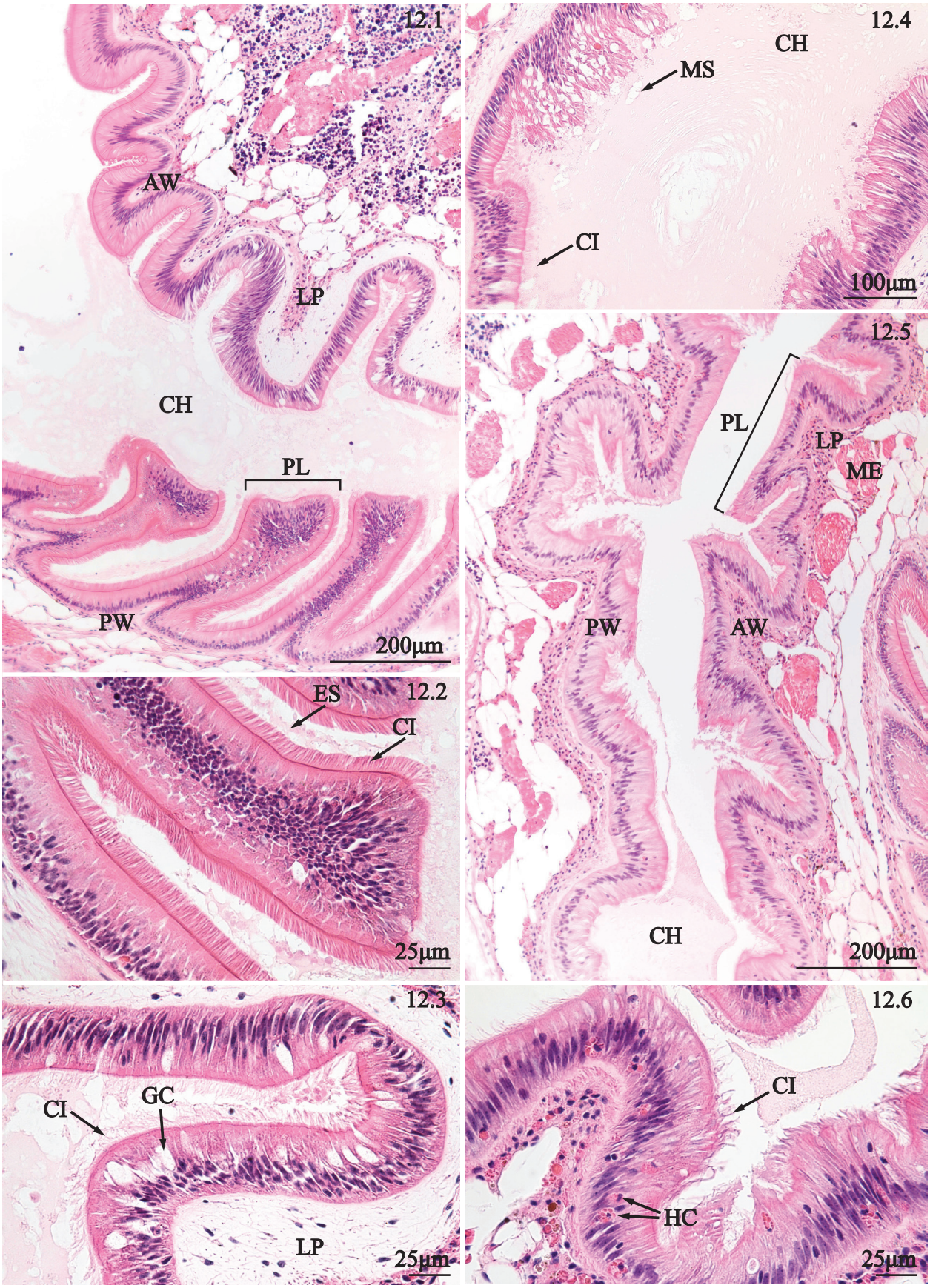
12.1
AW
LP
CH
PL
PW
200µm
12.4
CH
MS
CI
100µm
12.5
PL
LP
ME
PW
AW
CH
200µm
ES
12.2
CI
25µm
12.3
CI
GC
LP
25µm
12.6
CI
HC
25µm

PLATE 13. Third intestinal limb, fourth intestinal limb, and fifth intestinal limb of *Villosa nebulosa*. 1. Transverse section through the initial portion of the third intestinal limb located ventrally to the style sac, and featuring plicae (PL) along the intestinal walls, and a lamina propria (LP) surrounding the epithelium. 2. Sagittal section of the third intestinal limb featuring short plicae lined with cilia (CI), hemocytes (HC) between epithelial cells and a well-defined lamina propria (LP). 3. Transverse section through medial portion of the visceral mass portraying a large, ventrally pointed typhlosole (TY), surrounded by lamina propria (LP), and adipose tissue (AT). 4. Transverse section of the ventral wall of the fourth intestinal limb, emphasizing cilia (CI), eosinophilic granular cells (EC), lamina propria (LP), and adipocytes (AC). 5. Transverse section of the dorsal typhlosole of the fourth intestinal limb emphasizing a continuous line of cilia (CI) along the surface, and a well-defined lamina propria (LP) with hemolymph sinuses (HS). 6. Transverse section of the fifth intestinal limb emphasizing a large, dorsally oriented typhlosole (TY), lamina propria (LP), encircled by muscle tissue (MU). 7. Transverse section of the ventral typhlosole portraying cilia (CI), and goblet cells (GC) of the epithelium, and a thick lamina propria (LP). 8. Transverse section through the dorsal wall of the fifth intestinal limb where the tissue is organized into a series of small rectangular plicae possessing cilia (CI), and surrounded by a lamina propria (LP).

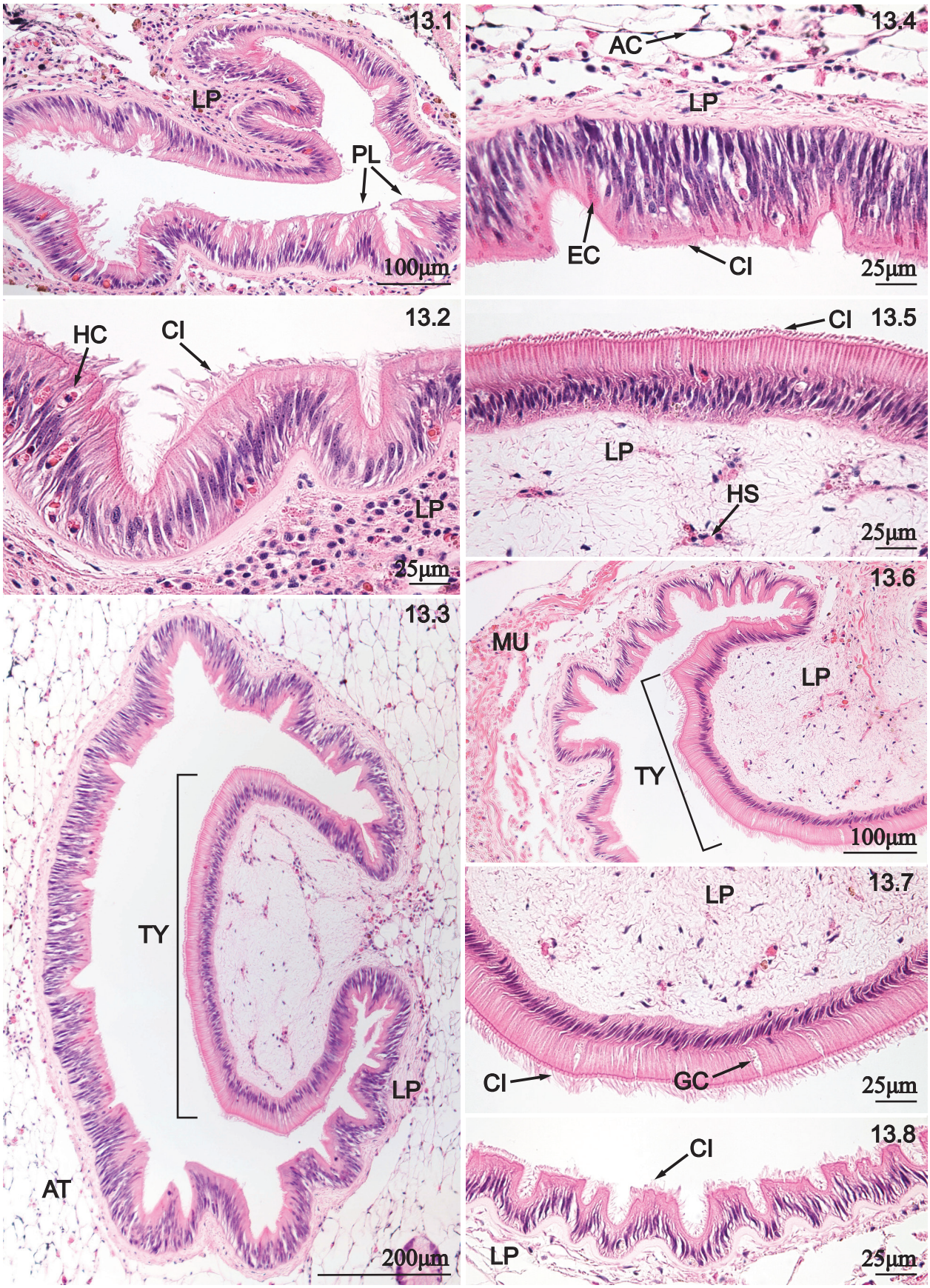
13.1
LP
PL
100µm
13.4
AC
LP
EC
Cl
25µm
13.2
HC
Cl
LP
25µm
Cl
13.5
LP
HS
25µm
13.3
TY
LP
AT
200µm
13.6
MU
LP
TY
100µm
13.7
LP
Cl
GC
25µm
13.8
Cl
LP
25µm

PLATE 14. Heart, and pericardial cavity of *Villosa nebulosa*. 1. Sagittal section through the dorsal portion of the visceral mass revealing the heart (HE), in relation to the intestine (IN), pericardial cavity (PC) and nephridium (NE). 2. Frontal section of the ventricle emphasizing the irregular cardiac muscle (CM), pericardial epithelium (PE), and pericardial cavity (PC). 3. Frontal section of the ventricle emphasizing the thin composition of the pericardial sac (PS), and irregularities in the pericardial epithelium (PE). 4. Frontal section of the ventricle portraying branched cardiac myocytes (MC) and hemocytes (HC). 5. Transverse section of the heart and pericardium belying the orientation of the left auricle (AU) ventricle (VE), pericardial cavity (PC), auriculoventricular valve (AV), nephridium (NE), and mantle (MA). 6. Transverse section of an auriculoventricular valve, emphasizing squamous epithelium (SE), cardiac muscle (CM), and hemocytes (HC).

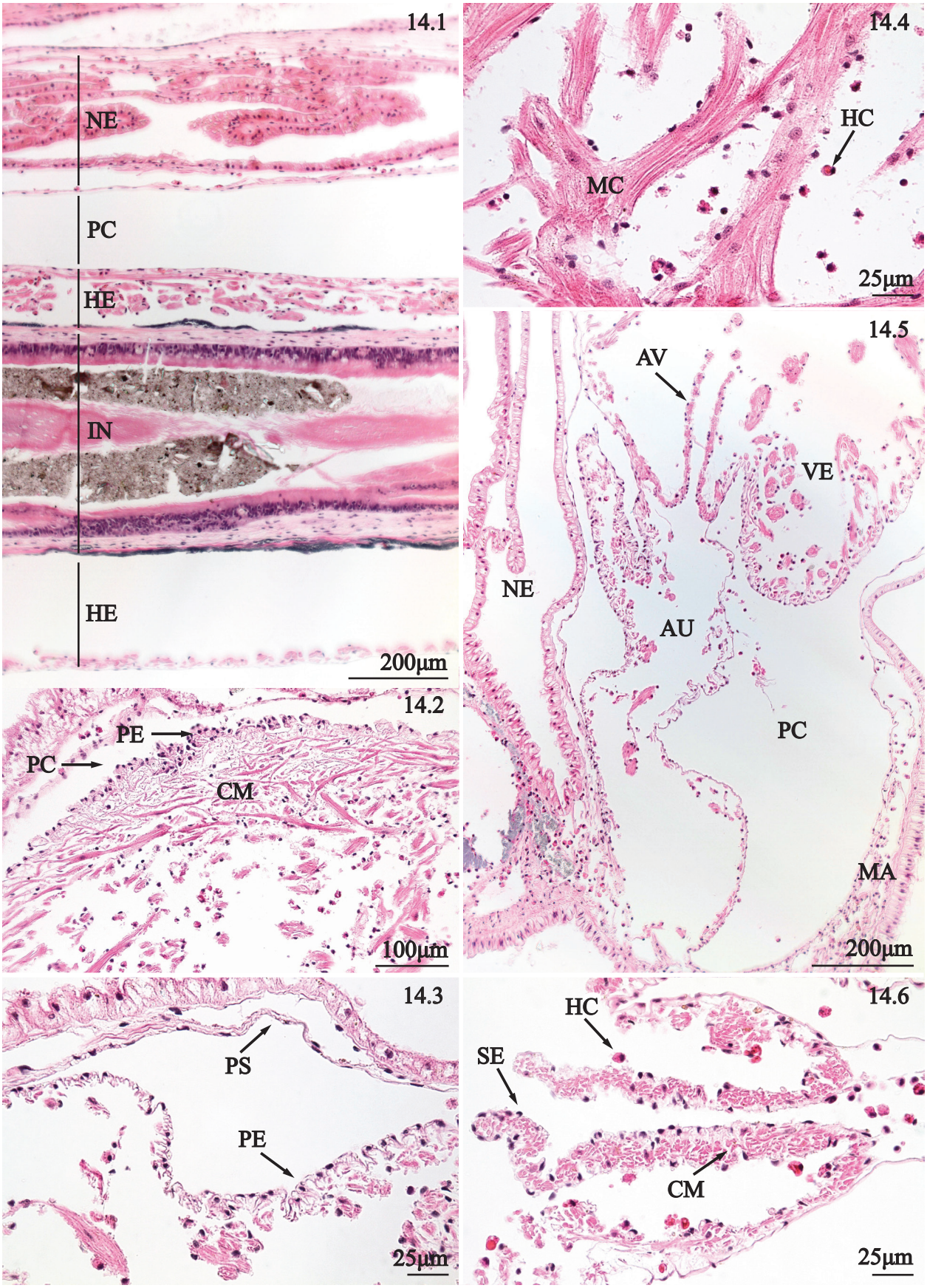
14.1
NE
PC
HE
IN
HE
200µm
14.2
PE
PC
CM
100µm
14.3
PS
PE
25µm
14.4
HC
MC
25µm
14.5
AV
VE
NE
AU
PC
MA
200µm
14.6
HC
SE
CM
25µm

PLATE 15. Hemolymph vessels of *Villosa nebulosa*. 1. Transverse section of visceral mass emphasizing the squamous epithelium (SE) of a vein (VE), surrounded by foci of hemolymph (HL), testicular acini (TA), and ciliated gonadal ducts (CD). 2. Transverse section of visceral mass showing squamous epithelium (SE) of a vein (VE), and tertiary tubules (TT). 3. Transverse section of visceral mass displaying an artery (AR), with squamous epithelium (SE), and concentric musculature (MU), among adipoctes (AC). 4. Transverse section of mantle edge revealing an artery (AR), between the outer epithelium (OE) and adipocytes (AC). 5. Sagittal section of posterior adductor (PA), emphasizing a capillary (CA), with a squamous epithelial lining (SE). 6. Transverse section of the base of the visceral mass showing a muscular arch (AR) between the visceral mass and nephridium. 7. Transverse section of the base of the ctenidia focusing on an afferent hemolymph sinus (HS) containing hemolymph (HL) before it enters the auricles. 8. Transverse section of the pericardial gland characterized by a network of loose connective tissue fibers (CT), hemocytes (HC), and senescent hemocytes (SH).

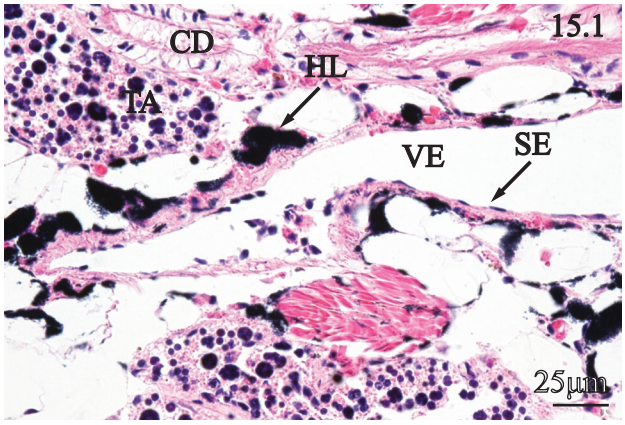
15.1
CD
HL
TA
VE
SE
25μm

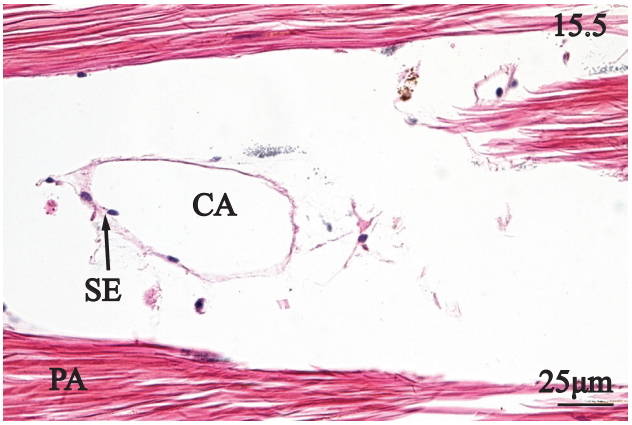
15.5
CA
SE
PA
25μm

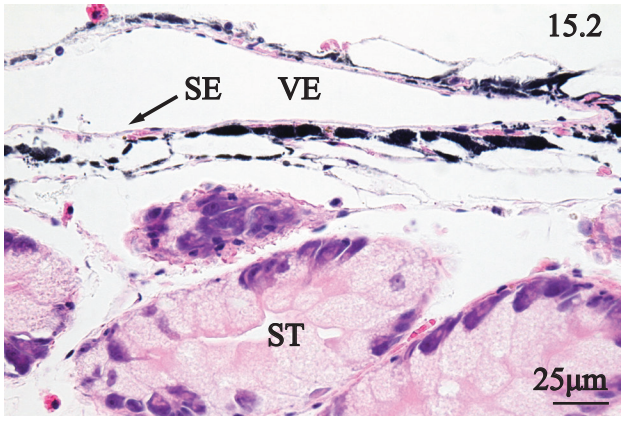
15.2
SE
VE
ST
25μm

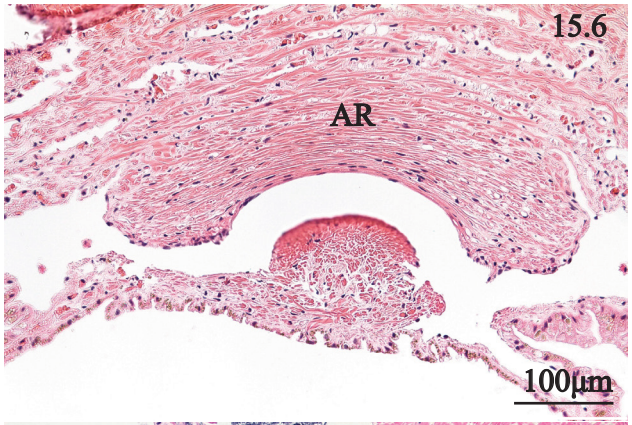
15.6
AR
100μm

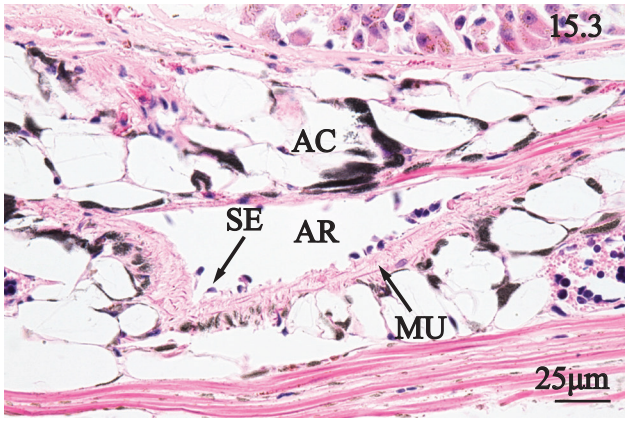
15.3
AC
SE
AR
MU
25μm

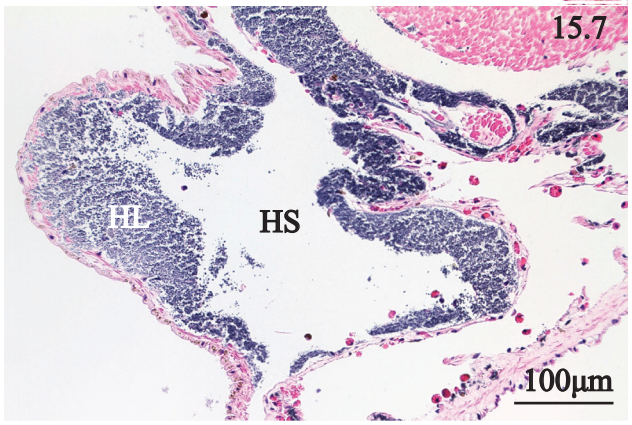
15.7
HL
HS
100μm

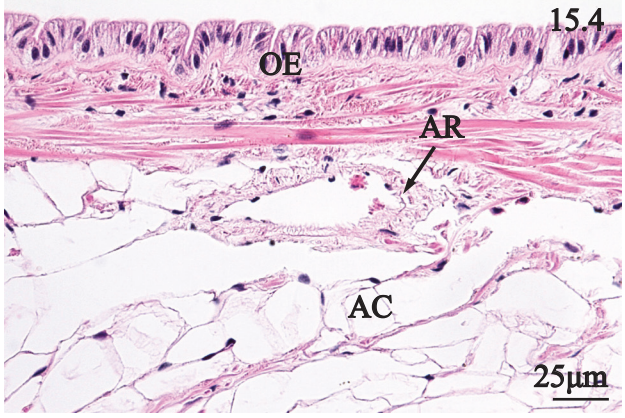
15.4
OE
AR
AC
25μm

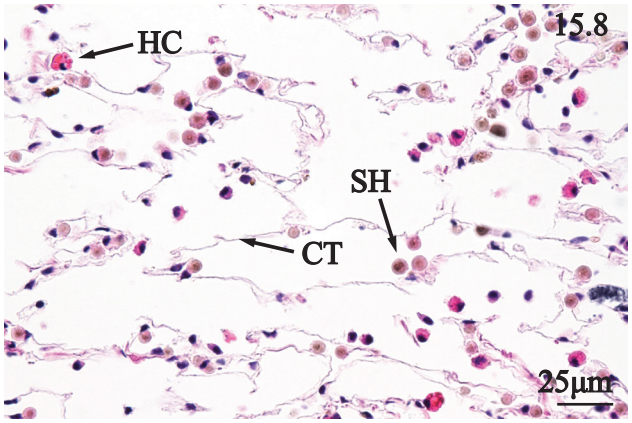
15.8
HC
SH
CT
25μm

PLATE 16. Anterior nephridium of *Villosa nebulosa*. 1. Transverse section through dorsal portion of the visceral mass revealing the general structural features of ventral nephridium (VN), dorsal nephridium (DN), and pericardial cavity (PC). 2. Transverse section through the nephridium emphasizing the morphological difference between the ventral (VL) and dorsal nephridial limbs (DL), including plications (PL) within ventral and dorsal nephridia. 3. Transverse section of the ventral nephridial limb showing plicae (PL) occupying a large proportion of the lumen, columnar cells containing brown intracellular granules (BG), hemolymph vessels (HV), and lamina propria (LP) comprising subepithelium. 4. Transverse section of the dorsal nephridial limb displaying a branched plicaton extending dorsally from the ventral wall, as well as teardrop cells (TC), and brown intracellular granules (BG). 5. Transverse section of the dorsal nephridium portraying a patch of teardrop cells (TC) at the dorso-lateral corner of the wall, and a sinus of hemolymph (HL) beneath the epithelium. 6. Transverse section of nephridium showing the urethra (UR) and reno-pericardial canal (RC). 7. Transverse section of a urethra revealing a short stretch of columnar cells bearing cilia (CI), mucus cells (MC), and connective tissue (CT). 8. Transverse section of a reno-pericardial canal emphasizing conical extensions of epithelial tissue bearing cilia (CI) and goblet ells (GC), encircled by a lamina propria (LP), and hemocytes (HC).

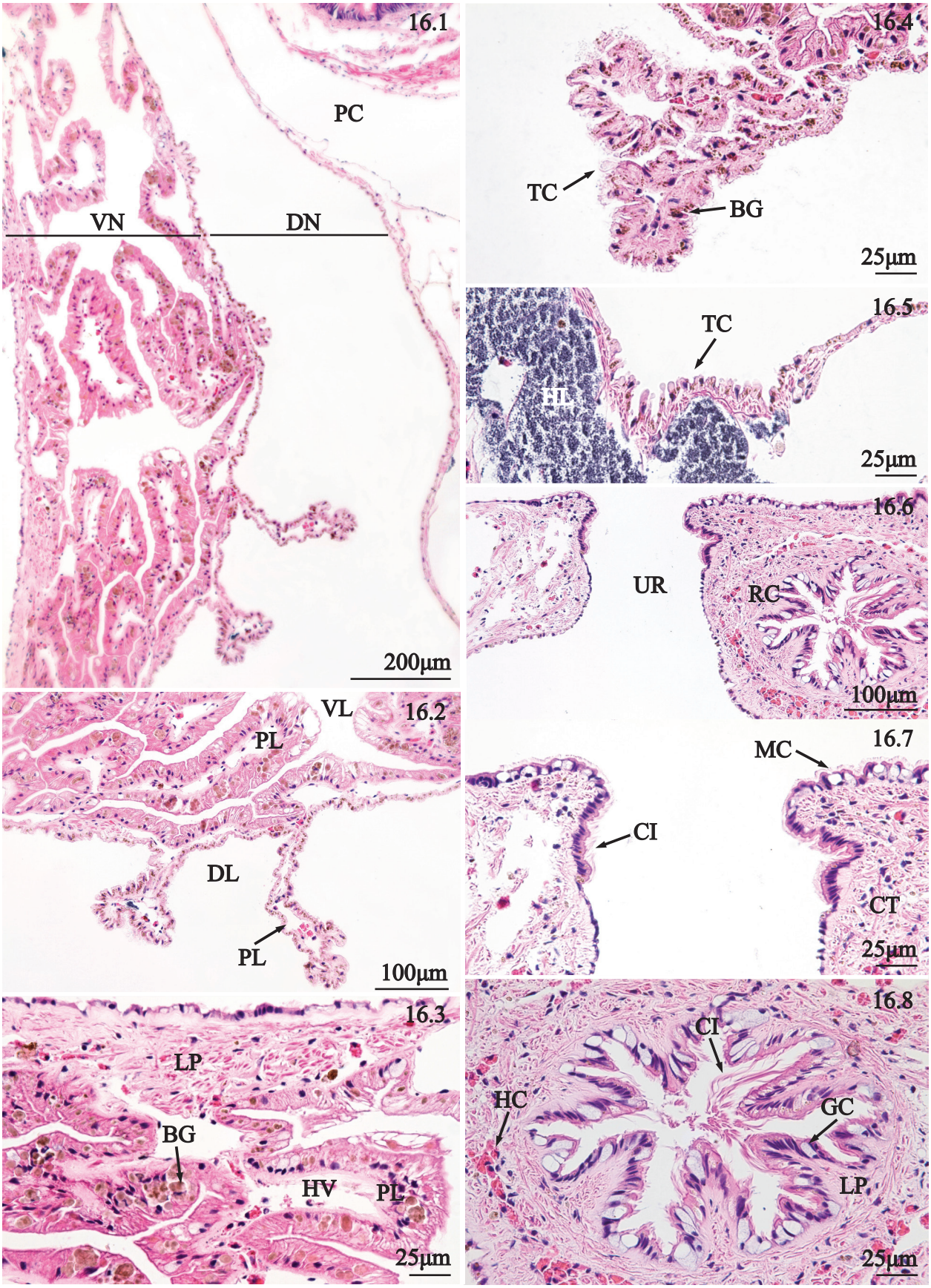
16.1
PC
VN
DN
200µm
16.2
VL
PL
DL
PL
100µm
16.3
LP
BG
HV
PL
25µm
16.4
TC
BG
25µm
16.5
TC
HL
25µm
16.6
UR
RC
100µm
16.7
MC
CI
CT
25µm
16.8
CI
HC
GC
LP
25µm

PLATE 17. Posterior nephridium of *Villosa nebulosa*. 1. Transverse section of the posterior end of the nephridium featuring a convoluted epithelium (CE), expansive nephridial lumen (NL), juxtaposed to the posterior pedal retractor (PR), and a large nerve (NE). 2. Transverse section of posterior nephridium portraying vesiculated columnar cells of convoluted epithelium (CE), and an underlying hemolymph vessel (HV). 3. Transverse section of the posterior nephridium showing a septum of connective tissue (CT) dividing the sinistral and dextral portions of the nephridium, and a pair of nerves (NE). 4. Transverse section of a large hemolymph vessel comprised of wavy myofibers (MF) and myocyte nuclei (MN) located medially to the sinistral and dextral nephridia. 5. Transverse section of pedal retractor (PR) displaying the thin perimysium (PM) surrounding the musculature, and neighboring nephridial epithelium (NE). 6. Transverse section of the posterior pedal retractor revealing densely packed myofibers (MF), and myocyte nuclei (MN). 7. Sagittal section of posterior adductor displaying thick chords of myofibers (MF), and myocyte nuclei (MN).

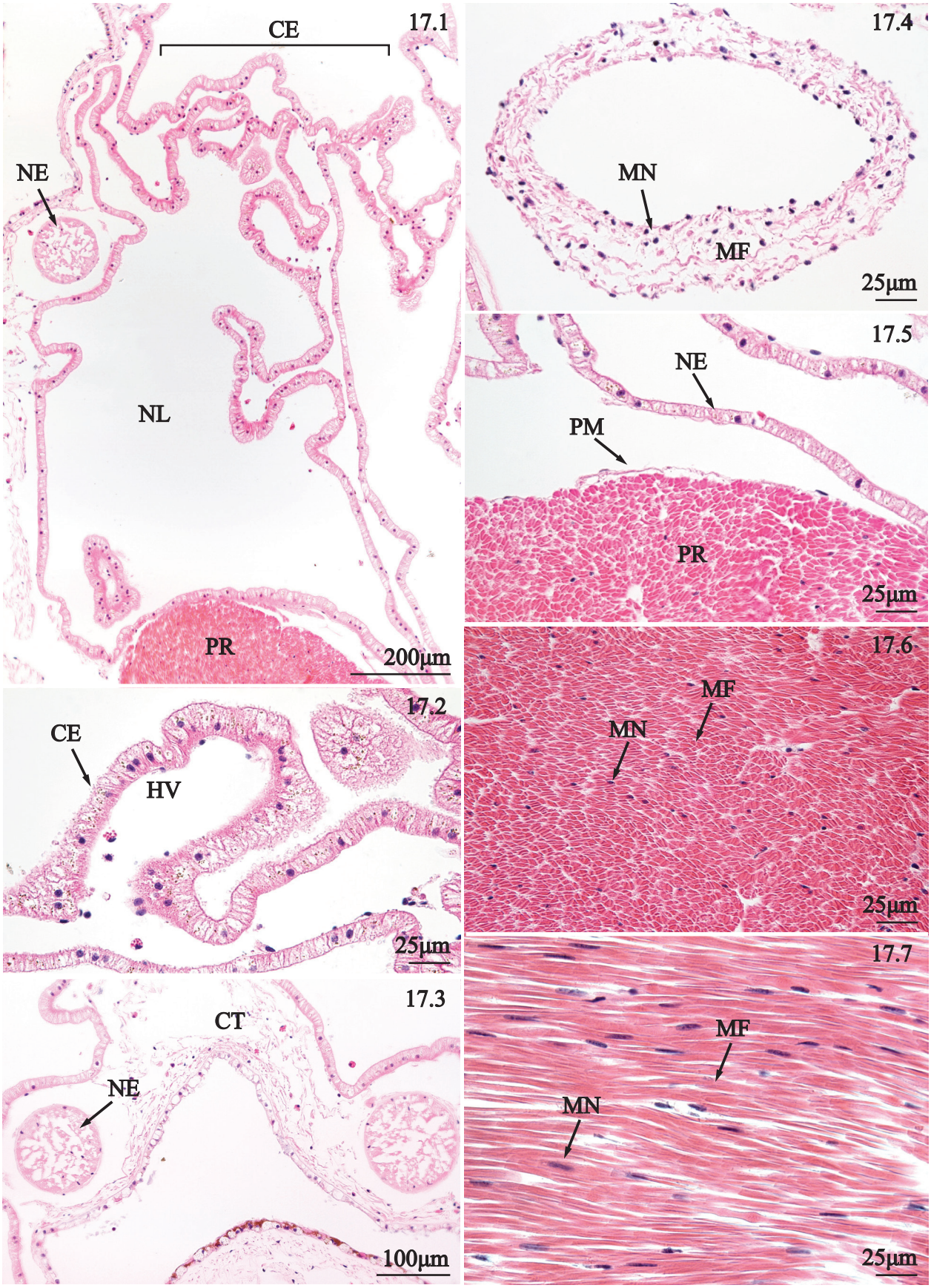
17.1
CE
NE
NL
PR
200µm
17.2
CE
HV
25µm
17.3
CT
NE
100µm
17.4
MN
MF
25µm
17.5
NE
PM
PR
25µm
17.6
MF
MN
25µm
17.7
MF
MN
25µm

PLATE 18. Pedal ganglion of *Villosa nebulosa*. 1. Transverse section of pedal ganglion portraying neural cortex (CO), neural medulla (ME), ventral fissure (VF), dorsal fissure (DF), central commissures (CC), and roots (RO). 2. Transverse section of the dorsal margin of the pedal ganglion revealing the median dorsal fissure (DF), hemocytes (HC), central commissures (CC), and neuron cell bodies (CB). 3. Transverse section of pedal ganglion medulla displaying cell bodies (CB), and axons (AX). 4. Transverse section of the pedal ganglion median where central commissures (CC) of axons communicating with the sinistral and dextral hemispheres. 5. Transverse section of the ventro-lateral aspect of the pedal ganglion revealing the medulla (ME), neural cortex (CO), perineurium (PN), and a ventral root (VR).

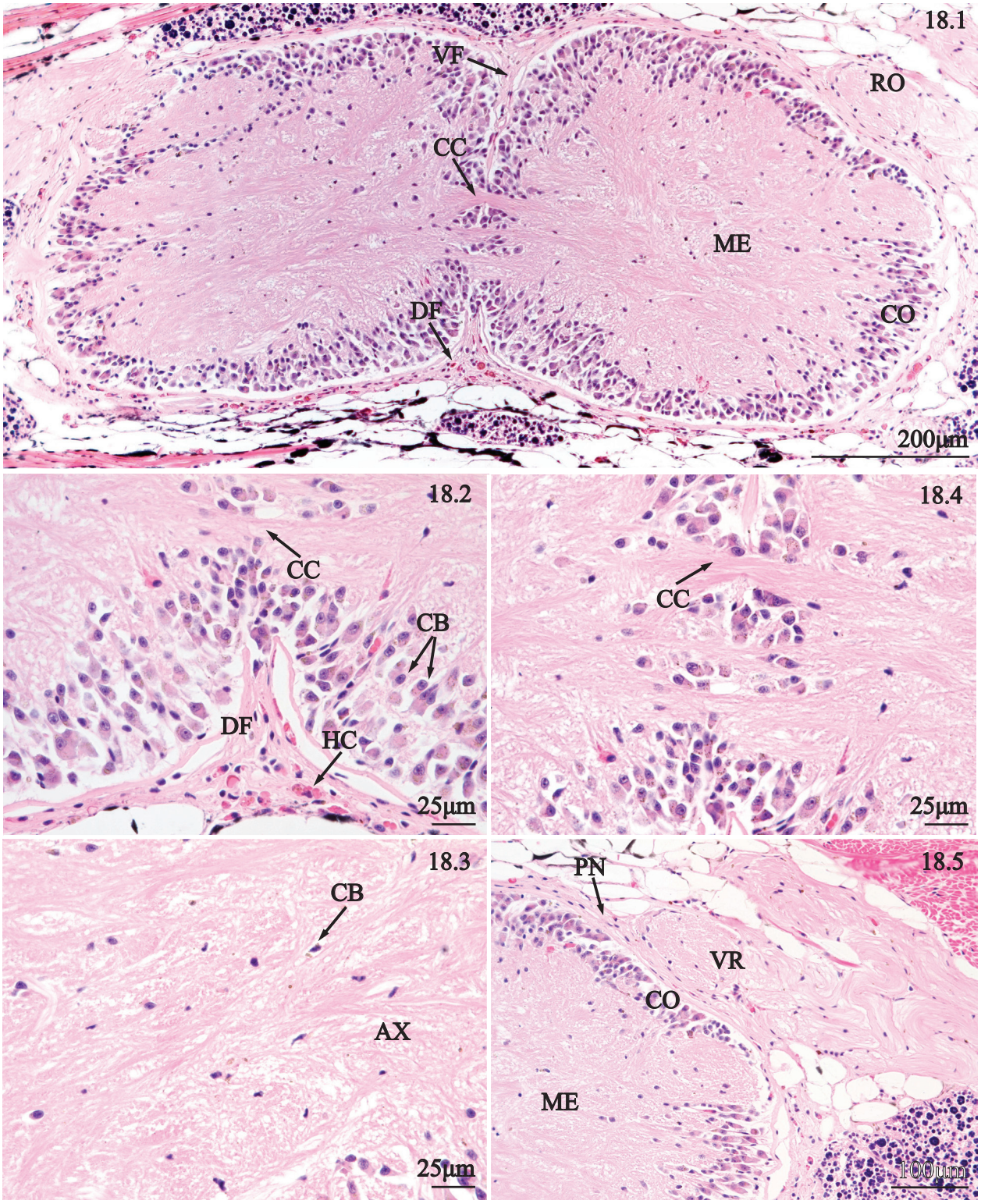
18.1
VF
RO
CC
ME
DF
CO
200µm
18.2
CC
CB
DF
HC
25µm
18.4
CC
25µm
18.3
CB
AX
25µm
18.5
PN
VR
CO
ME
100µm

PLATE 19. Cerebral ganglion, and visceral ganglion of *Villosa nebulosa*. 1. Sagittal section of anterior visceral mass showing the anterior adductor (AD), anterior pedal retractor (PR), and anterior ganglion (AG) with distinct neural cortex (CO), neural medulla (ME), and nerves (NE). 2. Sagittal section of posterior adductor (AD) emphasizing the posterior ganglia (PG) with distinct neural cortex (CO) and neural medulla (ME) located along the ventral surface of the posterior adductor (AD). 3. Transverse section of the free dorsal margin of the ctenidia anterior to the posterior adductor, emphasizing nervous tissue (NE) enclosed by musculature (MU) and teardrop cells (TC). 4. Sagittal section of the ventral margin of the posterior ganglion highlighting neuron cell bodies (CB), axons (AX), connective tissue (CT), goblet cells (GC) and cuboidal epithelium (CE) of the overlying the ganglion.

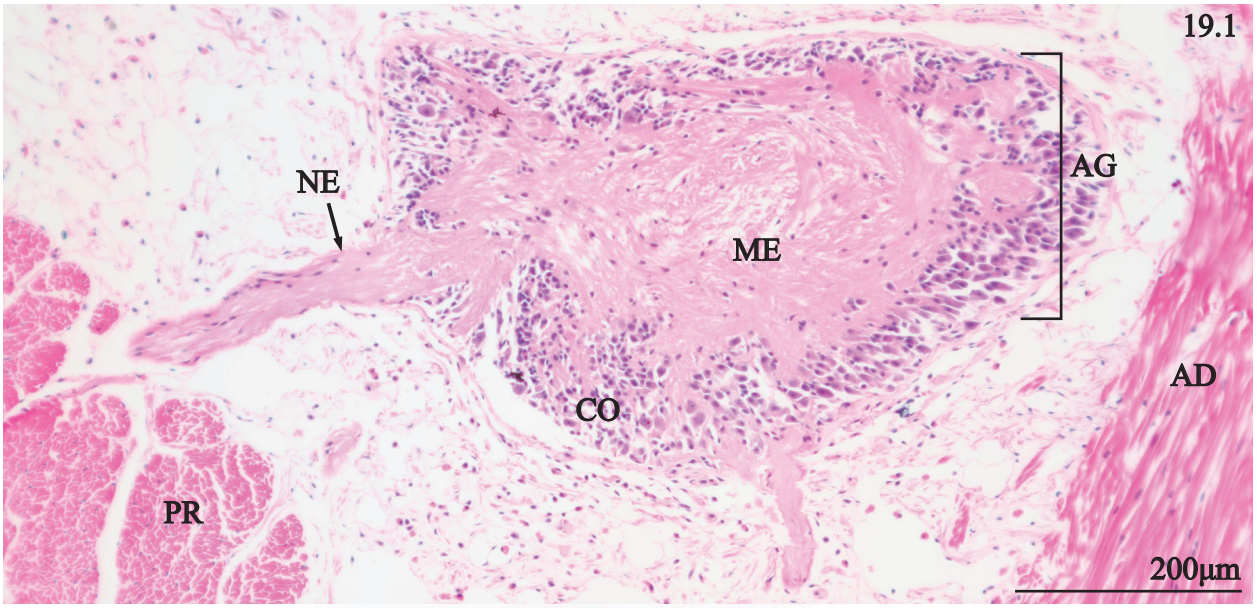
19.1
NE
AG
ME
AD
CO
PR
200µm

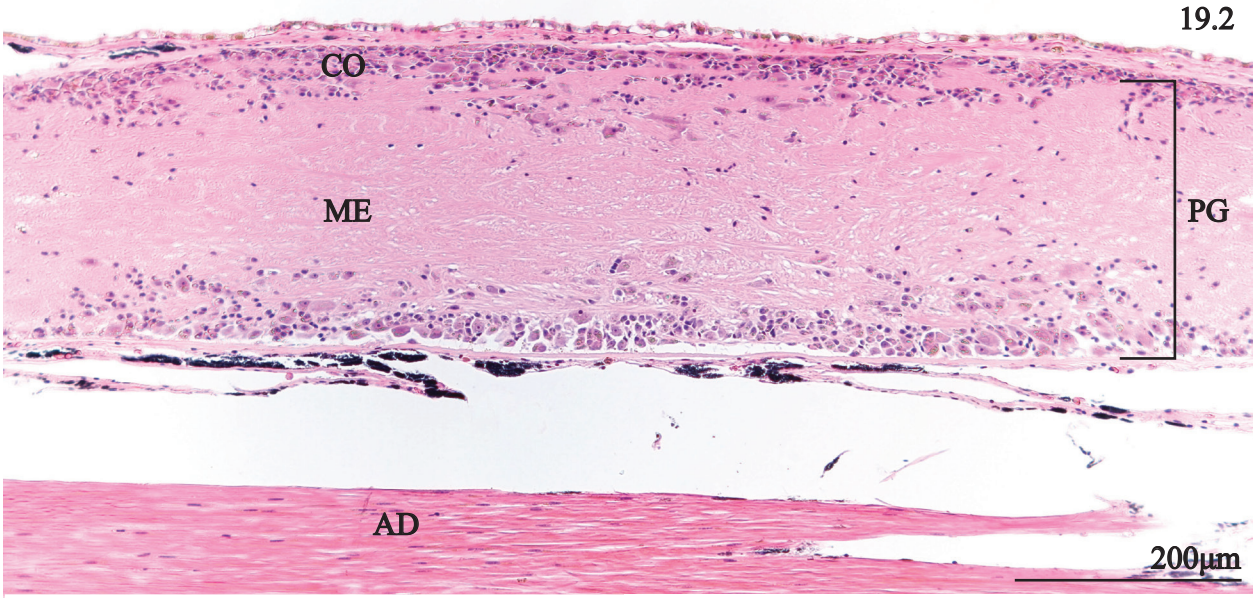
19.2
CO
ME
PG
AD
200µm

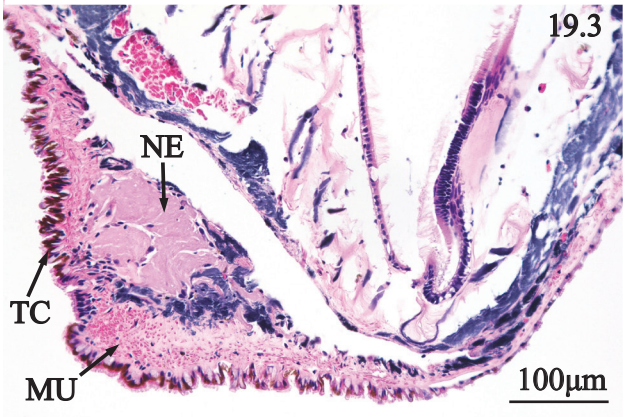
19.3
NE
TC
MU
100µm

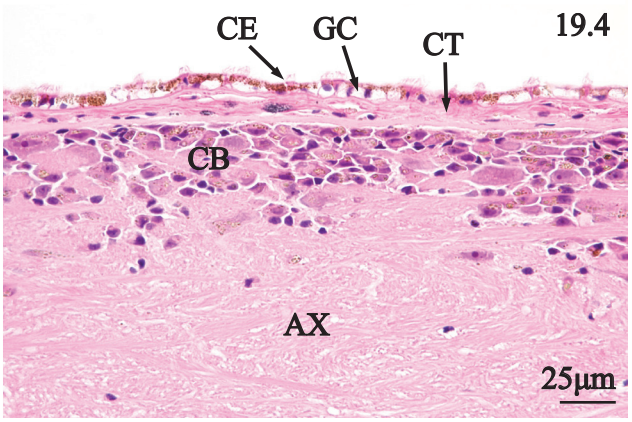
19.4
CE
GC
CT
CB
AX
25µm

PLATE 20. Nerves, and statocysts of *Villosa nebulosa*. 1. Transverse section of the lateral margin of the coelom revealing a visceral nerve (NE) between testicular acini (TA) and ciliated gonadal ducts (CD). 2. Sagittal section of posterior mantle edge portraying a pedal nerve branch (NE), foot musculature (FM). 3. Transverse section of a nephridial nerve with a distinct perineurium (PN), nerve fibers (NF) surrounded by concentric layers of musculature (MU). 4. Sagittal section of posterior mantle edge portraying pedal nerve branches (PN), musculature (MU), hemolymph sinuses (HS), and papillae (PA). 5. Transverse section of visceral mass revealing a statocyst (SC), connective tissue wrapping (CT), testicular acini (TA), and foot musculature (FM). 6. Transverse section of a statocyst emphasizing the ciliated columnar cells (CC) and a spherical statolyth (SL).

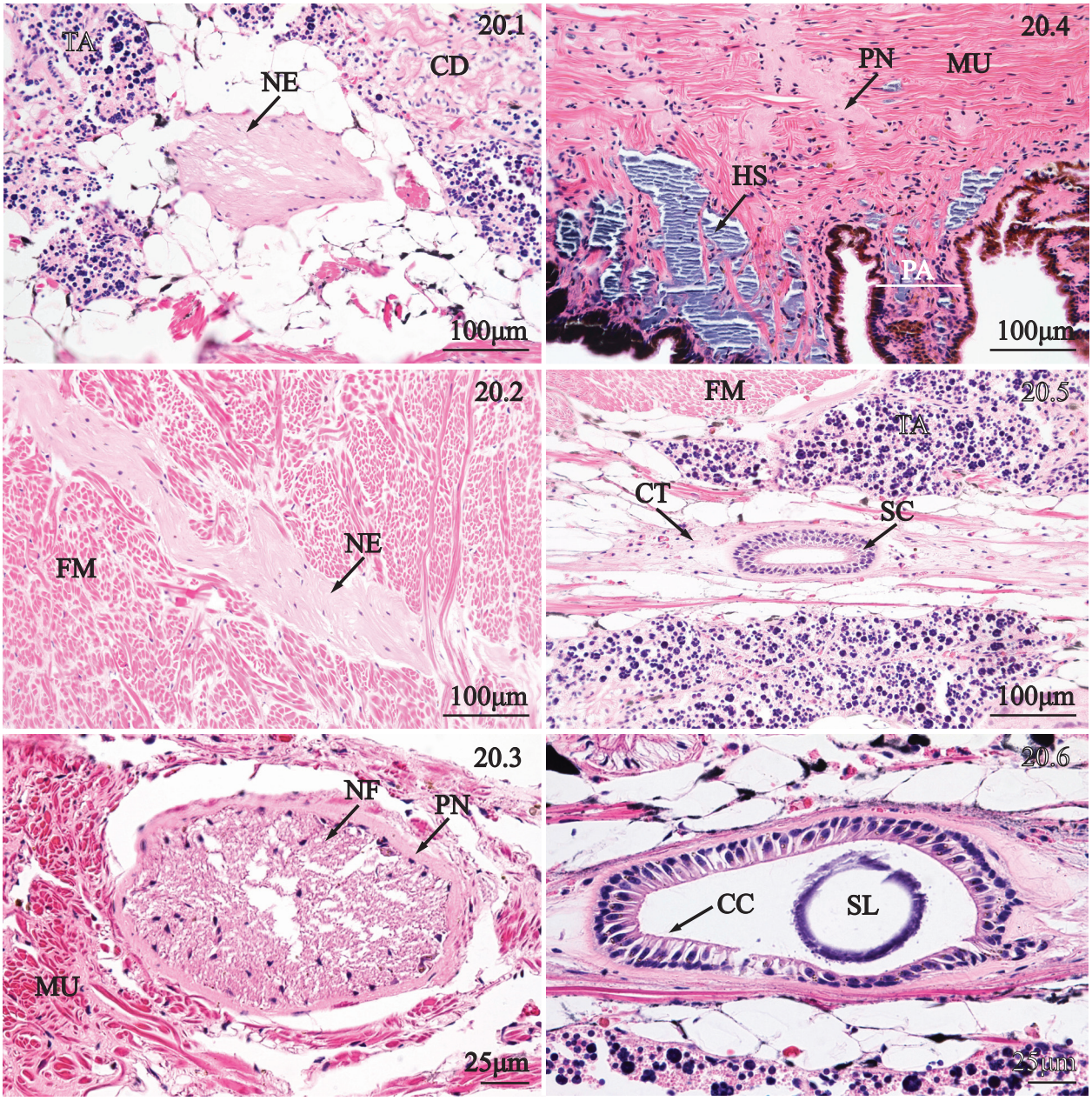
20.1
TA
CD
NE
100μm
20.4
PN
MU
HS
PA
100μm
20.2
FM
NE
100μm
FM
20.5
TA
CT
SC
100μm
20.3
NF
PN
MU
25μm
20.6
CC
SL
25μm

PLATE 21. Ovarian acini, testicular acini, and ciliated gonadal ducts of *Villosa nebulosa*. 1. Transverse section through the visceral mass of an adult female collected in May 2010 displaying a series of immature ovarian acini (OA), and ciliated gonadal ducts (GD). 2. Transverse section through the visceral mass of an adult female collected in May 2010 emphasizing immature oocytes (OC), cell body (CB), and the squamous epithelial lining of acini (SE). 3. Transverse section of a mature ovarian acinus of an adult female collected in August 2011 showing mature oocytes (MO), surrounded by vitelline (VI). 4. Transverse section through the visceral mass of an adult male collected in May 2010 portraying a series of immature testicular acini (TA) and ciliated gonadal ducts (GD). 5. Transverse section of immature testicular acini of an adult male collected in May 2010 portraying a preponderance of sperm morula (SM) within the acini, and ciliated gonadal ducts (GD) in close proximity to testicular acini. 6. Transverse section of mature testicular acini of a male collected in August 2011 emphasizing spermatogenesis (SG) and a preponderance of spermatozoa (SZ) in the lumen. 7. Transverse section through the visceral mass of a mature male collected in August 2011 portraying spermatozoa (SZ) traveling dorsally through a duct by means of cilia (CI). 8. Transverse section of the dorso-lateral portion of the visceral mass emphasizing the sinistral gonadal pore (GP) dorsal to the gill (GI).

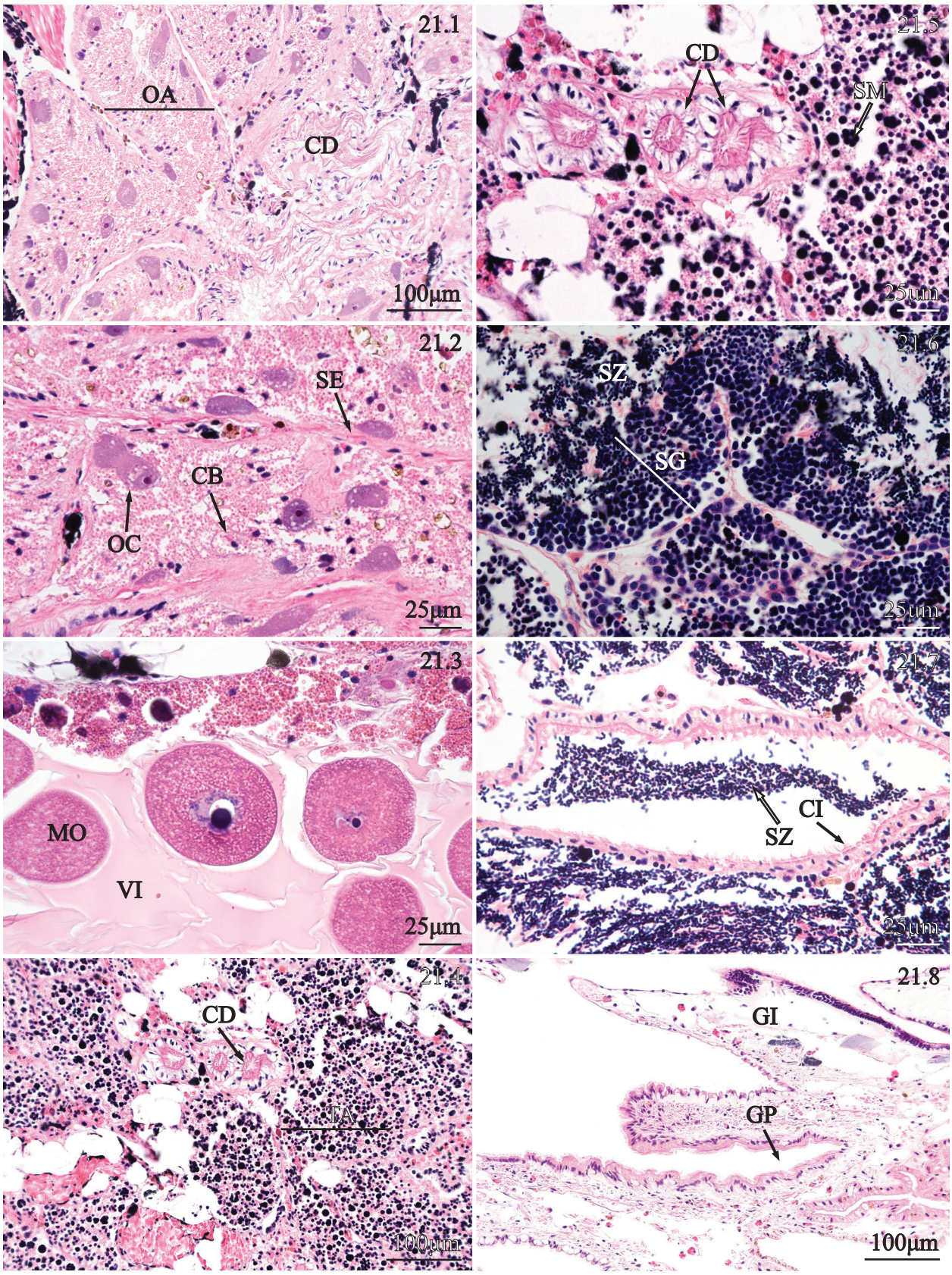
21.1
OA
CD
100μm
21.2
SE
CB
OC
25μm
21.3
MO
VI
25μm
21.4
CD
TA
100μm
21.5
CD
SM
25μm
21.6
SZ
SG
25μm
21.7
CI
SZ
25μm
21.8
GI
GP
100μm

Chapter 5

SHELL MORPHOLOGY, GROSS ANATOMICAL FEATURES OF THE MANTLE CAVITY, AND CELLULAR STRUCTURE OF MANTLE, GILL, FOOT, AND VISCERAL MASS OF THE GULF PIGTOE, *Fusconaia cerina* (CONRAD, 1838)

5.1. Shell morphology

The valves of *F. cerina* from Cahaba River are circular to rhomboidal and a well-defined posterior ridge may be present, represented by an obliquely oriented convex line. Shells are typically thick or heavy with a dark brown epidermis. The anterior and posterior margins are broad, but truncated in length. The umbo is broadly conical, high, extending beyond the hingeline. Furthermore, *F. cerina* from Cahaba River typically exhibit an inflated shell and umbo arches or curles dorsally to meet the hinge line (Fig. 22.1, 22.2). The nacre is white with a strongly developed and somewhat cuboidal pallial line. Anterior and posterior adductor scars are conspicuous with a somewhat irregular surface. Anterior adductor sacr is deeply inset and parallel with the anterior margin while the posterior adductor scar is shallow, parallel with the posterior margin. Pseudocardinal teeth are strongly developed with two on the left valve and one tooth located on the right valve, pseudocardinal teeth have a rough or grooved surface. Lateral teeth are strongly developed with two on the left valve and one on the right valve. Considering the arched umbo, there is a correspondingly deep umbo cavity. Additionally, the ligament is typically cylindrical, brown, and thickened along the dorsal margin (Fig. 22.3, 22.4).

5.2. Gross anatomical features of the mantle cavity

Fusconaia cernia were collected in shoal habitats in gravel or sandy substrate. Incurrent and excurrent apertures are lined with papillae and especially along the incurrent margin, papillae are conical to branched (Fig. 22.5). The body of F. cerina is typically pallid, grey to white. However, the mantle, foot and gill may become red to orange when mature. Inner and outer gills are broad and arched over the posterior adductor. Females are tetragenous brooders and each gill may be filled with linear or subcylindrical masses of embryos or conglutinates. Mature conglutinates may be red to orange and fill most of the vertical volume of the marsupial water

tubes (Fig. 22.6). During the summer months, white ovigerous female F. cerina may be collected. Conglutinates from white females consist entirely of unfertilized ova whereas mature, red to orange conglutinates consist of colored, developing embryos or glochdia adhered to unfertilized, white ova (Fig. 22.7). The mantle edge has a homogenous coloration with a fine, brown line across the ventral margin. Papillae along the siphonal aperrtures are located along a truncated posterior margin and appear mottled, brown to white. The foot of *F. cerina* is broad, and the visceral mass is creamy white. The mantle isthmus is broadly rounded and extends deep into the cavity between the sinistral and dextral dorsal margins (Fig. 22.8).

5.3. Cellular structure of mantle

5.3.1. Anterior mantle edge

The anterior portion of the mantle edge (lateral to labial palps) of *Fusconaia cerina* bears the same cell types as the anterior mantle edge of *Villosa nebulosa*. However, there are unique morphological features of mantle edge epithelium of *F. cerina* not observed on *V. nebulosa*. The outer mantle edge epithelium spanning the distance between the pallial line and outer lobe is sinuous and there are crypts along the ventral surface of the outer mantle lobe (Fig. 23.1, 7). The outer mantle lobe is branched with as many as three lobes, and the distal tip of each branch is bluntly rounded (Fig. 23.3). Each branch of the outer mantle lobe is pleated, and plicae are irregular such that each extension of the outer lobe is asymmetrical. The basal bulb of *F. cerina* is rounded posteriorly, differing from the flattened, cleft of *V. nebulosa* (Fig 23.2). The middle mantle lobe of *F. cerina* is bulbous with eosinophilic squamous cells extending approximately half the length of the ventral surface before abruptly becoming columnar. Given the abrupt transition from squamous to columnar, and considering how columnar cells maintain the same cytological characteristics as the squamous cells, these two cell types may differ only in

orientation (Fig. 23.4). Inner mantle lobe of *F. cerina* is triangular and plicated, but unlike *V. nebulosa*, the columnar cells along the inner surface of the inner mantle lobe appear to lack brown intracellular granules (Fig. 23.5). Inner lobe epithelium consists of irregularly shaped plicae becoming teardrop-shaped along the dorsal surface (Fig. 23.6). The columnar epithelium along the ventral surface of the mantle edge is wavy and isolated goblet cells may be interspersed among epithelial cells (Fig. 23.7)

5.3.2. Posterior mantle edge, middle mantle, and mantle isthmus

Posterior mantle edge was sampled adjacent to the posterior adductor. Posterior mantle edge of *F. cerina* maintains the same cell types from the anterior, but the shape of the mantle lobes is different (Fig. 24.1). Outer lobe is forked with minor epithelial undulations along the dorsal and ventral branches. The middle lobe is cylindrical and pleated along its dorsal surface and the inner lobe is broader at its base than it is anteriorly. Papillae along the posterior margin of *F. cerina* mantle edge primarily differ from *V. nebulosa* in appearing bluntly rounded to branched (Fig. 24.2). The columnar epithelium and musculature of *F. cerina* mantle edge papillae is indistinguishable from *V. nebulosa* (Fig. 24.3).

The middle mantle of *F. cerina* has an outer columnar epithelium, inner cuboidal epithelium, and subepithelial strata consisting of loose connective tissue fibers and hemolymph. (Fig. 24.4) The cellular composition of the middle mantle is not different from *V. nebulosa*.

Mantle isthmus of *Fusconaia cerina* is a well-defined median extension of mantle tissue. The dorsal epithelium around the visceral mass consists of pale eosinophilic columnar epithelial cells similar to the columnar epithelium of middle mantle. Isthmus epithelium is cuboidal along the lateral surfaces and basophilic columnar cells are localized to the dorsal margin (Fig. 24.5).

Additionally, isthmus epithelium features sparsely distributed goblet cells and a wavy subepithelium of connective tissue fibers and hemolymph.

5.4. Cellular structure of gill

5.4.1. Non-marsupial gill

Ctenidia of *Fusconaia cerina* feature cylindrical filaments across each inner and outer lamina, united by septa and vertical water tubes (Fig. 25.1). Tissue structure of each ctenidial face consists of cylindrical filaments with frontal, frontal-lateral, and lateral groups of ciliated cells across the apical surface. Filaments are occasionally separated by ostia, communicating with median water tubes and each filament has a medially located blood sinus. Each inner and outer lamina of a demibranch is joined by a septum, and septa possess teardrop-shaped goblet cells (Figs. 25.2). The distal margin of the outer gill has a rounded surface resembling the fusion of ctenidial filaments while the inner gill features a median, ciliated furrow (Figs. 25.3, 4).

Fusconaia cerina from Cahaba River (Shelby Co., AL) have a deep umbo cavity and a correspondingly arched abdomen represented by an expansive latticework of loose connective tissue and hemolymph. The cellular features of the base of the ctenidia of *F. cerina* and *V. enbulosa* are identical, however there are two structural features at the base of the ctenidia of *F. cerina* that differ from *V. nebulosa*. The inner lamina of *F. cerina* inner gill is attached at the anterior end of the visceral mass near the labial palps and becomes detached along the length of the body (Fig. 25.5) until the posterior adductor where it reattaches to the integument ventral to the posterior adductor. The inner ctenidium of *V. nebulosa* is attached to the visceral mass fro approximately half of its length. Secondly, muscle fascicles along the base of the ctenidia of F. cerina are most conspicuous in the posterior region of the body between the heart and posterior adductor (Figs. 25.6, 7). In contrast, the muscular supporting rods of *V. nebulosa* are

conspicuous throughout the length of the ctenidia. The junction of the outer lamina of outer ctenidium and middle mantle in *F. cerina* appears no different from *V. nebulosa* (Fig. 25.8).

5.4.2. Marsupial gill

Female *Fusconaia cerina* utilize both pairs of inner and outer ctenidia for larval incubation. Fertilized and unfertilized ova are packaged into strings or conglutinates and transported into the ctenidial water tubes such that a large proportion of the vertical length of the gill may be occupied by conglutinates. Marsupial ctenidia feature enlarged water tubes and intrabranchial septa as compared to male demibranchs (Fig. 26.1). Filaments, ostia and ctenidial vasculature of marsupial ctenidia appear to be no different from the structural elements of male ctenidia (Fig. 26.2). The main cytological difference between male and marsupial female ctenidia are the thickened septa. Septa have a broad, triangular base and generally become narrow at the water tube midline (Figs. 26.1, 2). Septum epithelium is pleated and typically there is a prominent, median fold extending into the water tube lumen. The epithelium of intrabranchial septa consists of teardrop-shaped columnar cells and goblet cells and septa contain an irregular subepithelium of fibrous tissue and a pale, eosinophilic ground substance (Fig. 26.4). In gravid female *F. cerina* collected from Cahaba River (Shelby Co., AL) in May 2011, water tubes contained clusters of unfertilized ova and spherical, early-stage embryos (Figs. 26.1-3). Morphologically, the unfertilized ova and early stage embryos are spherical and possess a series of sinuous branches extending from the surface of the ova (Fig. 26.3). Branches have a pale, basophilic pigmentation and typically have a sharply defined border similar to the appearance of a ribbon of periostracum. Embryos are typically spherical while unfertilized ova tend to have an irregular shape in histological sections. Unfertilized ova have an eosionphilic, homogenously granular composition, while early stage embryos are multinucleated, but lacking apparent cell membranes.

Nuclei of early-stage embryos are spherical and a small nucleolus may be observed in some cells. In female *F. cerina* collected from Cahaba River in August 2011, conglutinates had been shed, but the marsupia maintained the same histological characteristics as a filled ctenidium (Fig. 26.5).

5.5. Cellular structure of foot and associated tissues

5.5.1. Pedal musculature and byssal gland

At low magnification, and in a transverse plane of section, pedal tissue of *Fusconaia cerina* is characterized by a median triangle of somatic musculature flanked by strongly basophilic regions of chromatocytes (Fig. 27.1). The ventral margin has dark-staining and pale-staining basophilic chromatocytes intertwined among myofibers (Fig. 27.2). Granulocytes continue dorsally to the terminus of type-three epithelium. Pedal musculature consists of a ventral irregular or woven region with distinct horizontal and vertically oriented myofibers (Fig. 27.3) while the base of the foot consists of well-defined layers of vertical and horizontally oriented musculature (Fig. 27.4)

Fusconaia cerina has a diamond-shaped byssal gland located posterior to the pedal ganglion. The luminal surface of the byssal gland is ciliated with an emarginated epithelium and a densely fibrous subepitheium (Figs. 27.5, 6). There are a series of small, spherical, ciliated structures in the posterior region of the foot, possibly representing disconnected remnants of the byssal canal. Sagittal sections of *F. cerina* foot reveal groups of spherical, ciliated structures in an oblique, linear path between the dorsal base of the foot, where the coelomic cavity joins the pedal musculature, and the posterior margin of the pedal integument. Byssal canal remnants consist of a ciliated, columnar epithelium surrounding a lumen filled with debris. Luminal contents of byssal canal may appear to be a shapeless eosinohilic mass material, or a darkened, granular material (Fig. 27.7).

5.5.2. Pedal integument and mesentery

Pedal integument of *F. cerina* consists of five regions from ventral to dorsal. The most distinguishing cytological characteristic of *F. cerina* is the preponderance of violet chromatocytes in the ventral portion of the foot. The abundance of chromatocytes is so high that histological sections of foot have a distinctive violet tinge (Fig. 28.1). Type one epithelium of *F. cerina* is densely ciliated consisting of rectangular plicae (Fig. 28.1). Granulocytes within the subepithelium of type one plicae appear dorsoventrally compressed. Chromatocytes underlying type one plicae of *F. cerina* are so densely packed that it is difficult to determine the boundaries of some cells. Tall rectangular plicae become narrower and diminish in height between integumentary regions two and three (Figs. 28.2, 3). Plicae of F. cerina diminish to a simple columnar epithelium featuring subtle undulations in integumentary region four (Fig. 28.4). Columnar cells of integument four are ciliated and numerous goblet cells are present. Type four integument of *F. cerina* has a distinct subepithelium of connective tissue fibers overlying hemolymph sinuses and somatic musculature. Integumentary region five of *F. cerina* features a simple cuboidal epithelium, goblet cells and sparsely distributed tufts of cilia. Subepithelium of region five features a thin hemolymph sinus juxtaposed upon blocks of somatic musculature (Fig. 28.5). Overall, the integument around the foot is deeply sinuous at the ventral margin and flattened at the dorsal extent (regions four and five). The ventral portion of the foot, as seen in sagittal sections, is highly rugose and irregular (Fig. 28.6).

Histological sections of visceral mass reveal numerous horizontally to obliquely oriented bands of mesentery spanning coelom (Fig. 28.7). Bundles of mesentery are characterized by a series of eosinophilic filaments with slender, basophilic nuclei. Sagittal sections of coelom reveal a preponderance of mesentery fascicles throughout the coelom (Fig. 28.8).

5.6. Anterior adductor and anterior pedal protractors

Myofibers of the anterior protractors have a dark eosinophilic composition, and the tissue features distinct fascicles (Fig. 29.6). Adductor muscle features large fascicles and conspicuous permysium containing capillaries (Fig. 29.3). Myofibers of the anterior muscle group consists of spindle shaped cells with cylindrical nuclei. Fascicles are well organized and in sagittal sections, musculature has a woven appearance.

5.7. Cellular structure of digestive system tissues

5.7.1. Labial palps, oral groove, and esophagus

Labial palps of *Fusconaia cerina* feature plicae along the inner surface and a smooth outer surface (Fig. 29.1). Plicae of the inner surface are bulbous at the distal margin and have two small epithelial folds along the stem (Fig. 29.2). Ciliated columnar cells represent the main constituent of the inner palp epithelium and extend along the palp interior until the distal margin of each lip. The distal margin of the palp features prominent goblet cells the tissue transitions to a flattened epithelium (Fig. 29.5). The outer surface of each palp features a flattened epithelium with teardrop-shaped columnar cells (Fig. 29.4). Subepithelial strata of each palp is represented by eosinophilic fibers and a pale ground substance (Figs 29.2, 4)

Oral groove of *F. cerina* resembles a deep cavity located posteriorly to the anterior adductor. At the ventral entrance to the oral groove, there are two cylindrical extensions of tissue histologically resembling labial palp. The epithelium consists of teardrop-shaped columnar cells along the ventral surface and a pseudostratified, ciliated epithelium along the dorsal surface. The tip of each cylindrical extension of oral groove entrance consists of a preponderance of goblet cells. Subepithelium of the cylindrical extensions consists of muscle fibers and hemolymph sinuses (Fig. 30.1). Lateral to the cylindrical extensions, the walls of the oral groove curves

dorsally and become vertically oriented. The curved portion of the oral groove wall is pleated, while the straight or vertically oriented extent of the walls consists of uniform line of ciliated columnar cells (Figs. 30.2-3). Ciliated columnar cells of oral groove walls feature an eosinophilic cytoplasm and a homogenous, basophilic nucleus. The dorsal floor of the oral groove features ciliated plicae. Plicae of the dorsal aspect of the oral groove are histologically similar to the plications along the curved portion of the walls located at the ventral side of the organ.

The esophagus is an ovular tube characterized by deep sinuous folds extending into the lumen from the dorsal and ventral surfaces (Fig. 30.5). Esophagus has a well-defined lamina propria consisting of loose connective tissue fibers and a pale ground substance. Esophageal epithelium consists of ciliated columnar cells arranged along tall, rectangular to "Y"-shaped plicae (Fig. 30.4).

5.7.2. Digestive diverticulum

The stomach is a large rectangular chamber located in the medial aspect of the digestive diverticulum. The anterior portion of the stomach mainly comprises sinuous, ciliated ducts leading to the tubules of the digestive diverticulum. The esophagus of *F. cerina* enters the stomach on the left side of the body. The esophageal-stomach unction is characterized by a median typhlosole along the ventral surface of the esophagus. The typhlosole has a flattened, rectangular tip and a pleated stem. The ventral wall of the esophagus bends ventrally creating a rounded, sinistral fold of rounded plicae (Fig. 31.1). Rounded plicae feature ciliated columnar cells and such plicae are a repetitive feature of the stomach walls (Fig. 31.2). In contrast, the dorsal and lateral walls of the esophageal-stomach junction largely lack epithelial folds. Subepithelium of the stomach possesses a well-defined lamina propria.

Fusconaia cerina has primary, secondary and tertiary digestive tubules. The ciliated primary tubules feature thin, ciliated plicae extending to the midpoint of the lumen (Fig. 31.3). Given the compressed morphology of the plicae nuclei of the columnar cells are densely packed and created an accentuated basophilic stem of each individual plication. Additionally, cytoplasm of ciliated columnar cells lining the plicae has a strong eosinophilic characteristic (Fig. 31.4). Secondary tubules of *F. cerina* are similar feature columnar cells with an eosinophilic and vesiculated cytoplasm and apical microvilli (Fig. 31.5). However, columnar cells of secondary tubules tend to curl or become teardrop-shaped at the junction of tertiary tubules. The morphology of secondary tubule cells creates the appearance of cycle-shaped valves extending into the lumen of tertiary tubules (Fig. 31.6). Tertiary tubules have a vesiculated and eosinophilic cytoplasm. The nuclei of tertiary tubule cells have a strongly basophilic, triangular region containing a spherical nucleus, typically with a distinct nucleolus (Fig. 31.7).

5.7.4. Stomach

The main stomach chamber begins on the dextral side of the body. Transverse histological sections of the anterior visceral mass reveal a large triangular chamber located on the dextral side of the body. The shape of the chamber resembles a compressed pyramid, with the flattened, base of the pyramid oriented vertically and the apex in the sinistral direction. The apex of the pyramidal chamber unites with the main stomach chamber at the approximate vertical and horizontal midpoint of the anterior visceral mass. The stomach may contain layered mucoid masses that resemble the crystalline style or gastric shield (Fig. 32.1). Additionally there may be a less dense eosinophilic fluid surrounding the ciliated epithelium. The surface of the ciliated epithelium features small eosinophilic spheres possibly representing secretions or fluid agitated by ciliary action (Fig. 30.2).

At its widest portion, the stomach resembles a larege bag with a curved dextral wall and flattened dorsal, sinistral and ventral walls. Small, rounded, ciliated plicae are located throughout the lining of the stomach and some areas appear to be secreting an eosinophilic material into the lumen (Fig. 30.3). The junction between the bag-like dorsal portion of the stomach and the ovular, ventral stomach chamber features thin columnar cells with an eosinophilic, gelatinous covering (Fig. 32.4). A forked typhlosole extends obliquely into the the lumen of the stomach and possesses a conspicuous gelatinous coating (Fig. 32.5).

Ventral to the rectangular portion of the stomach is a large, ovular chamber leading to the crystalline style sac. The ventral wall has an irregular surface with numerous typhlosoles. There is a cycle-shaped sinistral wall leading to digestive diverticula, and a semicircular, dextral wall, also with digestive diverticulum ducts. A cylindrical typhlosole extends dorsally into the lumen of the ventral stomach chamber (Fig 33.1). Typhlosole epithelium consists of pale, eosinophilic, columnar cells bearing cilia. The epithelium surrounding the typhlosole appears pseudostratified, reflecting a rounded surface (Fig. 33.2). Directly dextral to the median typhlosole is a cone-shaped plication (Fig. 33.3. Epithelial cells along the surface of the cone appear indistinguishable from epithelium of the adjacent typhlosole. Between the cone and the oblique typhlosole, marking the junction between the ventral and dorsal stomach chambers, epithelial cells a columnar and ciliated and the epithelium lacks prominent plicae or typhlosoles. However, the apical surface of the ciliated epithelium varies between a covered or cuticularized epithelium (Fig. 33.4), to a ciliated surface lacking a distinct covering (Fig. 33.5).

5.7.4. Crystalline style sac

The crystalline style begins as a dorsal outpouching of the dorsal stomach chamber. The style sac consists of a large spherical chamber or style sac (Fig. 34.1), and a horizontal stem canal or

midgut (Fig. 34.2). The crystalline style is an eosinophilic rod style within the style sac extending anterior to posterior throughout the length of the style sac. Style sac epithelium consists of two types of ciliated columnar cells, herein referred to as types one and three. Type one epithelium lines the majority of the style sac and is represented by dark-staining, eosinophilic columnar cells with straight cilia. (Fig. 34.1). Type one epithelium consists of a single layer of cells and the luminal surface is almost completely rounded except for a slight sinistral and dextral cavitation. Type three epithelium is restricted to a small region of the dorsal style sac wall representing a junction between epithelium type one and type two epithelium of the stem canal (Fig. 34.3). Type three epithelium is pseudostratified consisting of thin, basophilic, ciliated columnar cells. Stem canal is a straightened chamber lateral to the style sac ending in a small, spherical chamber at the distal end (Fig. 34.4). In contrast to type one epithelium, the ciliated columnar type two cells of the stem canal have a pale staining cytoplasm and the epithelium is simple to pseudostratified (Figs. 34.3, 5). Crystalline style consists of a dense eosinophilic material that tends to form wrinkles during microtomy. The style appears to be layered with concentric, dark, granular lines. The central layers may contain small particulates and appear broken with an irregular space surrounding such particulate matter (Fig. 34.6).

5.7.5. Intestine

There are two ovular chambers located ventrally to the style sac. The sinistral chamber represents the ascending second intestinal limb while the dextral chamber constitutes the descending third limb (e.g., Fig. 35.1). Crystalline style sac extends posteriorly through the visceral mass, bends dorsally and represents the first intestinal limb. The walls of the first intestinal limb are pleated and deeply sinuous (Fig. 35.2). Subepithelium of first intestinal limb

consists of a well-defined lamina propria supporting the plicae becoming thinner around the straightened portions of the intestinal walls. Epithelium of the intestine alternates between style sac epithelium types one, two and three and creates a heterogenous luminal surface (Fig. 35.3).

In contrast to the sinuous epithelium comprising first intestinal limb, the second limb lacks deep epithelial folds (Figs. 35.1, 4). The ascending second intestinal limb consists of ciliated columnar cells with eosinophilic, granular vesicles. Cilia are thin and filamentous, similar to cilia of style sac type-three epithelium (Fig. 35.5). Transverse sections of second intestine reveal a generally flattened luminal surface (Fig. 35.1) while sagittal sections portray the intestine as a tube with bends characterized by a small inclination. High magnification shows the intestinal epithelium has having a slightly irregular surface (Fig. 35.5). Intestinal limb three represents a continuation of the second limb, but a flattened columnar epithelium is more abundant (Fig. 35.6).

The fourth and fifth intestinal limbs are each characterized by a large typhlosole occupying a large proportion of the lumen. The typhlosole of the fourth intestinal limb extends ventrally into the lumen (Fig 36.1). Ventral epithelium of the fourth intestinal limb is pleated around the lateral portion and smooth along the medial aspect. Epithelial cells of the ventral wall are ciliated and columnar with elliptical eosinophilic, granular inclusions (Fig. 36.2). Dorsal epithelium has a smooth surface, consisting of simple ciliated columnar cells (Fig. 36.3). Subepitheium of intestinal limb four is comprised of a distinct lamina propria containing a series of hemolymph sinuses. Lamina propria supporting dorsal epithelium is expansive while marginal connective tissue of ventral epithelium is thin.

Fifth intestinal limb is analogous to intestinal limb four as the alimentary canal bends dorsally and continues along the hinge towards the posterior adductor. The typhlosole of the

fifth intestinal limb projects dorsally from the base of the visceral mass (Fig. 36.4). Ventral epithelium lining the typhlosole is pleated with tall ciliated columnar cells (Fig. 36.5). Columnar cells of the dorsal epithelium are shorter than typhlosole cells. Dorsal epithelium is pleated around the lateral margins, but generally smooth in the median (Fig. 36.6). Unlike the fourth intestinal limb, dorsal epithelium lacks elliptical eosinophilic inclusions.

5.8. Cellular structure of cardiovascular system tissues

5.8.1. Heart

The most prominent feature of the heart is the thickened, muscular ventricle surrounding the intestine (Fig. 37.1). The ventricle consists of an epicardium, and a thickened myocardium of irregular muscle fibers. Epicardial surface is sinuous with teardrop-shaped cells, some of which have a transparent apical vesicle (Fig. 37.2). Epicardium and myocardium feature red-staining hemocytes between epithelial cells of the epicardium and juxtaposed among myofibers. Cardiac myocytes are spindle-shaped, and form rectangular bands of musculature generally oriented anterior to posterior or dorsal to ventral (Fig. 37.3).

Auricles are thin walled, tubular structures uniting the pericardial wall with the ventricle. Auricles are composed of an outer squamous epithelium, and inner myocardial fibers (Fig. 37.4). Each auricle has a ventral and a dorsal branch and the auricular branches may be closely apposed to the squamous pericardium. Blood flowing from auricles to the median ventricle is regulated by a pair of auriculoventricular valves (Fig. 37.5). Valves consist of an outer squamous epithelium covering the dark-staining myocardial and pale-staining connective tissue fibers.

5.8.2. Arteries, veins, capillaries, and pericardial gland

Throughout the body there are a series of blood vessels resembling arteries, veins, and capillaries based upon the overall size of the tissue and its cellular constituents. Possible arteries

consist of several layers of muscle encircling emarginated nuclei of endothelium (Fig. 38.1). Arteries and veins may be similar in size, but possible veins consist of a lesser-developed muscular wall encircling an endothelium (Fig. 38.2). Capillaries are small circular to ovular tubes consisting of endothelial cells. Capillaries are best observed within the perimysium of the adductors and pedal protractor and retractors (Fig. 38.3). The pericardial gland is a large latticework of adipocyte-like cells surrounding the pericardial cavity. Hemocytes are typically present within the lumen and there are emarginated hemocytes that appear to be attached to the lumen or incorporated within a narrow space between emarginated pericardial gland cells (Fig. 38.4).

5.9. Cellular structure of renal system tissues

5.9.1. Anterior nephridium

Nephridium is located directly underneath or dorsal to ctenidia and visceral mass. Nephridium has a ventral, convoluted limb while the dorsal limb has fewer epithelial folds extending into the lumen (Fig. 39.1). Anteriorly, ventral nephridium features numerous convoluted plicae restricting the lumen to a series of irregular, narrow spaces (Fig. 39.2). Columnar cells of ventral epithelium have a vesiculated, eosinophilic cytoplasm (Fig. 39.3). Ventral nephridial cells have a pale cytoplasm, but plicae appear mottled at a low magnification since wandering hemocytes are scattered throughout the plicated epithelium. Hemocytes are distinguished from epithelial cells by a red-staining cytoplasm, and a spherical nucleus. Subepithelium of nephridial plicae consists of connective tissue, endothelial cells and hemolymph (Fig. 39.3). Plicae of the dorsal nephridium are more sparsely distributed and may be distinguished from ventral plicae in having a convoluted surface whereas ventral nephridial plicae are smoother. Epithelium of dorsal plicae may be distinguished from ventral epithelium in

having brown intracellular granules (Fig. 39.4). A characteristic feature of dorsal nephridium is the presence of teardrop-shaped columnar cells with a transparent apical vesicle. Teardrop cells are distributed along the lateral and dorsal surfaces of dorsal nephridium and contain brown intracellular granules (Fig. 39.5).

Anterior nephridium with its extensively folded luminal branches is located anterior to the heart and pericardium. Pericardium unites with the ventral nephridial limb at the anterior-posterior midpoint of the visceral mass. Pericardial cavity forms a pleated tubule referred to as the reno-pericardial canal (Fig. 39.6). The reno-pericardial canal is lined with narrow, rounded plicae containing ciliated columnar cells and elliptical goblet cells (Fig. 39.7). The reno-pericardial canal is adjacent to the urethra representing the excurrent aperture of the dorsal nephridium. Urethra has a columnar epithelium with goblet cells lining the dorsal half of the tissue and a densely ciliated epithelium within the ventral half (Fig. 39.8). Goblet cells reappear along the ventral epithelium between the ctenidia and urethra.

5.9.2. Posterior nephridium

Between the posterior terminus of the visceral mass and the posterior adductor, the nephridial branches become elongated and the lumen greatly expands (Fig. 40.1). Nephridial epithelium encircles the posterior pedal retractors and nephridial branches resemble a series of stems and loops. Branches of posterior nephridium consist of columnar cells with pale, eosinophilic intracellular vesicles. Although the cell types of posterior nephridium appear morphologically similar to each other, all around the organ, it branches may represent the functional aspect of the tissue. At high magnification, cells of the nephridial branches typically have an eosinophilic, whispy material at the apical surface (Fig. 40.2). Cells lining the walls of the posterior

nephridium typically lack a whispy residue (Fig. 40.3). Additionally, the blood vessels underlying columnar cells of epithelial branches are wider than in the anterior nephridium.

5.10. Posterior adductor and posterior pedal retractors

Posterior pedal retractors unite with the posterior margin of the visceral mass and extend ventrally into the foot. Transverse histological sections of the posterior region of *F. cerina* reveal groups of retractor fascicles with a distinct perimysium and endomysium (Fig. 40.4). Additionally there are thin, elliptical capillaries located between fascicles. Posterior adductor, as seen in a sagittal plane, consists of filamentous myofibers with an elliptical nucleus and a distinct nucleolus (Fig. 40.5). Myofilaments overlap and at high magnification, dark striations are evident.

5.11. Cellular structure of nervous system tissues

5.11.1. Pedal ganglion, cerebral ganglia, and visceral ganglion

As in *Villosa nebulosa*, the four ganglia of *Fusconaia cerina* have similar histological characteristics and the description of the pedal ganglion is representative of the anterior and posterior ganglia. Pedal ganglion of *F. cerina* consists of a pair of vertically ovular lobes. Each lobe has a distinct outer cortex containing neuron cell bodies with axons extending into the inner medulla. Pedal ganglion has a distinct epineurium, dorsal and ventral fissures, with commisures uniting the two lobes (Fig. 41.1). Neuron cell bodies are polygonal, with a basophilic cytoplasm and a spherical, heterochromatic nucleus. Neurons have a homogenous cytoplasm and brown intracellular inclusions epineurium fibers appear granular and the tissue has a distinct filamentous appearance (Fig. 41.2). Axons are darkened and well defined as they extend from the neuron cell body into the medulla. Nerve fibers of pedal ganglion of *F. cerina* are distinctively filamentous (Figs. 41.3-4). Glial cells of the medulla have a darkened, homogenous

nucleus with a minimal amount of cytoplasm. Ganglionic roots are large bundles of axons extending dorso-laterally and ventral-laterally from each ganglionic lobe (Fig 41.5).

Anterior ganglia are paired spherical masses located between the anterior adductor and labial palps (Fig 42.1). The posterior ganglion is cylindrical, located anteriorly along the ventral surface of the adductor (Fig. 42.3). A horizontal band of connective tissue overlays the posterior ganglion and consists of fibrous tissue and hemolymph. Ventral to the hemolymph sinus is an apical layer of columnar cells and goblet cells (Fig. 42.2). The posterior ganglion extends into the base of the inner ctenidia and may appear as an ovular mass of nervous tissue at the base of the gill (Fig. 42.4).

5.11.2. Nerves and statocysts

Nerves are distributed throughout the visceral mass, foot, nephridium, and mantle edge. Tansverse sections of nerves reveal a thickened, eosinophilic epineurium encircling an irregular filamentous core of axons (Fig. 43.1). A sagittal view of a nerve illustrates how the tissue resembles a wavy band of filaments (Fig. 43.2). Additionally, there is a sinistral and dextral statocyst lateral to the pedal ganglion near the dorsal margin of the coelom. Statocysts appear stratified with ciliated columnar cells lining a spherical lumen (Fig. 43.3). Satocysts contain a spherical mass or statolyth in the median of the lumen.

5.12. Cellular structure of reproductive system tissues

Gonadal tissue consists of testicular and ovarian acini, ciliated gonadal ducts throughout the visceral mass, and a pair of ciliated gonadal pores located at the base of the visceral mass at the anterior end of the nephridium. Female and male Fusconaia cerina in Cahaba River (Bibb, Shelby Co., AL) sexually mature in May and females may bear glochidia during June. Males and females collected in May 2011 exhibited peak gametogenesis, while considerably less

gametogenesis was observed in individuals collected in August 2011. The luminal contents of immature ovaries mainly consisted of an eosinophilic granular material with minimal input of oocytes (Fig. 44.1). Walls of immature ovarian acini are lined with squamous cells with basophilic oocytes adhered to the luminal surface. Developing oocytes initially possess a violet cytoplasm and may appear to be attached to the acinus wall by a stem. Oocytes appear to grow and separate from the acinus wall. Separated oocytes have an irregular cell membrane, with a pale, basophilic margin. Immature oocytes feature a red, granular cytoplasm with a basophilic focus consisting of an irregular violet nuclear membrane and a spherical, black nucleolus (Fig. 44.2). Ovarian acini also produce a series of spherical, red, granular cells with a small basophilic nucleus. Given the small size and undifferentiated appearance, it is likely that the red cells are polar bodies. The lumen of immature ovarian acini also appears to contain the remnants of polar bodies considering the presence of an irregular, red, granular material and a series of nuclei lacking surrounding cytoplasm. Mature oocytes are enlarged, and densely packed within the acinus (Fig. 44.3). Mature oocytes have a pale basophilic nucleus with a distinct nucleolus within a red, granular cytoplasm. Oocytes released from the acinus wall feature a pale, basophilic membrane surrounding the cell body. Developing oocytes are attached to the acinus wall via a basophilic stem.

Immature testicular acini of individuals collected in August 2011 contained a preponderance of blackened single-celled spermatocytes and multicellular sperm morula (Fig. 44.4). Spermatozoa are present in some acini, but restricted to the center of the lumen. Primary spermatocytes are typically emarginated along the acinus wall and have a pale, basophilic cytoplasm. Violet spermatocytes appear to differentiate into sperm morula and cells of sperm morula become spermatozoa (Fig. 44.5). Additionally, immature testicular acini contain a series of small,

esoinophilic granules, possibly representing remnants of degenerative spermatocytes or fluid. A high level of spermiogenesis was evident in mature testicular acini in individuals collected in May 2011. Sperm morula as seen in immature testes were less consipicuous within mature testes. Violet spermatocytes along the acinus wall appear to differentiate into darkened, spherical cells. Darkened testicular cells have such a small size that it is difficult to determine whether these cells represent clusters of spermatocytes or single-celled spermatocytes (Fig. 44.6).

Gonadal ducts of *F. cerina* consist of pale, eosinophilic, ciliated cells with an ovular nucleus. Spermatozoa were observed in the testicular ducts of mature male *Fusconaia cerina* collected in May 2011 (Fig. 44.7). Gonadal ducts merge dorsally and extend along the lateral margins of the coelom to the base of the visceral mass. The gonadal pores of *F. cerina* feature a bulbous ventral ledge and a pleated, ciliated epithelium (Fig. 44.8).

PLATE 22. Shell morphology, and gross anatomical features of the mantle cavity of *Fusconaia cerina*. 1. Lateral view of the right valve showing the broad anterior margin (AM), arched umbo (UM), ligament (LI), posterior ridge (PR), and posterior slope (PS). 2. Lateral view of left valve showing the broad anterior margin (AM), conical umbo (UM), well-developed posterior ridge (PR), and posterior slope (PS). 3. Medial view of the left valve showing the pallial line (PL), anterior adductor scar (AS), posterior adductor scar (PS), strong pseudocardinal teeth (PT), interdentum (ID), deep umbo cavity (UC), lateral teeth (LT), ligament (LI), and umbo extending beyond the dorsal margin (UM). 4. Medial view of the left valve showing the pallial line (PL), anterior adductor scar (AS), posterior adductor scar (PS), strongly developed pseudocardinal tooth (PT), interdentum (ID), deep umbo cavity (UC), lateral tooth (LT), and well-developed ligament (LI). 5. Ventrolateral view of *Fusconaia cerina* (ca. 60 mm shell length) buried in gravel at Cahaba River with papillose mantle margins cupped to form an incurrent aperture (IA) and excurrent aperture (EA). 6. Medial view of the mantle cavity with the right valve and right mantle removed showing the orange mantle edge (ME), middle mantle (MM), foot (FO), anterior adductor (AA), labial palp (LP), and tetragenous inner gill (IG) and outer gill (OG), red conglutinates (CO), posterior adductor (PA), mantle isthmus (MI), and supra-anal aperture (SA). 7. Medial view of the mantle cavity with the right valve and right mantle removed emphasizing pallid mantle edge (ME), foot (FO), anterior adductor (AA), tetragenous inner gill (IG) and outer gill (OG), white conglutinates (CO), posterior adductor (PA), mantle isthmus (MI), and supra-anal aperture (SA). 8. Medial view of the mantle cavity with the right valve, right mantle, and right gills removed revealing the orange mantle edge (ME), middle mantle (MM), foot (FO), labial palp (LP), visceral mass (VM), anterior adductor (AA), left inner gill (IG), posterior adductor (PA), mantle isthmus (MI), and supra-anal aperture (SA).

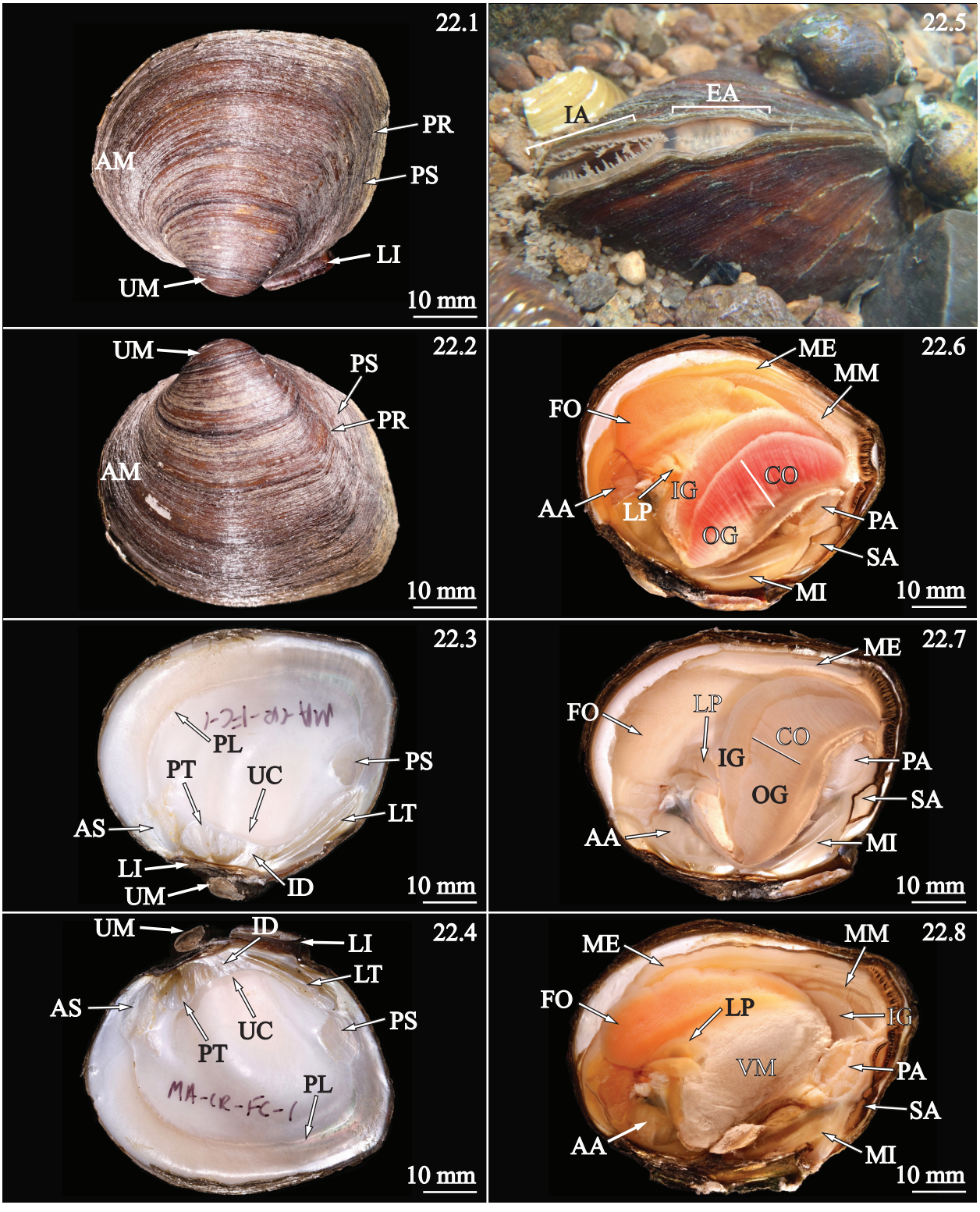
22.1
PR
AM
PS
LI
UM
10 mm
22.5
EA
IA
22.2
UM
PS
PR
AM
10 mm
22.6
ME
MM
FO
CO
IG
AA
LP
OG
PA
SA
MI
10 mm
22.3
PL
PT
UC
PS
LT
AS
LI
ID
UM
10 mm
22.7
ME
FO
LP
IG
CO
PA
OG
SA
AA
MI
10 mm
22.4
UM
ID
LI
LT
AS
UC
PS
PT
PL
10 mm
22.8
ME
MM
FO
LP
IG
VM
PA
SA
AA
MI
10 mm

PLATE 23. Anterior mantle edge of *Fusconaia cerina*. 1. Transverse section of anterior mantle edge showing the position of the outer lobe (OL), middle lobe (ML), and inner lobe (IL). 2. Transverse section of mantle edge emphasizing columnar epithelium (CE) of the outer lobe, basal bulb (BB), periostracal groove (PG), squamous epithelium (SE) of the middle lobe, and periostracum (PE). 3. Transverse section of the distal margin of outer mantle lobe revealing a basophilic columnar epithelium (CE) along branched plicae (PL) and a dense subepithelium of fibrous tissue (FT). 4. Transverse section of middle mantle lobe revealing a periostracum ribbon (PE) and squamous epithelium (SE), violet cells (VC), characterizing the dorsal margin consisting of a folded columnar epithelium (CE). 5. Transverse section of the inner mantle lobe edge portraying an irregular epithelium consisting of teardrop-shaped to flattened plicae (PL). 6. Transverse section of inner epithelium of proximal mantle edge defined by teardrop-shaped plicae (PL), granulocytes (GC), and a well-defined stratum of myofibers (MF). 7. Transverse section of the outer epithelium of proximal mantle edge characterized by a wavy columnar epithelium (CE), isolated goblet cells (GC), a horizontal lamina of myofibers (MF).

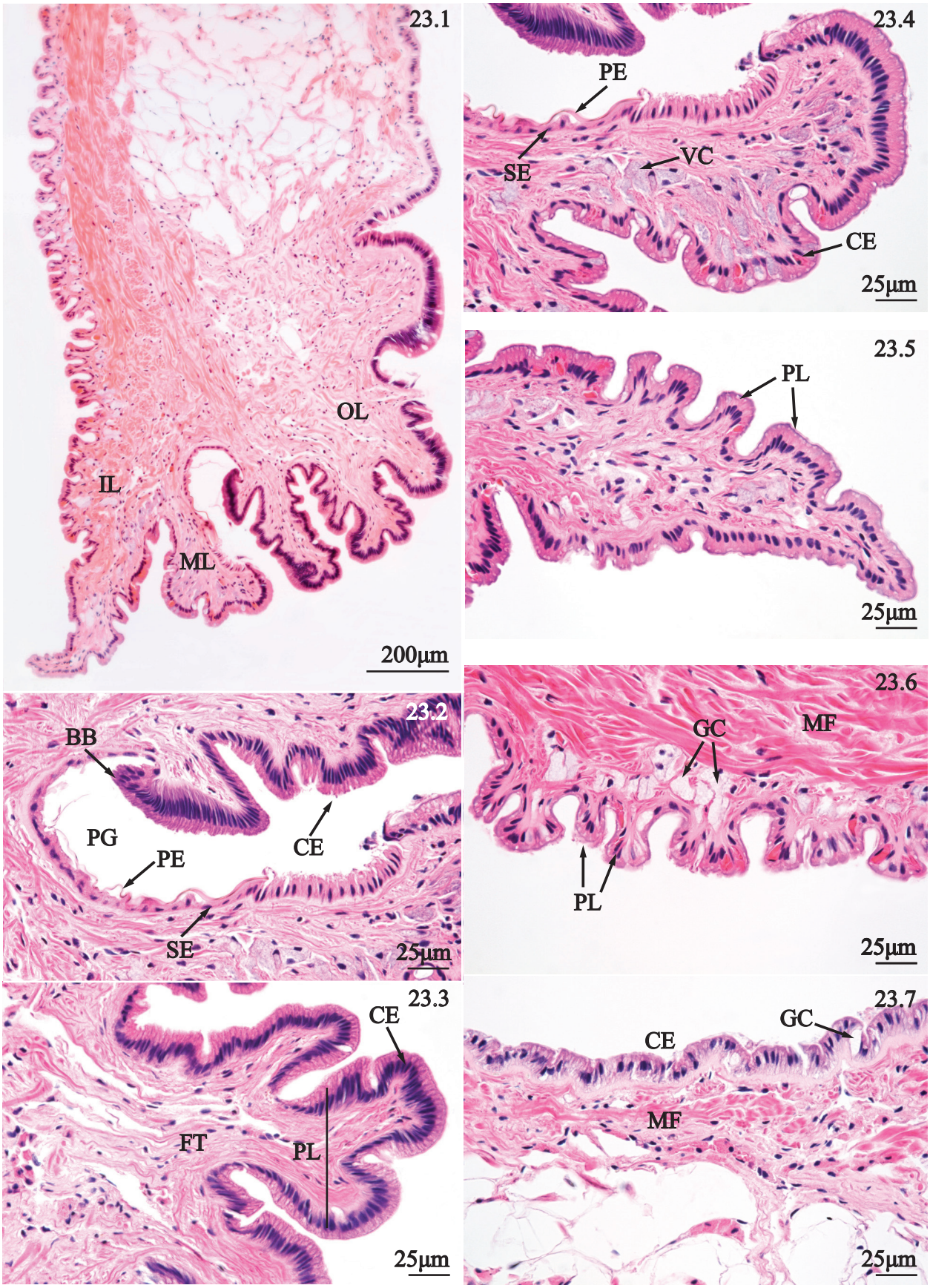
23.1
OL
IL
ML
200µm
23.4
PE
SE
VC
CE
25µm
23.5
PL
25µm
23.2
BB
PG
PE
CE
SE
25µm
23.6
GC
MF
PL
25µm
23.3
CE
FT
PL
25µm
23.7
GC
CE
MF
25µm

PLATE 24. Posterior mantle edge, middle mantle, and mantle isthmus of *Fusconaia cerina*. 1. Transverse section of posterior mantle edge showing a forked outer lobe (OL), conical middle lobe (ML), and triangular inner lobe (IL) with distinct plications (PL). 2. Sagittal section of posterior mantle edge characterized by conical papillae (PA) and oblique plications (PL) along the surface. 3. Sagittal section of a papilla displaying brown intracellular granules (BG) of the columnar epithelium and wandering hemocytes (HC) interspersed among epithelial cells, and a subepithelium endowed with connective tissue fibers (CT). 4. Transverse section of middle mantle displaying columnar cells of outer epithelium (OE), squamous cells of inner epithelium (IE) and a fibrous subepithelial strata of connective tissue (CT), and hemocytes (HC). 5. Transverse section of mantle isthmus revealing a well-organized basophilic epithelium (BE), goblet cells (GC), and sinuous connective tissue fibers (CT).

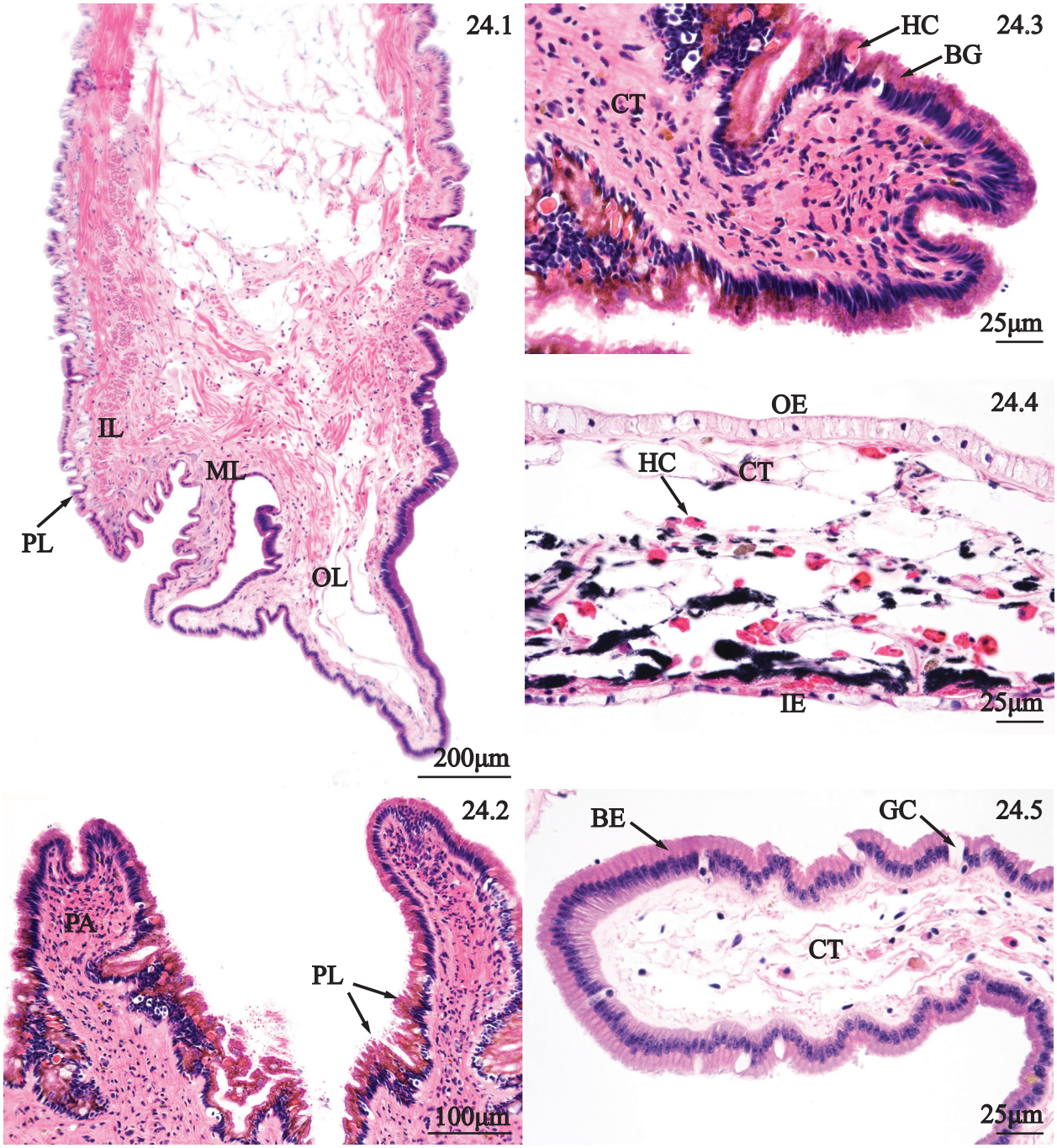
24.1
IL
ML
PL
OL
200µm
24.3
HC
BG
CT
25µm
24.4
OE
HC
CT
IE
25µm
24.2
PA
PL
100µm
24.5
BE
GC
CT
25µm

PLATE 25. Outer gill, and inner gill of *Fusconaia cerina*. 1. Transverse section of inner gill showing characteristic cylindrical filaments (FI), and a septum (SE) uniting inner and outer lamina along the length of a water tube (WT). 2. Transverse section of inner gill lamina emphasizing the functional components including lateral cilia (LC), frontal lateral cilia (FL), frontal cilia (FC), skeletal rods (SR), blood vessel (BV), ostium pore (OS), and corresponding water tube (WT). 3. Transverse section of the distal tip of an outer gill characterized by a convex distal margin (DM), derived from the fusion of filaments (FI). 4. Transverse section of the free distal margin (DM) of an inner ctenidium displaying a median ciliated groove (CG). 5. Transverse section of the free inner lamina (IL) of an inner gill showing its close proximity to the visceral mass (VM) and nephridium (NE). 6. Transverse section of the base of a gill displaying muscle fascicles (MU) in an anterior-posterio alignment, surrounded by a large mass of hemolymph (HE). 7. Transverse section of the base of a ctenidium revealing muscle fascicles (MU) and hemolymph (HE). 8. Transverse section of the base of an outer gill showing the union of the outer lamina (OL) and middle mantle (MA).

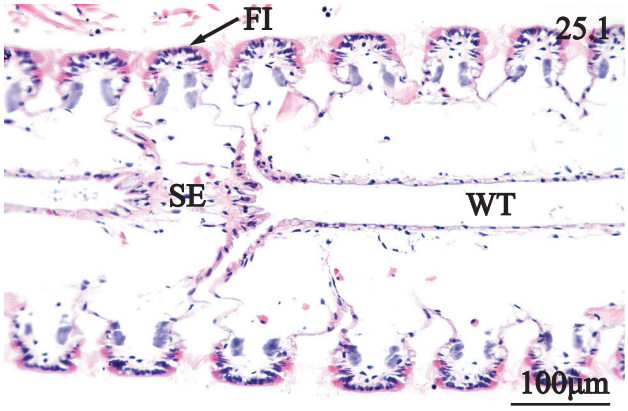
FI
25.1
SE
WT
100μm

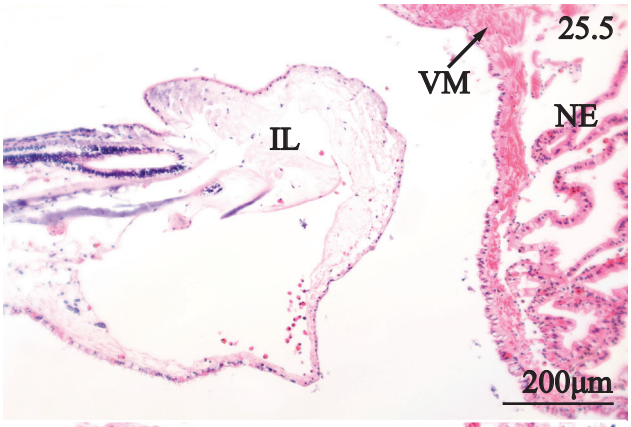
25.5
VM
NE
IL
200μm

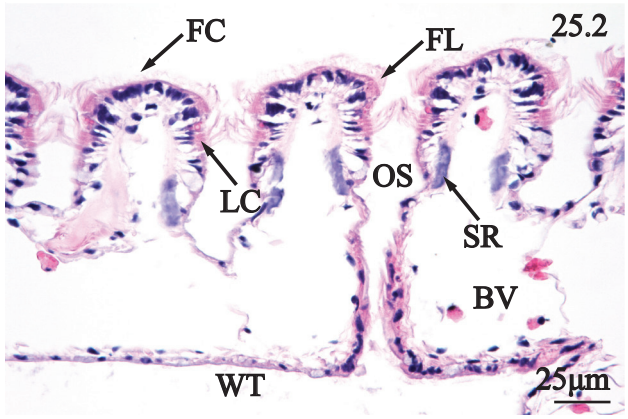
FC
FL
25.2
LC
OS
SR
BV
WT
25μm

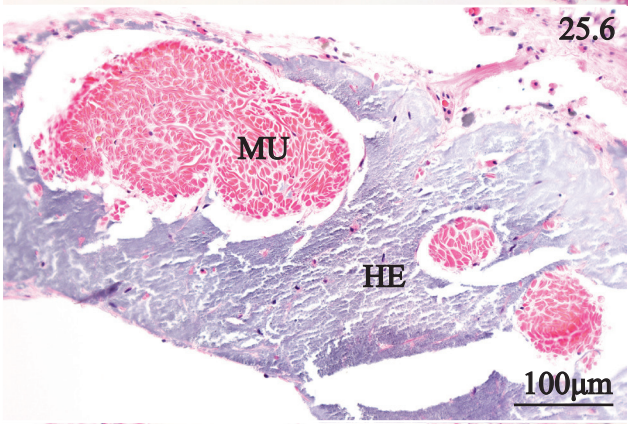
25.6
MU
HE
100μm

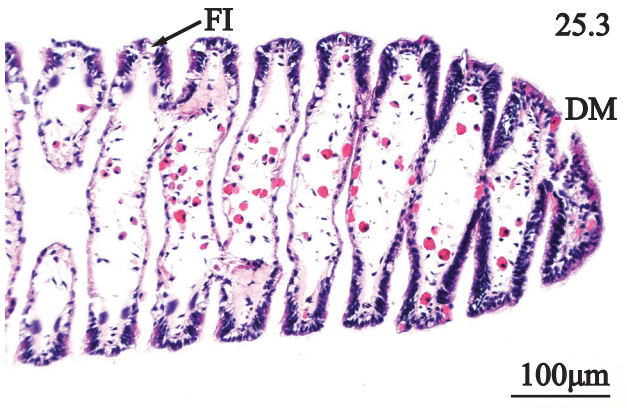
FI
25.3
DM
100μm

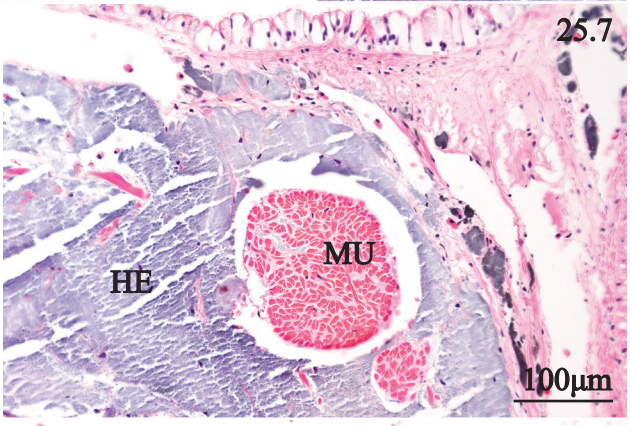
25.7
MU
HE
100μm

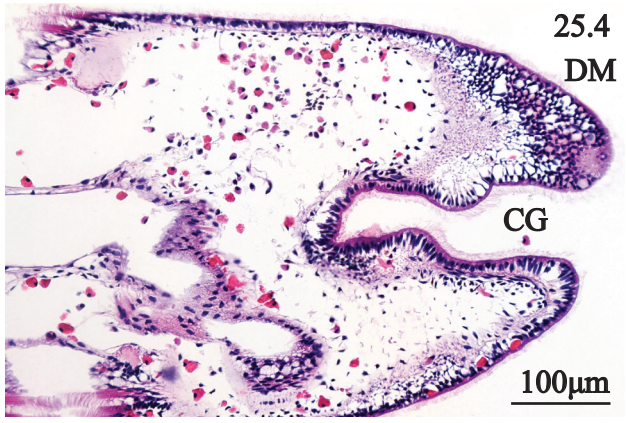
25.4
DM
CG
100μm

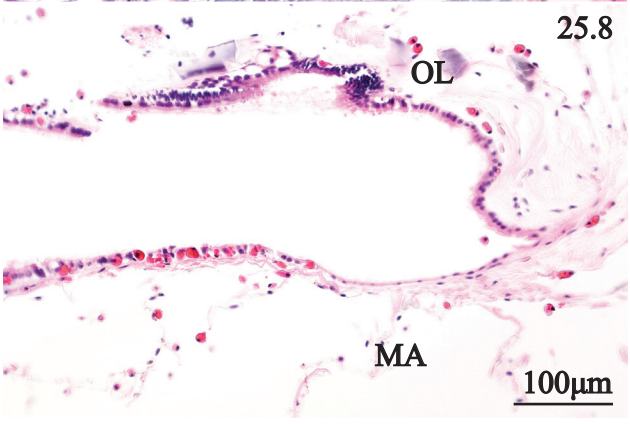
25.8
OL
MA
100μm

PLATE 26. Marsupium, and conglutinates of *Fusconaia cerina*. 1. Transverse section of a marsupial ctenidium containing a conglutinate (CO), within a distended water tube (WT), supported by thickened septa (SE). 2. Transverse section of the lateral margin of a filled marsupium portraying filaments (FI), an ostium (OS), blood vessels (BV), and a conglutinate consisting of early stage embryos (EE), and unfertilized ova (UO). 3. Transverse section of a marsupium portraying part of a conglutinate consisting of unfertilized ova (UO), early stage embryos (EE), both featuring basophilic apical branches (BR). 4. Transverse section of the marsupial septum consisting of a columnar epithelium (CE) containing goblet cells and a subepithelium consisting of fibrous connective tissue (CT), and hemocytes (HC). 5. Transverse section of an empty marsupium illustrating how the histological composition of filaments (FI), water tube (WT) and septa (SE) exhibit minimal change long after conglutinates are shed.

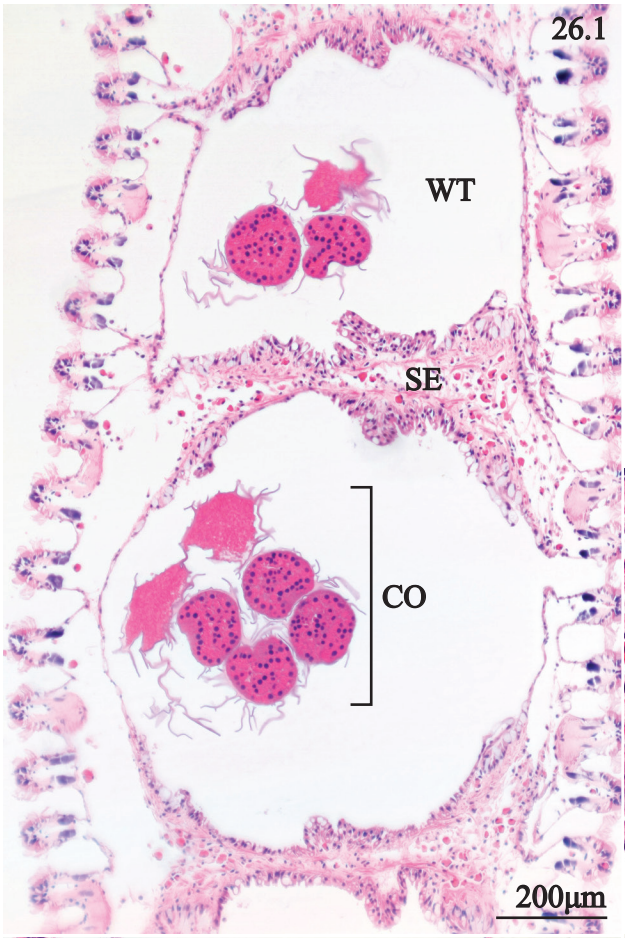
26.1
WT
SE
CO
200µm

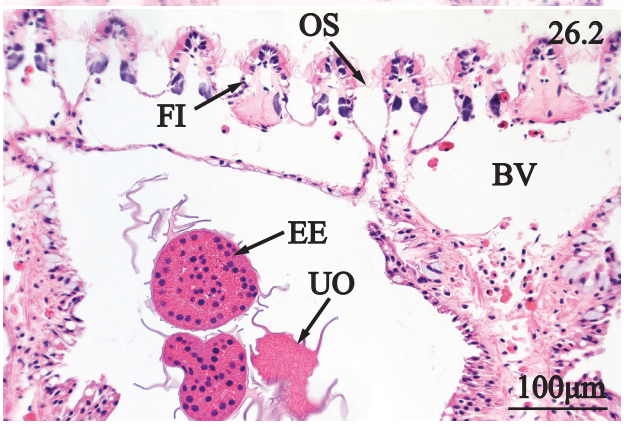
OS
26.2
FI
BV
EE
UO
100µm

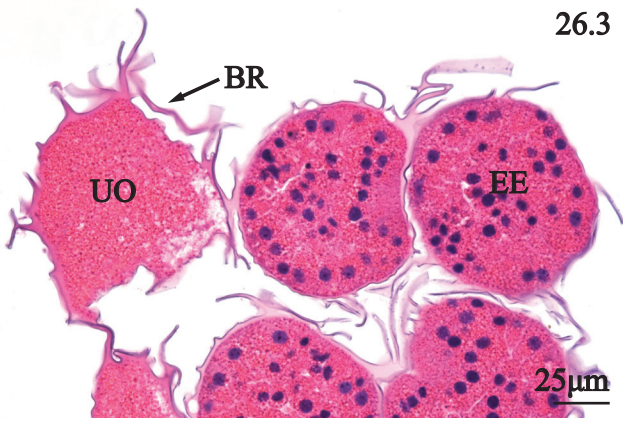
26.3
BR
UO
EE
25µm

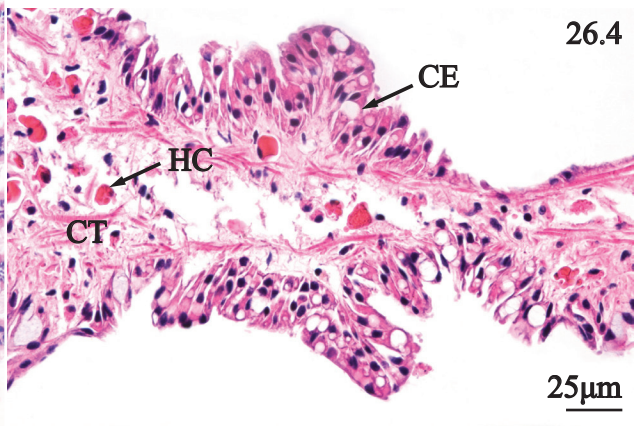
26.4
CE
HC
CT
25µm

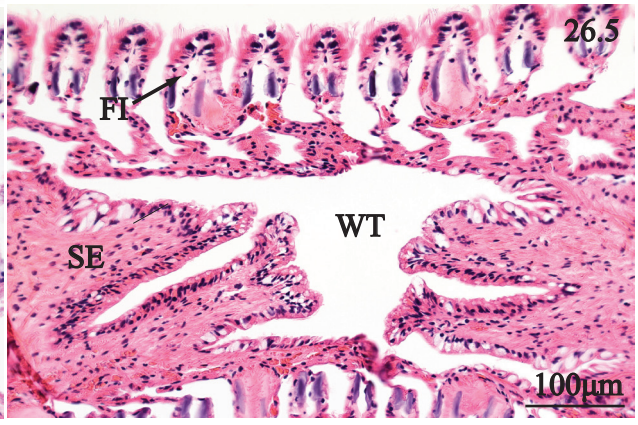
26.5
FI
WT
SE
100µm

PLATE 27. Pedal musculature, and byssal gland of *Fusconaia cerina*. 1. Transverse section of the ventral tip of the foot displaying a median triangular ray of somatic musculature (SM), and a darkened subeptihelium of granulocytes (GC). 2. Transverse section of foot subepithelium characterized by irregular myofibers (MF), pale, blue granulocytes (BC), and violet cells (VC). 3. Transverse section of ventral foot musculature emphasizing bundles of horizontal myofibers (HM), and vertical myofibers (VM). 4. Transverse section of the foot portraying a distinct stratum of vertical foot musculature (VM) overlying layers of horizontal musculature (HM). 5. Transverse section of the byssal gland (BG) encircled by a lamina propria (LP) and surrounded by ovarian acini (OA). 6. Transverse section of the byssal gland emphasizing cilia (CI) and squamous epithelium (SE). 7. Sagittal section of the posterior portion of the foot emphasizing possible remnants of the byssal canal consisting of a ciliated epithelium (CE), enclosing an eosinophilic mass (EM).

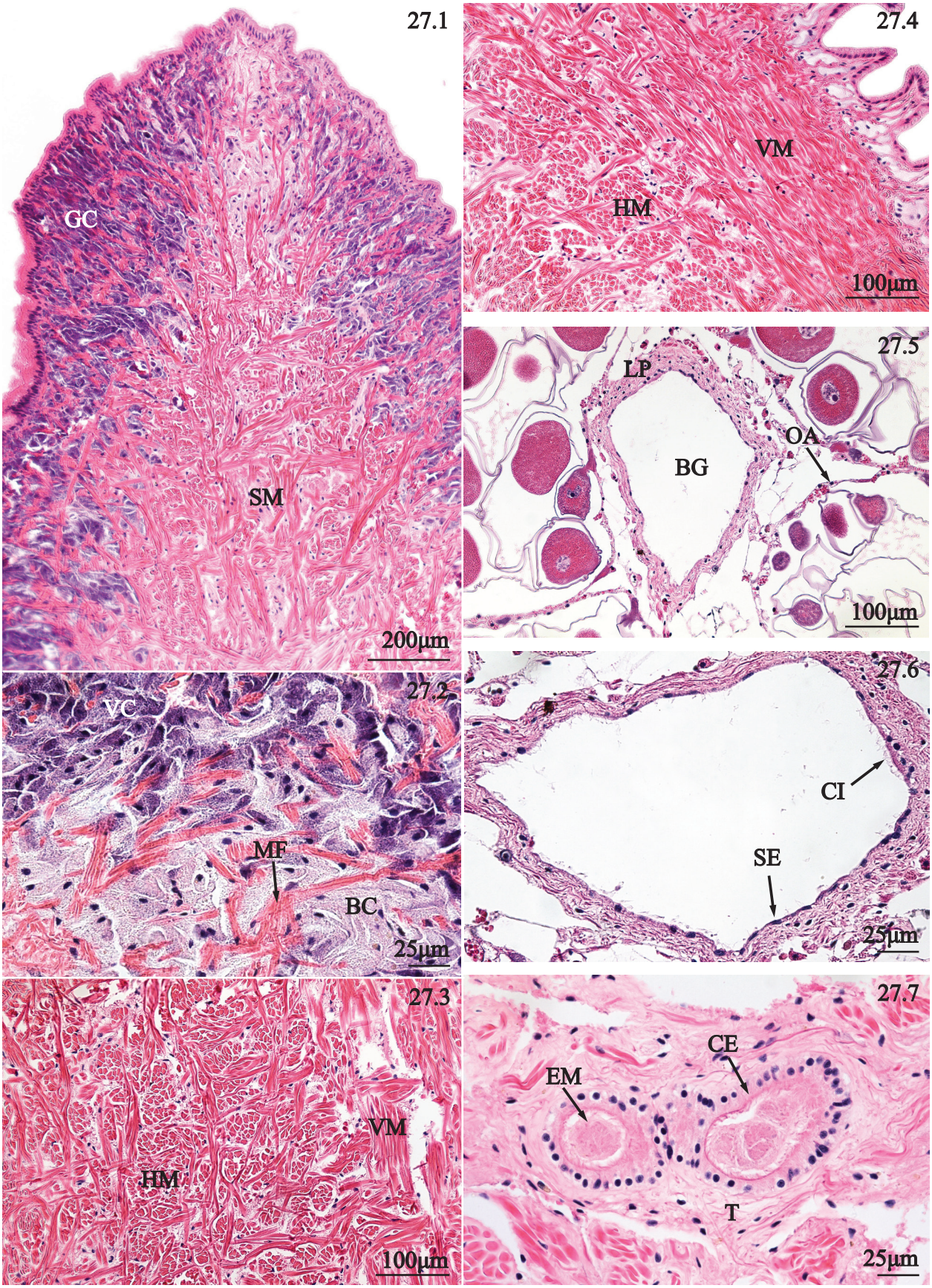
27.1
GC
SM
200µm
27.4
VM
HM
100µm
27.5
LP
OA
BG
100µm
27.2
VC
MF
BC
25µm
27.6
CI
SE
25µm
27.3
VM
HM
100µm
27.7
CE
EM
T
25µm

PLATE 28. Pedal integument, and mesentery of *Fusconaia cerina*. 1. Transverse section of pedal integument type 1, emphasizing rectangular plicae (PL), dense cilia (CI), and a large swath of violet cells (VC). 2. Transverse section of pedal integument type 2 characterized by thinner plicae (PL) with isolated patches of cilia (CI) and pale-staining violet cells (VC). 3. Transverse section of pedal integument type 3, displaying reduced, teardrop-shaped plicae (PL), cilia (CI), goblet cells (GC), horiztonal musculature (HM), and vertical musculature (VM). 4. Transverse section of pedal integument type 4, characterized by a flattened epithelium consisting of ciliated columnar cells (CI) and goblet cells (GC) overlying a subepithelium consisting of connective tissue (CT), hemolymph (HL), horitzontal muscle (HM) and vertical muscle (VM). 5. Transverse section of pedal integument type 5, featuring a flattened epithelium consisting of cilia (CI), goblet cells (GC), underlying hemolymph sinus (HS), horizontal musculature (HM), and mesentery (ME). 6. Sagittal section of pedal integument at the posterior margin of the foot, emphasizing cilia (CI) and plicae (PL). 7. Transverse section of the dorso-lateral aspect of the coelom illustrating chords of mesentery (ME) spanning the coelomic cavity with linkage to he lateral vertical muscle (VM), and horizontal muscle (HM) strata. 8. Sagittal section through the posterior visceral mass revealing a mesenteric fascicle (FA) encircled by adipocytes (AC).

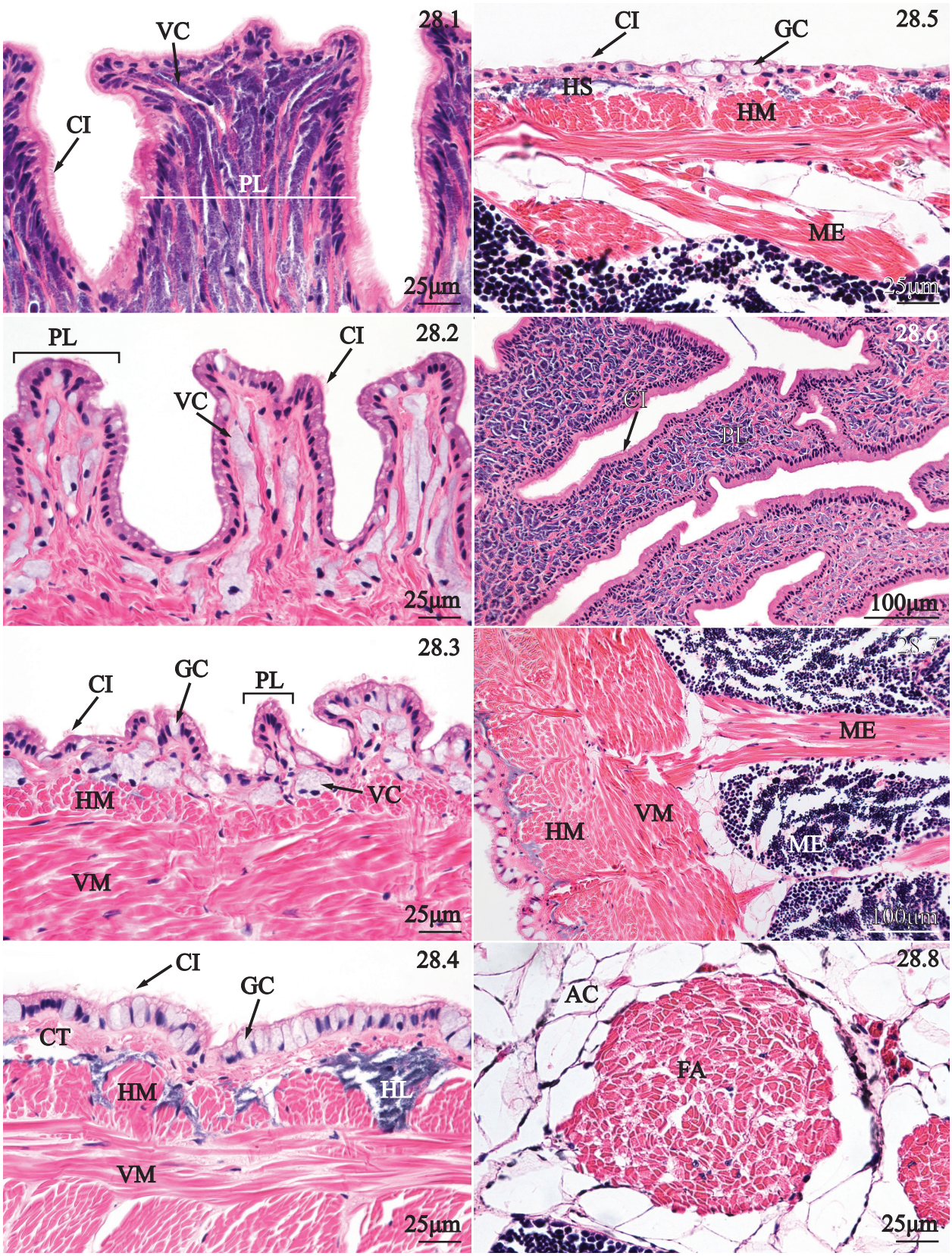
28.1
VC
CI
PL
25μm
28.5
CI
GC
HS
HM
ME
25μm
PL
CI
28.2
VC
25μm
28.6
CI
PL
100μm
28.3
CI
GC
PL
HM
VC
VM
25μm
28.7
ME
VM
HM
ME
100μm
28.4
CI
GC
CT
HM
HL
VM
25μm
28.8
AC
FA
25μm

PLATE 29. Labial palps, anterior pedal protractor, and anterior adductor of *Fusconaia cerina*. 1. Transverse section of labial palps revealing plicae (PL) along the inner epithelium (IE), and flattened outer epitheliu (OE). 2. Transverse section of the inner palp epithelium featuring ciliated plicae (PL), and connective tissue fibers (CT) of the subepithelium. 3. Sagittal section of anterior adductor portraying myofibers (MF), myocyte nuclei (MN), and a pale eosinophilic perimysium (PM). 4. Transverse section of outer epithelium emphasizing teardrop-shaped columnar cells (TC), and subepithelial connective tissue (CT). 5. Transverse section of distal palp margin showing cilia (CI) and goblet cells (GC). 6. Transverse section of anterior pedal protractor illustrating densely packed myofibers (MF), scattered myocycte nuclei (MN) and perimysium (PM).

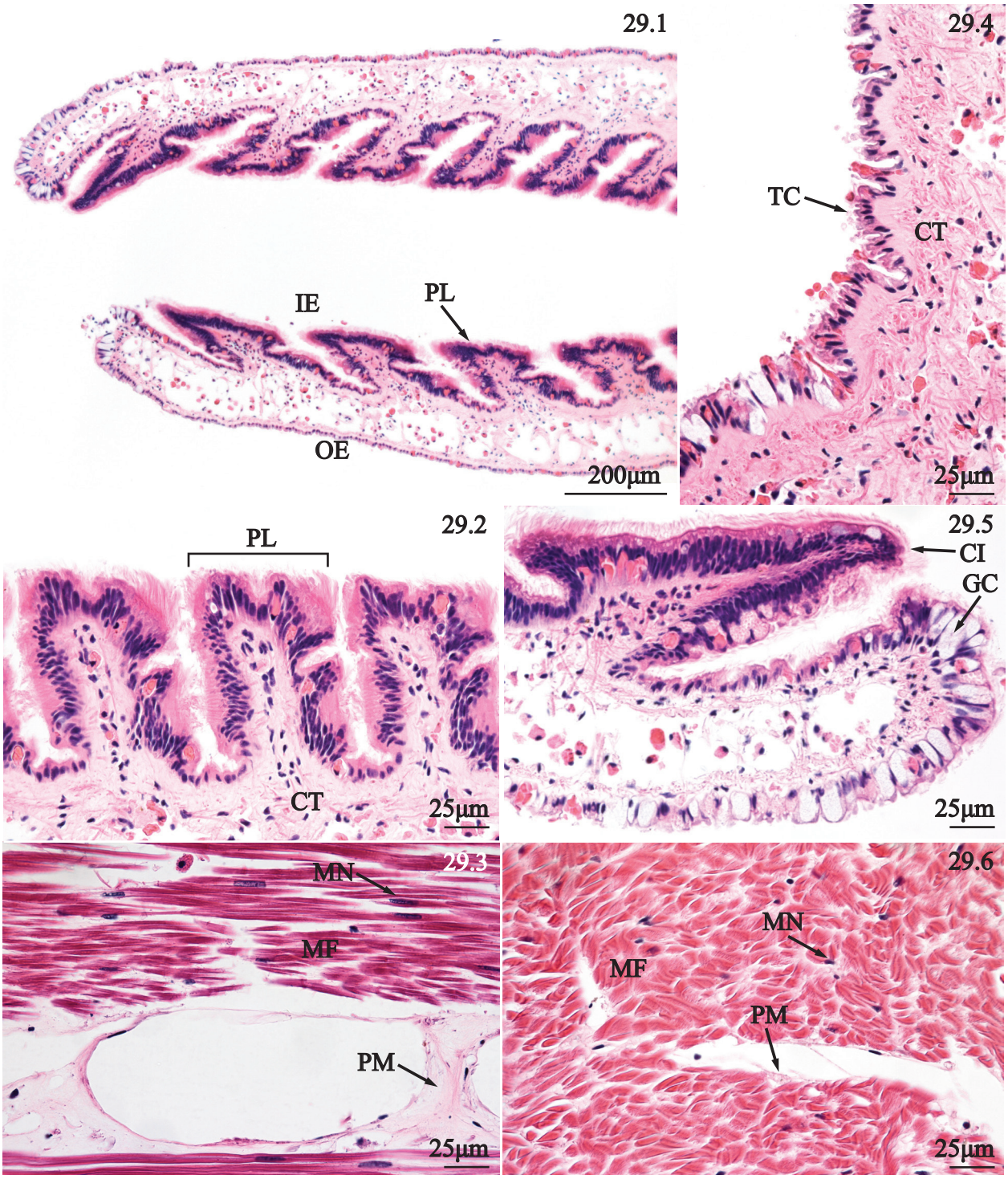
29.1
IE
PL
OE
200µm
29.4
TC
CT
25µm
29.2
PL
CT
25µm
29.5
CI
GC
25µm
29.3
MN
MF
PM
25µm
29.6
MN
MF
PM
25µm

PLATE 30. Oral groove, and esophagus of *Fusconaia cerina*. 1. Transverse section of the ventral portion of the oral groove featuring a muscular extension (MU) of ciliated columnar cells (CC), and goblet cells (GC). 2. Transverse section of ventral oral groove wall showing an extension of cilia (CI) along the surface of plicae (PL) and a subepithelium of connective tissue fibers (CT). 3. Transverse section of lateral oral groove epithelium emphasizing flattened columnar epithelial cells endowed with cilia (CI) and subepithelial myofibers (MF). 4. Transverse section of the esophagus revealing plicae (PL) and a densely ciliated epithelium (CI). 5. Transverse section of the dorsal aspect of anterior visceral mass portraying an ovoid esophagus (ES) with a distinct lamina propria (LP), closely associated with digestive diverticulum tubules (DD).

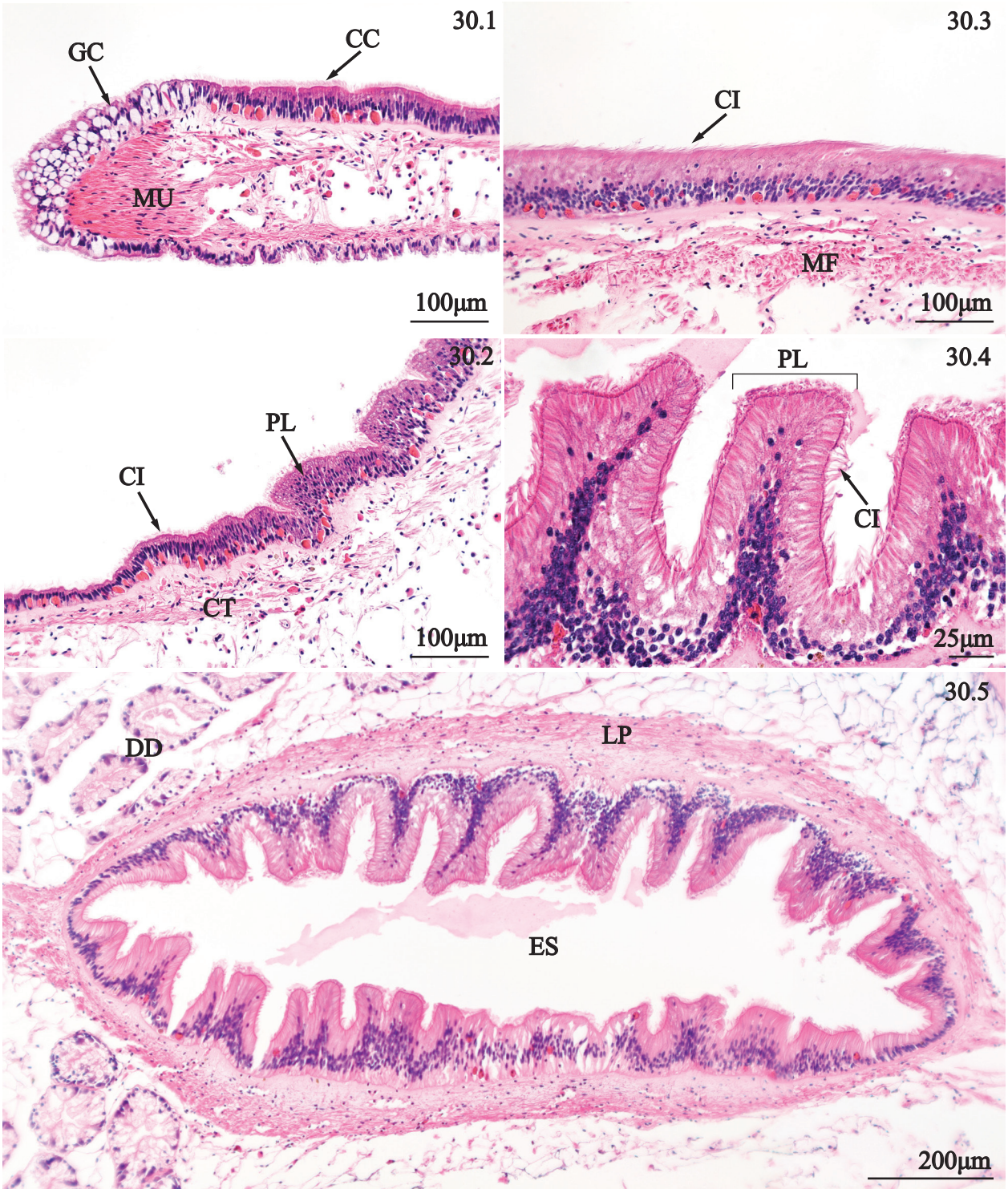
30.1
GC
CC
MU
100μm
30.3
CI
MF
100μm
30.2
PL
CI
CT
100μm
30.4
PL
CI
25μm
30.5
DD
LP
ES
200μm

PLATE 31. Digestive diverticulum of *Fusconaia cerina*. 1. Transverse section of the junction of esophagus (ES) and stomach (ST) showing the position of plicae (PL) in relation to the typhlosole (TY) and the non-plicated dorsal wall (DW). 2. Transverse section of anterior stomach emphasizing rounded, ciliated plicae (PL) with a distinct lamina propria (LP). 3. Transverse section of digestive diverticulum portraying the deeply infolding plicae (PL) of a primary tubule. 4. Transverse section of a primary digestive diverticulum tubule illustrating cilia (CI) extending from conical plicae (PL). 5. Transverse section of secondary digestive diverticulum tubule emphasizing vesiculated epithelium (VE), apical microvilli (MV), and a thin subepithelium of eosinophilic connective tissue fibers (EF). 6. Transverse section of digestive diverticulum showing the valve-like (VA) appearance of the secondary tubules (ST) as they unite with tertiary tubules (TT). 7. Transverse section of tertiary digestive diverticulum tubules emphasizing the characteristic basophilic nuclear region (BN) and eosinophilic intracellular vesicles (EV).


31.1
ST
PL
DW
TY
ES
200µm

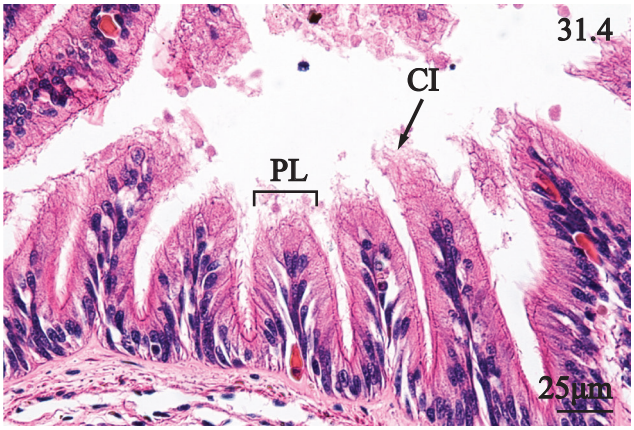
31.4
CI
PL
25µm

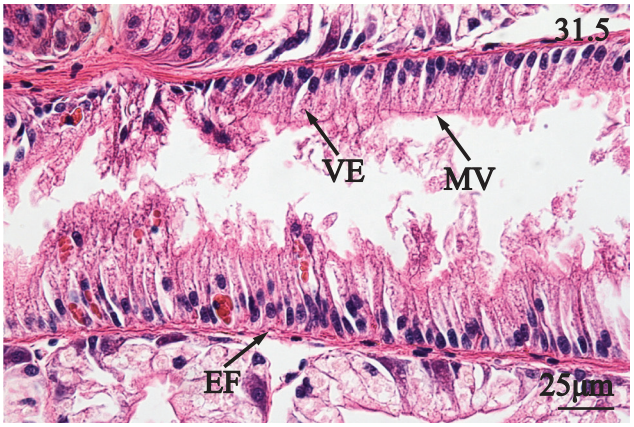
31.5
VE
MV
EF
25µm

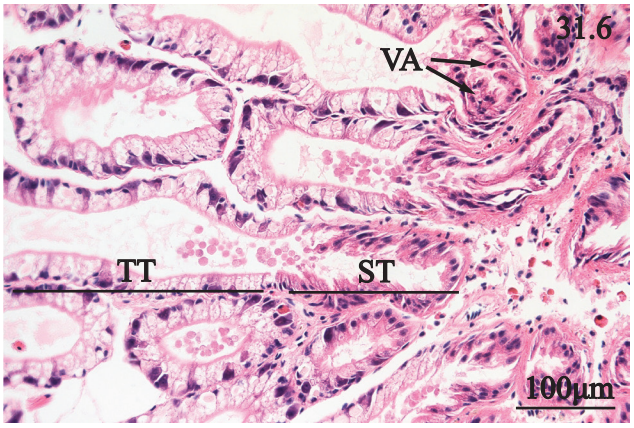
31.6
VA
TT
ST
100µm


31.2
PL
LP
100µm

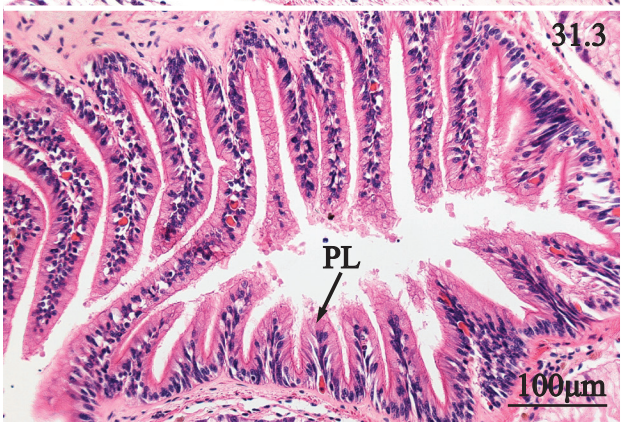
31.3
PL
100µm


31.7
BN
EV
25µm

PLATE 32. Anterior stomach chamber of *Fusconaia cerina*. 1.Transvere section of the dextral stomach chamber showing a large eosinophilic rod (ER) extending into the lumen, ciliated plicae (PL) along the chamber wall, and an eosinophilic fluid (EF) throughout the lumen. 2. Transverse section of the dextral stomach chamber showing the close relationship between cilia (CI) of plicae (PL), and the eosinophilic fluid (EF) and eosinophilic rod (ER). 3. Transverse section of the dorsal wall of the rectangular stomach chamber portraying plicae (PL) and an eosinophilic fluid (EF). 4. Transverse section of the stomach wall emphasizing a layered eosinophilic cuticle (CU), overlying densely packed columnar cells (CC). 5. Transverse section of the stomach emphasizing an obliquely oriented typhlosole (TY) with a thickened eosinophilic cuticle (CU).

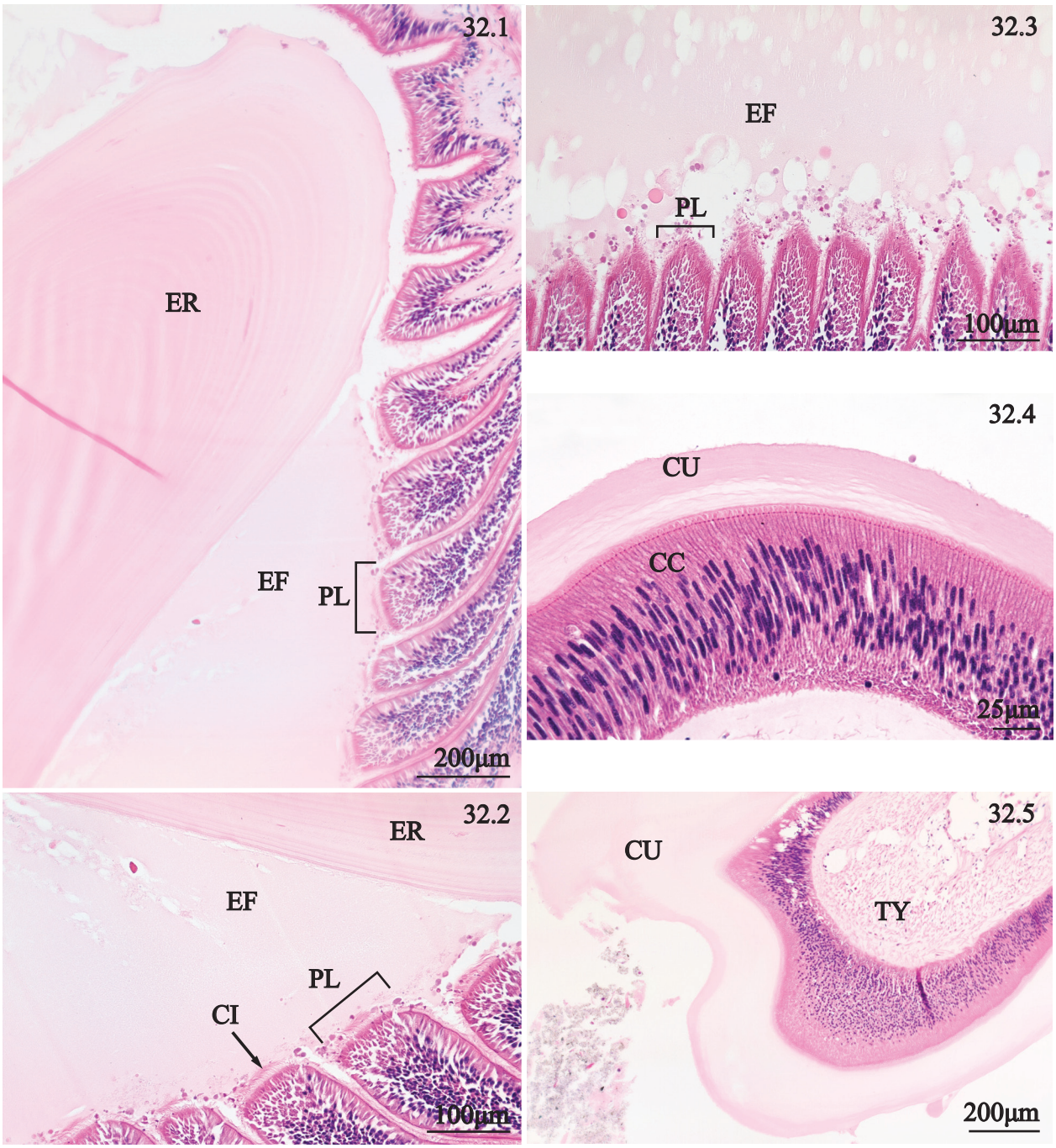
32.1
ER
EF
PL
200μm
32.3
EF
PL
100μm
32.4
CU
CC
25μm
32.2
ER
EF
PL
CI
100μm
32.5
CU
TY
200μm

PLATE 33. Posterior stomach chamber of *Fusconaia cerina*. 1.Transverse section of ventral stomach wall showing a cylindrical typhlosole (TY) with a well defined lamina propria (LP). 2. Transverse section of the cylindrical typhlosole portraying the densely ciliated (CI) columnar epithelium overlying the lamina propria (LP). 3. Transverse section of the ventral stomach epithelium revealing a conical plica (PL) with a densely ciliated surface (CI) supported by connective tissue of the lamina propria (LP). 4. Transverse section of ventral stomach epithelium emphasizing a layered cuticle (CU) overlying cilia (CI) of the columnar epithelial cells (CE). 5. Transverse section of ventral stomach epithelium emphasizing cilia (CI) extending from a reduced columnar epithelium (CE) and subepithelial adipocytes (AC).

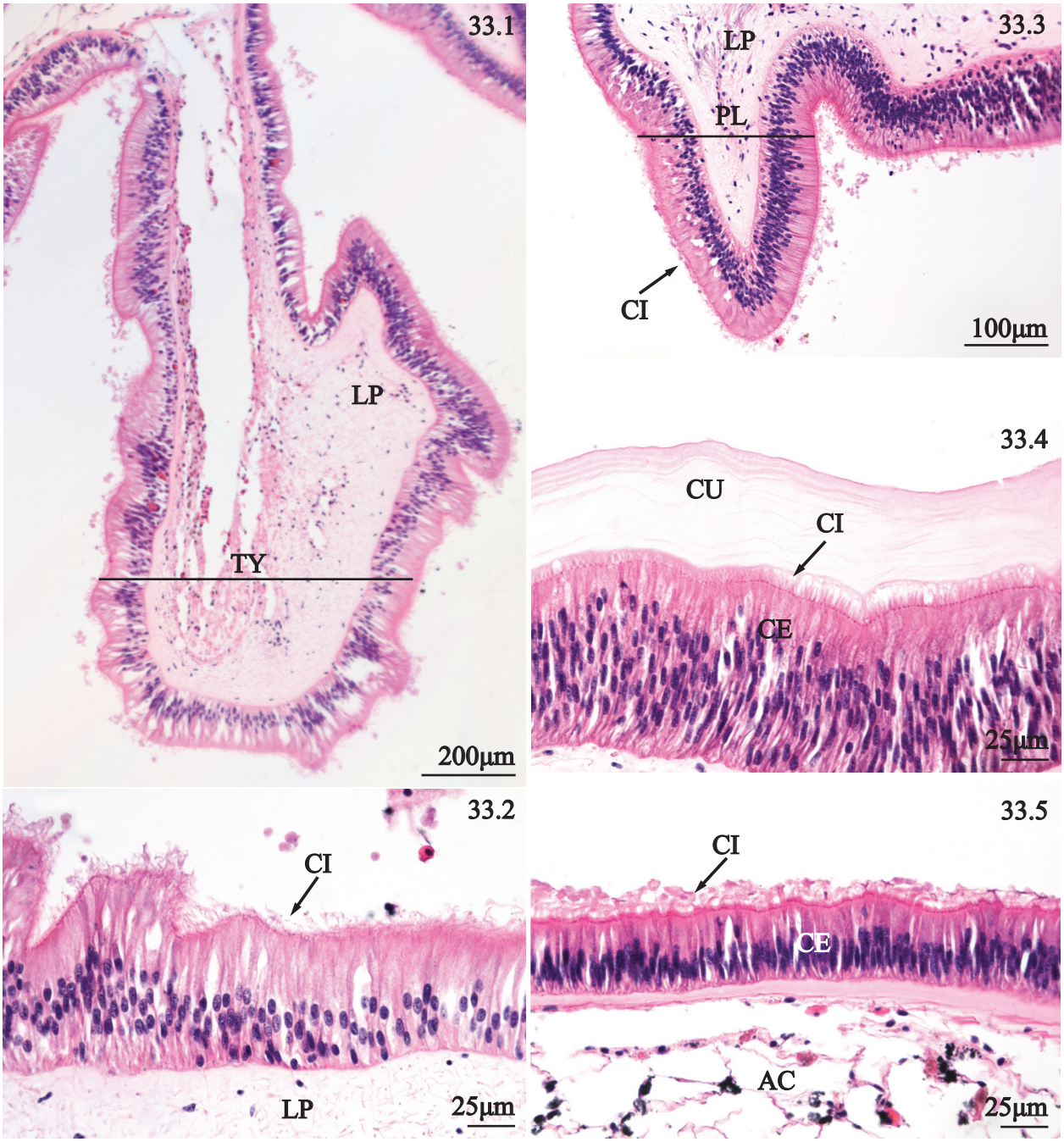
33.1
LP
TY
200µm
33.3
LP
PL
CI
100µm
33.4
CU
CI
CE
25µm
33.2
CI
LP
25µm
33.5
CI
CE
AC
25µm

PLATE 34. Crystalline style sac of *Fusconaia cerina*. 1. Transverse section emphasizing overall structure of the style sac including the crystalline style (SY), style sac epithelium type 1 (E1), epithelium type 2 (E2), and epithelium type 3 (E3). 2. Transverse section of style sac showing the straightened cilia (CI) of type one epithelium and the close proximity of cilia to the style (SY). 3. Transverse section of the style sac portraying the junction between style sac epithelium type two (E2), epithelium type three (E3), and the underlying lamina propria (LP). 4. Transverse section of the style sac showing the style (SY) and laterally extending midgut (MG). 5. Transverse section of the style sac showing the junction between epithelium type one (E1) and type two (E2) and their respective ciliated surfaces (CI). 6. Transverse section of the crystalline style revealing darkened concentric layers (CL), and particulates (PA) near the center of the style.

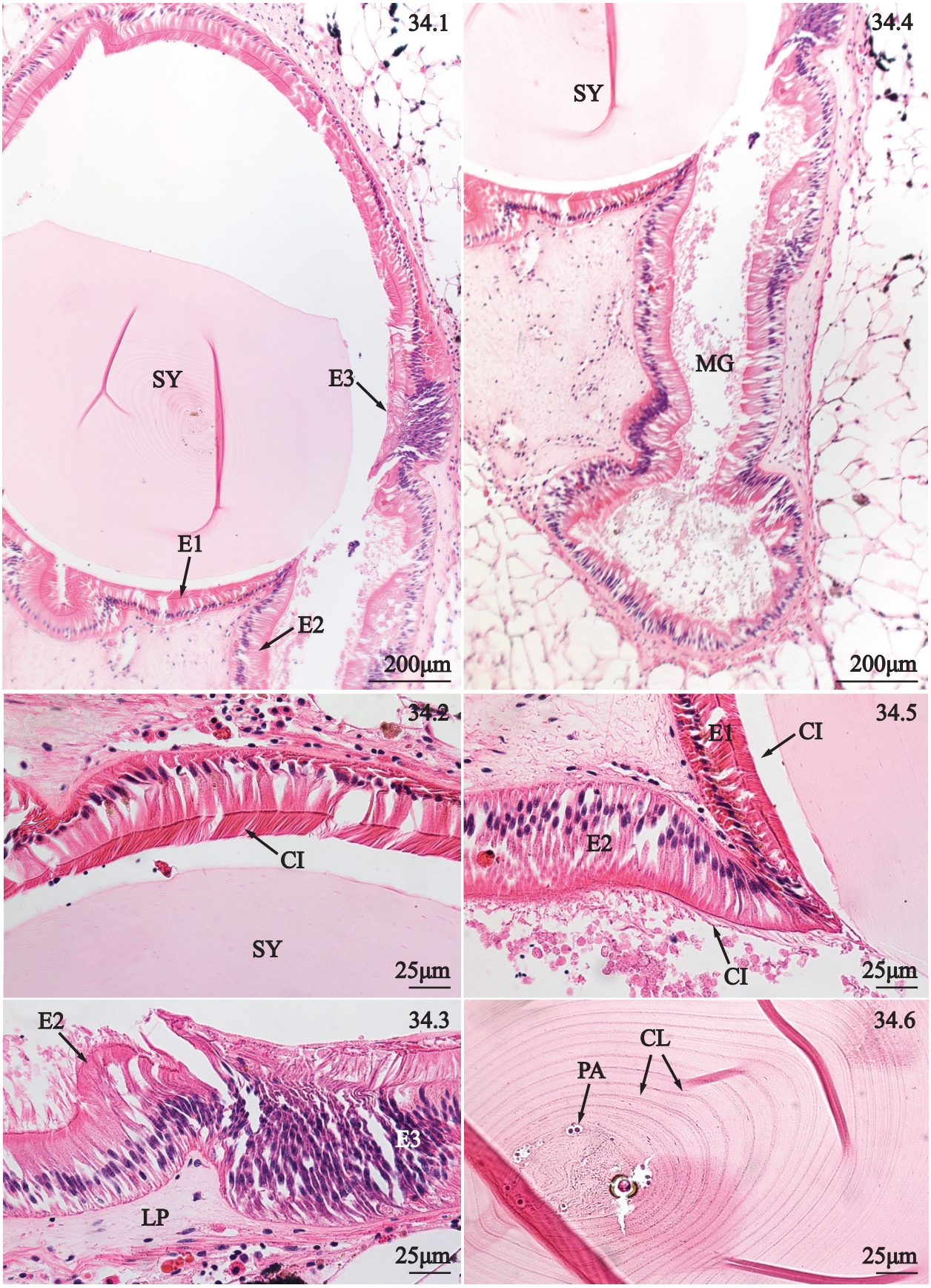
34.1
SY
E3
E1
E2
200μm
34.4
SY
MG
200μm
34.2
CI
SY
25μm
34.5
E1
CI
E2
CI
25μm
E2
34.3
E3
LP
25μm
34.6
CL
PA
25μm

PLATE 35. First intestinal limb, second intestinal limb, and third intestinal limb of *Fusconaia cerina*. 1. Transverse section of the ventral portion of the coelom portraying a cylindrical portion of the third intestinal limb (IN). 2. Sagittal section of descending first intestinal limb emphasizing plicae along the anterior wall (AW) and posterior wall (PW) of the first intestinal limb. 3. Sagittal section of the posterior intestinal wall showing a junction between style sac epithelium types one (E1) and three (E3) with their respective, contrasting ciliated surfaces (CI). 4. Sagittal section through the ascending second intestinal limb displaying sinuous anterior wall (AW), posterior wall (PW) and eosinophilic chyme (CH) occupying the lumen. 5. Sagittal section of second intestinal limb showing tall, thin columnar cells with cilia (CI) and eosinophilic vesicles (EV) overlying a fibrous lamina propria (LP). 6. Sagittal section of the third intestinal limb showing a homogenous columnar epithelium (CE), cilia (CI), and a thin lamina propria (LP) and underlying adipocytes (AC).

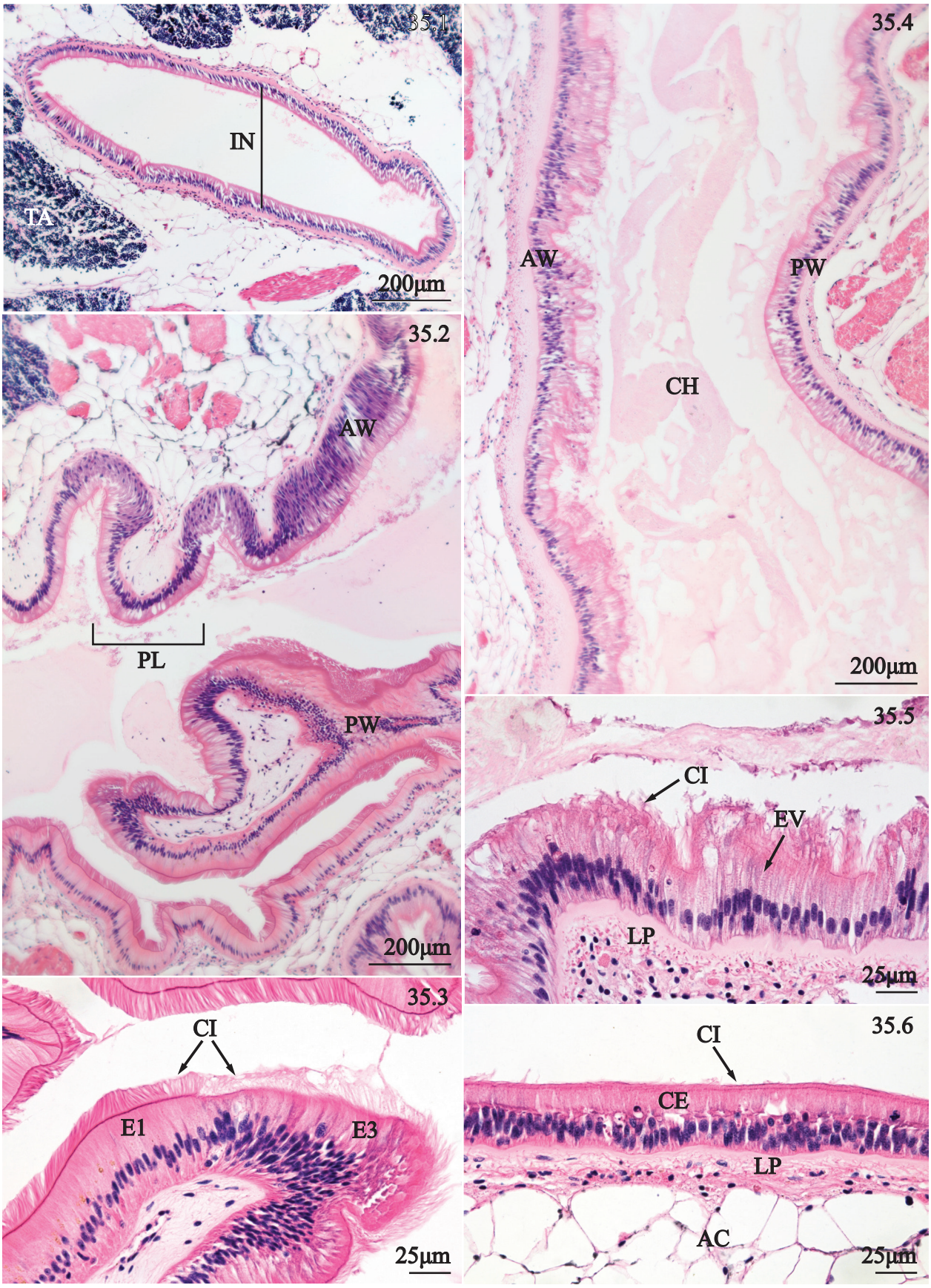
35.1
IN
TA
200µm
35.2
AW
PL
PW
200µm
35.3
CI
E1
E3
25µm
35.4
AW
PW
CH
200µm
35.5
CI
EV
LP
25µm
35.6
CI
CE
LP
AC
25µm

PLATE 36. Fourth intestinal limb, and fifth intestinal limb of *Fusconaia cerina*. 1. Transverse section through the fourth intestinal limb emphasizing a large median typhlosole (TY), lamina propria (LP), and surrounding adipose tissue (AT). 2. Transverse section of the fourth intestinal limb showing eosinophilic columnar cells (EC) and cilia (CI) along the ventral wall, and a fibrous lamina propria (LP) and subepithelial hemocytes (HC). 3. Transverse section of fourth intestinal limb portraying the dense cilia (CI) of the typhlosole, hemocytes (HC) juxtaposed among epithelial cells as well as within sinuses within the lamina propria (LP). 4. Transverse section of the fifth intestinal limb showing a large median typhlosole (TY) with an expansive lamina propria (LP). 5. Transverse section of the dorsal epithelium surrounding the typhlosole consisting of ciliated columnar cells (CI), plicae (PL), and a distinct lamina propria (LP). 6. Transverse section of dorsal intestinal wall featuring cilia (CI), lamina propria (LP) and wandering hemocytes (HC).

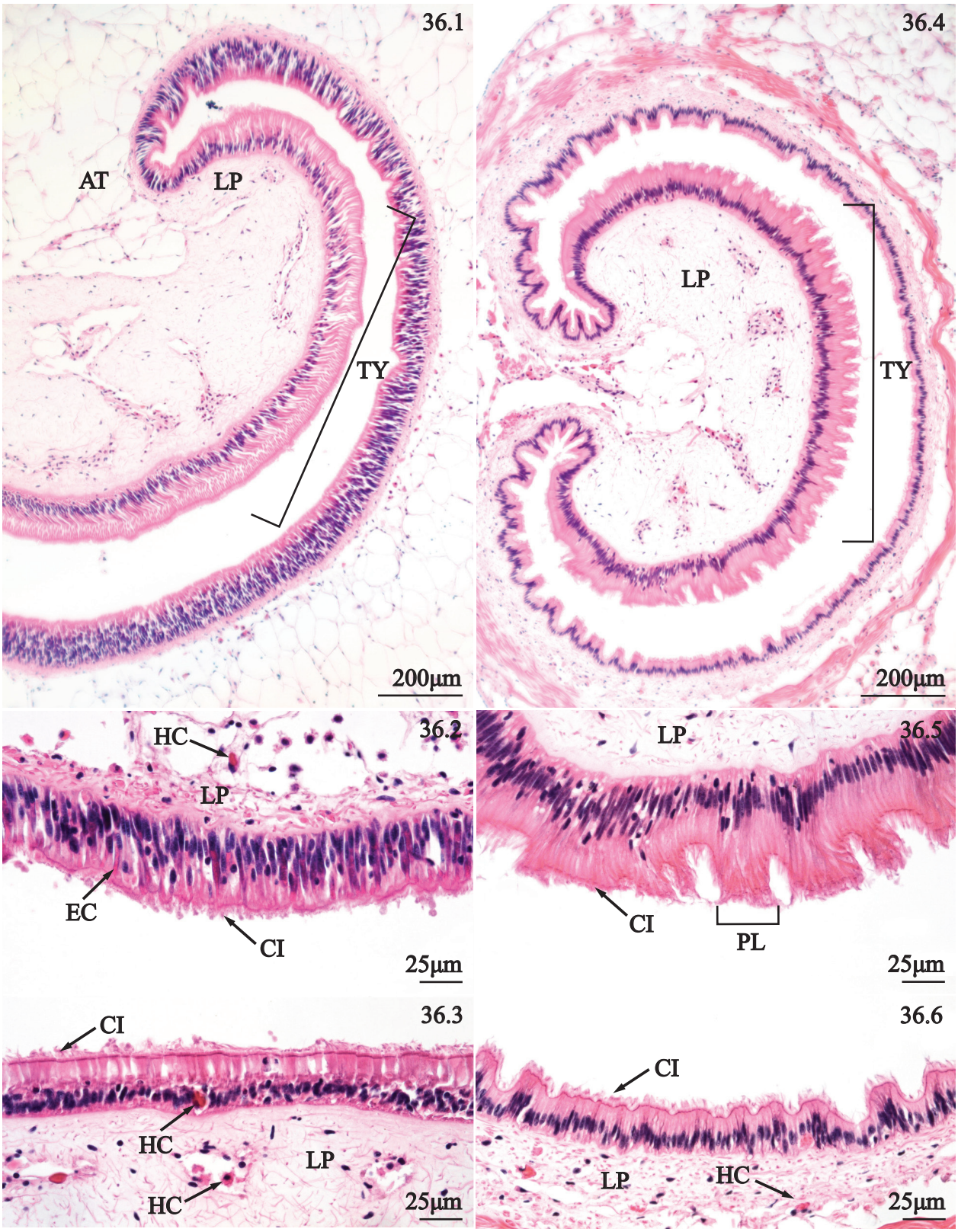
36.1
AT
LP
TY
200µm
36.4
LP
TY
200µm
36.2
HC
LP
EC
CI
25µm
36.5
LP
CI
PL
25µm
36.3
CI
HC
LP
HC
25µm
36.6
CI
LP
HC
25µm

PLATE 37. Heart, and pericardial cavity of *Fusconaia cerina*. 1. Transverse section through the dorsal portion of the visceral mass revealing branching myofibers of the ventricle (VE) surrounding the intestine (IN). 2. Transverse section of the ventricle revealing the epicardium (EC) and myocardium (MC). 3. Transverse section of the ventricle illustrating horizontal and verticle myofibers (MF). 4. Transverse section of the auricle (AU) emphasizing squamous epithelium (SE), cardiac muscle (CM), and adjacent pericardium (PC). 5. Transverse section of the ventricle focusing on an auriculoventricular valve (AV), endowed with connective tissue fibers (CT), and cardiac muscle (CM).

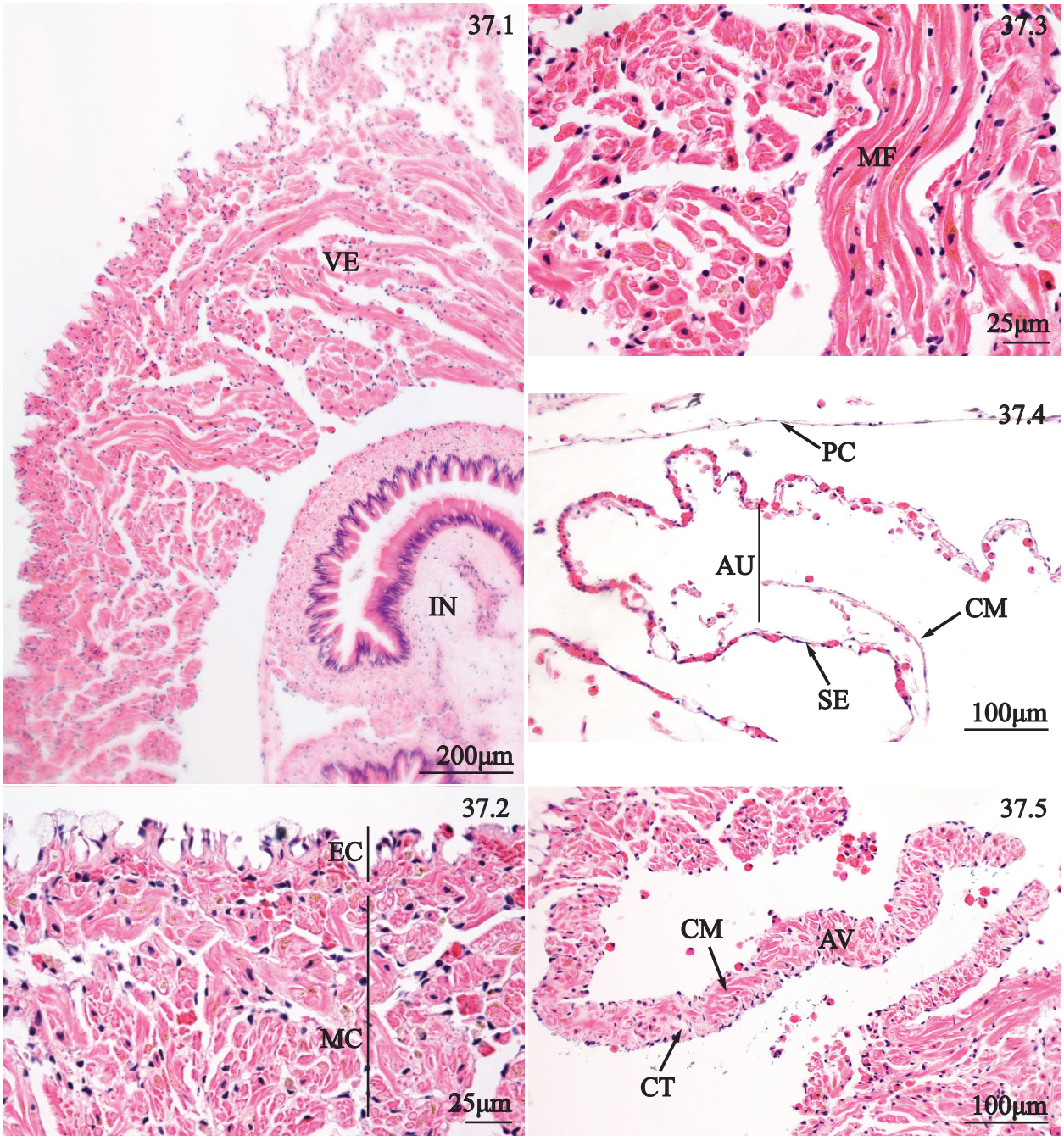
37.1
VE
IN
200µm
37.3
MF
25µm
37.4
PC
AU
CM
SE
100µm
37.2
EC
MC
25µm
37.5
CM
AV
CT
100µm

PLATE 38. Hemolymph vessels of *Fusconaia cerina*. 1. Transverse section of the base of the foot showing a potential artery containing a thick muscular wall (MU), emarginated nuclei of endothelial cells (EN), and surrounding connective tissue (CT). 2. Transverse section of digestive diverticulum revealing a potential vein consisting of a thin muscular wall (MU), emarginated nuclei of endothelial cells (EN), and supporting adipocytes (AC). 3. Sagittal view of adductor muscle portraying a capillary and its endothelium (EN) within the perimysium (PM). 4. Transverse section of the pericardial gland displaying hemocytes (HC), emarginated hemocytes (EH), and emarginated nuclei (EN) of connective tissue cells.

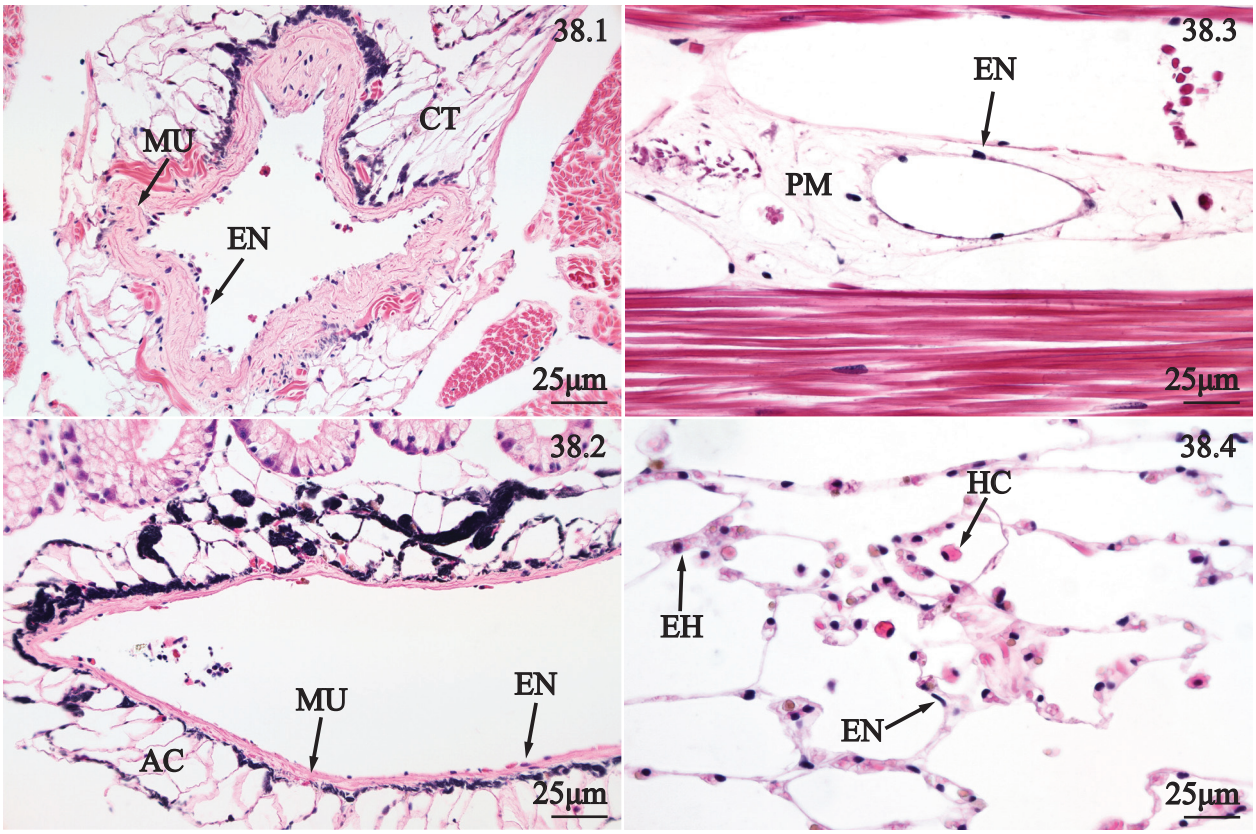
38.1
MU
CT
EN
25µm
38.3
EN
PM
25µm
38.2
MU
EN
AC
25µm
38.4
HC
EH
EN
25µm

PLATE 39. Anterior nephridium of *Fusconaia cerina*. 1. Transverse section of anterio nephridium contrasting the convoluted ventral nephridium (VN), and relatively unbranched dorsal nephiridum (DN). 2. Transverse section of ventral nephridium illustrating convoluted plicae (PL), restricting the ventral lumen (VL). 3. Transverse section of ventral nephridium portraying vesiculated columnar cells (VC), wandering hemocytes (HC) in the epithelium, and emarginated nuclei of endothelial cells (EN). 4. Transverse section of a dorsal nephirdial limb emphasizing plicae (PL), brown, granular epithelial cells (BG), and hemocytes (HC). 5. Transverse section of dorsal nephridum displaying teardrop cells (TC) and underlying dense connective tissue (CT). 6. Transverse section of nephridium showing the ciliated reno-pericardial canal (RC) and adjacent urethra (UR). 7. Transverse section of nephrostome and urethra detailing cilia (CI), and goblet cells (GC). 8. Transverse section of urethra focusing on a dense layer of cilia (CI), and outer layer of goblet cells (GC).

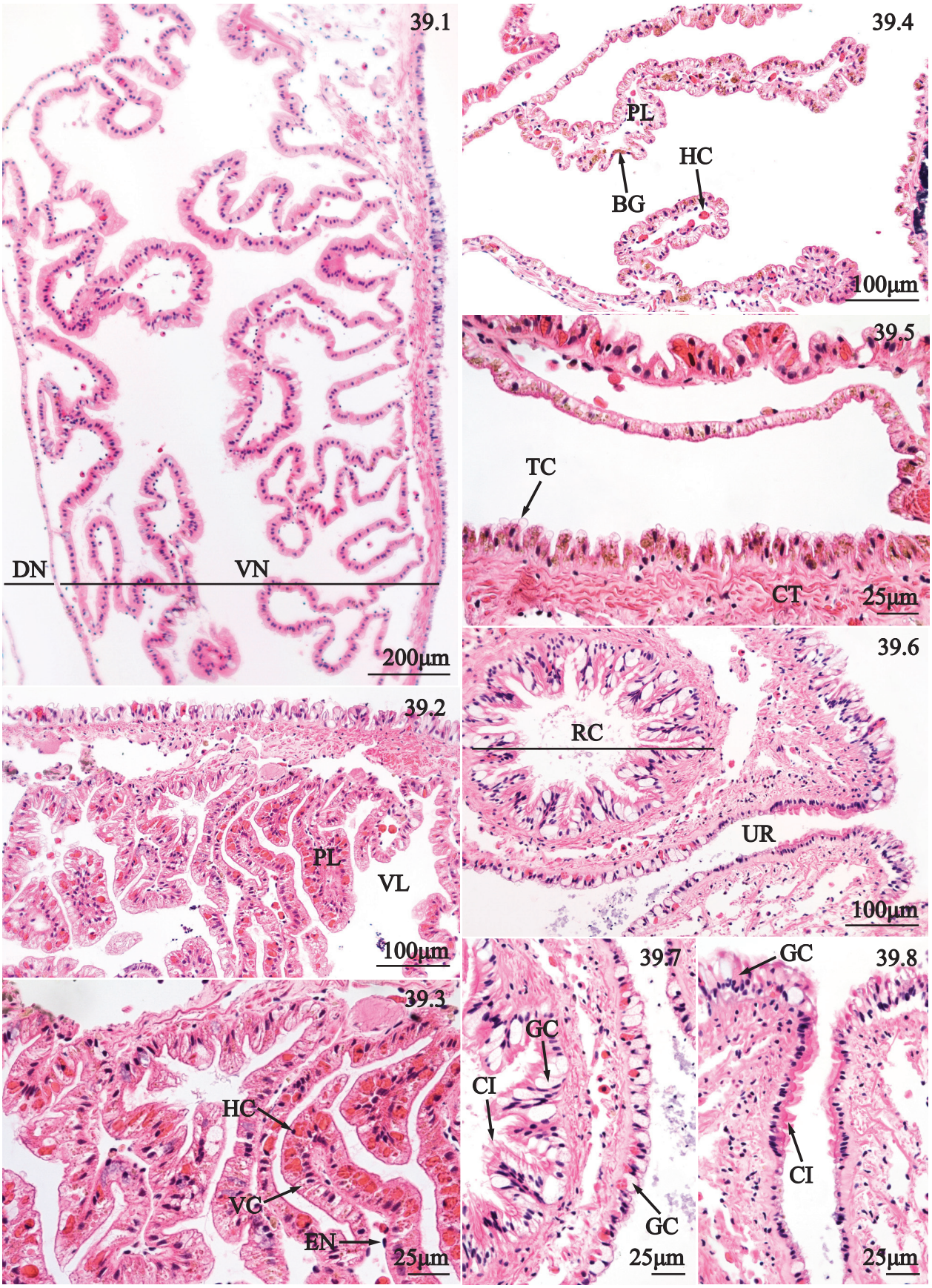
39.1
DN
VN
200µm
39.4
PL
HC
BG
100µm
39.5
TC
CT
25µm
39.6
RC
UR
100µm
39.2
PL
VL
100µm
39.3
HC
VG
EN
25µm
39.7
GC
CI
GC
25µm
39.8
GC
CI
25µm

PLATE 40. Posterior nephridium of *Fusconaia cerina*. 1. Transverse section of the posterior nephridium featuring nephridial branches (NB) and posterior pedal retractor (PR). 2. Transverse section of posterior nephridium detailing columnar epithelium (CE), and fibrous material (FM) of the apical surface, and underlying blood vessels (BV). 3. Transverse section of posterior nephirdium consisting of a nerve fascicle (NE), and a smooth surfaced columnar epithelium (CE). 4. Transverse section of posterior retractor illustrating myofibers (MF), myocyte nuclei (MN),a and a capillary (CA). 5. Sagittal view of posterior adductor portraying spindles of myofibers (MF) and cylindrical myocyte nuclei (MN).

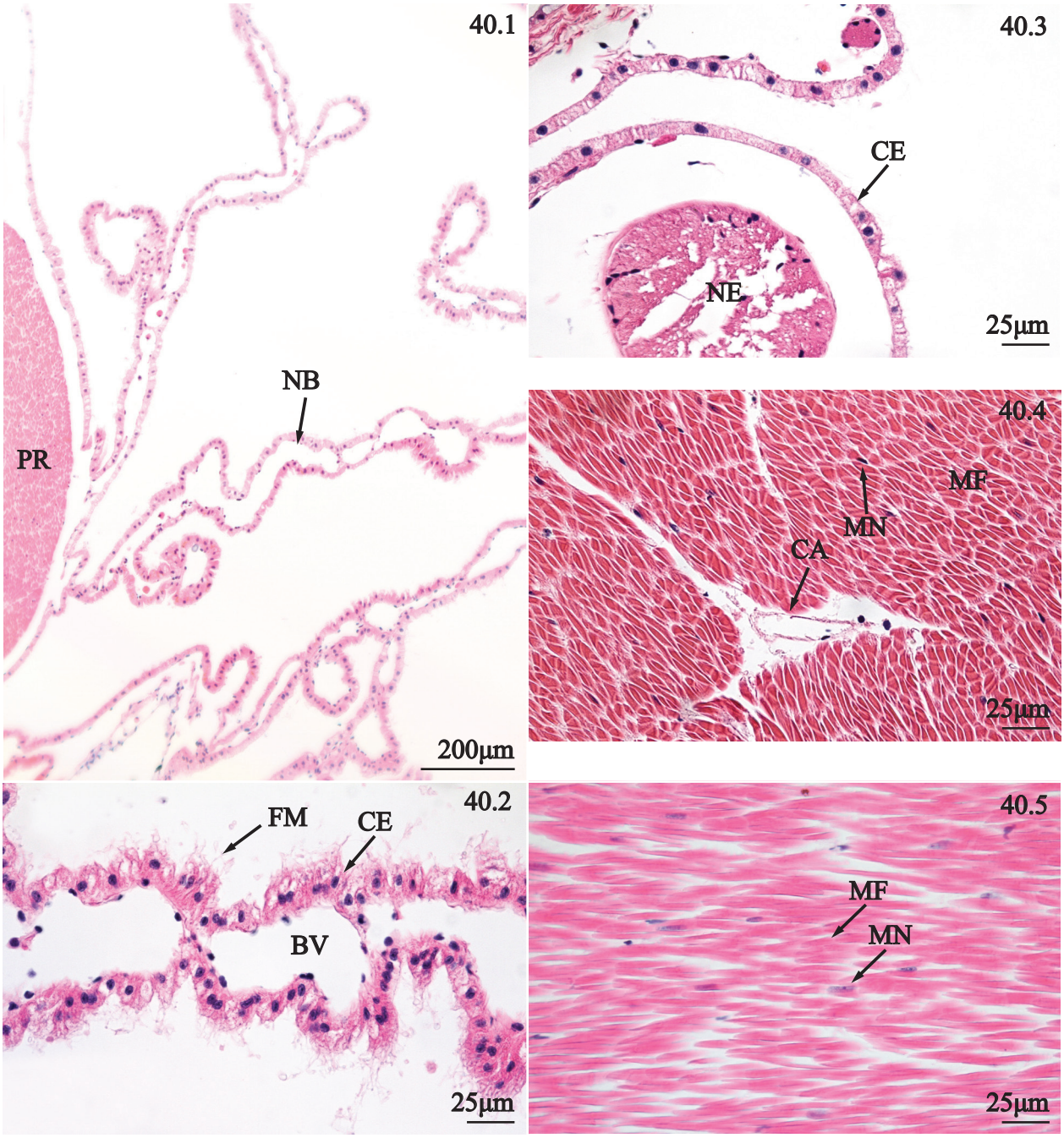
40.1
NB
PR
200µm
40.3
CE
NE
25µm
40.4
MF
MN
CA
25µm
40.2
FM
CE
BV
25µm
40.5
MF
MN
25µm

PLATE 41. Pedal ganglion of *Fusconaia cerina*. 1. Transverse section of pedal ganglion portraying neural cortex (CO), inner medulla (ME), central commissures (CC), dorsal fissure (DF) and ventral fissure (VF). 2. Transverse section of pedal ganglion showing neuron cell bodies (CB), and fibrous epineurium (EN). 3. Transverse section of the median of the pedal ganglion showing central commissures (CC), and dorsal fissure (DF). 4. Transverse section of the pedal ganglion medulla emphasizing the irregular meshwork of axons (AX) and cell bodies (CB). 5. Transverse section of pedal ganglion revealing axons (AX) bundled within a root (RO) and surrounded by membranous connective tissue of the epineurium (EN).

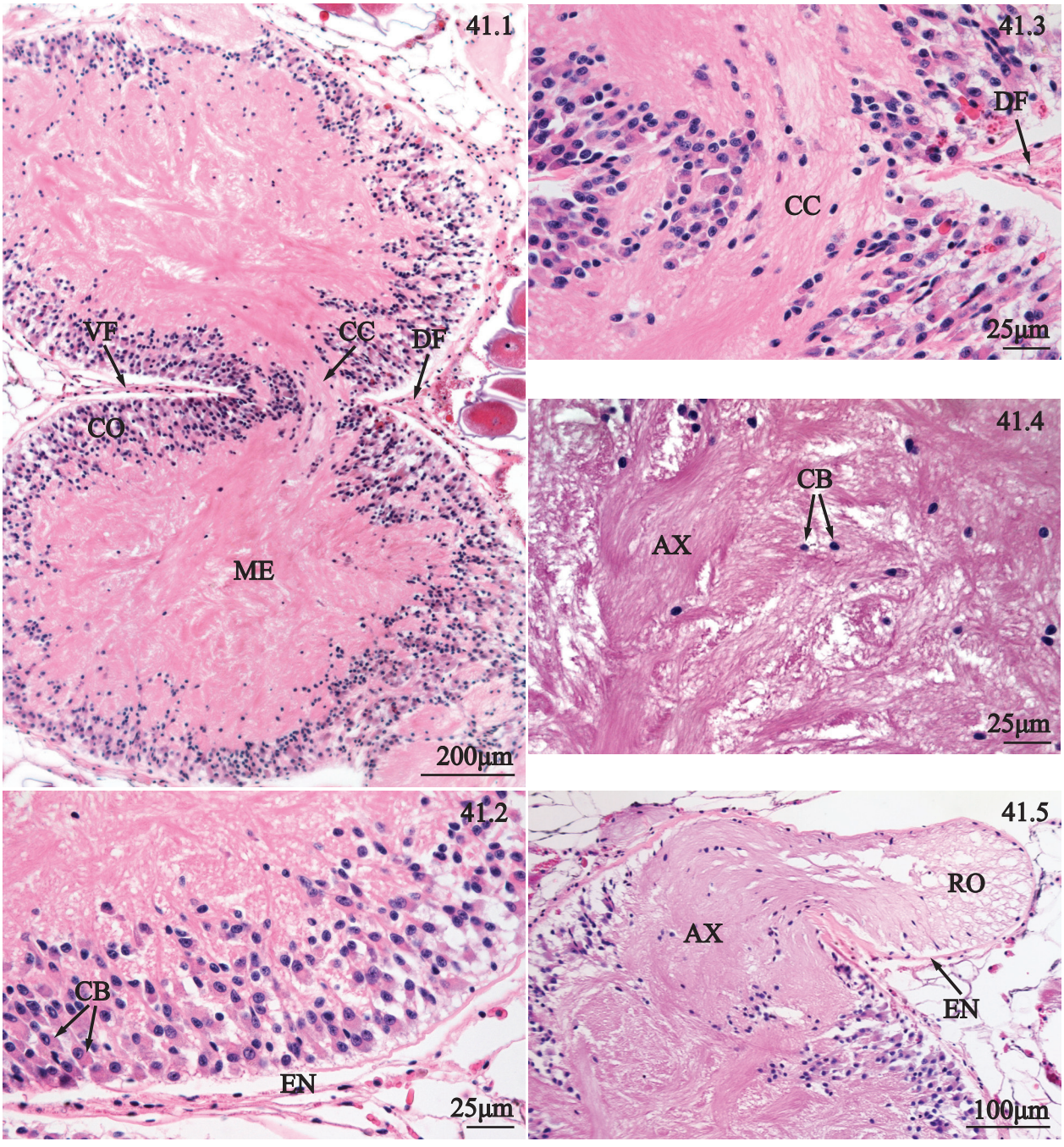
41.1
VF
CC
DF
CO
ME
200µm
41.3
DF
CC
25µm
41.4
CB
AX
25µm
41.2
CB
EN
25µm
41.5
RO
AX
EN
100µm

PLATE 42. Anterior ganglion, and posterior ganglion of *Fusconaia cerina*. 1. Transverse section of anterior ganglion revealing the neural cortex (CO), neural medulla (ME) and a large nerve root (RO). 2. Transverse section of the ventral surface of the posterior ganglion revealing cell bodies (CB) of the neural cortex, and a thick layer of hemolymph (HE) between neural tissue and columnar epithelial cells (CE) facing the suprabranchial cavity. 3. Transverse section of posterior ganglion showing the neural cortex (CO), neural medulla (ME), and a nerve root (RO). 4. Transverse section of the base of the ctenidia showing an anterior nerve (NE) branch of the posterior ganglion juxtaposed with columnar epithelial cells (CE), and a muscle fascicle (MU).

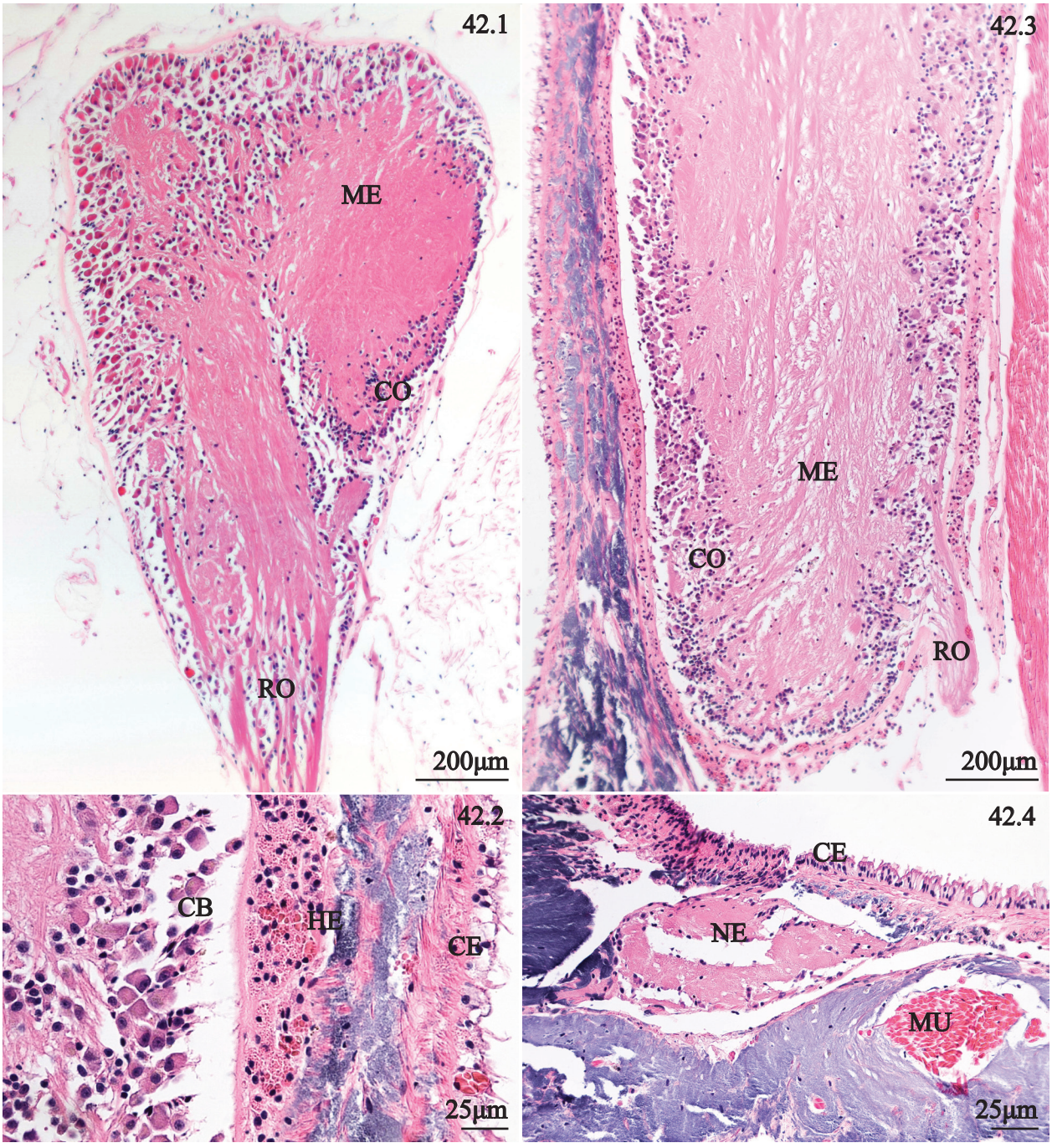
42.1
ME
CO
RO
200µm
42.3
ME
CO
RO
200µm
42.2
CB
HE
CE
25µm
42.4
CE
NE
MU
25µm

PLATE 43. Nerves, and statocysts of *Fusconaia cerina*. 1. Transverse section gonad emphasizing a large nerve consisting of nerve fibers (NF) and a pale, eosinophilic perineurium (PN). 2. Transverse section of foot musculature (FM) detailing a nerve chord (NE) with filamentous axons. 3. Transverse section of a statocyst revealing stratification of columnar cells (CC) and the spherical, median statolyth (SL).

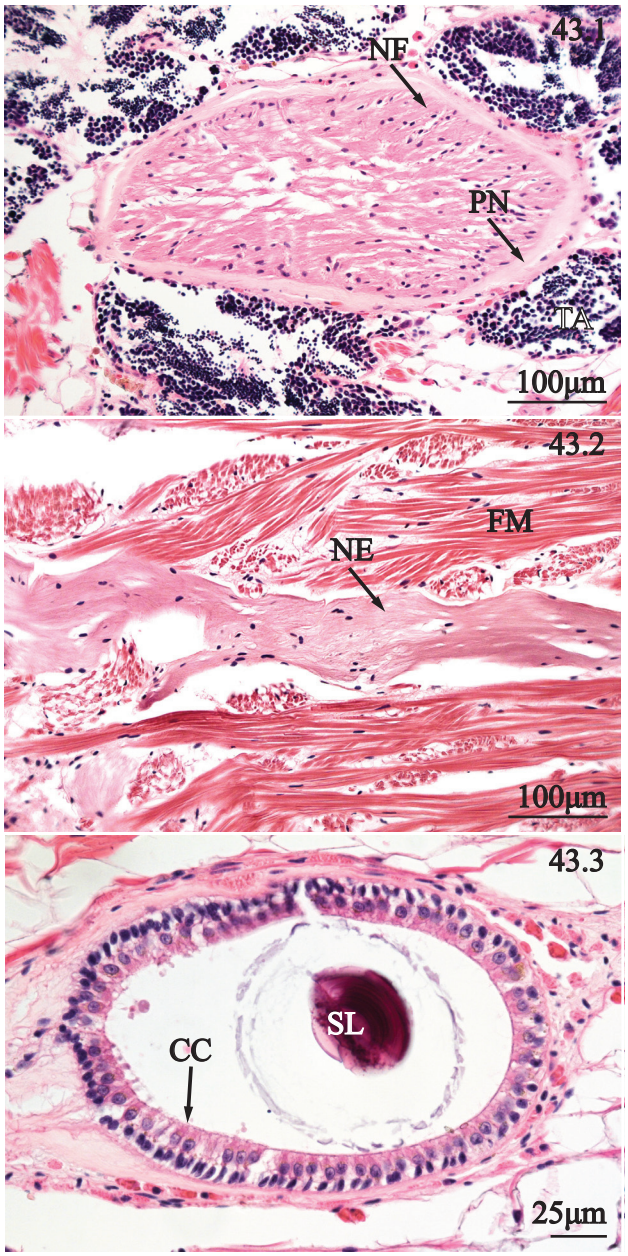
43.1
NF
PN
TA
100µm
43.2
FM
NE
100µm
43.3
SL
CC
25µm

PLATE 44. Ovarian acini, testicular acini, and ciliated gonadal ducts of *Fusconaia cerina*. 1. Transverse section through the visceral mass of an adult female collected in August 2011 displaying immature ovarian acini (OA), and ciliated gonadal ducts (CD). 2. Transverse section of the visceral mass of an adult female collected in August 2011 emphasizing immature oocytes (OC), cell bodies (CB), and emarginated nuclei (EN) of an acinus wall. 3. Transverse section of visceral mass of an adult female collected in May 2011 detailing developing oocytes (DO), enlarged mature oocytes (OC), and a surrounding vitelline membrane (OM). 4. Transverse section of the visceral mass of an adult male collected in August 2011 illustrating a series of immature testicular acini (TA). 5. Transverse section of the visceral mass of an adult male collected in August 2011 emphasizing primary spermatocytes (PS), sperm morula (SM), spermatozoa (SZ), and emarginated nuclei (EN) of an acinus. 6. Transverse section of a mature testicular acinus of a male collected in May 2011 detailing spermiogenesis (SG), and a large quantity of medially located spermatozoa (SZ). 7. Transverse section of the visceral mass of a mature male collected in May 2011 illustrating the passage of spermatozoa (SZ) though a gonadal duct via the action of luminal cilia (CI). 8. Transverse section of the base of the visceral mass of a mature male collected in May 2011 illustrating a gonadal pore (GP) with a pleated epithelial lining (PL).

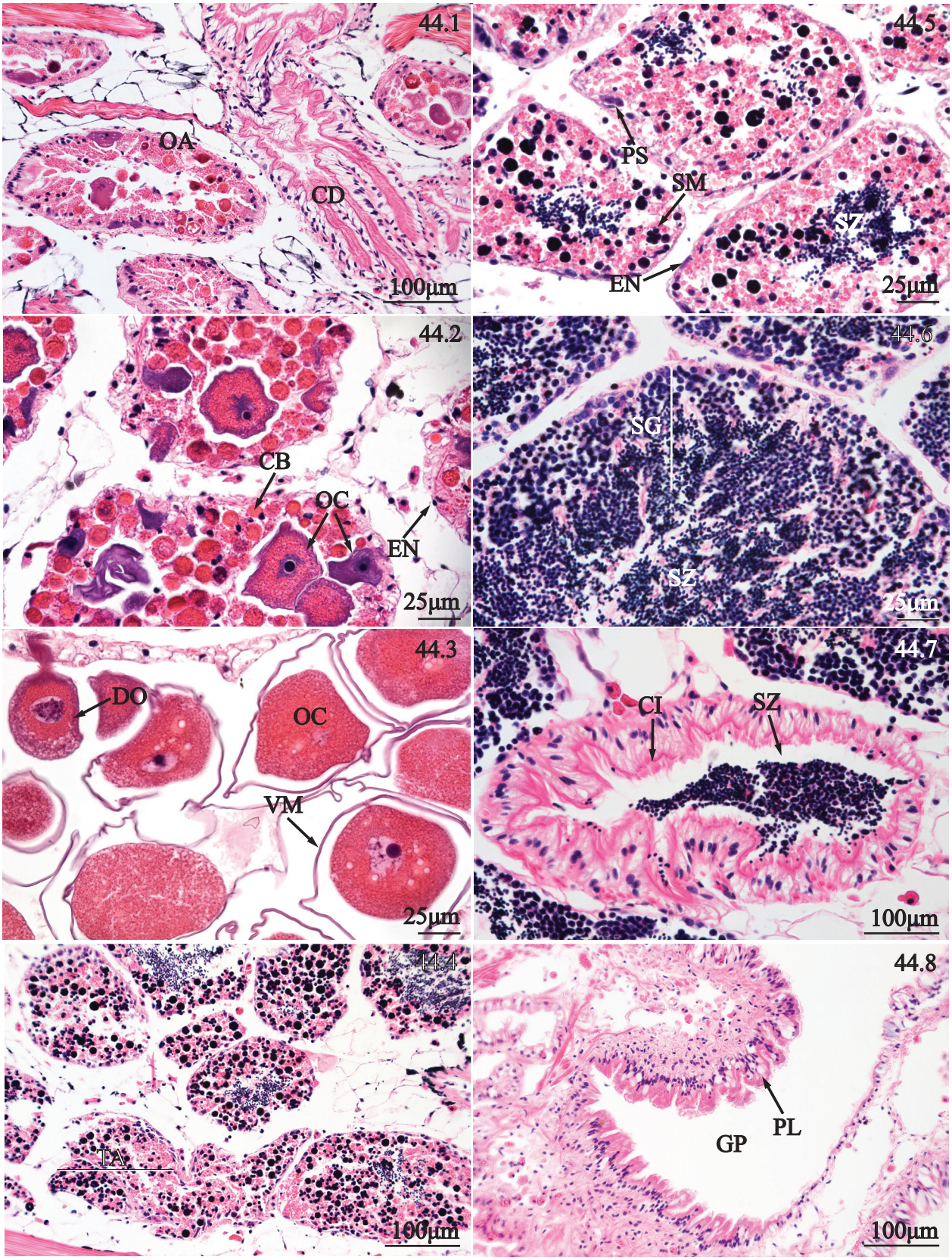
44.1
OA
CD
100µm
44.5
PS
SM
SZ
EN
25µm
44.2
CB
OC
EN
25µm
44.6
SG
SZ
25µm
44.3
DO
OC
VM
25µm
44.7
CI
SZ
100µm
44.4
TA
100µm
44.8
GP
PL
100µm

Chapter 6

SHELL MORPHOLOGY, GROSS ANATOMICAL FEATURES OF THE MANTLE CAVITY, AND CELLULAR STRUCTURE OF MANTLE, GILL, FOOT, AND VISCERAL MASS OF THE ALABAMA CREEKMUSSEL, *Strophitus connasaugaensis* (LEA, 1858)

6.1. Shell morphology

Valves of *Strophitus connasauagaensis* are elongated, and ovular to rhomboidal. The shell is characterized by a light-to-dark brown periostracum and there may be thin to thick black lines along the posterior surface. Each valve is asymmetrical with the ventral margin approximately double the length of the dorsal margin or hinge line. Ventral shell margin may be straightened to slightly concave and the posterior margin may form a rounded point or be truncated with a short, flattened edge. Shell height from umbo to umbo may be moderately compressed to moderately inflated. The umbo extends obliquely towards the anterior shell margin giving the appearance of a sharp dorsal to the anterior shell margin. The posterior side of the shell may have a well-defined longitudinal crease or posterior ridge defining the shape and extent of the posterior slope. The posterior slope of *S. connasaugaensis* may be slightly flattened as compared to the convex ventral surface (Figs. 45.1-45.2).

The inside of the shell is lustrous with a silver nacre. The pallial line is a scar forming an incomplete ellipse around the ventral margin of the nacre between the anterior adductor scar and posterior adductor scar. The anterior adductor is a triangular depression between the anterior shell margin and interdentum. The posterior adductor scar is broad, ovular and flattened with a smaller, circular marking positioned anteriorly demarking the posterior pedal retractor scar. Pseudocardinal teeth are reduced to small, rounded triangular extensions of the shell at the anterior end of the hinge line between the interdentum and ligament. Lateral teeth are virtually absent, and appear as low, rounded ridgeline ventral to the ligament. The umbo cavity is small, forming a narrow cavity that curves dorsally and anteriorly behind the interdentum (Figs 45.3, 45.4).

6.2. Gross anatomical features of the mantle cavity

The posterior aspect of the mantle edge forms a short, incomplete siphon when the sinistral and dextral mantle edges are cupped. The siphon of *S. connasaugaensis* is grey, uniformly pigmented externally, but with irregular transverse lines along the internal surface. When mantle edges are cupped, incurrent and excurrent apertures or openings are formed. The incurrent and excurrent apertures are not divided by a septum, but rather mantle tissue is curled medially and forms trapezoidal flaps that may meet medially or overlap. The incurrent aperture is papillose and papillae are uniramous. Papillae are reduced or absent along the excurrent aperture (Fig. 45.5).

The mantle edge is orange, flattened and pigmentation continues posteriorly to the blackened siphon, just posterior to the posterior adductor. The middle mantle is white and somewhat transluscent, spanning the nacre. A transluscent, trapezoidal keel of mantle tissue, the isthmus, extends dorsally into a cleft between the left, right halves of the shell. The ctenidia are paired consisting of elongated inner and outer gills (Fig. 45.6). Ovigerous females brood using the outer gills and red lines of glochidia are present in marsupia of gravid females (Fig. 45.7). Removing the mantle and gill on one side exposes the foot and visceral mass. The foot of *S. connasaugaensis* is orange, forming a right triangle with a vertical anterior face, and a posterior slope. Visceral mass is white and extends dorsally to the base of the ctenidia. Labial palps are transluscent lips located antero-laterally between the foot and visceral mass. The anterior adductor is pale, white to orange, ovular in outline and oriented vertically between the anterior shell margin and foot. Posterior adductor is grossly identical to the anterior adductor, but is parallel with the posterior shell margin. The gill is supported by a thickened, white line of

connective tissue, and the white line represents the beginning of the abdomen. The abdomen is transluscent and triangular between the visceral mass and posterior adductor. (Fig. 45.8)

6.3. Cellular structure of mantle

6.3.1. Anterior mantle edge

Anterior mantle edge of *Strophitus connasaugaensis* is dorsoventrally compressed with outer, middle and inner lobes nearly equidistant from the base of the mantle edge (Fig. 46.1). The outer mantle lobe is generally flattened except for a few trapezoidal plications along the ventral margin (Figs. 46.1-46.3), and pleated distal end (Figs. 46.1, 46.3). The outer lobe has a simple columnar epithelium with deeply basophilic cells ventrally located along the medial half of the lobe. Outer lobe columnar cells feature an ovular, monochromatic nucleus, obliquely oriented in relation to the horizontal plane of the outer lobe, and the cytoplasm may contain a single, apical, transparent vesicle. In contrast, dorsal epithelium of the outer lobe is largely flattened and columnar cells characterizing dorsal epithelium have an eosinophilic cytoplasm, but are otherwise indistinguishable from ventral columnar cells (Figs. 46.2-46.3). Dorsal epithelium of the outer lobe terminates at the small, cleft-like basal bulb, and abruptly transitions to simple, squamous epithelium (Fig. 46.2). The middle lobe is flattened along the ventral surface, and pleated along the dorsal margin. Middle lobe cell types include a simple squamous epithelium along the ventral margin and a simple columnar epithelium lining the dorsal surface. Squamous cells of the ventral surface consist of an eosinophilic cytoplasm and a monochromatic, nucleus. Secreted periostracum is sometimes observed in histological sections of outer and middle lobes, appearing as an eosinophilic filament, and may be closely apposed to the ventral surface. Columnar cells of the dorsal margin are eosinophilic with an ovular, monochromatic nucleus. Plications of the dorsal surface of the middle lobe give an irregularity to the spacing of columnar cells such that

some cells appear more laterally compressed than others (Fig. 46.4). The inner mantle lobe is triangular with thin, teardrop-shaped plicae along the dorsal and ventral surfaces. Columnar cells of the inner lobe are indistinguishable from those of the dorsal surface of the middle lobe (Fig. 46.5). The dorsal bend to the middle lobe and the ventral bend to the inner lobe may represent fixation artifacts. Teardrop-shaped plicae with columnar epithelial cells extend medially towards the base of the mantle edge and are replaced by plicae endowed with goblet cells. Goblet cells may contain a single transparent vesicle or a series of wispy, basophilic lines, suggesting that mucins are housed within a series of vesicles, and goblet cell nuclei are ovular to emarginated (Fig. 46.6). Dorsal epithelium of anterior mantle edge is flattened with a simple columnar epithelium and the tissue maintains a flattened surface along the medial aspect of the tissue until the base of the outer mantle lobe. Columnar cells of dorsal mantle epithelium have a densely staining, basophilic cytoplasm and an ovular, monochromatic nucleus (Fig. 46.7).

Muscle tissue a large constituent of the mantle edge (Fig. 46.1). The subepithelium of mantle lobes consists of linear tracts of muscle fibers. Myofibers are wavy, and organized into dense bands in the outer and middle lobes (Figs. 46.2-46.4). Myofibers of the inner lobe are arranged in an irregular meshwork (Fig. 46.5). Other tissue components of the mantle edge include irregular sinuses containing blackened hemolymph, nerve fibers (Fig. 46.6), and blue to violet, granular cells beneath the epithelium of the inner mante lobe (Fig. 46.5).

6.3.2. Posterior mantle edge, middle mantle, and mantle isthmus

Mantle lobe morphology differs from anterior mantle edge in several respects. The outer and middle lobes become a forked extension of mantle tissue, each lobe equidistant from its base. Inner mantle lobe is reduced in comparison to the outer and middle lobes. Outer and middle lobes each feature flattened ventral and dorsal epithelia while epithelium surrounding the inner

lobe is plicated. The distal tip of the outer lobe is rectangular and there is a single obliquely oriented crease near the dorsal margin. Inner mantle lobe is reduced and does not extend to the margins of the outer and middle lobes. The epithelium of the outer lobe and middle lobe is flattened, while plicae extend along the inner lobe (Fig. 47.1). Papillae are conical extensions of the mantle edge along the narrow, posterior shell margin. Papillae are darkened, consisting of a simple columnar epithelium containing brown to black intracellular granules and an ovular, monochromatic nucleus. Subepithelium is fibrous and irregular consisting of somatic musculature, hemolymph sinuses, and nerve fibers. The epithelium and subepithelium of the papillae is wavy, giving the surface a folded texture with sharply defined crypts (Fig. 47.2). Darkened granules in posterior mantle edge are located in the epithelium and subepithelial musculature and the preponderance of granules conspicuously blackens the tissue (Fig. 47.3).

Middle mantle is a thin integument between mantle edge and visceral mass. An outer epithelium of columnar cells and goblet cells is adjacent to the nacre. Inner epithelium consists of cuboidal cells and there is a fibrous subepithelium of connective tissue between the outer and inner epithelial layers. Connective tissue of the middle mantle consists of wavy fibers interspersed among hemocytes (Fig. 47.4).

The isthmus is a keel-like structure extending dorsally from the base of the visceral mass. Mantle isthmus originates anteriorly at the beginning of the digestive diverticulum and terminates posterior to the posterior adductor. Isthmus epithelium is simple columnar with an isolated goblet cells epithelium extends around the isthmus and the surface may appear flattened to irregular. The isthmus has a simple columnar epithelium with isolated goblet cells. Isthmus epithelial cells have a pale, eosinophilic cytoplasm and a monochromatic, ovular nucleus, but

columnar cells along the dorsal margin are strongly basophilic. Mantle isthmus has a subepithelium consisting of connective tissue fibers and hemocytes (Fig. 47.5).

6.4. Cellular structure of gill

6.4.1. Non-marsupial gill

Gills are non-plicate, each consisting of an inner and outer lamina with a series of horizontally oriented filaments. Inner and outer gill laminae are joined by a regular arrangement of septa. Gill is porous with cylindrical, vertical sinuses between inner and outer laminae called water tubes (Fig. 48.1). Branchial filaments are cylindrical with three groups of cilia (lateral, latero-frontal, and frontal) along the lateral and distal surfaces. Filaments are each supported by a pair of basophilic skeletal rods and a pale, eosinophilic matrix of connective tissue. The medial aspect of gill filaments consists of a simple squamous epithelium and comprises a blood vessel. Groups of two or more ctenidial filaments are separated by horizontal pores or ostia. Water is admitted into the water tubes through a series of ostia distributed throughout the gill (Fig 48.2). The structure of the inner and outer gills is functionally identical (except for marsupial gills, see below) until the ventral margin. Outer gill have a convex ventral margin (Fig. 48.3) and the ventral margin of an inner ctenidium is furrowed to allow particles captured along the lateral surfaces to accumulate in the median (Fig. 48.4).

Inner ctenidia and outer ctenidia also differ in the way gill tissue is joined to the abdomen. The inner lamina of the inner gill is united with the base of the visceral mass until the anterior-posterior midline of the visceral mass, after the terminus of the digestive diverticulum. The inner lamina of the inner gill becomes separated from the body at the anterior margin of the nephridium, near the urethra (Fig. 48.5). Outer lamina of the inner ctenidium is connected to the abdomen throughout the length of the visceral mass. At the base of the inner gill are a pair of

muscle fascicles spanning the length of the gill (Fig. 48.6). The inner lamina of the outer ctenidium is joined to the abdomen by connective tissue and muscle fascicles are absent from the base of the outer gill (Fig. 48.7). Outer lamina of outer gill joins a narrow region of abdominal connective tissue at the junction of the middle mantle (Fig. 48.8).

6.4.2. Marsupial gill

Female *S. connasaugaensis* brood their glochidia larva in the outer gill and virtually the whole gill is used for larval incubation. A marsupial ctenidium is expanded and includes a cylindrical mass of connective tissue and hemolymph and a sac containing glochidia. Overall, the marsupium of *S. connasaugaensis* is moderately enlarged (Fig. 49.1). The ventral margin of the marsupium is convex and thickened with loose connective tissue and hemolymph (Fig. 49.2). Interbranchial setpa consists of numerous spherical, goblet cells with a basophilic cytoplasm, and a vacuole containing pale, basophilic fibers (Fig. 49.4). Glochidia within a filled marsupium appear to be held together by strands of fibrous tissue, possibly representing a binding substance of a conglutinate of embryos. Glochidia are semicircular with a prominent, median adductor. The valves consist of two tissue components; there is an eosinophilic, granular constituent and a basophilic material with a homogenous staining character. Glochidia of *S. connasuagaensis* attach to fish skin and glochidial valves have spines along the ventral margin of the valves (Fig. 49.5).

6.5. Cellular structure of foot and associated tissues

6.5.1. Pedal musculature and byssal gland

The ventral margin of the foot features a triangular array of overlapping muscle fibers in the median, subepithelial granulocytes, and a highly folded integument (Fig. 50.1). Violet staining granulocytes are located directly beneath the pedal epithelium, while pale, blue-staining

granulocytes are medial in respect to violet cells (Figs 50.2). Foot muscle is composed of regions of irregular and regular muscle fibers. Musculature in the ventral region of the foot has a woven appearance with fibers arranged into a vertical and horizontal plane (Fig. 50.3). The somatic muscle at the base of the foot is organized with distinct vertical and horizontal layers (Fig. 50.4). The base of the foot is broadly triangular with an ovular byssal gland located medially at the ventral margin of the coelom, posterior to the pedal ganglion (Fig. 50.5). The byssal gland is supported by concentric connective tissue fibers and musculature. The lumen is lined with a simple, ciliated columnar epithelium with occasional, pale, basophilic goblet cells. Goblet cells are interspersed among columnar cells in the lumen and the contents of goblet cells appear granular to wispy. Byssal gland goblet cells are similar in some respects to goblet cells of marsupial septa (See Fig. 49.3). The vestiges of the byssus is represented by a spherical, mass containing a pale to darkened eosinophilic material. The byssal mass occupies the center of the byssal gland lumen and is surrounded by an irregular, eosinophilic mass, likely constituting a fluid (Fig. 50.6). Vestiges of the byssal canal were not observed in histological sections of the foot.

6.5.2. Pedal integument and mesentery

There are five epithelium types surrounding the foot and visceral mass. From ventral to dorsal, the integument is initially pleated with a deeply folds and the folds become shorter in height and narrower in width. In the first two regions, plicae are tall and thickened with subepithelial musculature. The first region possesses ciliated, columnar cells with a subepithelium consisting of irregular myofibers and violet granulocytes. Ciliated cells have an eosinophilic cytoplasm, similar to the coloration of the underlying muscle tissue, and cilia are short and nearly straight. Nuclei of type one epithleium are ovular and have a homogenous

staining character (Fig. 51.1). Epithelial region two consists of tall plicae with a more conspicuous space between the folds. Columnar cells largely lack cilia and have an ovular, monochromatic nucleus. Numerous goblet cells are present and closely juxtaposed give the tissue the appearance of large, ovular to teardrop-shaped mucus pores. Subepithelial tissue of integument type two consists of horizontally arranged myofibers (Fig. 51.2). Plicae are noticeably reduced in height and width in region three cells in the second region have similar cytological characteristics as region one, however ciliated cells are sparsely distributed. Region three is characterized by an underlying layer of horizontal muscle and vertical muscle (Fig. 51.3). Integument four consists of a squamous epithelium around rectangular folds of connective tissue. There is a prominent space between the epithelium and pedal musculature of region four. The space possibly represents a hemolymph sinus as observed in *V. nebulosa* and *F. cerina* (Fig. 51.4). The fifth integumentary region of the foot is flattened with squamous cells and goblet cells. Only a subtle waviness of the tissue layer is reminiscent of the plications further down the length of the foot. Musculature under the fifth epithelium is thinner and is separated from the overlying epithelium except for occasional fibrous, connective tissue linkages (Fig. 51.5). Plications of the pedal integument give the surface an irregularly grooved appearance (Fig. 51.6).

The sinistral and dextral halves of the visceral mass are joined by mesentery fascicles distributed throughout the coelom (Fig. 51.7). Fascicles are composed of eosinophilic fibrils with a pale to darkened cytoplasm and fibrils are quadrangular to polygonal. Furthermore, there does not appear to be an obvious pattern of fibril arrangement within a fascicle and the mesentery bundles are histologically identical to pedal muscle fibers (Fig. 51.8).

6.6. Anterior adductor and anterior pedal protractors

Anterior adductor consists of bands of eosinophilic myofilaments longitudinally oriented across the viscera. Fibers are eosinophilic and typically appear wavy in histological sectios. Myocytes have emarginated and elongated nuclei and nuclei are granular. Perimysium consists of thin wispy connective tissue fibers, and form ellipsoid chambers that may contain hemolymph. Additionally, the underlying space of perimysium consists of black granules (Fig. 52.5). The anterior pedal retractors are located between the labial palps and mantle and fascicles are arranged in a transverse orientation when the visceral mass is sectioned transversely. The epimysium, perimysium and endomysium are present, but these structures are delicate, and thin (Fig. 52.6).

6.7. Cellular structure of digestive system tissues

6.7.1. Labial palps, oral goove, and esophagus

Labial palps of *S. connasaugaensis* have an inner palp surface lined with ciliated, rectangular plicae and a smooth outer surface (Fig. 52.1). Plicae of the inner palp surface are rectangular a flattened dorsal margin and a pleated ventral surface. Ciliated columnar cells represent the main constituent of the inner palp epithelium and extend along the palp interior until the distal margin of each lip. Ciliated cells of the inner palp surface have a pale, basophilic cytoplasm and an ovular, monochromatic nucleus. The surface of the epithelium is densely ciliated and cilia are wispy (Fig. 52.2). The free distal palp tip transitions from a pleated, ciliated epithelium to a non-ciliated mucosa characterized by ovular goblet cells (Fig. 52.3). The external palp surface is flattened with non-ciliated cuboidal cells with a monochromatic nucleus (Fig. 52.4). Subpeithelial tissue of the labial palp is composed of loose connective tissue and hemolymph sinuses.

Oral groove is a derivation of labial palp wrapping around the anterior visceral mass. In transverse sections of visceral mass, the oral groove appears as a large chamber posterior to the anterior adductor. The ventral wall of the oral groove resembles the distal margin of a labial palp. The ventral epithelium of the lip resembles the flattened epithelium along the outer surface of the palp while the elongated, rectangular plicae appear to be a continuation of inner palp epithelium. Additionally, the plicae contain elliptical, basophilic goblet cells (Fig. 53.1). Note the similarity between the columnar epithelium of the oral groove ledge (Fig. 53.1) with the epithelia along the inner surfaces of the palps, located at the base of the palps (Fig. 52.1). The lateral walls of the oral groove consist of cuboidal cells bearing cilia and a loose matrix of connective tissue fibers comprises the subepithelium (Fig. 53.2). The dorsal epithelium is flattened with ciliated columnar cells (Fig. 53.3).

The esophagus is tubular continuation of the palps since the walls feature, tall, rectangular plicae. The esophagus is ovular with concentric connective tissue fibers forming a distinct lamina propria (Fig. 53.4). The esophagus is located at the base of the visceral mass, located between digestive gland tubules and the mantle isthmus. Ciliated, rectangular folds extend from the dorsal and ventral esophageal walls. Epithelial cells are pseudostratified and ciliated, with an eosinophilic cytoplasm and an elliptical, monochromatic nucleus. Cilia along the apical surface of esophageal cells are short and generally straight. The lumen of the esophagus may contain a shapeless, eosinophilic mass, which may represent mucus and ingested substances. Additionally, the esophageal epithelium is supported by concentric layers pink and red eosinophilic fibers, creating a heterogenous lamina propria. The esophagus is lined with plicae featuring ciliated columnar cells and there is a subtle, median furrow to the surface of each plication (Fig. 53.5).

6.7.2. Digestive diverticulum

The esophagus opens sinistrally into the digestive diverticulum and the junction of these two organs is marked by a large "L"-shaped chamber. The walls of the vestibular chamber feature cylindrical plicae similar to the constituents of the esophageal-digestive diverticulum junction of *F. cerina*. The lumen of the vestibular chamber contains irregular patches of an eosinophilic fluid, possibly mucus (Fig. 54.1). Plicae of the vestibule are cylindrical and ciliated and the subepithelium features a well-defined connective tissue support (Fig. 54.2). The cell types of the vestibule resemble digestive diverticulum type one epithelium. Cells are ciliated and columnar with a conspicuously eosinophilic cytoplasm and contain a granular nucleus with a small nucleolus. Plicae of type one tubules are flattened to rounded, and some plicae have a single, median furrow (Fig. 54.3, 54.4). Secondary tubules have a homogenous, eosinophilic character and a minute brush border membrane (Fig. 54.5). Furthermore, type two tubules of *S. connasaugaensis* do not appear vesiculated (Fig. 54.6). Tertiary tubules of *S. connsaugaensis* consist of columnar cells with an esosinophilic, vesiculated cytoplasm and triangular rays of basophilic cells. Basophilic cells are somewhat triangular with the apex extending to the lumen. A small, spherical nucleus may be located at the base of basophilic cells and the nucleus has a darker staining character than the surrounding cytoplasm (Fig. 54.7)

6.7.3. Stomach

The stomach is a large chamber between the digestive diverticulum and style sac. Stomach begins as a dextrally placed ovular cavity and merges with a medially located, rectangular chamber. The dextral chamber is widest at the dorsal base and tapers ventrally. Short, rounded plicae with ciliated columnar cells are placed along the sinistral wall, and plicae are absent from the dextral wall (Fig. 55.1). Ciliated cells of the short plicae have an eosinophilic cytoplasm and

an ovular, monochromatic nucleus (Fig. 55.2). The junction between the two anterior chambers has a dorsally placed fold and there are a series of short, rounded plicae along the surface of the fold (Fig. 55.3). The rectangular aspect of the stomach features a series of simple, ciliated, columnar cells organized into short plicae similar to the plicae along the walls of the dextrally placed stomach chamber (Fig. 55.4). A characteristic feature of the stomach is the gastric shield, an obliquely oriented typhlosole with a prominent cuticle. The typhlosole is a rectangular extension of the stomach wall, but the distal portion is rounded and asymmetrical with a broad, dorsal extension of epithelium. Furthermore, the cuticle is pale, eosinophilic, resembling a gelatinous coating and the cuticle generally conforms to the shape of the typhlosole (Fig. 55.5).

The rectangular portion of the stomach connects ventrally to a horizontal chamber before uniting with the style sac. A cuticular covering extends along the epithelium of the ventral stomach chamber. Columnar cells of the ventral chamber are thin, tall and vesiculated with a dense ciliary mat. The cuticle appears to closely adhere to the ciliated surface of the columnar epithelium, but it does not represent a continuous lining around the ventral chamber (Fig. 55.6).

The ventral stomach chamber has different structural features from the dorsal chamber. The ventral wall has an irregular composition alternating between a pleated to a flattened epithelium. The ventral wall has a conspicuous median furrow with a ventrally situated, horizontal cavity (Fig. 55.1). The sinistral margin of the ventral stomach chamber leads to digestive tubules and features rounded, ciliated plicae (Fig. 55.2). Dextral to the median groove is a region of ciliated columnar epithelium with an attached cuticle (Fig. 55.3). The stomach walls on the right side of the stomach are flattened in comparison to the left side of the stomach (Fig. 55.4).

6.7.4. Crystalline style sac

The crystalline style sac is an ovular chamber spanning the length of the body from the stomach to the posterior margin of the visceral mass. The style is a pale, eosinophilic rod located sinistrally, within the circular aspect of the organ. Extending dextrally from the style sac is a horizontal chamber known as the midgut. The style sac consists of three different types of epithelium based on cell size, staining characteristics, and cilium morphology (Fig. 57.1).

The style sac is lined with rectangular, eosinophilic columnar cells with thick, rigid cilia and a conspicuous cell membrane. Nuclei of type-one cells are ovular and contain a distinct nucleolus (Fig. 57.2). Type-two epithelium is located along the ventral surface of the midgut, dextral to the median fold. There are a series of short plicae along the dextral wall of the midgut and they are subtle in the anterior portion of the style sac, but become more prominent posteriorly. Columnar cells of type-two epithelium have a slightly more basophilic and vesiculated cytoplasm. Cilia of type-two epithelium are thinner than type-one cilia and appear correspondingly more flexible given their wispy appearance. Nuclei of type-two cells have an ovular nucleus and a median nucleolus (Fig. 57.3). Type-two epithelium represents the main constituent of the midgut until the median, dorsal surface. Type-three epithelium comprises a distinct region of tall, thin, basophilic columnar cells with short cilia. Nuclei of type-three cells are elliptical, laterally compressed with a nucleolus (Fig. 57.4). The style consists of concentric layers of an eosinophilic, colloid material similar to the cuticular covering of the stomach (Fig. 57.5). The crystalline style sac is surrounded by loose connective tissue comprising a lamina propria (Fig. 57.1). Connective tissue is well developed around the folds, characterized by a lattice of thin fibers, a pale, eosinophilic ground substance, and spindle-shaped nuclei (Figs. 57.2, 57.3).

6.7.5. Intestine

Transverse sections of visceral mass reveal two limbs of the intestine ventral to the crystalline style sac in a sinistral and dextral position. The sinistral limb comprises the ascending second intestinal limb while the dextral intestinal limb represents the third, descending portion of the intestine (Fig. 58.1). The style sac represents the first limb of the intestine and it descends dorsally with an anteriorly directed curvature (Fig. 58.2). Sagittal sections of the posterior visceral mass reveal a complex epithelial structure at the posterior margin of the visceral mass. Style sac epithelium is consistent through the descending portion of its length considering the union of tissue across the lumen (Fig. 58.2). However, the dorsal extent of the first intestinal limb features thin, conical plicae similar to the finger-like plicae along the dextral wall of the midgut (Fig. 58.3). Connective tissue surrounding the first intestinal limb as it descends is identical to lamina propria of the straightened portion of the style sac.

The second intestinal limb is characterized by short plicae that give the lumen a slightly undulating appearance (Fig. 58.4). There are two types of epithelium comprising the lining of the second intestinal limb. The first type of epithelium is located at the beginning of the second intestinal limb as it begins to ascend along the posterior visceral margin. Type-one cells are columnar, with a pale, eosinophilic and vesiculated cytoplasm. Additionally, there are transparent bubbles located at the ciliated surface, possibly representing mucus secretions. Nuclei of type-one cells are ovular with a distinct nucleolus (Fig. 58.5). Type-two cells are more widely distributed throughout the second intestinal limb. Ciliated columnar cells comprising type-two epithelium are distinguished by a darker eosinophilic cytoplasm. Nuclei of type-two epithelial cells are ovular and contain a distinct nucleolus (Fig. 58.6). The second intestinal limb travels anteriorly to the mid-point of the visceral mass, and becomes the third intestinal limb

when it bends to extend posteriorly. Epithelial tissue of the third intestinal limb is not different from the second intestinal limb. Connective tissue surrounding the second and third intestinal limbs is different from the supporting tissue surrounding the first intestinal limb. The tissue has a darker eosinophilic character and nuclei are larger and more spherical than connective tissue surrounding the style sac.

The fourth limb of the intestine is characterized by a prominent, ventrally extending typhlosole. The typhlosole is a large extension of the dorsal intestinal wall consisting of pale, eosinophilic, columnar cells. The ventral wall of the fourth intestine is pleated with short, rounded to flattened plicae (Fig. 59.1). The ventral and dorsal epithelial are both ciliated and cilia are short. Ventral epithelium consists of darkened, basophilic columnar cells. The nucleus of ventral epithelial cells is compressed and teardrop-shaped, and there is a slightly more eosinophilic granular region in the apical portion of the cell. Cytoplasm of ventral epithelial cells is thin and most conspicuous at the apical and lateral portions of plicae (Fig. 59.2). Nuclei of typhlosole columnar cells are ovular and contain a distinct nucleolus. Epithelial cells of the typhlosole are well defined in comparison to the darkened, basophilic cells. Additionally, typhlosole epithelium contains isolated goblet cells. The nuclei of dorsal epithelial cells are ovular and a distinct nucleolus (Fig. 59.3). Connective tissue supporting the typhlosole consists of a latticework of loose connective tissue and spindle-shaped nuclei.

The fifth limb of the intestine is located medially and runs parallel to the hinge line. The intestine is enclosed within the heart, and there is a ring of cardiac muscle surrounding the anterior portion of the intestine. The most prominent feature of the fifth intestinal limb is the large typhlosole extending dorsally into the lumen and the dorsal wall has numerous, narrow plicae (Fig. 59.4). Epithelium of the typhlosole is ciliated and columnar with a pale, eosinophilic

cytoplasm, and an ovular nucleus with a distinct nucleolus (Fig. 59.5). Plications around the dorsal intestinal wall consist of pale, eosinophilic columnar cells bearing cilia. Columnar cells of dorsal and ventral epithelium of intestinal limb five bear a close resemblance to each other (Fig. 59.6). Connective tissue comprising lamina propria of the fifth intestinal limb consists of a lattice of fibers within a pale ground substance and spindle-shaped nuclei. However, there is a thin, darkened layer of fibrous tissue, possibly representing musculature, surrounding the intestine.

6.8. Cellular structure of cardiovascular system tissues

6.8.1. Heart

The heart is located dorsally in relation to the visceral mass and it begins at the anterior margin of the nephridium and terminates between the posterior margin of the visceral mass and posterior pedal retractors. Ventricular cardiac muscle begins as a thin wrapping around the intestine and progressively becomes thicker posteriorly. The ventricle is large, bulbous and medially located while the auricles are thin, irregular extensions of cardiac tissue extending obliquely and medially into the ventricle from the lateral pericardium (Fig. 60.1). The ventricle consists of a thin epicardiaum and a thickened myocardium. Epicardium is a pale, eosinophilic, simple squamous epithelium enclosing the underlying myocardium and epicardium is highly irregular (Fig. 60.2). Myocardium consists of thick bands of myofibers oriented in a transverse and longitudinal plane. Cardiac myocytes have a dark, red, eosinophilic composition with spherical to ovular, monochromatic nuclei (Fig. 60.3). Auricles are thin, incorporate a small amount of cardiac muscle, and have an irregular epicardium. Auricles may be closely positioned to the pericardial sac and pericardium is constructed from squamous epithelial cells (Fig. 60.4). Blood flow traveling into the ventricle is regulated on the sinistral and dextral sides of the

ventricle by the auriculoventricular valves. The auriculoventricular valves are composed of squamous cells and cardiac muscle. Inner and outer valve surfaces feature squamous cells and there is an inner layer of muscle tissue (Fig. 60.5).

6.8.2. Arteries, veins, capillaries, and pericardial gland

Hemolymph is located throughout the viscera and mantle of *S. connasaugaensis*. Adipose tissue represents a significant portion of the connective tissue of the coelomic cavity and mantle and there is a preponderance of black, ink-like granules located within the interstitial spaces of adipose tissue. Additionally, there are isolated hemocytes located within interstitial spaces of coelom and mantle (See Figs. 47.4, 52.2, 55.4 for examples). However, the circulatory system has numerous circular to ovular tubes representing blood vessels. *S. connasaugaaensis* has a network of arteries, veins, and capillaries similar to *V. nebulosa* and *F. cerina*. Blood vessels consisting of thickened musculature may comprise arteries (Fig. 61.1). Blood vessels that incorporate less muscle tissue are potential veins and veins have a more irregular shape (Fig. 61.2). Capillaries are also apparent, especially within adductor muscle and mantle edge. Capillaries are characterized by a ring of squamous cells and correspondingly have a small diameter (Fig. 61.3).

The dorsal aspect of the visceral mass consists of an extensive fibrous tissue surrounding the pericardium. The fibrous tissue represents the pericardial gland and it is characterized by pale, eosinophilic fibers and hemocytes. Pericardial gland cells are irregularly oriented and possess an emarginated nucleus. Hemocytes are located freely within the lumen of the pericardial gland and some hemocytes seem to adhere to the pericardial gland cells (Fig. 61.4).

6.9. Cellular structure of renal tissues

6.9.1. Anterior nephridium

The nephridium is a large tubular organ located dorsally to the left and right of the visceral mass. Nephridium extends down the length of the body from the midpoint of the visceral mass to the posterior adductor. Nephridium consists of distinct ventral and dorsal limbs and the morphology of each limb changes posterior to the visceral mass. At its anterior extent, the ventral nephridium has a convoluted epithelium and the dorsal limb is a simple cavity underlying the ventral region (Fig. 62.1). Ventral nephridium features a simple columnar epithelium consisting of strongly eosinophilic, vesiculated cells. The surface of the ventral nephridial cells is smooth, seemingly lacking cilia or microvilli. The branching pattern of the ventral nephridium of *S. connasauagaensis* is more simplified in comparison to nephridial branching of *V. nebulosa* and *F. cerina*. The subepithelium of ventral nephirdium consists of a pale, eosinophilic layer of squamous cells comprising the endothelium (Fig. 62.2). The dorsal nephridium consists of cuboidal cells with a pale, eosinophilic cytoplasm and a spherical, monochromatic nucleus. Dorsal nephridium has isolated regions of columnar cells containing a pallid median vesicle. Some vesiculated columnar cells are teardrop shaped with an apical vesicle (Fig. 62.3). Dorsal nephridium largely lacks branches, but a small number of reduced plicae are present (Fig. 62.4). Fluid from the pericardial cavity is flushed into the ventral nephridium through a ciliated duct or reno-pericardial canal at the anterior end of the nephridium. The reno-pericardial canal merges with ventral nephridium at the lateral margin of the ventral nephridium, but appears to be a circular duct at its midpoint. Transverse histological sections of the nephridium show a circular duct representing the midpoint of the renal-pericardial canal and the adjacent, laterally positioned urethra (Fig. 62.5). Epithelial tissue comprising the renal-pericardial canal features ciliated

columnar cells, and goblet cells organized into conical plicae enclosed within a thickened circumferential lamina propria (Fig. 62.6). The histological composition of the urethra resembles the dorsal nephridial chamber until the distal most portion near the communication between the nephridium and suprabranchial cavity. The urethra of *S. connasaugaensis* is characterized by darkend, basophilic columnar cells bearing cilia. Cilia are short and densely distributed across the surface of the epithelium towards the distal end of the urethra (Fig. 62.7).

6.9.2. Posterior nephridium

Nephridial branches expand, and the tissue becomes enlarged between the posterior margin of the visceral mass and posterior adductor. Nephridial epithelium is convoluted, consisting of epithelial folds with a repeating stem-loop configuration (Fig. 63.1). Posterior nephridial branches are spaced farther apart from each other than in the anterior nephridium. Epithelial cells are cuboidal to columnar with a pale eosinophilic and granular cytoplasm. Cytoplasm of nephridial cells may contain brown granules while the apical surface of some cells has a filamentous, eosinophilic residue, possibly representing a secretion. Each half of a nephridial branch is united by filamentous, connective tissue septa. The medial portion of a nephridial branch constitutes a blood vessel and emarginated nuclei of endothelial cells are present (Fig. 63.2). The ventral margin of the posterior nephridium features a pair of large nerves. Each nerve consists of an outer epineurium and an inner, granular focus of axons (Fig. 63.3).

6.10. Posterior adductor and posterior pedal retractors

Posterior pedal retractors are located within the nephridial septum, between the posterior adductor and visceral mass. Pedal retractors have a distinct epimysium surrounding a series of fascicles. Connective tissue of pedal retractors is delicate, especially the epimysium and perimysium. Endomysium consists of a pale, eosinophilic membranous material between

myofibers. Myofibers are polygonal in a transverse orientation, and have a dark, eosinophilic cytoplasm (Fig. 63.4). The posterior adductor is located posterior to the retractors and is oriented longitudinally when mussels are transversely cut. Adductor myofibers are organized into large fascicles with a simple, squamous epimysium and a delicate, fibrous perimysium. Myofibers of the posterior adductor are long, eosinophilic filaments with elliptical, heterochromatic nuclei and a distinct nucleolus (Fig. 63.5). Perimysium is thin, membranous and contains a series of ellipsoid capillaries.

6.11. Cellular structure of nervous system tissues

6.11.1. Pedal ganglion, cerebral ganglia, and visceral ganglion

Nervous system of *S. connasaugaensis* consists of four ganglia, each with a series of nerve fibers extending throughout the body. A pair of cerebral ganglia is located anteriorly; each ganglion is positioned laterally along the body between the anterior adductor and labial palp. The third ganglion is referred to as the pedal ganglion since it is located at the ventral margin of the coelom between the digestive diverticulum and gonad, dorsal to the base of the foot. Finally, the pleural ganglion is located on the ventral surface of the posterior adductor. Each ganglion has a distinct outer cortex of neuron cell bodies, and a fibrous inner medulla. Furthermore, there is not an obvious difference between the cellular characteristics of all ganglia and therefore the foregoing description of the neural cortex and medulla of the pedal ganglion is representative of the anterior and posterior ganglia.

Pedal ganglion is bi-lobed, each hemisphere is surrounded by a distinct epinurium, and separated by a median fissure. Central commissures oriented horizontally represent communications between the hemispheres (Fig. 64.1). Neuron cell bodies in the cortex are conical to polygonal, with the apex extending towards the medulla neuron. Cell bodies have a

pale, basophilic cytoplasm and a spherical nucleus and a nucleolus may be observed in some cells (Fig. 64.2). Fissures separating the hemispheres are fibrous with a pale, eosinophilic character. The medulla has an irregular array of axons and isolated cell bodies. Commissures represent a continuation of the medulla, joining each ganglionic lobe by means of horizontal bundles of axons (Fig. 64.3). Cell bodies of the medulla have a spherical to spindle shaped nucleus and only a small amount of darkened, eosinophilic cytoplasm is visible (Fig. 64.4). Axons leave the hemispheres at lateral extensions of the medulla at dorsal and ventral margins of the hemispheres. Roots along the lateral margins of the pedal ganglion consist of large bundles of axons and supporting cells (Fig. 64.5). Nerves derived from the ventral aspect of each hemisphere extend ventrally through the pedal musculature. Pedal nerves from dorsal roots span the vertical length of the visceral mass.

The cerebral ganglia are spherical to ovular, located within connective tissue between the palp, anterior pedal retractor, and adductor (Fig. 65.1). Nerves derived from anterior ganglia extend into the anterior adductor, retractor, foot, and mantle edge. The visceral ganglion is cylindrical, and closely applied to underlying myofibers of the posterior adductor (Fig. 65.3). The ventral surface of the visceral ganglion consists of a thin layer of connective tissue and an epithelium represented by simple columnar cells and goblet cells. Additionally, columnar cells contain brown intracellular granules and the entire cytoplasm is darkened (Fig. 65.2). The inner gill reunites with the body at the anterior margin of the posterior adductor. At ctenidial-adductor junction, ganglionic tissue extends ventrally into the base of the gill tissue (Fig.65.4).

6.11.2. Nerves and statocysts

Nerves may be distinguished from connective tissue by the pale eosinophilic membrane or perineurium, surrounding nerve fascicles. The perineurium is thickened with a homogenous

staining character while groups of axons have small, irregularly by polygonal spaces between each other. Transverse sections show how the contents of a bundle of nerves are irregular or vesiculated mass of fibers (Fig. 66.1). Longitudinal sections of nerves portray bundles of axons as sinuous ribbons of fine, eosinophilic, fibers (Fig. 66.2). Additionally, nerves contain a series of nuclei; cylindrical to emarginated nuclei near the perineurium are possible Schwann cells. Spindle-shaped to polygonal nuclei medially located within a nerve appear to be neuron cell bodies. Nuclei of neuron cell bodies have a small perimeter of basophilic cytoplasm. Given the above, the smallness of nerve cells precludes definitive identification with hematoxylin and eosin-stained tissue sections.

Statocysts represent accessory structures of the nervous system associated with the pedal ganglion. A statocyst is an ovular capsule located at the ventral margin of the coelom, lateral to the pedal ganglion. Statocyst epithelium consists of ciliated columnar cells lining the lumen and a basal layer of cuboidal cells. Columnar cells of a statocyst have a pale eosinophilic cytoplasm and a spherical, basophilic nucleus containing a small nucleolus. The lumen of the statcyst contains a dark, spherical mass called the statolyth. The statolyth has a dark, violet character and may appear fragmented. A thickened, pale, eosinophilic capsule surrounds the statocyst and connective tissue becomes continuous with coelomic connective tissue associated with the pedal ganglion (Fig. 66.3).

6.12. Cellular structure of reproductive system tissues

Ovarian and testicular tissues are organized into ovular acini. Ovarian and testicular acini were immature during May 2011 from individuals collected in Shoal Creek while peak gametogenesis was evident in one male and one female *S. connasaugaensis* collected from South Fork Terrapin Creek in August 2011. Immature ovarian acini are widely dstributed amongst

connective tissues and ciliated gonadal ducts (Fig. 67.1). Immature ovarian acini contain a large concentration of eosinophilic matter consisting of small, spherical granules and larger cells, possibly representing polar bodies. The eosinophilic granules may represent the remains of polar bodies and apoptotic oocytes. Oocytes of immature acini are spherical to ovular, basophilic with a distinct, spherical nucleus, and a series of transparent cytoplasmic vescicles. Immature oocytes may be free within the lumen of attached to the acinius wall by a pellicle (Fig. 67.2).

Mature females sampled in August were characterized by enlarged acini with correspondingly enlarged mature oocytes. Ovarian acini of mature females contain mature oocytes and a well-defined perimeter of eosinophilic, granules and small irregular nuclei. Mature oocytes begin as a small basophilic cell with a distinct nucleus and nucleolus. Oocytes are attached to the acinus wall by a pellicle and eventually separate from the wall when they reach a certain size. As oocytes mature, they become larger and eosinophilic cytoplasm becomes more prominent. Mature oocytes of *S. connasaugaensis* have a red, granular cytoplasm and a pale, basophilic nucleus with dark patches of chromatin. The membrane of mature oocytes is irregular, with a pale staining character. However, the distal margin of the vitelline membrane appears to be more condensed and fibrous. Mature oocytes are greatly enlarged, occupying the majority of the lumen of the acinus (Fig. 67.3).

Immature testicular acini are small and positioned within a matrix of adipocytes and ciliated ducts (Fig. 67.4). The most characteristic feature of immature testicular acini is the clusters of sperm morula. Spermatocytes undergo a cell division process resulting in a series of smaller, closely spaced cells. Spermatocytes of sperm morula appear to largely lack cytoplasm and consist of a darkened cell body. Small eosinophilic granules are interspersed among sperm

morula possibly representing a fluid or the remains of broken down spermatocytes. A small quantity of spermatozoa may be present within the center of the acinus (Fig 67.5).

Mature testicular acini are enlarged and distinguished by a plethora of spermatozoa. The luminal contents contain such a large quantity of actively dividing spermatocytes and spermatozoa that virtually the entire acinus is darkened. Dividing spermatocytes are spherical and have a pale basophilic character. Sperm morula are also present, but less abundant than in immature testicular acini. As in immature testicular acini, the small size and dark staining character of spermatocytes and sperm morula make observations of specific meiotic phases difficult (Fig. 67.6). When acini are mature, ciliated gonadal ducts carry sperm and ova from acini to the gonopores. Presently spermatozoa and mature ova were observed descending to the gonopores (Fig. 67.7). The gonopores are located at the dorsal end of the visceral mass, ventral, and anterior to the nephridium. Gonopores appear C-shaped in histological sections and the lining consists of ciliated columnar cells and goblet cells. Goblet cells are more numerous just outside of the gonopores (Fig. 67.8).

PLATE 45. Shell morphology, and gross anatomical features of the mantle cavity of *Strophitus connasaugaensis*. 1. Lateral view of right valve showing the anteriorly directed umbo (UM), dorsally located ligament (LI), posterior slope (PS), and posterior ridge (PR). 2. Lateral view of left valve showing the anteriorly directed umbo (UM), dorsally located ligament (LI), posterior slope (PS), and a well-defined posterior ridge (PR). 3. Medial view of the right valve showing the leading edge of the periostracum (PE), nacre (NA), pallial line (PL), anterior adductor scar (AS), posterior adductor scar (PS), pseudocardinal tooth (PT), interdentum (ID), umbo cavity (UC), and ligament (LI). 4. Medial view of the left valve showing the leading edge of the periostracum (PE), nacre (NA), pallial line (PL), anterior adductor scar (AS), posterior adductor scar (PS), pseudocardinal tooth (PT), interdentum (ID), umbo cavity (UC), and ligament (LI). 5. Ventrolateral view of *Strophitus connasaugaensis* (ca. 80 mm shell length) buried in sand at Shoal Creek with its mantle cupped forming an incurrent aperture (IA) and excurrent aperture (EA). 6. Medial view of the mantle cavity with the right valve and right mantle removed to show the position of the mantle edge (ME), middle mantle (MM), foot (FO), anterior adductor (AA), labial palp (LP), inner gill (IG), outer gill (OG), posterior adductor (PA), mantle isthmus (MI), and supraanal aperture (SA). 7. Medial view of the mantle cavity with the right valve and right mantle removed to show the position of the mantle edge (ME), middle mantle (MM), foot (FO), anterior adductor (AA), inner gill (IG), outer gill (OG), glochidia (GL), posterior adductor (PA), mantle isthmus (MI), and supraanal aperture (SA). 8. Medial view of the mantle cavity with the right valve, right mantle, and right gills removed to show the position of the mantle edge (ME), middle mantle (MM), foot (FO), labial palp (LP), visceral mass (VM), anterior adductor (AA), left inner gill (IG), posterior adductor (PA), mantle isthmus (MI), and supraanal aperture (SA).

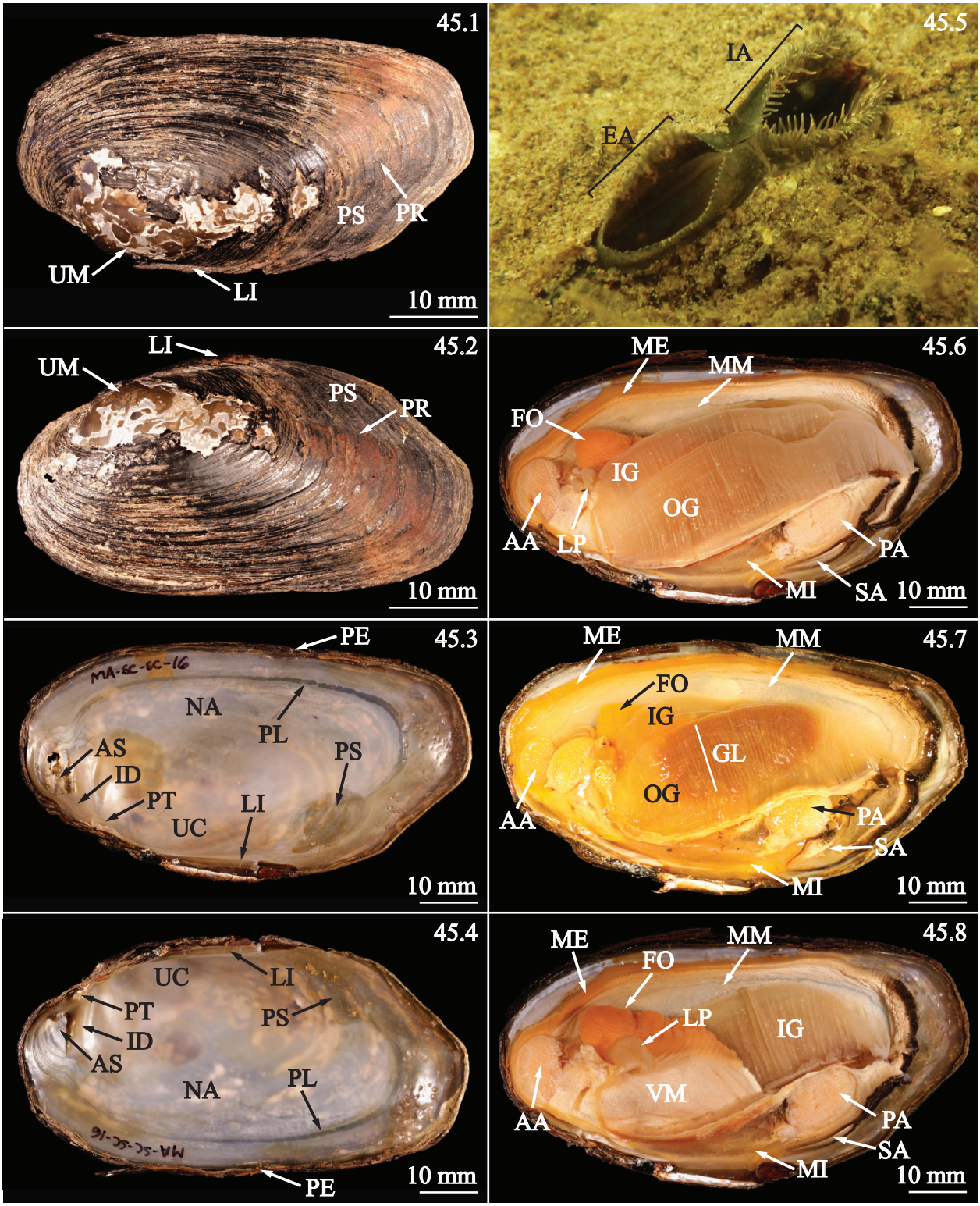
45.1
PS
PR
UM
LI
10 mm
45.5
IA
EA
45.2
LI
UM
PS
PR
10 mm
45.6
ME
MM
FO
IG
OG
AA
LP
PA
MI
SA
10 mm
45.3
PE
NA
PL
AS
ID
PT
UC
LI
PS
10 mm
45.7
ME
MM
FO
IG
GL
OG
AA
PA
SA
MI
10 mm
45.4
UC
LI
PT
PS
ID
AS
NA
PL
PE
10 mm
45.8
ME
MM
FO
LP
IG
VM
AA
PA
SA
MI
10 mm

PLATE 46. Anterior mantle edge of *Strophitus connasaugaensis*. 1. Transverse section of the mantle edge portraying the position of the outer lobe (OL), middle lobe (ML), and inner lobe (IL). 2. Transverse view of the base of the outer and inner mantle lobes showing columnar epithelium (CE) and basal bulb (BB) of the outer lobe, squamous epithelium (SE) of the middle lobe, periostracal groove (PG) and periostracum ribbon (PE). 3. Transverse section of the free distal tip of the outer mantle lobe featuring columnar epithelium (CE), plicae (PL), and fibrous tissue (FT) in the subepithelium. 4. Transverse section of the middle mantle lobe revealing squamous epithelium (SE) and periostracum (PE) along the ventral surface, and columnar epithelial cells (CE) of the dorsal surface. 5. Transverse section of the inner mantle lobe featuring narrow plicae (PL), violet cells (VC), and irregular fibrous tissue (FT). 6. Transverse section of the dorsal epithelium of the base of the mantle edge featuring plicae (PL), goblet cells (GC), and a subepithelium consisting of myofibers (MF), hemolymph sinuses (HS), and nerves (NE). 7. Transverse section of the base of the mantle edge revealing a deeply basophilic columnar epithelium (CE), and myofibers (MF) in the subepithelium.

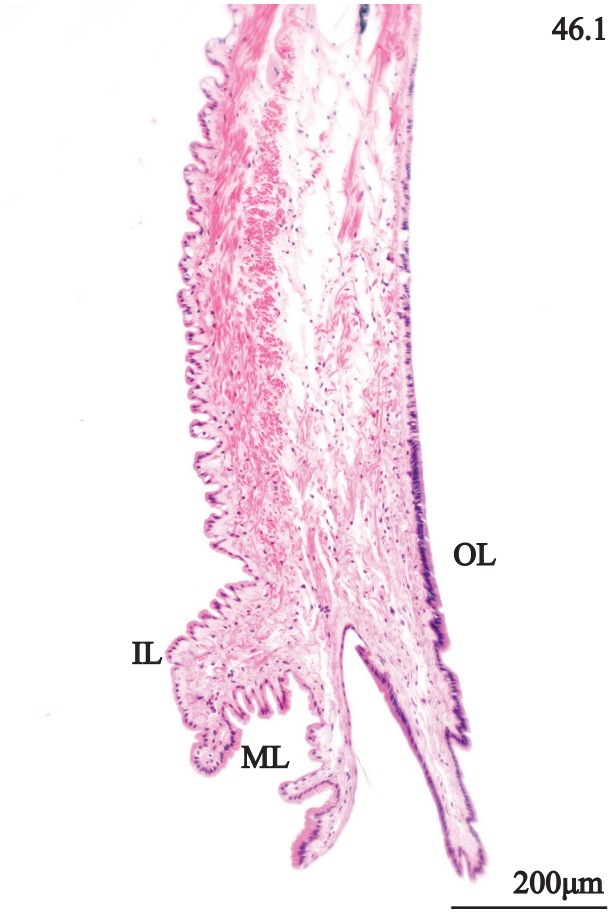
46.1
OL
IL
ML
200µm

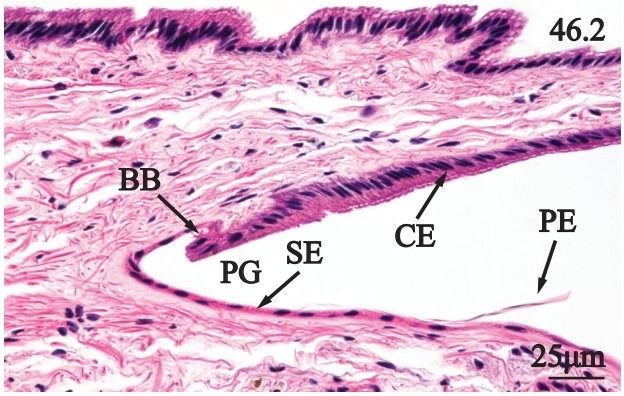
46.2
BB
CE
PE
PG
SE
25µm

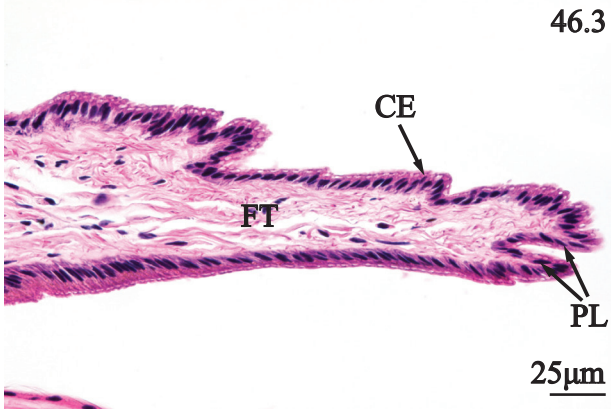
46.3
CE
FT
PL
25µm

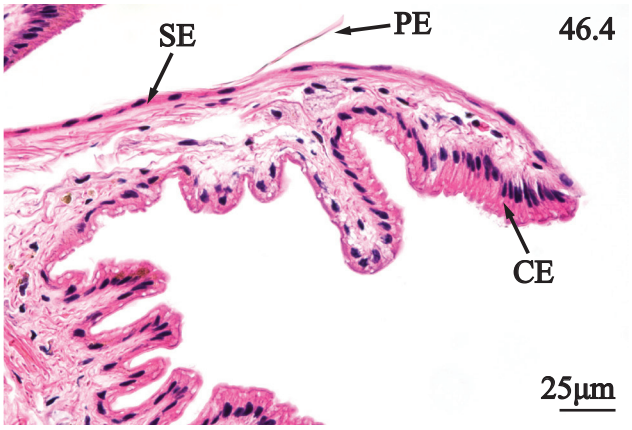
46.4
SE
PE
CE
25µm

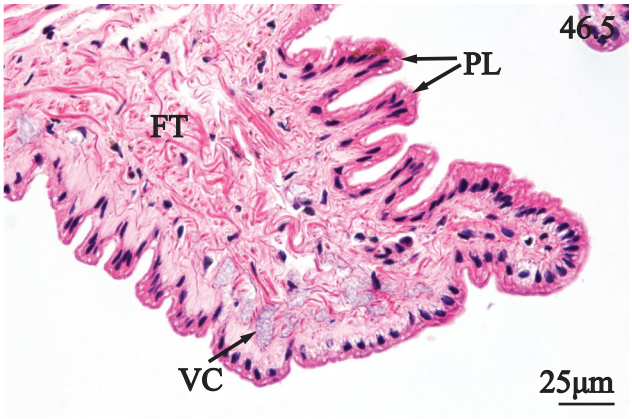
46.5
PL
FT
VC
25µm

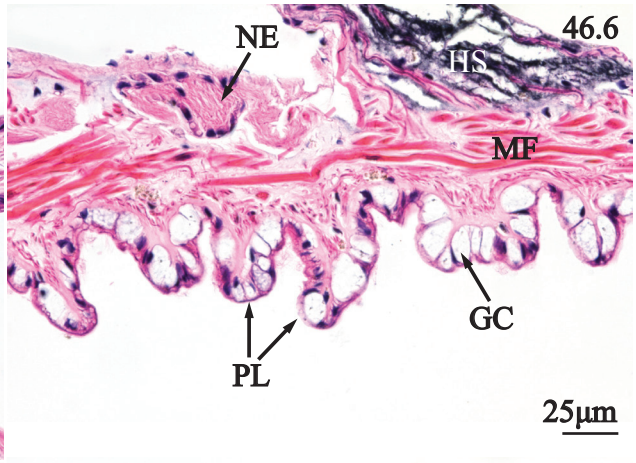
46.6
NE
HS
MF
GC
PL
25µm

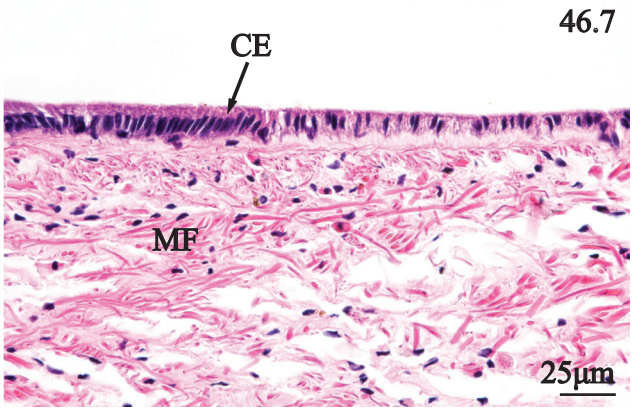
46.7
CE
MF
25µm

PLATE 47. Posterior mantle edge, middle mantle, and mantle isthmus of *Strophitus connasaugaensis*. 1. Transverse section of posterior mantle edge revealing thin outer lobe (OL) and middle lobe (ML) and a triangular inner lobe (IL) featuring plicae (PL) along the dorsal and ventral surfaces. 2. Sagittal section of posterior mantle edge characterized by conical papillae (PA) with brown-pigmented epithelium (BE), and a subepithelium consisting of hemolymph sinuses (HS), nerves (NE) and myofibers (MF). 3. Sagittal section of posterior mantle edge emphasizing brown intracellular granules (BG) present in columnar epithelium (CE), and subepithelial musculature (MU). 4. Transverse section of middle mantle displaying a outer epithelium (OE) of columnar cells bearing cilia (CI), goblet cells (GC) inner epithelium (IE), connective tissue (CT), and hemocytes (HC). 5. Transverse section of mantle isthmus emphasizing columnar epithelium (CE), goblet cells (GC), and irregular connective tissue (CT) and hemocytes (HC) in the subepithelium.

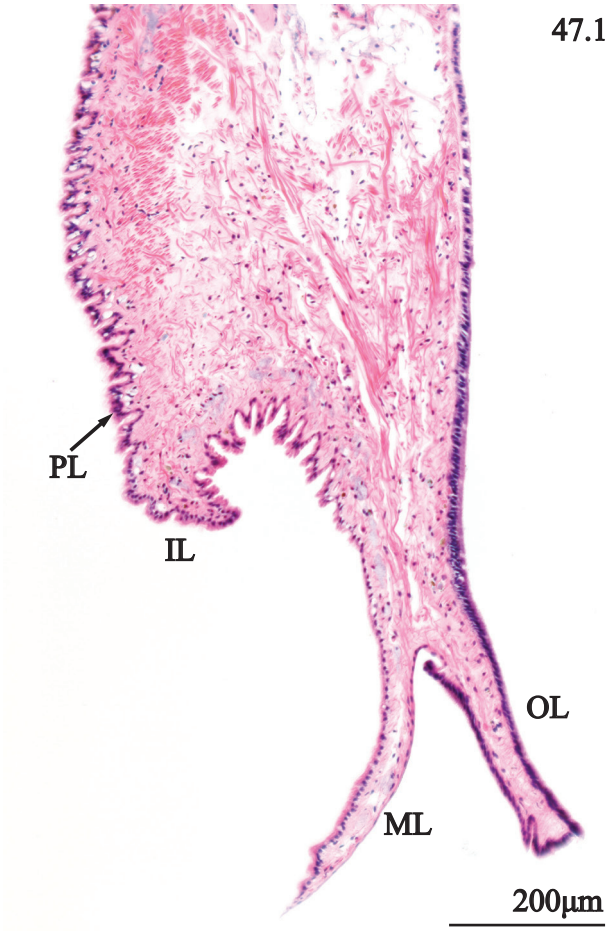
47.1
PL
IL
OL
ML
200µm

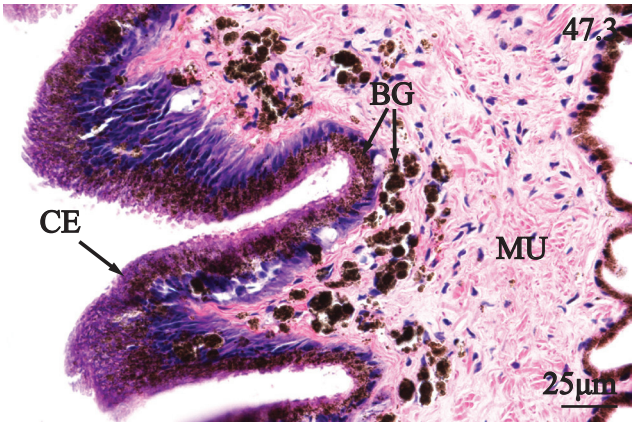
47.3
BG
CE
MU
25µm

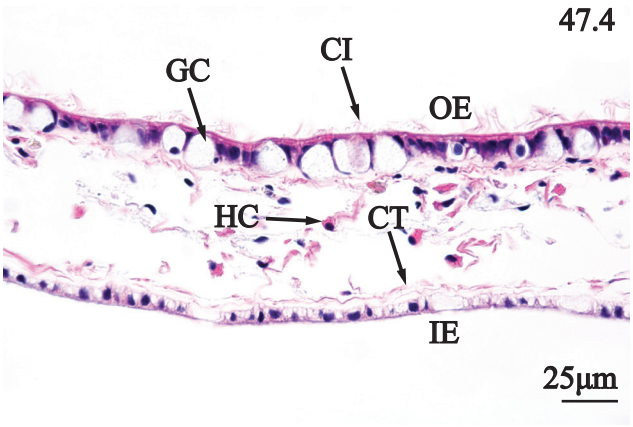
47.4
GC
CI
OE
HC
CT
IE
25µm

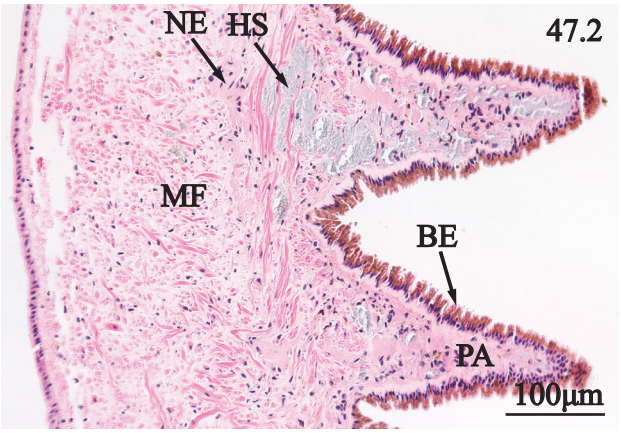
NE
HS
47.2
MF
BE
PA
100µm

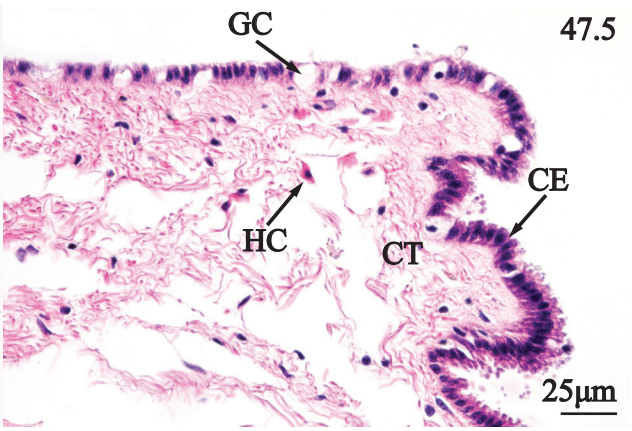
GC
47.5
CE
HC
CT
25µm

PLATE 48. Outer gill and inner gill of *Strophitus connasaugaensis*. 1. Transverse section of inner gill displaying horizontally oriented filaments (FI), a septum (SE) linking the inner and outer lamina, and a median water tube (WT). 2. Transverse section of the inner lamina of inner gill showing the main tissue components of gill including frontal cilia (FC), frontal-lateral cilia (FL), lateral cilia (LC), ostia (OS), blood vessels (BV), hemocytes (HC) skeletal rods (SR), and a water tube (WT). 3. Transverse section of the distal tip of outer gill characterized by a rounded distal margin (DM), resembling merged branchial filaments (FI). 4. Transverse section of the distal margin (DM) of the inner gill characterized by a median ciliated groove (CG). 5. Transverse section of the inner lamina (IL) of the inner gill showing its separation from the base of the visceral mass (VM). 6. Transverse section of the base of the inner gill where muscle fascicles (MU) are aligned anterior to posterior. 7. Transverse section of the base of the gill showing the junction of the outer lamina of the inner gill (OL), and inner lamina of the outer gill (IL), and loose connective tissue (CT) of the abdomen. 8. Transverse section of the base of the gill showing the junction between the outer lamina of outer gill (OL) and middle mantle (MM).

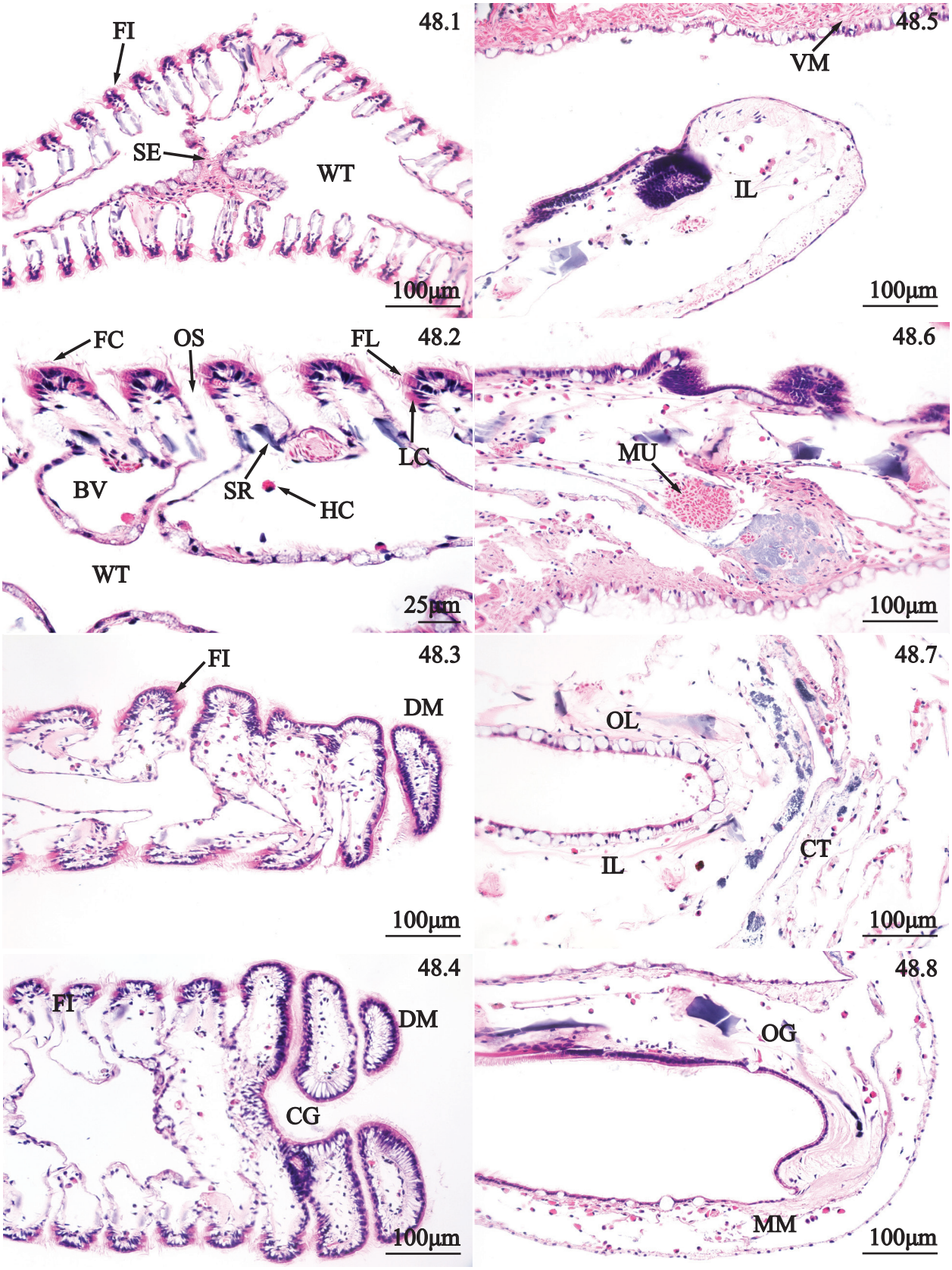
48.1
FI
SE
WT
100μm
48.2
FC
OS
FL
LC
BV
SR
HC
WT
25μm
48.3
FI
DM
100μm
48.4
FI
DM
CG
100μm
48.5
VM
IL
100μm
48.6
MU
100μm
48.7
OL
IL
CT
100μm
48.8
OG
MM
100μm

PLATE 49. Marsupium, and glochidia of *Strophitus connasaugaenesis*. 1. Transverse section of a filled marsupium showing distended filaments (FI), water tube (WT), and a cylindrical placenta-like sac (PL) containing glochidia (GL). 2. Transverse section of the distal margin (DM) of a marsupium portraying distended filaments (FI) and loose connective tissue (CT). 3. Transverse section of a marsupial septum emphasizing basophilic cells (BC) between basophilic goblet cells (GC). 4. Transverse section of a marsupium emphasizing the shell (SH), mantle (MA), and adductor muscle (AM) of glochidia. 5. Transverse section of a marsupium near a septum (SE) emphasizing spines (SP) and mantle tissue (MA) at the ventral extent of glochidium valves. 6. Transverse section of an empty marsupium showing distended filaments (FI), water tube (WT), and a contracted placenta (PL).

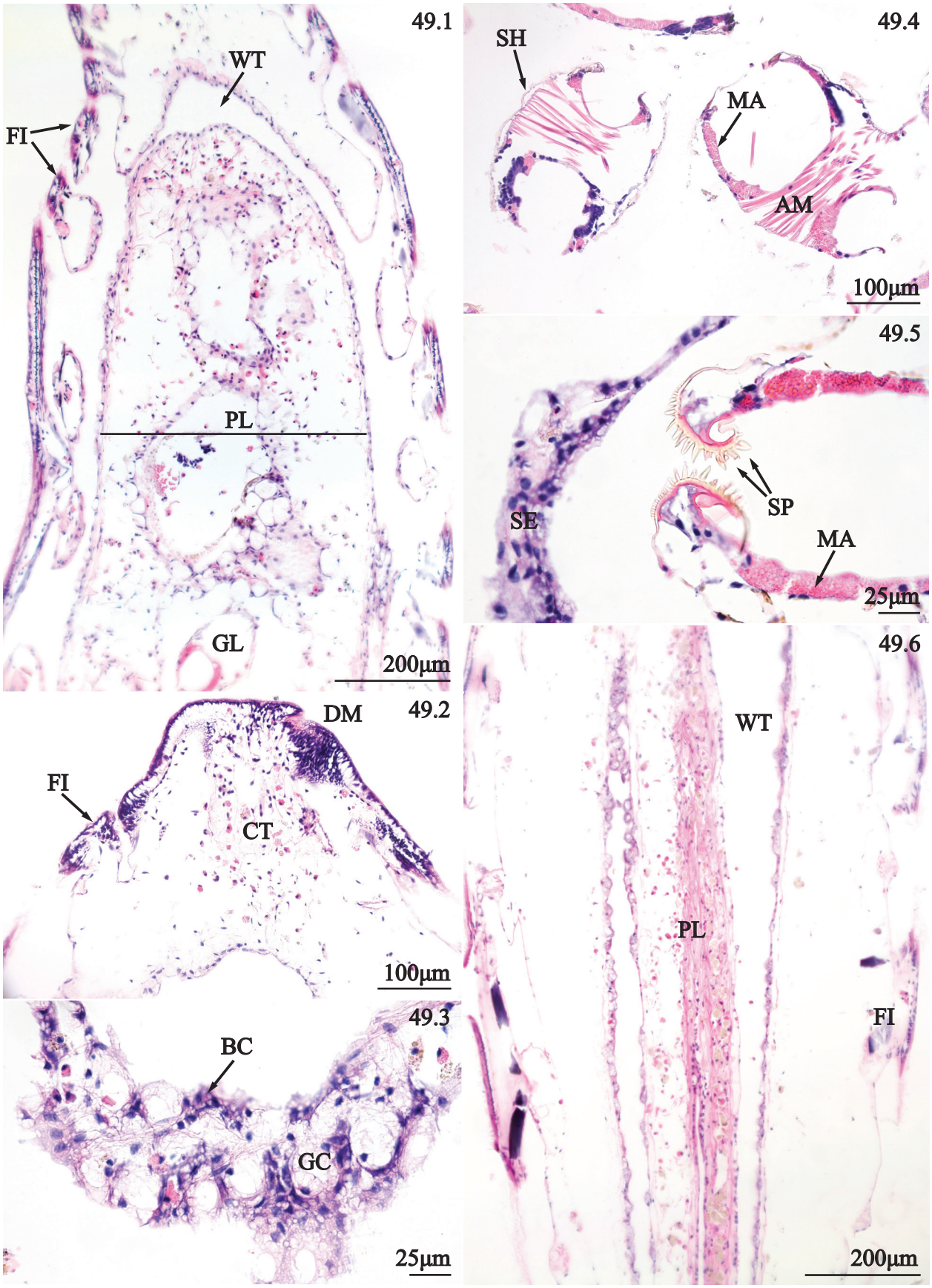
49.1
WT
FI
PL
GL
200µm
49.2
DM
FI
CT
100µm
49.3
BC
GC
25µm
49.4
SH
MA
AM
100µm
49.5
SP
SE
MA
25µm
49.6
WT
PL
FI
200µm

PLATE 50. Pedal musculature, and byssal gland of *Strophitus connasaugaensis*. 1. Transverse section of the ventral margin of the foot characterized by an inner core of somatic musculature (SM), and peripheral, basophilic granulocytes (BG). 2. Transverse section of pedal subepithelium characterized by myofibers (MF) pale, blue granulocytes (GC) in the median, and violet-staining granulocytes (VC) between the blue cells and the epithelium. 3. Transverse section of ventral pedal musculature featuring an irregular meshwork longitudinal fibers (LF), and transverse fibers (TF). 4. Transverse section of dorso-lateral foot musculature characterized by transverse myofibers (TF) and type-two pedal epithelium (E2). 5. Transverse section of the byssal gland showing its close proximity to ovarian acini (OA), hemolymph (HL), and mesentery (ME) characterizing the ventral margin of the coelom. 6. Transverse section of the byssal gland displaying ciliated columnar cells (CC), goblet cells (GC), byssus (BY) and an outer wrapping of fibrous tissue (FT).


50.1
GC
SM
200μm

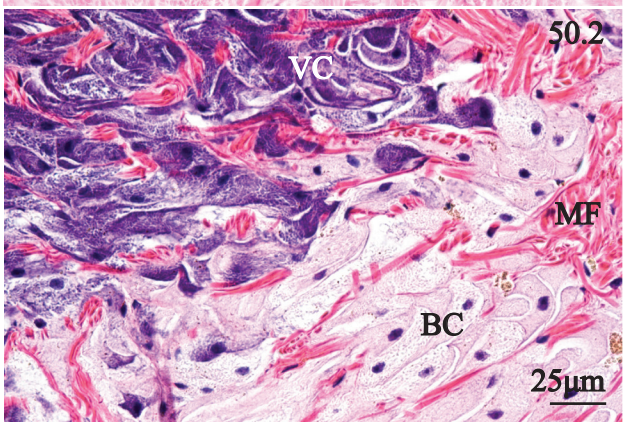
50.2
VC
MF
BC
25μm

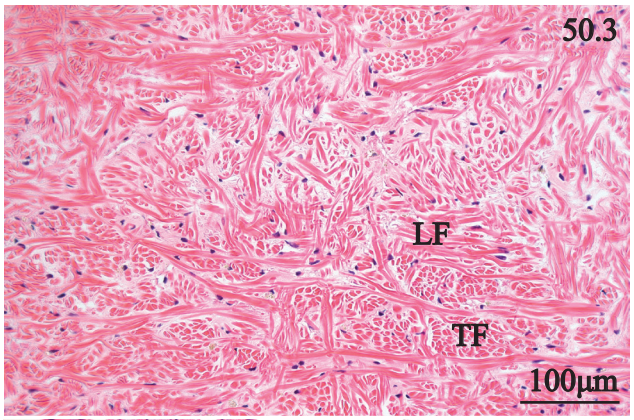
50.3
LF
TF
100μm

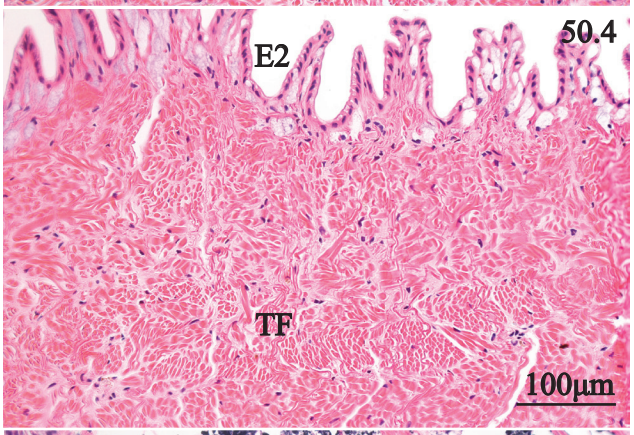
50.4
E2
TF
100μm

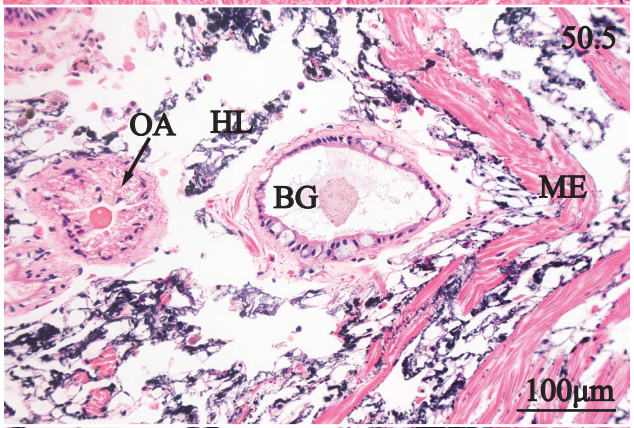
50.5
OA
HL
BG
ME
100μm

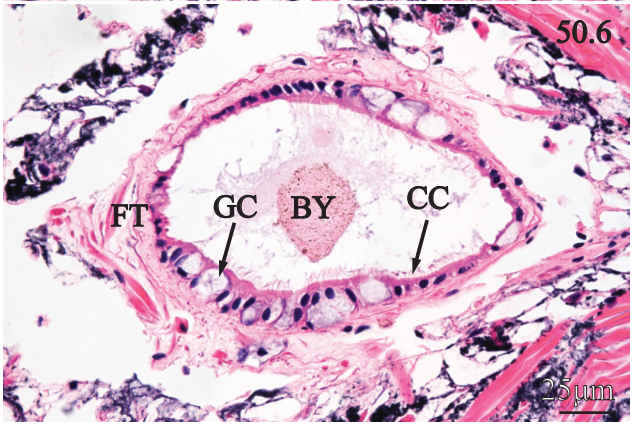
50.6
FT
GC
BY
CC
25μm

PLATE 51. Pedal integument, and mesentery of *Strophitus connasaugaensis*. 1. Transverse section of pedal integument type-one, emphasizing tall irregular plicae (PL) with densely packed cilia (CI) overlying a subepithelium of irregular fibers (IF), and basophilic granulocytes (BG). 2. Transverse section of pedal integument type-two represented by tall plicae (PL), columnar cells (CC), goblet cells (GC), and transverse myofibers (TF). 3. Transverse section of pedal integument type-three, characterized by shorter, thinner plicae (PL) bearing goblet cells (GC), cilia (CI), and a distinct subepithelium of connective tissue (CT), and underlying stata of transverse myofibers (TF). 4. Transverse section of pedal integument type-four, characterized by a sinuous, but more flattened integument of cuboidal epithelium (CE), cilia (CI), goblet cells (GC), and a subepithelium of hemolymph sinues (HS), and transverse myofibers (TF). 5. Transverse section of pedal integument type-five, revealing the flattened squamous epithelium (SE), cilia (CI), goblet cells (GC), and longitudinal myofibers (LF). 6. Sagittal section of pedal integument featuring irregular plicae (PL) giving the integument a rugose structure. 7. Transverse section of the lateral coelomic margin emphasizing longitudinal myofibers (LF), and struts of musculature forming mesentery (ME). 8. Sagittal section through the coelom revealing a mesentery fascicle (FA) surrounded by adipocytes (AC) and hemolymph (HL).

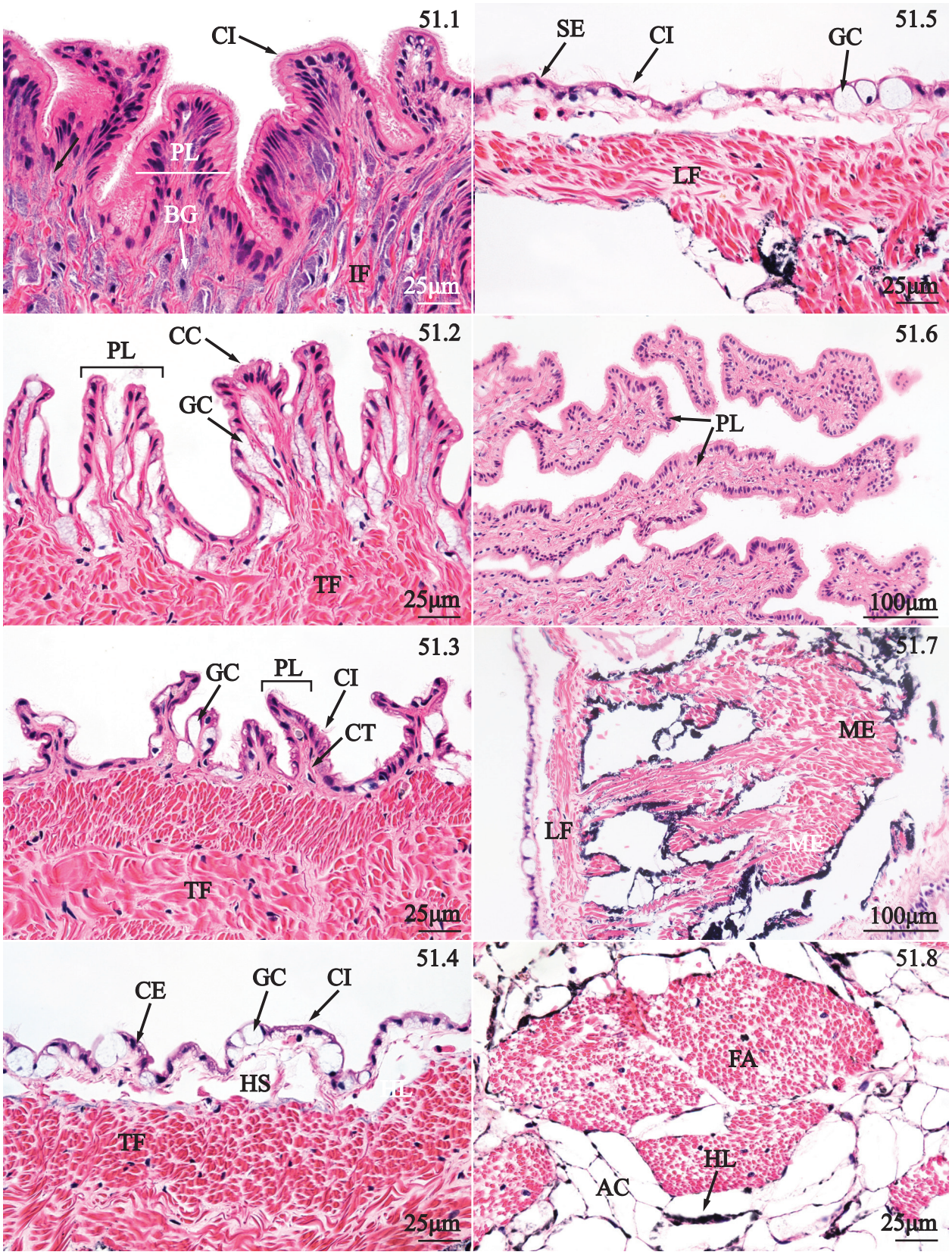
51.1
CI
PL
BG
IF
25μm
51.5
SE
CI
GC
LF
25μm
51.2
PL
CC
GC
TF
25μm
51.6
PL
100μm
51.3
GC
PL
CI
CT
TF
25μm
51.7
ME
LF
ME
100μm
51.4
CE
GC
CI
HS
TF
25μm
51.8
FA
HL
AC
25μm

PLATE 52. Labial palps, anterior pedal protractor, and anterior adductor of *Strophitus connasaugaensis*. 1. Sagittal view of a labial palp portraying plicae (PL) constituting inner epithelium (IE), and the smooth outer epithelium (OE). 2. Sagittal section of labial palps revealing plicae (PL), with ciliated columnar cells (CC), and subepithelial connective tissue (CT) and hemocytes (HC). 3. Sagittal section of the distal labial palp margin featuring the flattened outer epithelium of cuboidal cells (CU), goblet cells (GC), ciliated columnar cells (CC), hemocytes (HC) and subepithelial connective tissue (CT). 4. Sagittal section of outer palp surface highlighting squamous cells (SC), and subepithelial connective tissue (CT). 5. Sagittal section of anterior adductor showing longitudinal myofibers (MF), flattened myocyte nuclei (MN), and perimysium (PM). 6. Transverse section of anterior pedal retractor displaying thin perimysium (PM), endomysium (EM), polygonal myofibers (MF), myocyte nuclei (MN) and a capillary (CA) between adjacent fascicles.

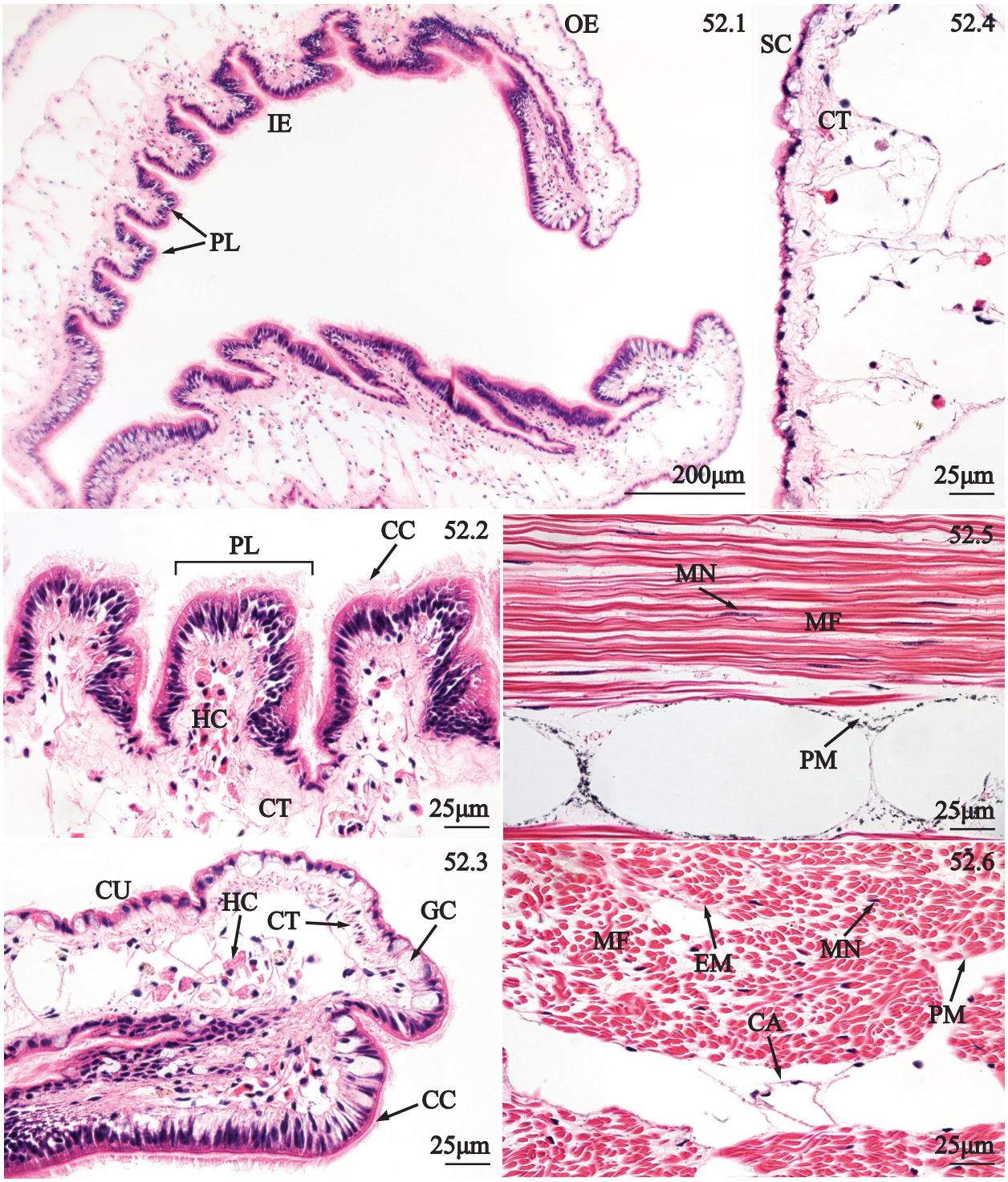
OE
52.1
IE
PL
200µm
SC
52.4
CT
25µm
PL
CC
52.2
HC
CT
25µm
52.5
MN
MF
PM
25µm
52.3
CU
HC
CT
GC
CC
25µm
52.6
MF
EM
MN
PM
CA
25µm

PLATE 53. Oral groove, and esophagus of *Strophitus connasaugaensis*. 1. Transverse section of oral groove showing a cylindrical shelf consisting of musculature (MU), goblet cells (GC), and a ciliated columnar epithelium (CC). 2. Transverse section of the lateral oral groove wall displaying ciliated columnar cells (CC) and a subepithelium of loose connective tissue (CT). 3. Transverse section of the dorsal oral groove wall displaying cilia (CI), and loose connective tissue (CT). 4. Transverse section through dorsal aspect of visceral mass showing the esophagus (ES) lined with plicae (PL), enclosed within a distinct lamina propria (LP), and surrounded by tubules of the digestive diverticulum (DD). 5. Transverse section of esophagus emphasizing plicae (PL) consisting of ciliated columnar cells (CC) supported by a dense matrix of fibrous connective tissue (CT).

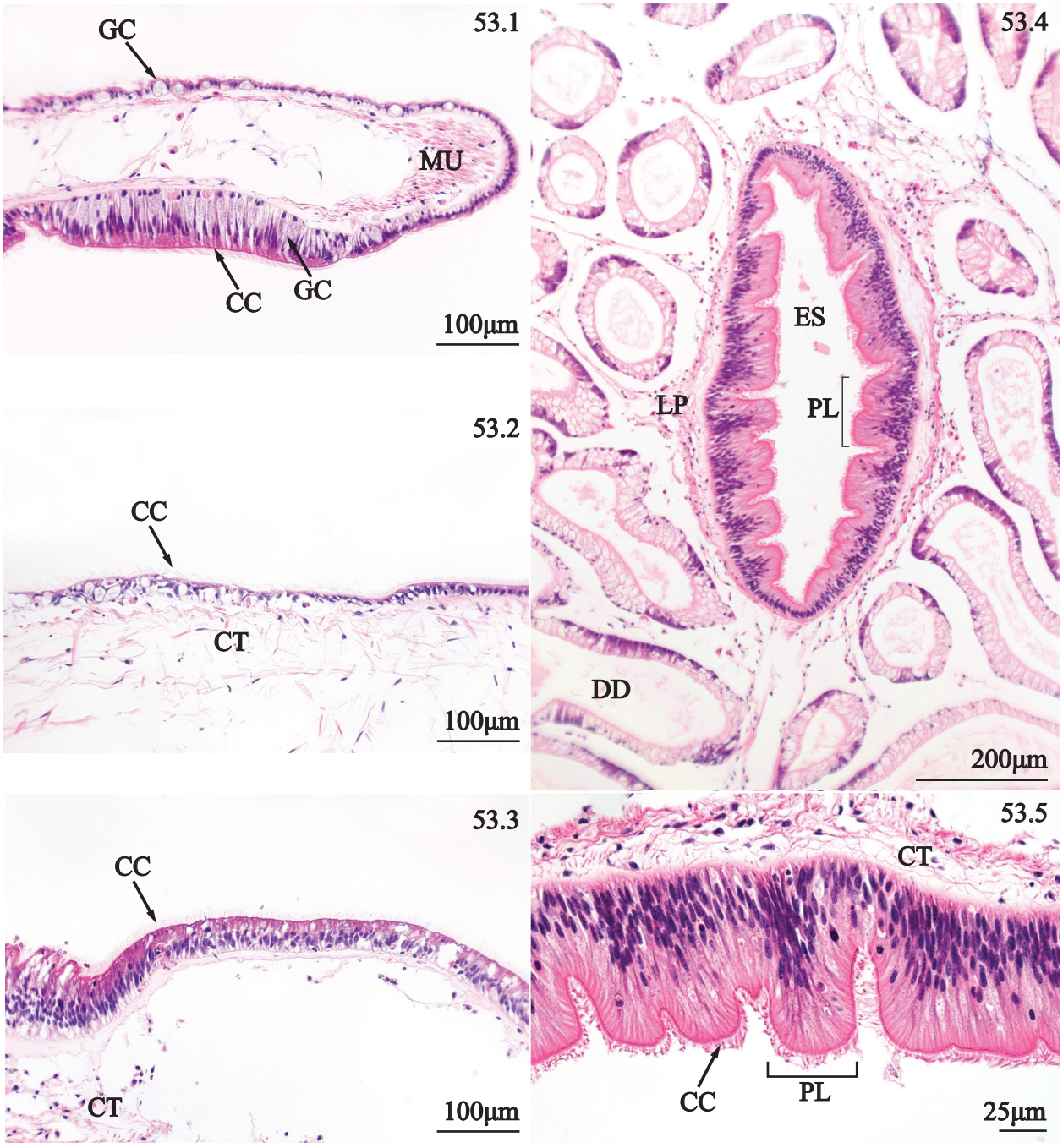
53.1
GC
MU
CC
GC
100µm
53.2
CC
CT
100µm
53.3
CC
CT
100µm
53.4
ES
LP
PL
DD
200µm
53.5
CT
CC
PL
25µm

PLATE 54. Digestive diverticulum, and stomach of *Strophitus connasaugaensis*. 1. Transverse section of the junction between the esophagus (ES) and digestive diverticulum (DD) revealing a large vestibular chamber characterized by ciliated plicae (PL). 2. Transverse section of the junction between the esophagus and digestive diverticulum, emphasizing conical plicae (PL) bearing cilia (CI) and underlying lamina propria (LP). 3. Transverse section of digestive diverticulum portraying plicae (PL) and ciliated columnar cells (CC) of primary digestive tubules. 4. Transverse section of digestive diverticulum showing dense cilia (CI) on the surface of plicae (PL) of a primary tubule. 5. Transverse section digestive diverticulum portraying the darkened eosinophilic character of secondary tubules (ST), and the pale eosinophilic content of tertiary tubules (TT). 6. Transverse section of digestive diverticulum revealing the minute structure of microvilli (MV) of secondary tubules (ST) and the contrasting cellular features of tertiary tubules (TT). 7. Transverse section of the digestive diverticulum focusing on tertiary tubule structure including eosinophilic vesicles (EV), and basophilic nuclei (BN) set within triangular rays of basophilic cytoplasm.

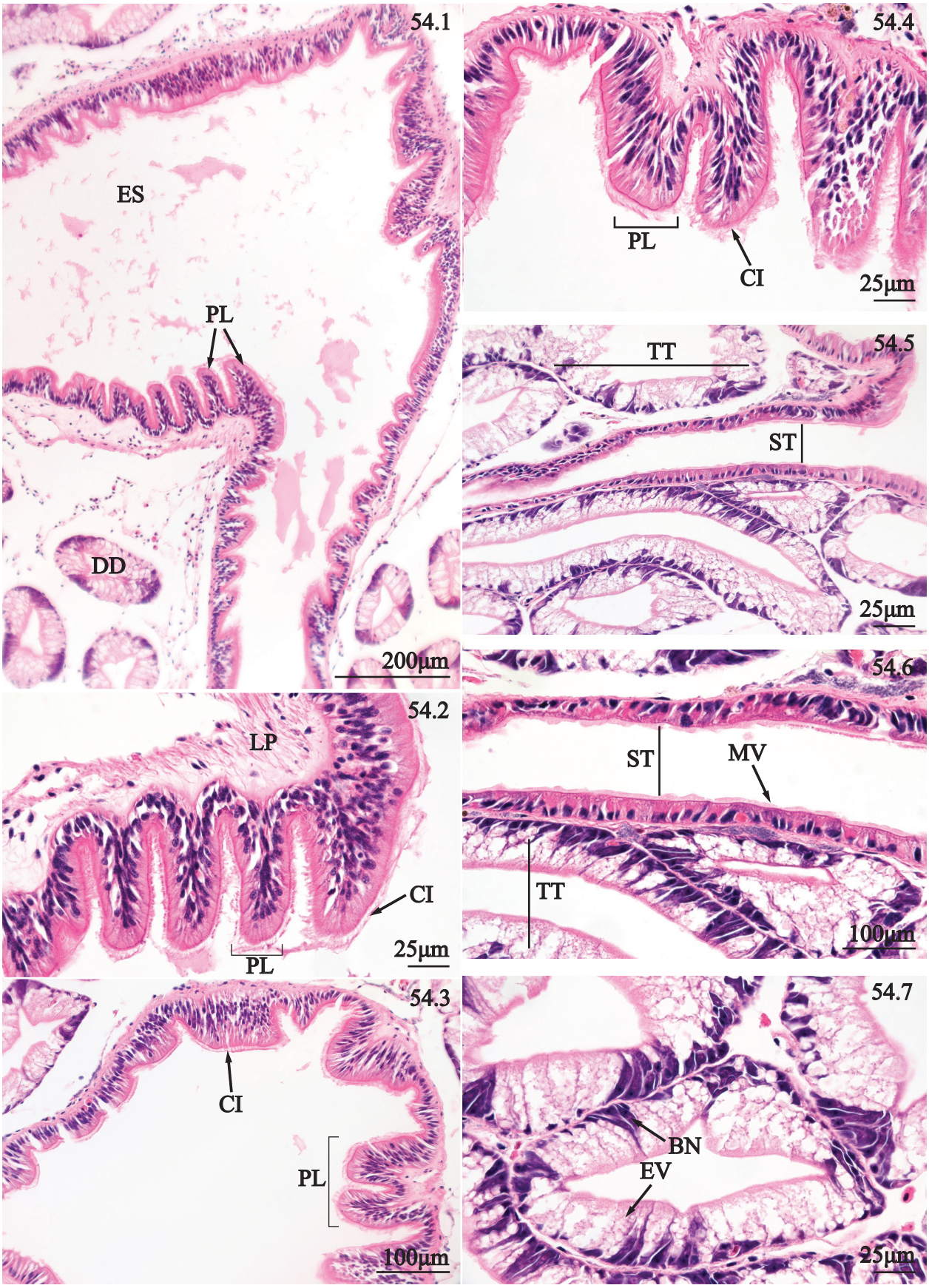
54.1
ES
PL
DD
200µm
54.2
LP
CI
PL
25µm
54.3
CI
PL
100µm
54.4
PL
CI
25µm
54.5
TT
ST
25µm
54.6
ST
MV
TT
100µm
54.7
BN
EV
25µm

PLATE 55. Anterior stomach chamber of *Strophitus connasaugaensis*. 1. Transverse section through visceral mass showing plicae (PL) along the walls of the dextral stomach chamber and an eosinophilic mass within the lumen (ES). 2. Transverse section of the wall of the dextral stomach chamber showing an eosinophilic mass (ES) mass in the lumen, and cilia (CI) along the surface of plicae (PL). 3. Transverse section of the dorsal stomach wall featuring a large fold of tissue featuring plicae (PL) supported by the underlying lamina propria (LP). 4. Transverse section of the dorsal stomach wall emphasizing low plicae (PL) formed by ciliated columnar cells (CC) of different heights. 5. Transverse section of the main stomach chamber featuring the obliquely oriented gastric shield (GS) and a cuticle (CU) along the surface. 6. Transverse section of the posterior stomach chamber featuring a columnar epithelium (CE), bearing cilia (CI), with an attached cuticle (CU), and subepithelial connective tissue (CT).

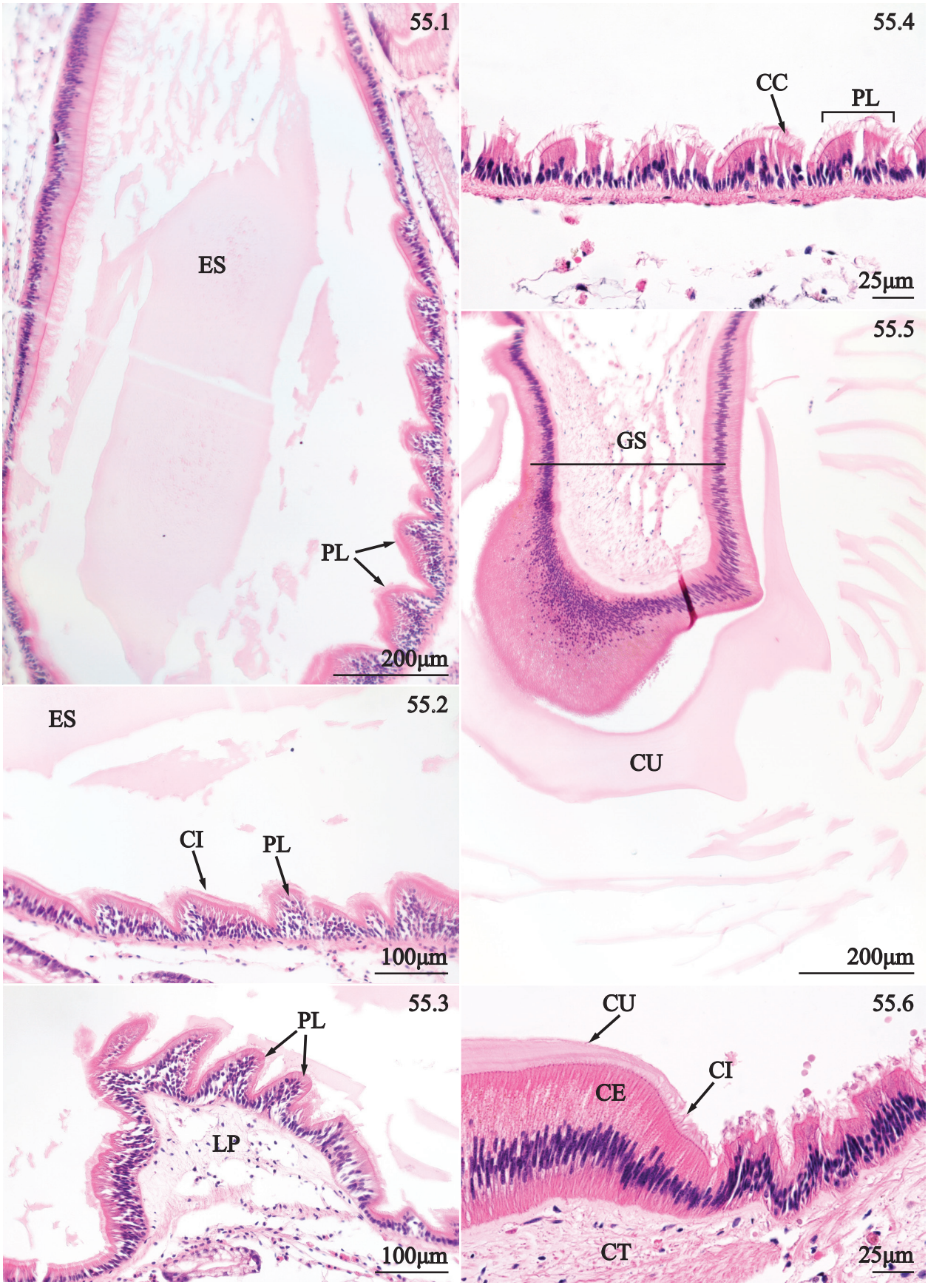
55.1
ES
PL
200μm
55.4
CC
PL
25μm
55.5
GS
CU
200μm
ES
55.2
CI
PL
100μm
55.3
PL
LP
100μm
55.6
CU
CI
CE
CT
25μm

PLATE 56. Posterior stomach chamber of *Strophitus connasaugaensis*. 1. Transverse section of the ventral stomach wall showing a median groove (MG), ciliated columnar cells (CC), and a well-defined lamina propria (LP). 2. Transverse section of the sinistral end of the posterior stomach chamber featuring rounded plicae (PL) bearing cilia (CI). 3. Transverse section of the ventral stomach wall near the median groove portraying a cuticle (CU) attached to the columnar epithelium (CE) supported by an underlying lamina propria (LP). 4. Transverse section of the dextral portion of the posterior stomach featuring a continuous line of ciliated columnar cells (CC), and a thin lamina propria (LP).

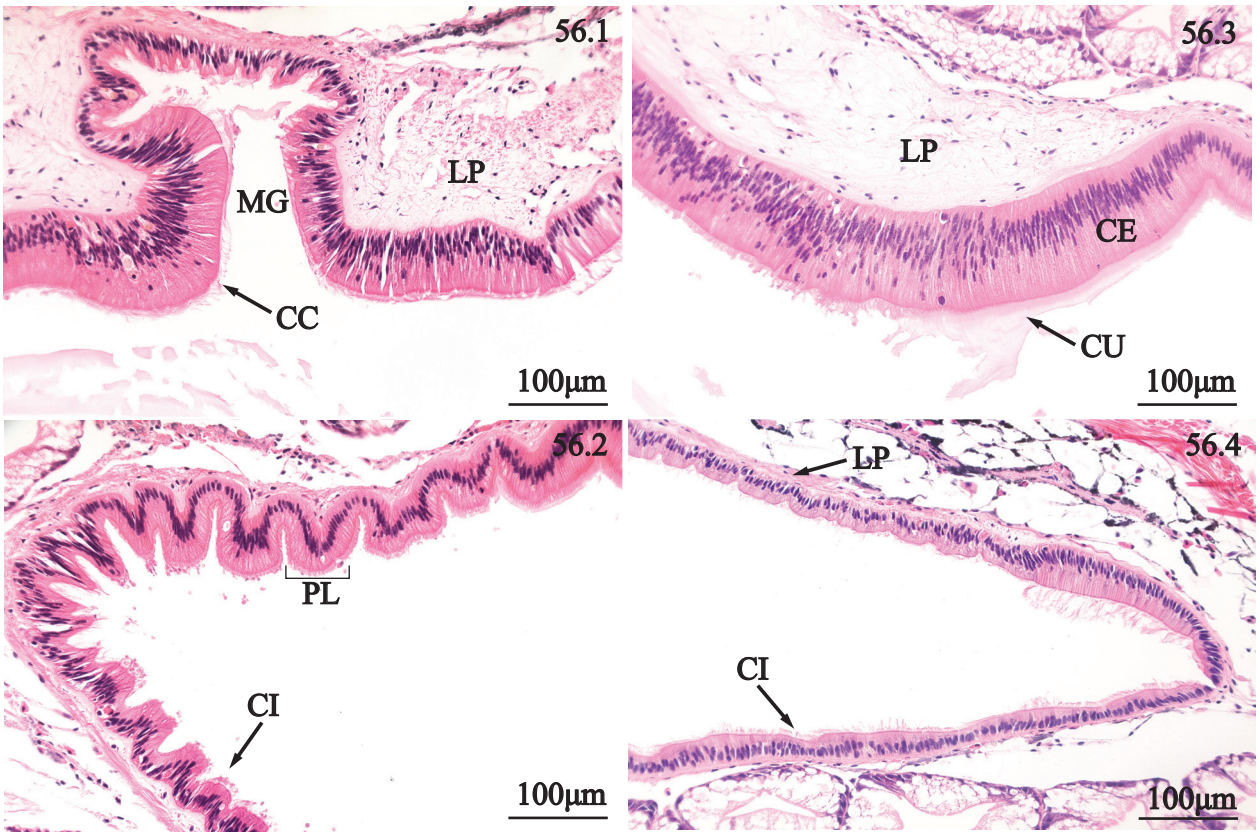
56.1
MG
LP
CC
100µm
56.3
LP
CE
CU
100µm
56.2
PL
CI
100µm
56.4
LP
CI
100µm

PLATE 57. Crystalline style sac of *Strophitus connasaugaensis*. 1. Transverse section through the crystalline style sac showing the position of the style sac (SS), midgut (MG), epithelium type-one (E1), epithelium type-two (E2), epithelium type-three (E3), style (ST) and the surrounding lamina propria (LP). 2. Transverse section of the crystalline style sac type-one epithelium, consisting of eosinophilic columnar cells bearing cilia (CI), the wispy margin of the style (SY), and the lamina propria (LP). 3. Transverse section of style sac epithelium type-two, emphasizing eosinophilic and vesiculated columnar cells bearing cilia (CI) and the underlying lamina propria (LP). 4. Transverse section of style sac type-three epithelium featuring thin, tall, basophilic columnar cells bearing cilia (CI). 5. Transverse section of the style (ST) showing concentric layers of an eosinophilic material.

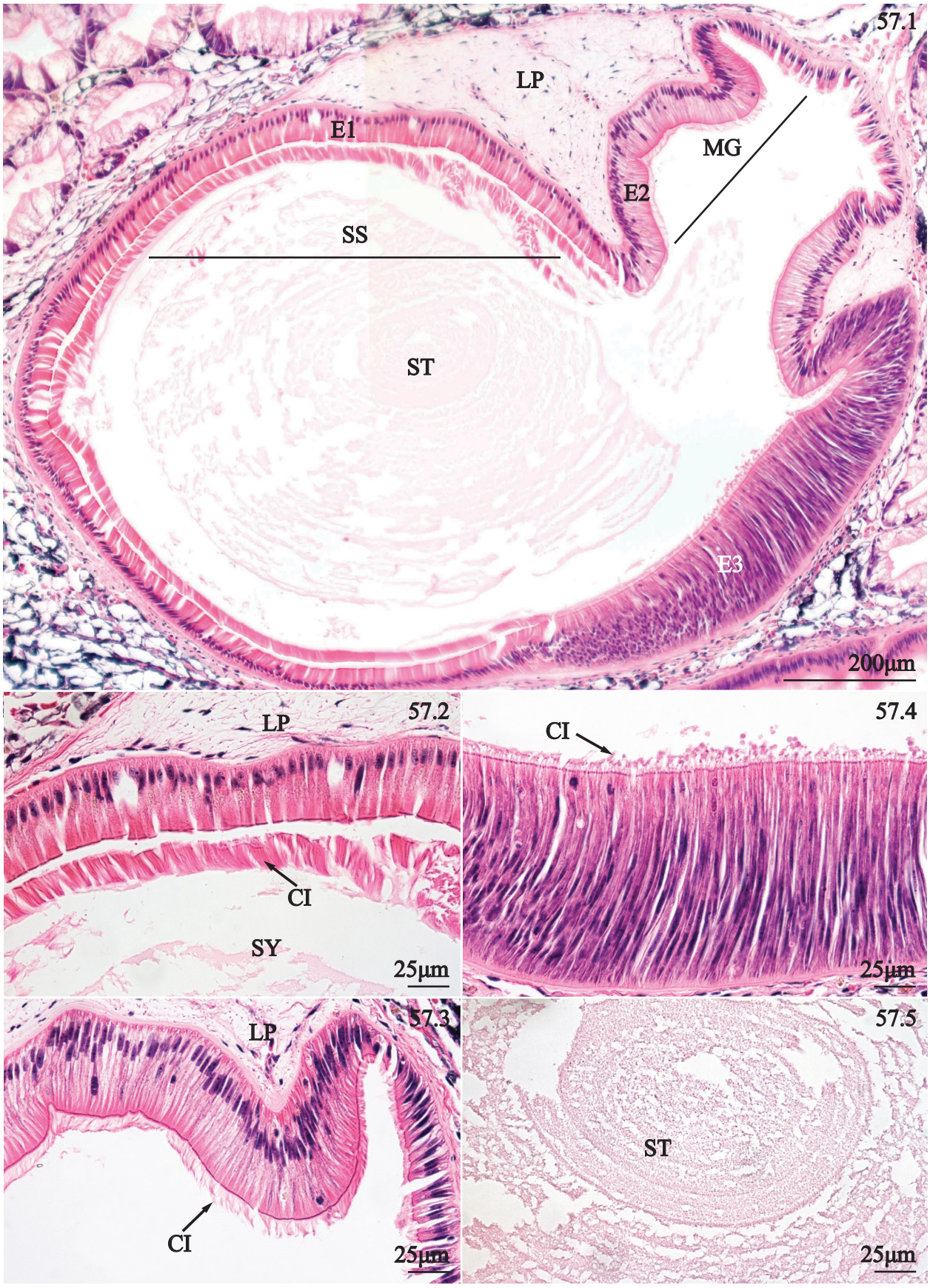
57.1
LP
E1
MG
E2
SS
ST
E3
200μm
57.2
LP
CI
SY
25μm
57.4
CI
25μm
57.3
LP
CI
25μm
57.5
ST
25μm

PLATE 58. First intestinal limb, and second intestinal limb of *Strophitus connasaugaensis*. 1. Transverse section through visceral mass revealing the second intestinal limb (IN) and surrounding lamina propria (LP), mesentery (ME), adipose tissue (AT), and ovarian acini (OA). 2. Sagittal section of the first, descending intestinal limb showing plicae (PL) along the anterior (AW) and posterior walls (PW), supported by lamina propria (LP). 3. Sagittal section of first intestinal limb showing style sac epithelium types one (E1), two (E2), and three (E3). 4. Sagittal section of the ascending portion of the second intestinal limb showing the sinuous epithelium of the anterior (AW) and posterior walls (PW), and surrounding lamina propria (LP). 5. Sagittal section of the second intestinal limb focusing on plicae (PL), vesicular cells bearing cilia (CI), chyme (CH) in the lumen. 6. Sagittal section of the second intestinal limb showing rounded to flattened plicae (PL), bearing cilia (CI), supported by lamina propria (LP).

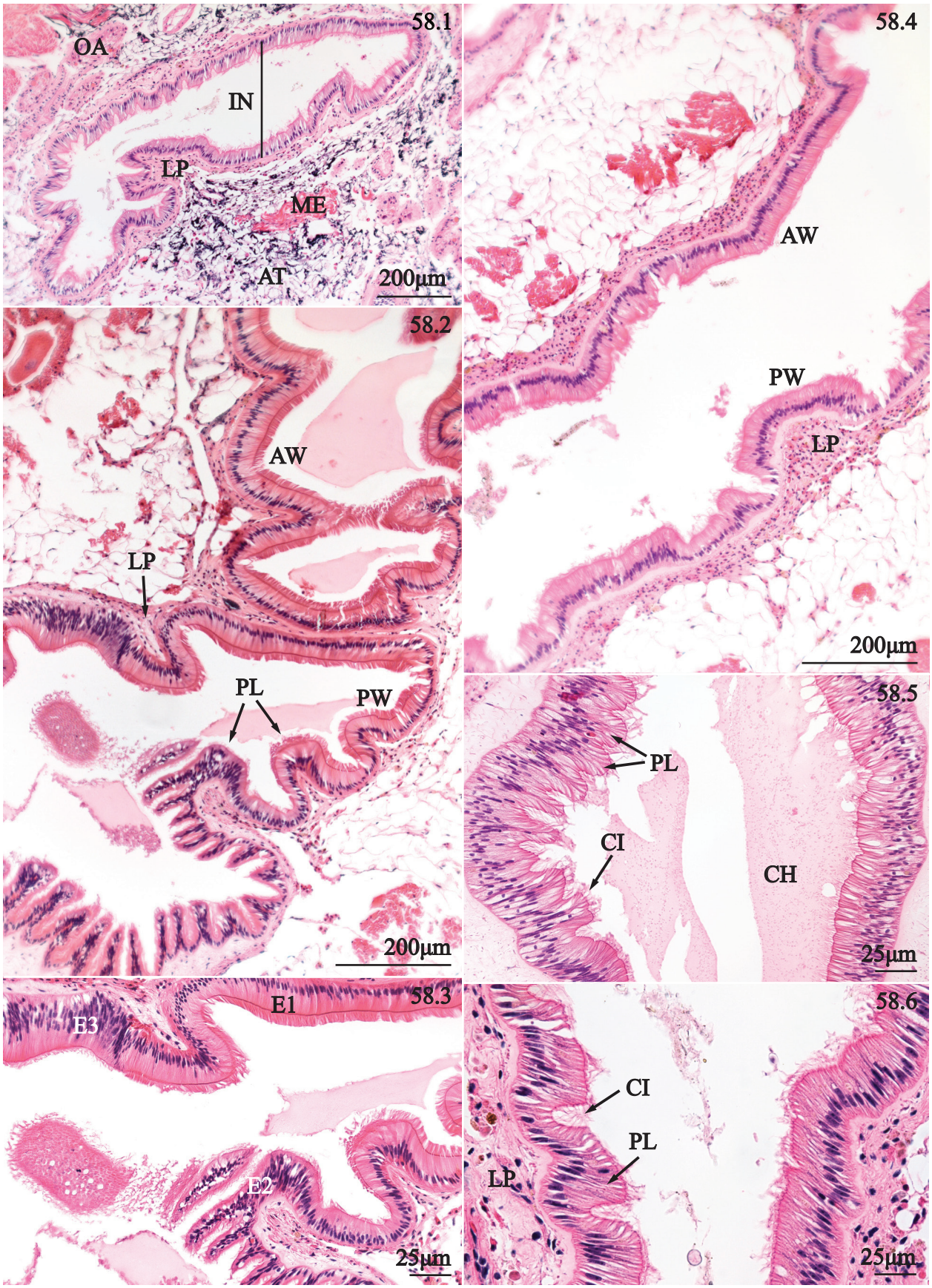
58.1
OA
IN
LP
ME
AT
200μm
58.2
AW
LP
PL
PW
200μm
58.3
E1
E3
E2
25μm
58.4
AW
PW
LP
200μm
58.5
PL
CI
CH
25μm
58.6
CI
PL
LP
25μm

PLATE 59. Fourth intestinal limb, and fifth intestinal limb of *Strophitus connasaugaensis*. 1. Transverse section of the fourth intestinal limb featuring a large, ventrally extending typhlosole (TY), with a correspondingly large lamina propria (LP), and plicae along the lateral-dorsal wall (PL.). 2. Transverse section of ventral epithelium (VE) of the fourth intestinal limb focusing on basophilic cells (BC) containing vesicles (VE) and a thin lamina propria (LP). 3. Transverse section of dorsal epithelium of the fouth intestinal limb featuring ciliated columnar cells (CC), and the underlying lamina propria (LP). 4. Transverse section of the fifth intestinal limb revealing a large, dorsally extending typhlosole (TY), with an extensive lamina propria (LP), plications (PL) along the dorsal wall, and thin tissue layers comprising the ventricle (VE) and pericardium (PC). 5. Transverse section of the ventral epithelium of the typhlosole emphasizing ciliated columnar cells (CC), containing a median vesicle (VE), and extensive lamina propria (LP). 6. Transverse section of dorsal epithelium portraying conical plicae (PL), bearing cilia (CI), and underlying tissues including a thin lamina propria (LP) and rim of myofibers (MF).

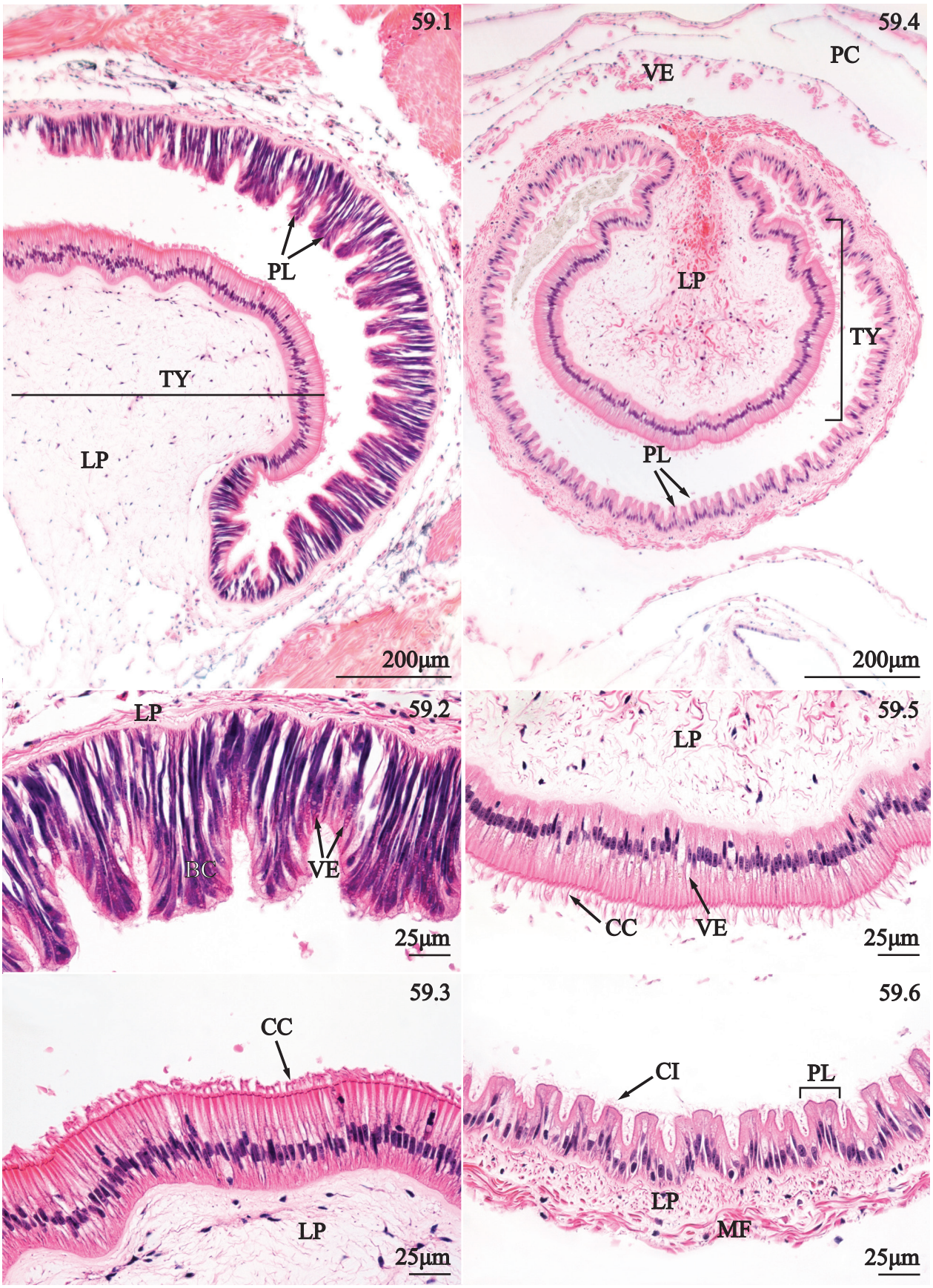
59.1
PL
TY
LP
200μm
59.4
PC
VE
LP
TY
PL
200μm
LP
59.2
BC
VE
25μm
59.5
LP
CC
VE
25μm
59.3
CC
LP
25μm
59.6
CI
PL
LP
MF
25μm

PLATE 60. Heart, and pericardium of *Strophitus connasaugaensis*. 1. Transverse section the lateral portion of the heart showing the fifth intestinal limb (IN), ventricle (VE), auricle (AU), auriculoventircular valve (AV), and pericardial gland (PG). 2. Transverse section through the ventricle focusing on the thin epicardium (EC), and underlying myocardium (MC). 3. Transverse section of the ventricle emphasizing transverse and longitudinal myofibers (MF), and interspersed hemocytes (HC). 4. Transverse section of the auricle (AU) showing epicardium (EC), cardiac muscle (CM), pericardial sac (PC), hemocytes (HC), and pericardial gland (PG). 5. Transverse section of an auriculoventricular valve showing cardiac muscle (CM), enveloped by a thin endothelium (EN).

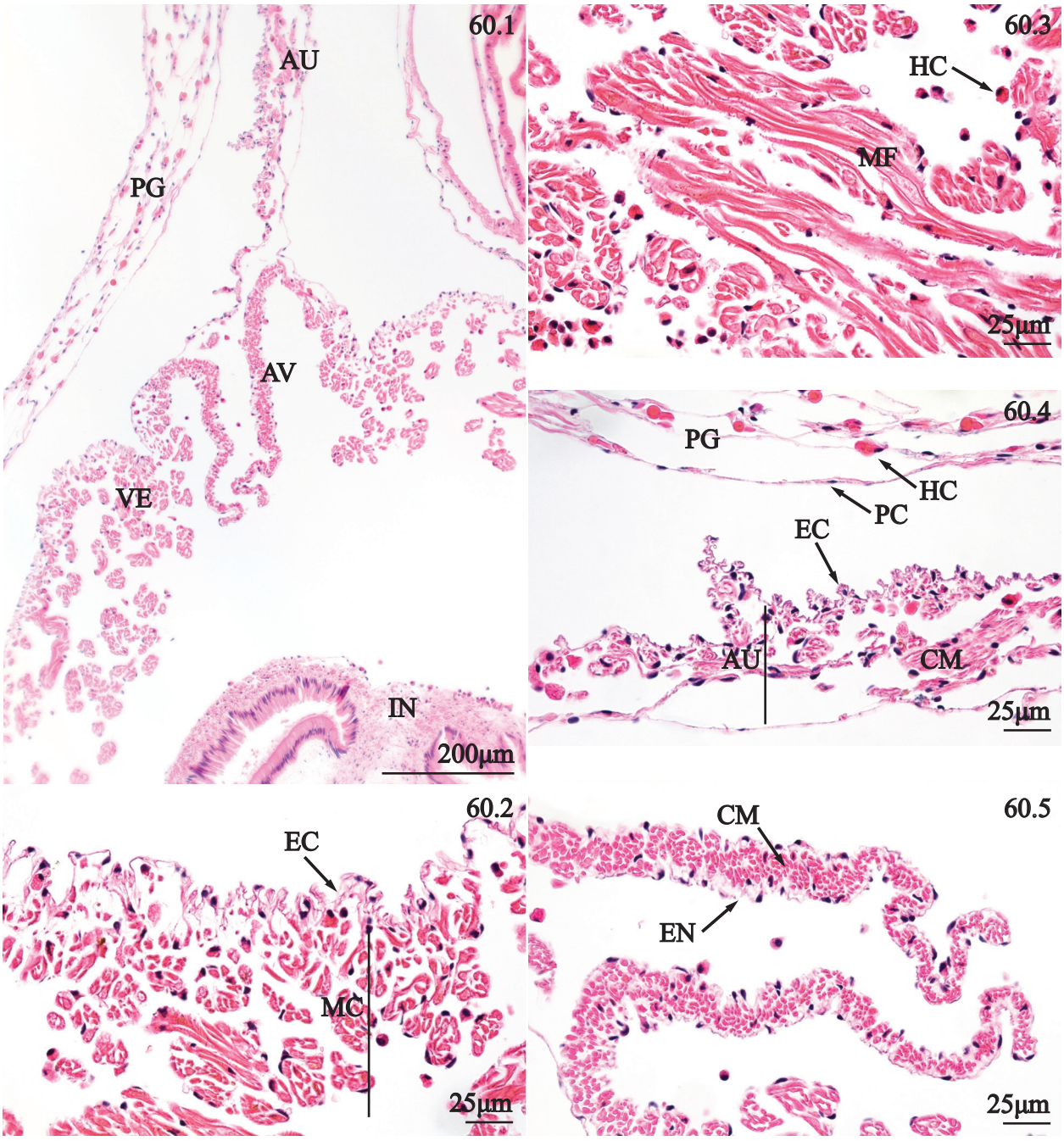
60.1
AU
PG
AV
VE
IN
200μm
60.3
HC
MF
25μm
60.4
PG
HC
PC
EC
AU
CM
25μm
60.2
EC
MC
25μm
60.5
CM
EN
25μm

PLATE 61. Hemolymph vessels, and pericardial gland of *Strophitus connasaugaensis*. 1. Transverse section of visceral mass showing a possible artery featuring an endothelium (EN), and thick muscular wrapping (MU), and surrounding pockets of hemolymph (HL). 2. Transverse section through the visceral mass featuring a possible vein demarcated by its endothelium (EN), and surrounded by adipocytes (AC) and pockets of hemolymph (HL). 3. Sagittal section through posterior adductor emphasizing longitudinal myofibers (MF), thin perimysium (PM), and a capillary consisting of endothelium (EN). 4. Transverse section of the pericardial gland showing emarginated nuclei of pericardial gland cells (EN), and hemocytes (HC).

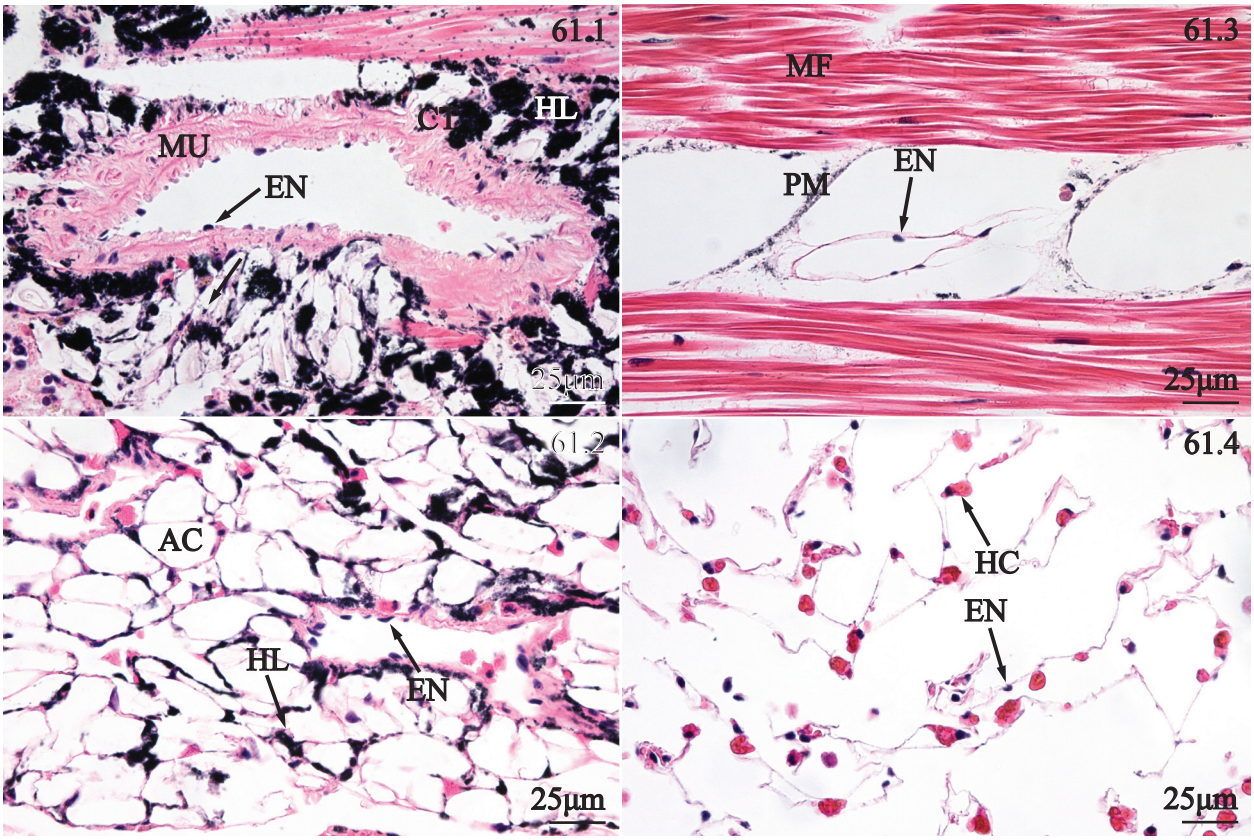
61.1
MU
CT
HL
EN
25µm
61.3
MF
PM
EN
25µm
61.2
AC
HL
EN
25µm
61.4
HC
EN
25µm

PLATE 62. Anterior nephridium of *Strophitus connasaugaensis*. 1. Transverse section of the dorsal aspect of the visceral mass (VM) showing the branched ventral nephridium (VN), dorsal nephridium (DN), pericardium (PC) and ventricle (VE). 2. Transverse section of the ventral nephirdium emphasizing the sinuous nephridial lumen (NL), eosinophilic intracellular granules (EG) of nephridial epithelium and subepithelial blood vessels (BV), and endothelium (EN). 3. Transverse section of dorsal nephridium consisting of teardrop-shaped columnar cells (TC), an expansive nephridial lumen (NL), and adjacent hemolymph (HL) and ventral nephridium (VN). 4. Transverse section of ventral nephridium focusing on the flattened, columnar epithelium (CE) of the dorsal wall, short, rounded plicae (PL) along the ventral surface, and hemocytes (HC). 5. Transverse section of the lateral margin of the nephridium showing the ventral nephridial branches (VN), urethra (UR), ciliated renal-pericardial canal (RC), and hemolymph (HL). 6. Transverse section of the renal-pericardial canal featuring ciliated columnar cells (CC), goblet cells (GC), and an encircling lamina propria (LP). 7. Transverse section of the urethra showing basophilic columnar cells bearing cilia (CI), goblet cells (GC), and lamina propria (LP).

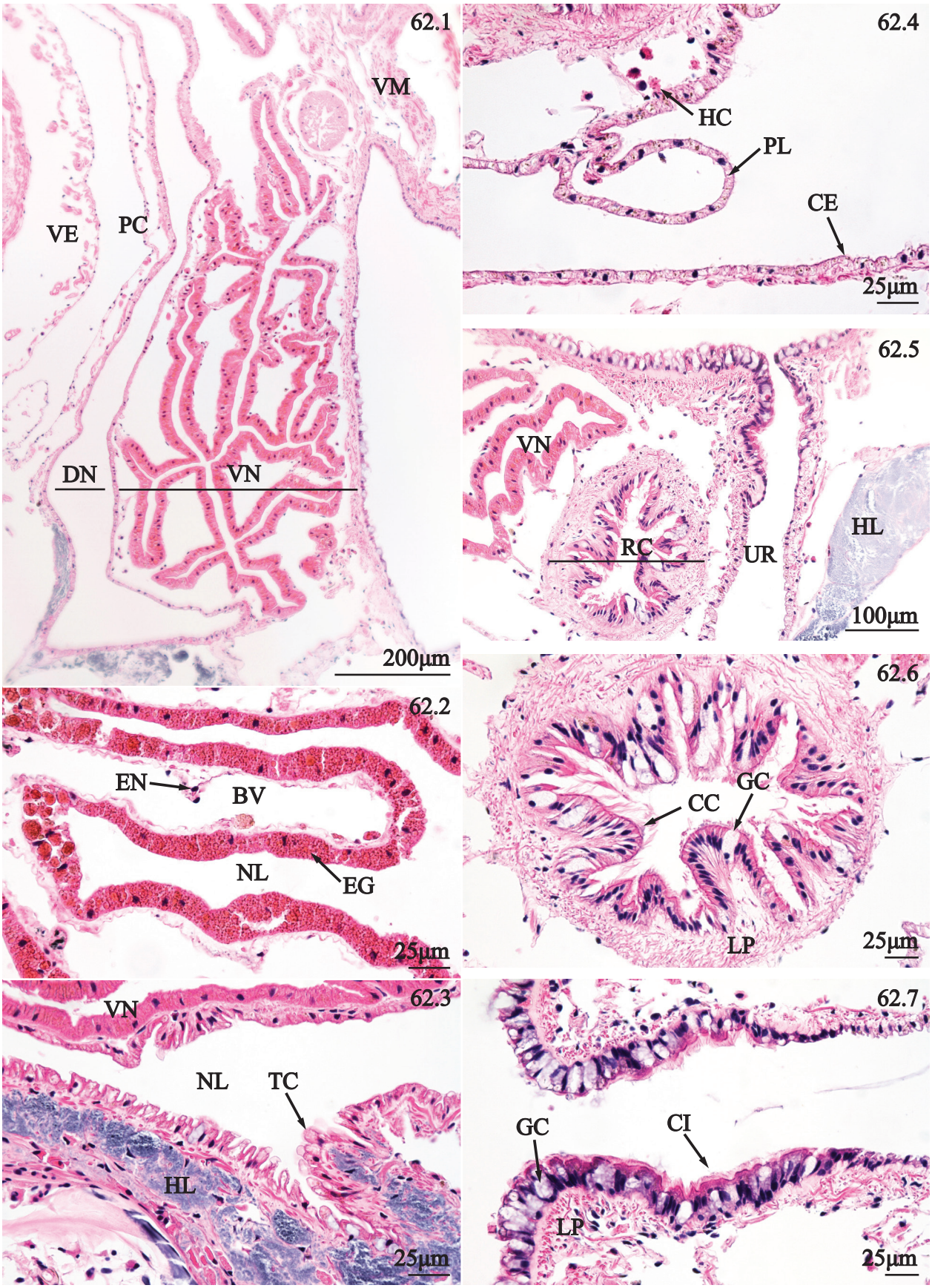
62.1
VM
VE
PC
DN
VN
200µm
62.2
EN
BV
NL
EG
25µm
62.3
VN
NL
TC
HL
25µm
62.4
HC
PL
CE
25µm
62.5
VN
RC
UR
HL
100µm
62.6
GC
CC
LP
25µm
62.7
GC
CI
LP
25µm

Plate 63. Posterior nephridium, posterior pedal retractor, and posterior adductor of *Strophitus connasaugaensis*. 1. Transverse section of posterior nephridium showing nephridial branches (NB) in relation to the posterior pedal retractor (PR). 2. Transverse section of nephridial branches showing a columnar epithelium (CE), brown intracellular granules (BG), and underlying blood vessels (BV). 3. Transverse section of posterior nephridium revealing a short nephridial branch (NB), and a large transverse nerve (NE). 4. Transverse section of posterior retractor showing epimysium (EM), myocyte nuclei (MN), and myofibers (MF). 5. Sagittal section of posterior adductor showing linear myofiber (MF), elliptical myocyte nuclei (MN), perimysium (PM), and endothelium (EN) of capillaries.

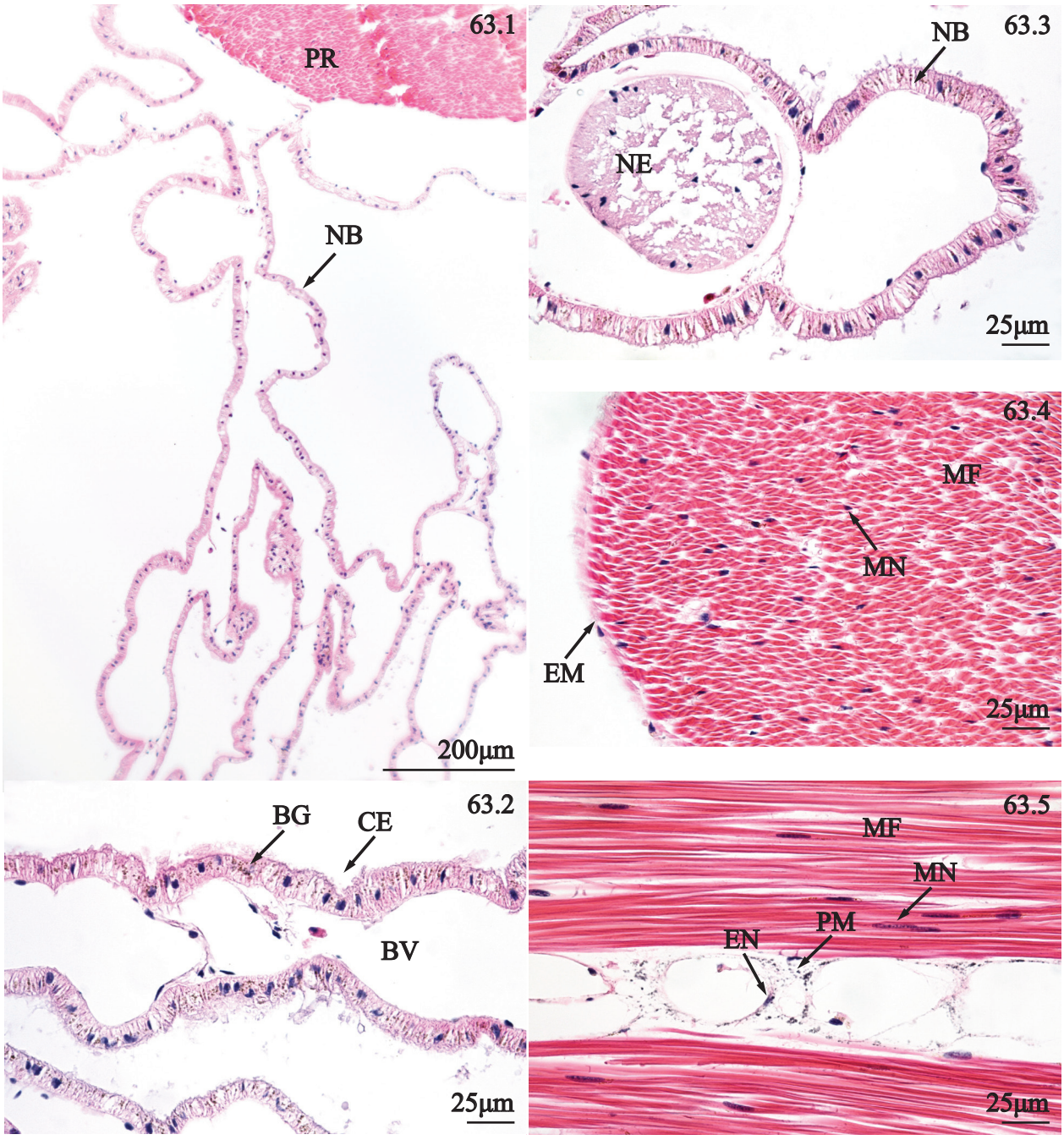
63.1
PR
NB
200µm
63.3
NB
NE
25µm
63.4
MF
MN
EM
25µm
63.2
BG
CE
BV
25µm
63.5
MF
MN
PM
EN
25µm

PLATE 64. Pedal ganglion of *Strophitus connasaugaensis*. 1. Transverse section of the pedal ganglion showing the neural cortex (CO), medulla (ME), dorsal fissure (DF), ventral fissure (VF), and central commissures (CC). 2. Transverse section of pedal ganglion showing the epineurium (EN), dorsal fissure (DF), and neuron cell bodies (CB). 3. Transverse section of neural medulla showing axons (AX), neuron cell bodies (CB), and central commissures (CC). 4. Transverse section of the neural medulla showing axons (AX) and isolated cell bodies (CB). 5. Transverse section of pedal ganglion showing a nerve (NE) extending from a ventral root (RO).

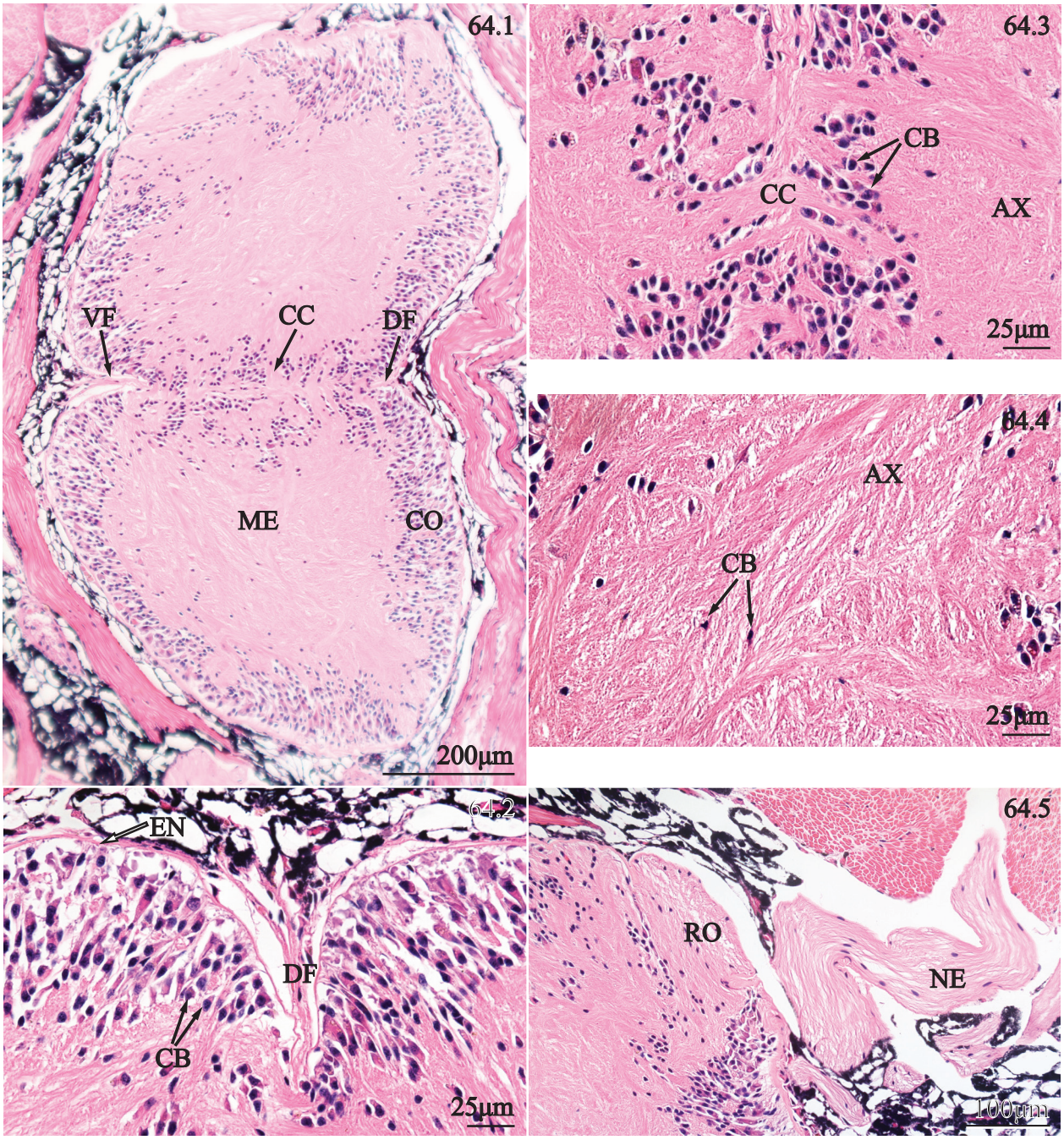
64.1
VF
CC
DF
ME
CO
200µm
64.3
CB
CC
AX
25µm
64.4
AX
CB
25µm
64.2
EN
DF
CB
25µm
64.5
RO
NE
100µm

PLATE 65. Cerebral ganglia, and visceral ganglion of *Strophitus connasaugaensis.* 1. Transverse section through cerebral ganglion showing neural cortex (CO), and medulla (ME). 2. Transverse section of visceral ganglion showing axons (AX), neuron cell bodies (CB), and a ventral layer of columnar epithelium (CE) containing brown intracellular granules. 3. Transverse section of visceral ganglion showing the cortex (CO), medulla (ME), and longitudinal myofibers of the posterior adductor (PA). 4. Transverse section of the base of the ctenidia near the posterior visceral mass showing goblet cells (GC), musculature (MU), and cell bodies (CB) and axons (AX) of a ventral extension of visceral ganglion.

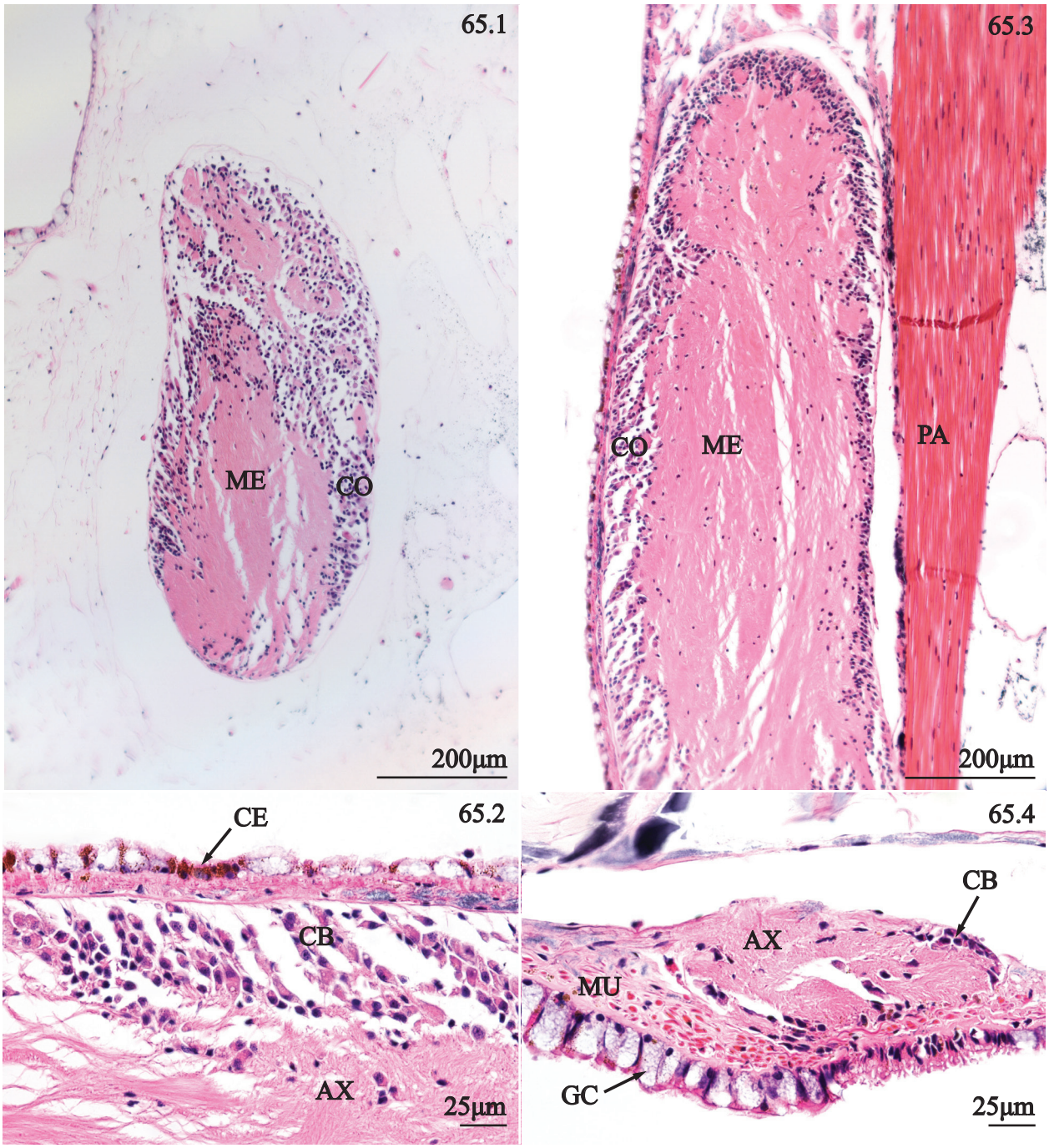
65.1
ME
CO
200µm
65.3
CO
ME
PA
200µm
CE
65.2
CB
AX
25µm
65.4
CB
AX
MU
GC
25µm

PLATE 66. Nerves, and statocysts of *Strophitus connasaugaensis.* 1. Transverse section through nerves (NE) extending from the pedal ganglion showing perineurium (PN), and cell bodies (CB). 2. Transverse section of visceral mass showing a longitudinally oriented nerve (NE) containing cell bodies (CB) and the outer perineurium (PN). 3. Transverse section of a statocyst showing ciliated columnar cells (CC) and the circular statolyth (SL) in the lumen.

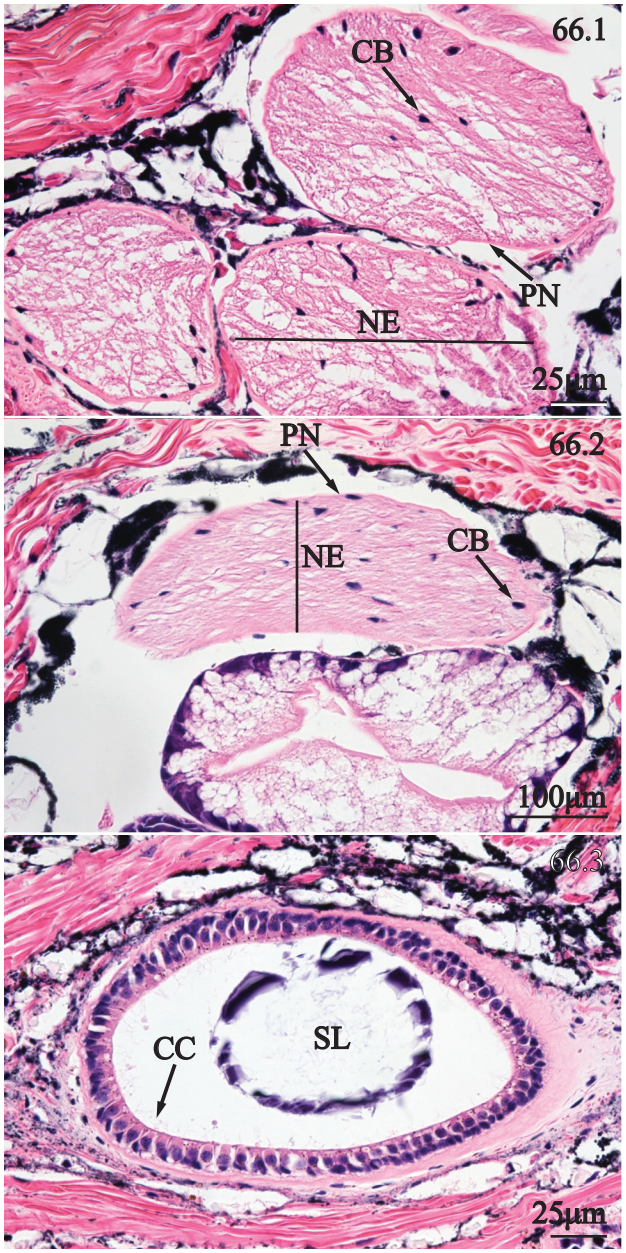
66.1
CB
PN
NE
25µm
PN
66.2
NE
CB
100µm
66.3
CC
SL
25µm

PLATE 67. Ovarian acini, testicular acini, and ciliated gonadal ducts of *Strophitus connasaugaensis.* 1. Transverse section of visceral mass revealing immature ovarian acini (OA) and adjacent ciliated gonadal duct (CD). 2. Transverse section of an ovarian acinus emphasizing emarginated nuclei (EN) constituting the acinus wall, developing oocytes (OC), and cell bodies (CB). 3. Transverse section of a mature ovarian acinus showing a developing oocyte (DO) arising from a pellicle (PE), larger, mature oocytes (MO), and an irregular vitelline membrane (VM). 4. Transverse section of immature testicular acini (TA), and an adjacent ciliated gonadal duct (CD). 5. Transverse section of an immature testicular acinus revealing emarginated nuclei (EN) constituting the acinus wall, primary spermatocytes (PS), and sperm morula (SM). 6. Transverse section of a mature testicular acinus showing prodigious spermatogenesis (SG), and spermatozoa (SZ) occupying the lumen. 7. Transverse section of a gonadal duct emphasizing ciliated columnar cells (CC), and preponderant spermatozoa (SZ) in the lumen. 8. Transverse section of a gonopore showing ciliated columnar cells (CC), and goblet cells (GC).

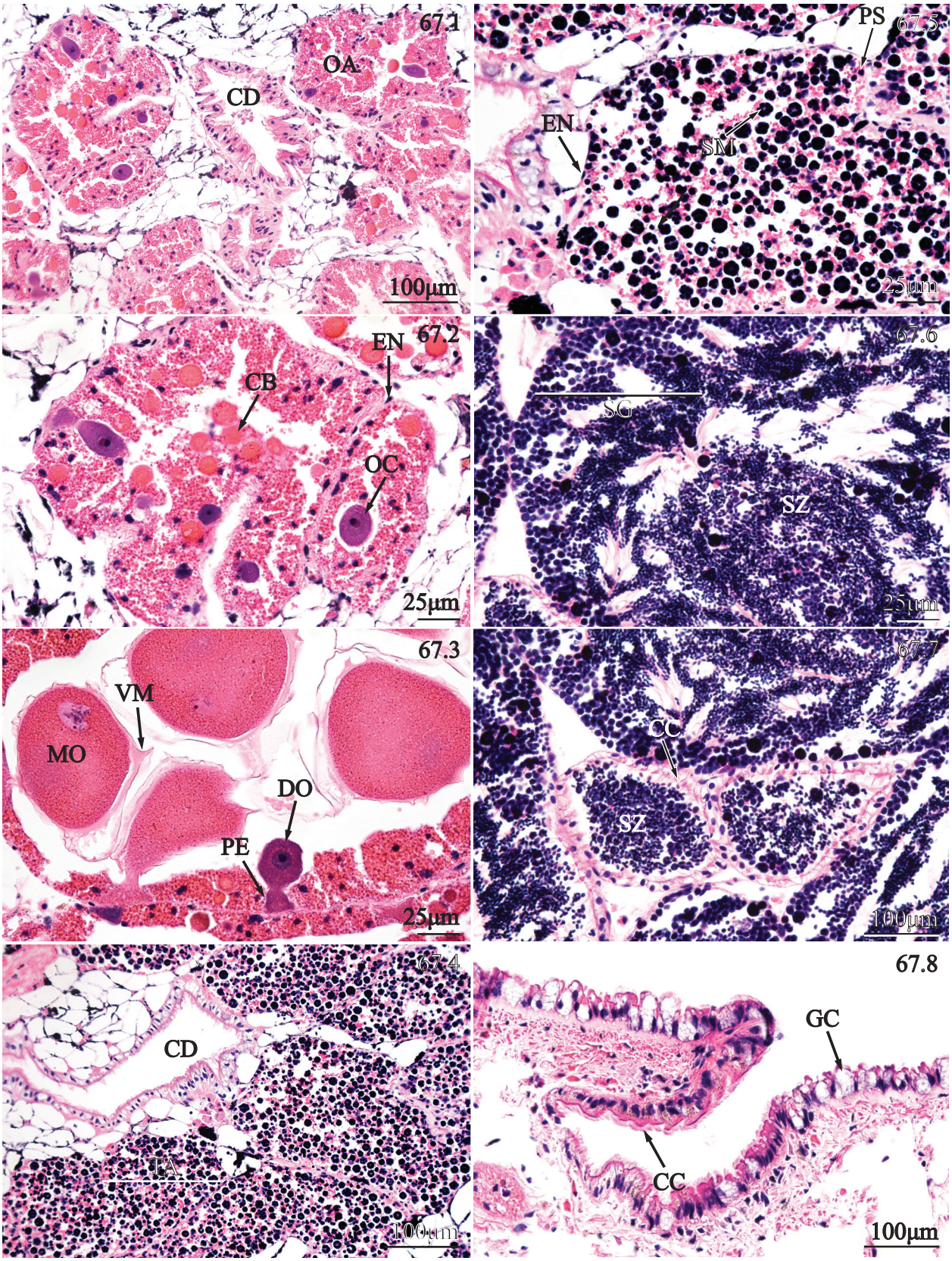
67.1
OA
CD
100μm
67.5
PS
EN
SM
25μm
67.2
EN
CB
OC
25μm
67.6
SG
SZ
25μm
67.3
VM
MO
DO
PE
25μm
67.7
CC
SZ
100μm
67.4
CD
TA
100μm
67.8
GC
CC
100μm

Chapter 7

COMPARISON OF INTERSPECIFIC STRUCTURAL DIFFERENCES BETWEEN ALABAMA RAINBOW (*Villosa nebulosa*), GULF PIGTOE (*Fusconaia cerina*), AND ALABAMA CREEKMUSSEL (*Strophitus connasaugaensis*)

7.1. Introduction

Given the descriptions of the tissues of *Villosa nebulosa*, *Fusconaia cerina*, and *Strophitus connasaugaensis*, it is evident that there are structurally conserved tissues, and tissues that exhibit interspecific structural variation. A list of structurally conserved and structurally distinct tissues is presented in Table 4. This comparative anatomy chapter describes structural differences between *V. nebulosa*, *F. cerina*, and *S. connasaugaensis* and the morphological characteristics of each tissue type that exhibited interspecific variation are summarized in tables.

7.2. Anterior mantle edge

There was conspicuous histological variation in the anterior portion of the mantle edge of *Villosa nebulosa*, *Fusconaia cerina,* and *Strophitus connasaugaensis* (Figs. 68.1–68.3). The mantle edge of *V. nebulosa* and *S. connasaugaensis* generally consisted of a dorsoventrally compressed outer lobe and middle lobe (Figs. 68.1, 68.3, Table 5). The outer mantle lobe of *V. nebulosa* and *S. connasaugaensis* was generally smooth except for the plicae located on the dorsal surface of the outer lobe. A flattened epithelium continues around the ventral surface of the outer lobe of *V. nebulosa* and *S. connasaugaensis*. The mantle edge of *F. cerina* has a thickened, and branched outer lobe (Fig. 68.2, Table 5). The epithelium surrounding the outer lobe of *F. cerina* is extensively folded and irregular and the irregular epithelium continues around the ventral side. Correspondingly, the musculature supporting the individual mantle lobes of *F. cerina* has a dense consistency. *F.usconaia cerina* has a bulbous middle mantle lobe (Fig. 68.2) while *V. nebulosa* and *S. connasaugaensis* lack a distal rounded margin (Figs. 68.1, 68.3, Table 5). The inner mantle lobe of *V. nebulosa* is shaped as an equilateral triangular and does not extend beyond the length of the middle lobe. The inner lobe of *F. cerina* and *S. connasaugaensis* extends nearly to the free margin of the middle lobe (Figs. 68.2, 68.3, Table 5).

Additionally in the anterior portion of the mantle edge of *V. nebulosa*, the basophilic granulocytes appeared to have a higher affinity for hematoxylin than the granulocytes of *F. cerina* and *S. connasaugaensis* (Table 5).

7.3. Posterior mantle edge

Overall the outer and middle lobes become compressed towards the posterior adductor. *Villosa nebulosa* and *S. connasauganesis* have long, thin outer and middle lobes extending from a triangular base of musculature (Figs. 69.1, 69.3, Table 6). There is additionally a reduction in plicae of outer and middle lobes. Outer lobe of *F. cerina* is bifurcated with reduced plicae (Fig. 69.2, Table 6). An irregular epithelium along the ventral surface of the mantle edge features a series of conspicuous clefts. In contrast, the ventral epithelium surrounding the mantle lobes of *V. nebulosa* and *S. connasaugaesis* is flattened with little or no crypts. The most conspicuous detail is the enlarged, bulbous inner mantle lobe of *V. nebulosa*. Plicae surrounding the inner lobe have deeply sinuous makeup.

Mantle papillae of *V. nebulosa* are narrow and triangular with an irregular surface (Fig. 70.1). Papillae of *F. cerina* are branched with a rounded distal margin (Fig. 70.2). The posterior mantle edge of *S. connasaugaensis* consists of conical papillae (Fig. 70.3, Table 6).

7.4. Gill

Non-marsupial gills of *V. nebulosa*, *F. cerina*, and *S. connasaugaensis* were indistinguishable. However, there were differences in fascicle structure in the base of the gills from anterior to posterior. *Villosa nebulosa* features two prominent fascicles along the length of the inner gill and an additional two fascicles along the length of the outer gill (Figs. 71.1, 71.4, Table 7). Correspoding pairs of fascicles in *F. cerina* become reduced between the posterior margin of the visceral mass and posterior adductor (Figs. 71.2, 71.5, Table 7). In *S. connasaugaensis*, only the

inner gill was supported by fascicles and there was a general reduction in fascicle diameter between the posterior margin of the visceral mass and posterior adductor (Figs. 71.3, 71.6, Table 7).

Marsupia were different between *V. nebulosa*, *F. cerina*, and *S. connasaugaensis*. The marsupium of *V. nebulosa* was bulbous and distended ventrally (Fig. 72.1). The lining of marsupial water tubes of *V. nebulosa* consisted of ciliated plicae and ciliated columnar cells with brown intracellular granules. The water tube walls are supported by prominent, muscle fibers and connective tissue. Distension of gill tissues of *F. cerina* and *S. connasaugaensis* was more evenly distributed in comparison to the progressively increasing distension of *V. nebulosa* water tubes. Septa of *F. cerina* have rounded to rectangular plicae with conspicuous goblet cells. Plicae are irregular and typically there is a median plica that is taller than the surrounding structures (Fig. 72.2). Glochidia of *S. connasaugaensis* were contained within a cylindrical sac or placenta within the central water tube (Fig. 72.3). The sac consisted of squamous epithelium, connective tissue, and hemolymph. Additionally, interbranchial septa have numerous spherical basophilic goblet cells and surrounding darkened basophilic cells (Table 7).

7.5. Foot

Pedal epithelium was different across each species. Overall, pedal epithelium at the ventral margin of the foot consisted of irregular, ciliated plicae (Figs. 73.1, 73.6, 73.11, Table 8). However, when plicae are distinctly separated from each other in integument regions one and two, plicae may resemble a "Y" (Fig. 73.1, 73.2), a rectangle (Fig. 73.6, 73.7) or may appear branched (Figs. 73.11, 73.12). Basophilic granulocytes are present.in the subepithelium of each species, but were most abundant in integument region one of *F. cerina* (Fig 73.6). The integument of *V. nebulosa* is irregular and sinuous at the ventral margin of the foot and the plicae

become shorter, towards the dorsum and are reduced to a series of convex squamous cells or teardrop-shaped columnar cells (Fig 73.1–73.5, Table 8). The pedal integument of *F. cerina*, and *S. connasaugaensis* ranges from a series of deep, irregular folds at the ventral margin, to a flattened epithelium at the dorsal end of the visceral mass (Figs. 73.6–73.15, Table 8).

7.6. Oral groove

The oral groove of *V. nebulosa* is tubular extension of the labial palps characterized by a concave track and longitudinal grooves (Fig. 74.1, Table 9). The oral groove of *F. cerina* and *S. connasauagaensis* ifeatures a pair of lip-like structures that demarcate a vertical entrance to a deep cavity (Figs. 74.2, 74.3, Table 9). The dorsal margin of the oral groove has a flattened and columnar epithelium with ciliated cells (Fis. 74.4–74.6).

7.7. Digestive diverticulum

The esophagus opens into the digestive diverticulum on the sinistral and dextral sides of the body in *V. nebulosa* (Fig. 75.1, Table 9). The ciliated tubules leading into the organ are narrow and extend obliquely into the viscera. The entrance of the digestive diverticulum of *F. cerina* and *S. connasaugaensis* is located on the sinistral side of the body and it is a large "L"-shaped cavity (Figs. 75.2, 75.3, Table 9).

Digestive tubules of *V. nebulosa* and *S. connasaugaensis* were similar to each other. Primary tubules consist of low, rounded plicae with ciliated columnar cells (Figs. 76.1, 76.3, Table 9). Secondary tubules are eosinophilic with microvilli and a vesiculated cytoplasm (Figs. 76.4–76.6). Primary tubules in *F. cerina* consist of narrow, rounded plicae that extend into the middle of the tubule lumen (Figs. 76.2, Table 9). Secondary tubules of *F. cerina* were strongly vesiculated and the cells are teardrop shaped such that opposing walls of a secondary tubule may resemble a pair of valves (Fig. 76.5, 31.5).

7.8. Crystalline style sac

The crystalline style sacs of *V. nebulosa*, *F. cerina* and *S. connasaugaensis* have similar morphological characteristics overall. However, the blind end of the midgut exhibited a subtle structural difference. In *V. nebulosa*, the blind end of the midgut was cylindrical (Fig. 77.1, Table 10). The blind end of the midgut was circular in *F. cerina* (Fig. 77.2, Table 10), and laterally compressed in *S. connasaugaensis* (Fig. 77.3, Table 10).

7.9. Intestine

The second and third intestinal limbs were structurally identical, but there are prominent interspecific structural differences in the shape of the intestinal lumen. *V. nebulosa* and *S. connasuagaensis* have prominent plicae or typhlosoles extending into the lumen (Figs. 78.1, 78.3, Table 10). In contrast, the lumen of the second and third intestinal limbs of *F. cerina* generally lacks such conspicuous folds (Figs. 78.2, Table 10).

7.10. Pedal ganglion

The pedal ganglion of *F. cerina* has filamentous connective tissue surrounding the neural cortex (Fig. 79.2, Table 10). Pedal ganglion axons of *V. nebulosa* and *S. connasauagaensis* were thinner and the medulla has a fine wispy appearance (Figs. 79.1, 79.3, Table 10).

7.11. Ovarian acini

Mature ova of *V. nebulosa*, *F. cerina*, and *S. connasaugaensis* were unique. Specifically, the vitelline of *V. nebulosa* is fluidic with an inconspicuous vitelline membrane (Fig. 80.1, Table 10). Conversely, *F. cerina* has a dense, well-defined vitelline membrane and there is little or no fluid surrounding the cytoplasm of the oocyte (Fig. 80.2, Table 10). The vitelline membrane of *S. connasaugaensis* represents a combination of the former tow types (Fig. 80.3, Table 10).

Table 5. List of structurally conserved and structurally distinct tissues of Alabama rainbow (*Villosa nebulosa*), Gulf pigtoe (*Fusconaia cerina*), and Alabama creekmussel (*Strophitus connasauagaensis*).

Structurally conserved	Structurally distinct
Middle mantle	Mantle edge
Mantle isthmus	Marsupium
Non-marsupial gill	Foot
Labial palp	Inner gill-abdomen junction
Adductor/pedal retractor/protractor	Outer gill-abdomen junction
Byssal gland	Digestive diverticulum
Esophagus	Stomach
Statocyst	Crystalline style sac
Intestinal limbs 4, 5	Intestinal limbs 2, 3
Pericardial gland	Ganglia
Heart	Ovarian acini
Nephridium	
Testicular acini	

Table 6. Summary of structural differences in anterior mantle edge of Alabama rainbow (*Villosa nebulosa*), Gulf pigtoe (*Fusconaia cerina*), and Alabama creekmussel (*Strophitus connasaugaensis*).

Species	Anterior mantle edge		
	Outer lobe	Middle lobe	Inner lobe
Villosa nebulosa	Dorsoventrally compressed, tapering distally	Dorsoventrally compressed, tapering distally	Equilateral triangle, not extending past outer, middle lobes
	Ventral epithelium flattened	Ventral epithelium flattened	Presence of basophilic granulocytes
	Dorsal epithelium flattened with plicae along distal end of lobe	Dorsal epithelium flattened	
Fusconaia cerina	Branched and bulbous	Rounded distally	Compressed triangle, extending beyond outer and middle lobes
	Ventral epithelium with plicae	Ventral epithelium flattened	Absence of basophilic granulocytes
	Dorsal epithelium with plicae	Dorsal epithelium with plicae	
Strophitus connasaugaensis	Dorsoventrally compressed, tapering distally	Dorsoventrally compressed	Compressed triangle, not extending beyond outer and middle lobes
	Ventral epithelium flattened	Ventral epithelium flattened	Presence of basophilic granulocytes
	Dorsal epithelium with reduced, sparsely distributed plicae	Dorsal epithelium with irregular plicae	

Table 7. Summary of structural differences in posterior mantle edge of Alabama rainbow (*Villosa nebulosa*), Gulf pigtoe (*Fusconaia cerina*), and Alabama creekmussel (*Strophitus connasaugaensis*).

Species	Posterior mantle edge			
	Outer lobe	Middle lobe	Inner lobe	Papillae
Villosa nebulosa	Dorsoventrally compressed, tapering distally, extending from an elongated base	Dorsoventrally compressed, tapering distally, extending from an elongated base	Bulbous, enlarged, extending to outer and middle lobes	Finely conical
	Ventral epithelium flattened	Ventral epithelium flattened	Epithelial cells with conspicuous black or brown, intracellular granules	
	Dorsal epithelium flattened	Dorsal epithelium flattened		
Fusconaia cerina	Outer lobe branched with two triangular lobes	Middle lobe straightened, not rounded distally	Triangular, compressed, not extending past outer, middle lobes	Subtriangular, branched
	Ventral epithelium flattened	Ventral epithelium flattened		
Strophitus connasaugaensis	Dorsoventrally compressed	Dorsoventrally compressed	Triangular, short, not extending beyond outer and middle lobes	Conical
	Flattened epithelium	Flattened epithelium		

Table 8. Summary of structural differences in gill of Alabama rainbow (*Villosa nebulosa*), Gulf pigtoe (*Fusconaia cerina*), and Alabama creekmussel (*Strophitus connasaugaensis*).

	Gill		
Species	Outer gill base	Inner gill base	Marsupium
Villosa nebulosa	Two conspicuous fascicles spanning anterior-posterior	Two conspicuous fascicles spanning anterior-posterior	Water tube distension increases ventrally Water tubes thickened with fibrous tissue Small, ciliated plicae lining water tubes Glochidia enclosed by a thin membrane
Fusconaia cerina	Well developed fascicles between posterior third of visceral mass and posterior adductor	Reduced fascicles between posterior third of visceral mass and posterior adductor	Laterally distended, branchial width is the same dorsal to ventral Water tubes lined with squamous epithelium Septa with irregular plicae, plicae become tall in the median Glochidia and unfertilized ova linked together in conglutinate
Strophitus connasaugaensis	Reduced fascicles between posterior third of visceral mass and posterior adductor	Fascicles absent	Laterally distended, branchial width is the same dorsal to ventral Water tubes lined with squamous epithelium Septa with irregular plicae that become tall in the median Glochidia contained within a cylindircal placenta

Table 9. Summary of structural differences in pedal epithelium of Alabama rainbow (*Villosa nebulosa*), Gulf pigtoe (*Fusconaia cerina*), and Alabama creekmussel (*Strophitus connasaugaensis*).

Species	Pedal epithelium				
	Type 1	Type 2	Type 3	Type 4	Type 5
Villosa nebulosa	Tall, irregular plicae	Medium-sized, irregular plicae	Short, irregular plicae	Epithelium plicated to papillose, folds becoming reduced	Epithelium papillose with teardrop-shaped columnar cells and convex squamous cells
	Violet basophilic granulocytes moderately abundant	Violet basophilic granulocytes sparsely distributed			
Fusconaia cerina	Tall, rectangular plicae	Tall, irregular plicae, may appear coalescing	Short, teardrop-shaped plicae, irregular shape	Columnar epithelium, epithelium is furrowed	Cuboidal epithelium, epithelium flattened
	Basophilic granulocytes very abundant	Basophilic granulocytes sparsely distributed			
Strophitus connasaugaensis	Tall, irregular, branched plicae	Tall, irregular, branched plicae	Short, thin, irregular plicae	Squamous epithelium, epithelium is furrowed	Squamous epithelium, epithelium flattened
	Basophilic granulocytes moderately abundant	Subepithelial glands, abundant			

Table 10. Summary of structural differences in oral groove, and digestive diverticulum of Alabama rainbow (*Villosa nebulosa*), Gulf pigtoe (*Fusconaia cerina*), and Alabama creekmussel (*Strophitus connasaugaensis*).

Species	Oral groove	Entrance to digestive diverticulum	Digestive diverticulum tubules	
			Type 1	Type 2
Villosa nebulosa	Concave, tubular	Esophagus opens directly into sinistral and dextral tubules	Tubules with short, rounded plicae	Columnar cells rectangular, vesiculated, with microvilli Seamless transition between secondary and tertiary tubules
Fusconaia cerina	Deep cavity	Esophagus opens into a large sinistral chamber	Tubules with long, thin plicae	Tubules with teardrop-shaped columnar cells Abrupt transition between secondary and tertiary tubule cells, resembles valves
Strophitus connasaugaensis	Deep cavity	Esophagus opens into a large sinistral chamber	Short, thin, irregular plicae	Columnar cells rectangular, vesiculated, with microvilli Seamless transition between secondary and tertiary tubules

Table 11. Summary of structural differences in crystalline style sac, intestine, pedal ganglion, and ovarian acini of Alabama rainbow (*Villosa nebulosa*), Gulf pigtoe (*Fusconaia cerina*), and Alabama creekmussel (*Strophitus connasauagaensis*).

Species	Style sac	Intestinal limbs 2 and 3	Pedal ganglion	Ovarian acini
Villosa nebulosa	Midgut bends around sinistrally directed typhlosole	Presence of numerous plicae, lumen is folded	Axons fine, filamentous	Mature ova with a thin vitelline membrane
			Surrounding connective tissue is fine	Abundance of fluid between vitelline membrane and ova
Fusconaia cerina	Midgut extends horizontally from style sac	Plicae largely absent, lumen is flattened	Axons thickened, conspicuous	Mature ova with thickened vitelline membrane
			Surrounding connective tissue is thickened, conspicuous	Little or no fluid between vitelline membrane and ova
Strophitus connasaugaensis	Midgut bends around sinistrally directed typhlosole	Presence of numerous plicae, lumen is folded	Axons fine, filamentous	Mature ova with a thin vitelline membrane
			Surrounding connective tissue is fine	Moderate quantitiy of fluid between vitelline membrane and ova

PLATE 68. Anterior mantle edge of *Villosa nebulosa*, *Fusconaia cerina*, and *Strophitus connasaugaensis*. 1. Anterior mantle edge of *Villosa nebulosa.* 2. Anterior mantle edge of *Fusconaia cerina.* 3. Anterior mantle edge of *Strophitus connasaugaensis*.

68.1

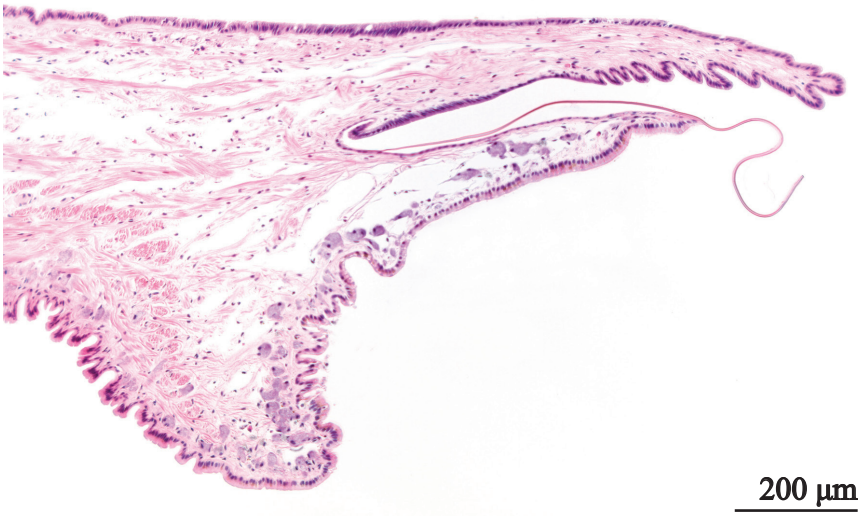

200 µm

68.2

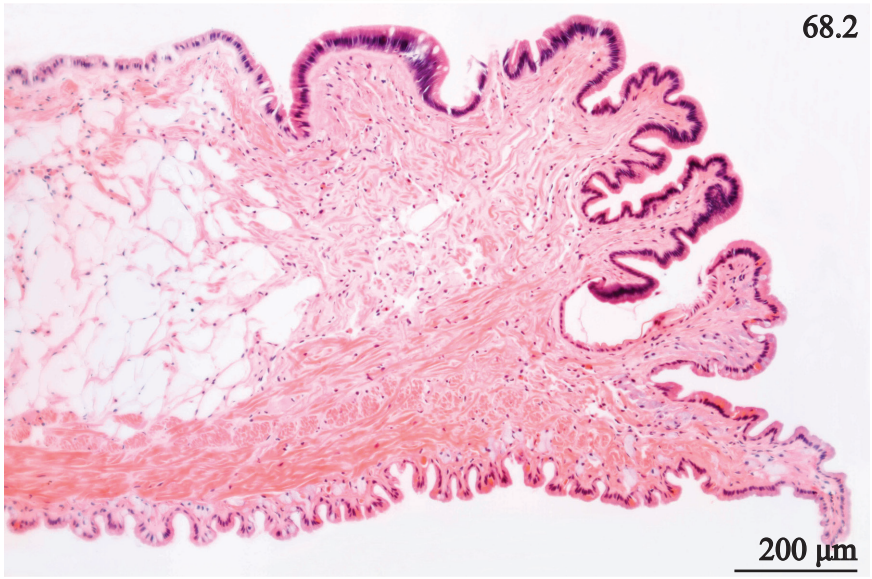

200 µm

68.3

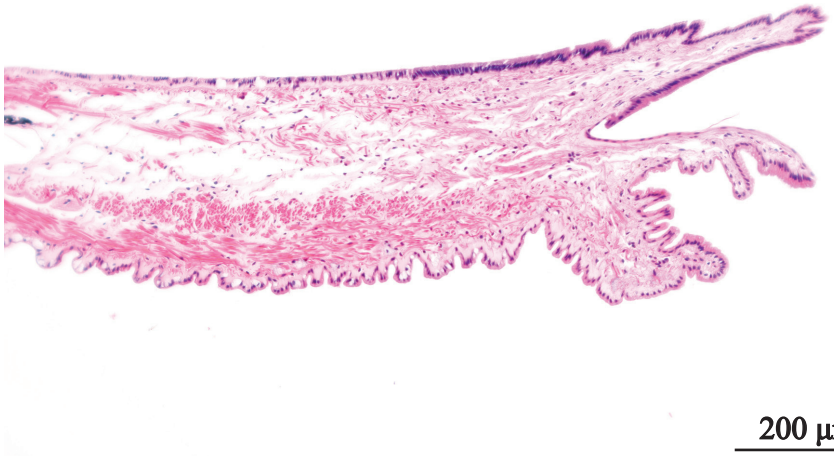

200 µm

PLATE 69. Posterior mantle edge of *Villosa nebulosa*, *Fusconaia cerina*, and *Strophitus connasaugaensis*. 1. Posterior mantle edge of *Villosa nebulosa*. 2. Posterior mantle edge of *Fusconaia cerina*. 3. Posterior mantle edge of *Strophitus connasaugaensis*.

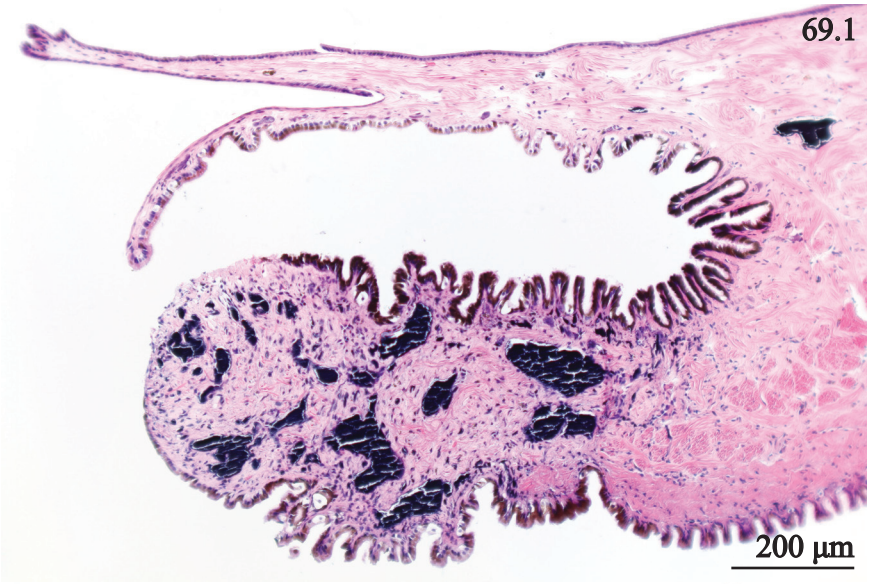

69.2

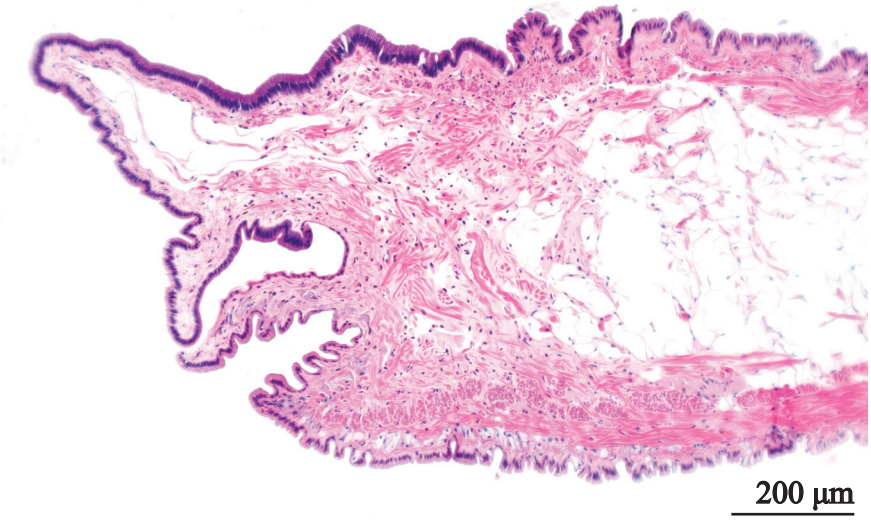

69.3

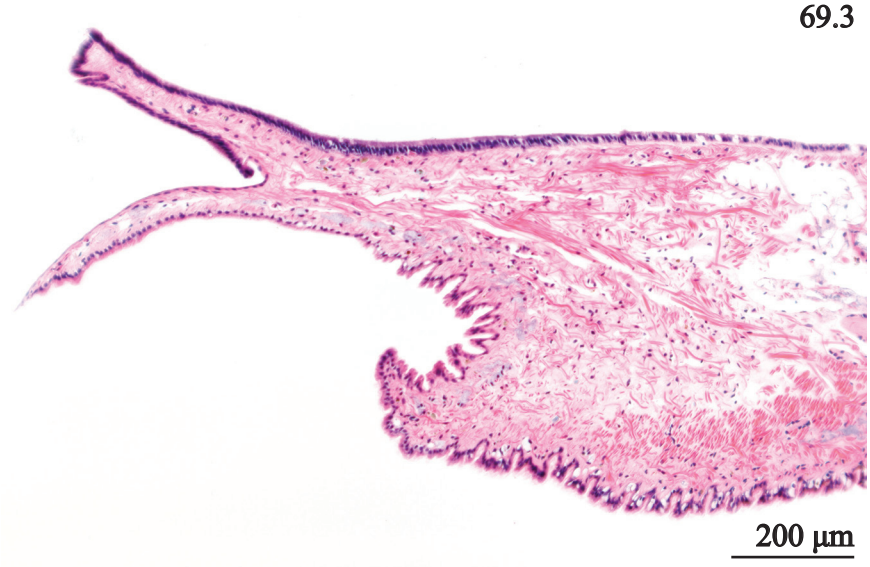

PLATE 70. Mantle edge papillae of *Villosa nebulosa*, *Fusconaia cerina*, and *Strophitus connasaugaensis.* 1. Mantle edge papillae of *Villosa nebulosa*. 2. Mantle edge papillae of *Fusconaia cerina*. 3. Mantle edge papillae of *Strophitus connasaugaensis*.

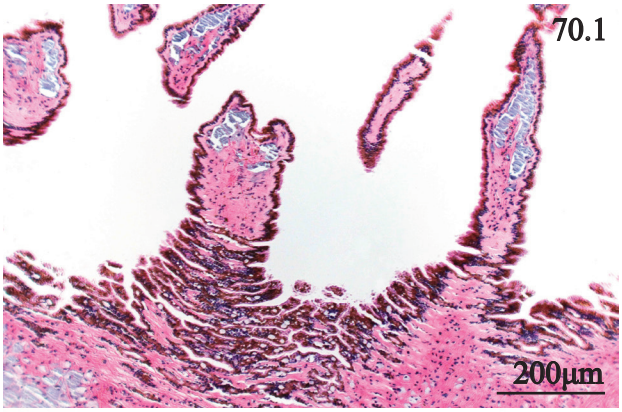
70.1
200µm

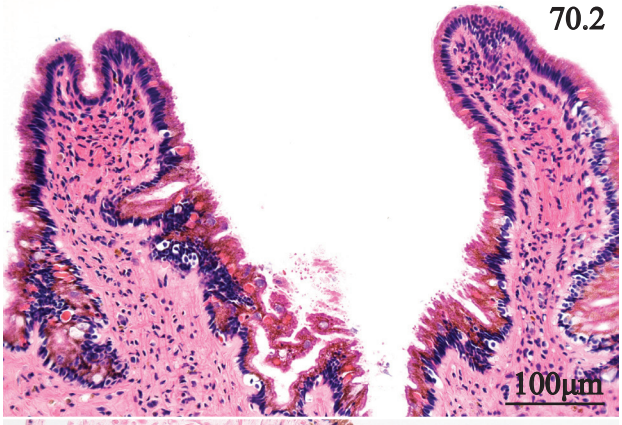
70.2
100µm

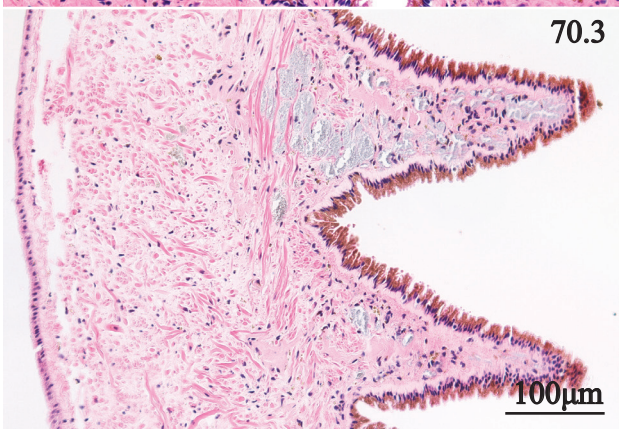
70.3
100µm

PLATE 71. Gill-abdomen junctions of *Villosa nebulosa*, *Fusconaia cerina*, and *Strophitus connasaugaensis.* 1.Inner gill-abdomen junction of *Villosa nebulosa*. 2. Inner gill-abdomen junction of *Fusconaia cerina*. 3. Inner gill-abdomen junction of *Strophitus connasaugaensis*. 4. Outer gill-abdomen junction of *Villosa nebulosa*. 5. Outer gill-abdomen junction of *Fusconaia cerina*. 6. Outer gill-abdomen junction of *Strophitus connasaugaensis*.

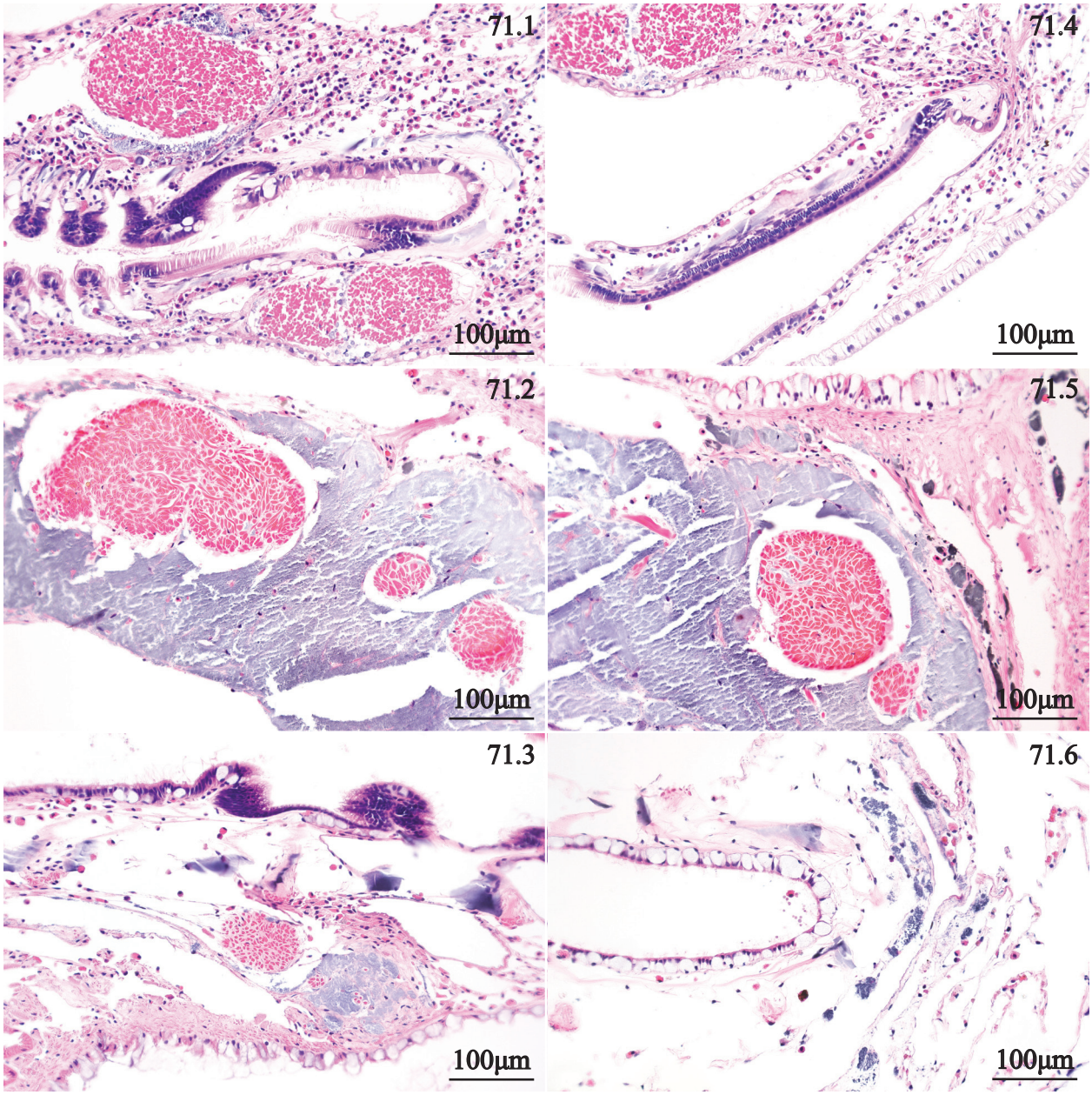
71.1
100µm
71.4
100µm
71.2
100µm
71.5
100µm
71.3
100µm
71.6
100µm

PLATE 72. Marsupial gill of *Villosa nebulosa*, *Fusconaia cerina*, and *Strophitus connasaugaensis.* 1. Marsupial gill of *Villosa nebulosa*. 2. Marsupial gill of *Fusconaia cerina*. 3. Marsupial gill of *Strophitus connasaugaensis*.


72.1
200 µm
72.2
200 µm
72.3
200 µm

PLATE 73. Pedal integument of *Villosa nebulosa*, *Fusconaia cerina*, and *Strophitus connasaugaensis.* 1. Pedal integument type 1 of *Villosa nebulosa*. 2. Pedal integument type 2 of *Villosa nebulosa*. 3. Pedal integument type 3 of *Villosa nebulosa*. 4. Pedal integument type 4 of *Villosa nebulosa*. 5. Pedal integument type 5 of *Villosa nebulosa*. 6. Pedal integument type 1 of *Fusconaia cerina*. 7. Pedal integument type 2 of *Fusconaia cerina*. 8. Pedal integument type 3 of *Fusconaia cerina*. 9. Pedal integument type 4 of *Fusconaia cerina*. 10. Pedal integument type 5 of *Fusconaia cerina*. 11. Pedal integument type 1 of *Strophitus connasaugaensis*. 12. Pedal integument type 2 of *Strophitus connasaugaensis*. 13. Pedal integument type 3 of *Strophitus connasaugaensis*. 14. Pedal integument type 4 of *Strophitus connasaugaensis*. 15. Pedal integument type 5 of *Strophitus connasaugaensis*.

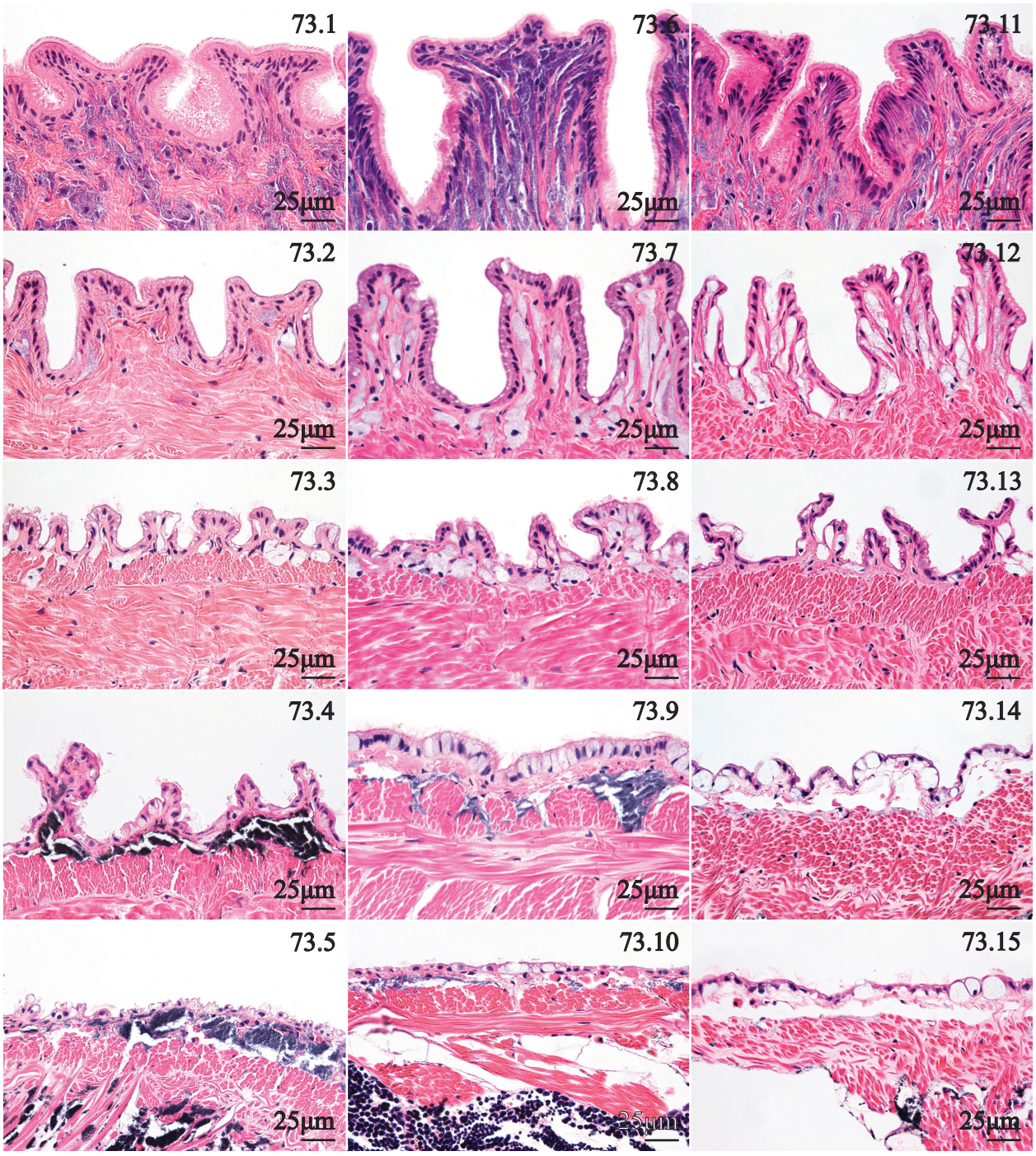
73.1
25µm
73.6
25µm
73.11
25µm
73.2
25µm
73.7
25µm
73.12
25µm
73.3
25µm
73.8
25µm
73.13
25µm
73.4
25µm
73.9
25µm
73.14
25µm
73.5
25µm
73.10
25µm
73.15
25µm

PLATE 74. Oral groove of *Villosa nebulosa*, *Fusconaia cerina*, and *Strophitus connasaugaensis.* 1. Ventral margin of the oral groove of *Villosa nebulosa*. 2. Ventral margin of the oral groove of *Fusconaia cerina*. 3. Ventral margin of the oral groove of *Strophitus connasaugaensis*. 4. Dorsal margin of the oral groove of *Villosa nebulosa*. 5. Dorsal margin of the oral groove of *Fusconaia cerina*. 6. Dorsal margin of the oral groove of *Strophitus connasaugaensis*.

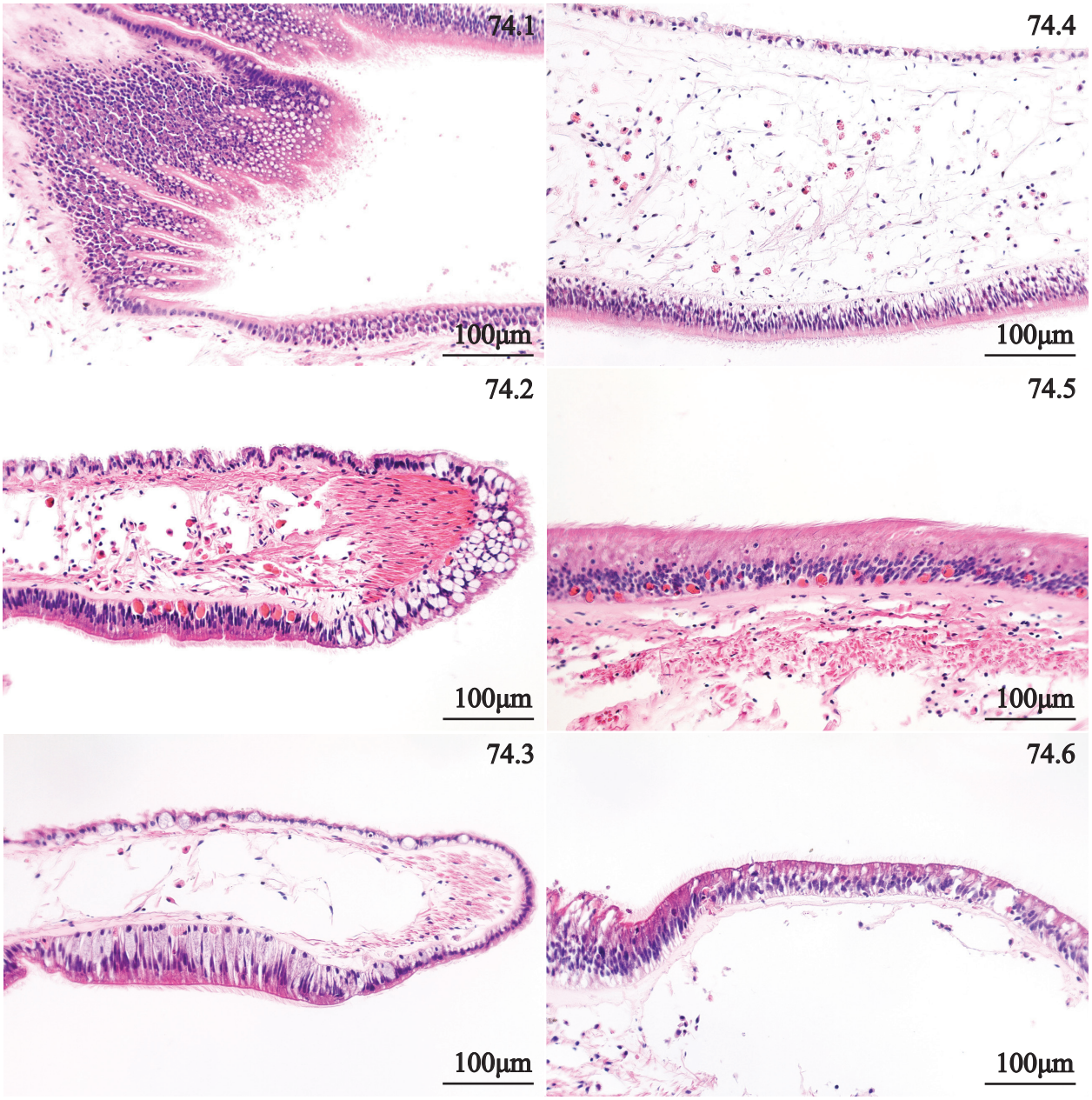
74.1
100μm
74.4
100μm
74.2
100μm
74.5
100μm
74.3
100μm
74.6
100μm

PLATE 75. Esophageal-digestive diverticulum junction of *Villosa nebulosa*, *Fusconaia cerina*, and *Strophitus connasaugaensis.* 1. Esophageal-digestive diverticulum junction of *Villosa nebulosa*. 2. Esophageal-digestive diverticulum junction of *Fusconaia cerina*. 3. Esophageal-digestive diverticulum junction of *Strophitus connasaugaensis*.

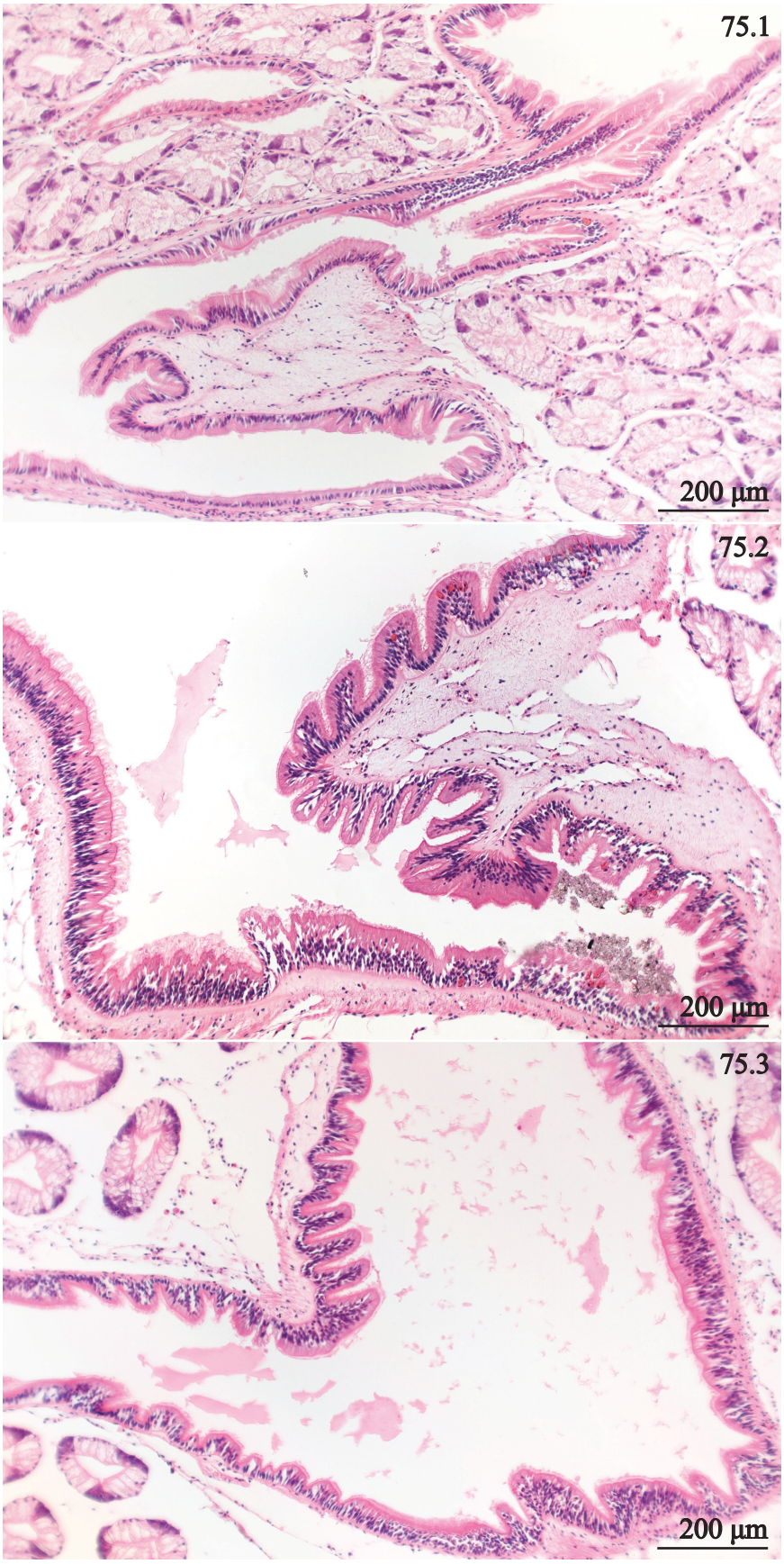
75.1
200 µm
75.2
200 µm
75.3
200 µm

PLATE 76. Primary, and secondary digestive diverticulum tubules of *Villosa nebulosa*, *Fusconaia cerina*, and *Strophitus connasaugaensis*. 1. A primary digestive tubule of *Villosa nebulosa*. 2. Primary digestive tubule of *Fusconaia cerina*. 3. Primary digestive tubule of Strophitus connasaugaensus. 4. Secondary digestive tubule of *Villosa nebulosa*. 5. Secondary digestive tubule of *Fusconaia cerina*. 6. Secondary digestive tubule of *Strophitus connasaugaensis*.

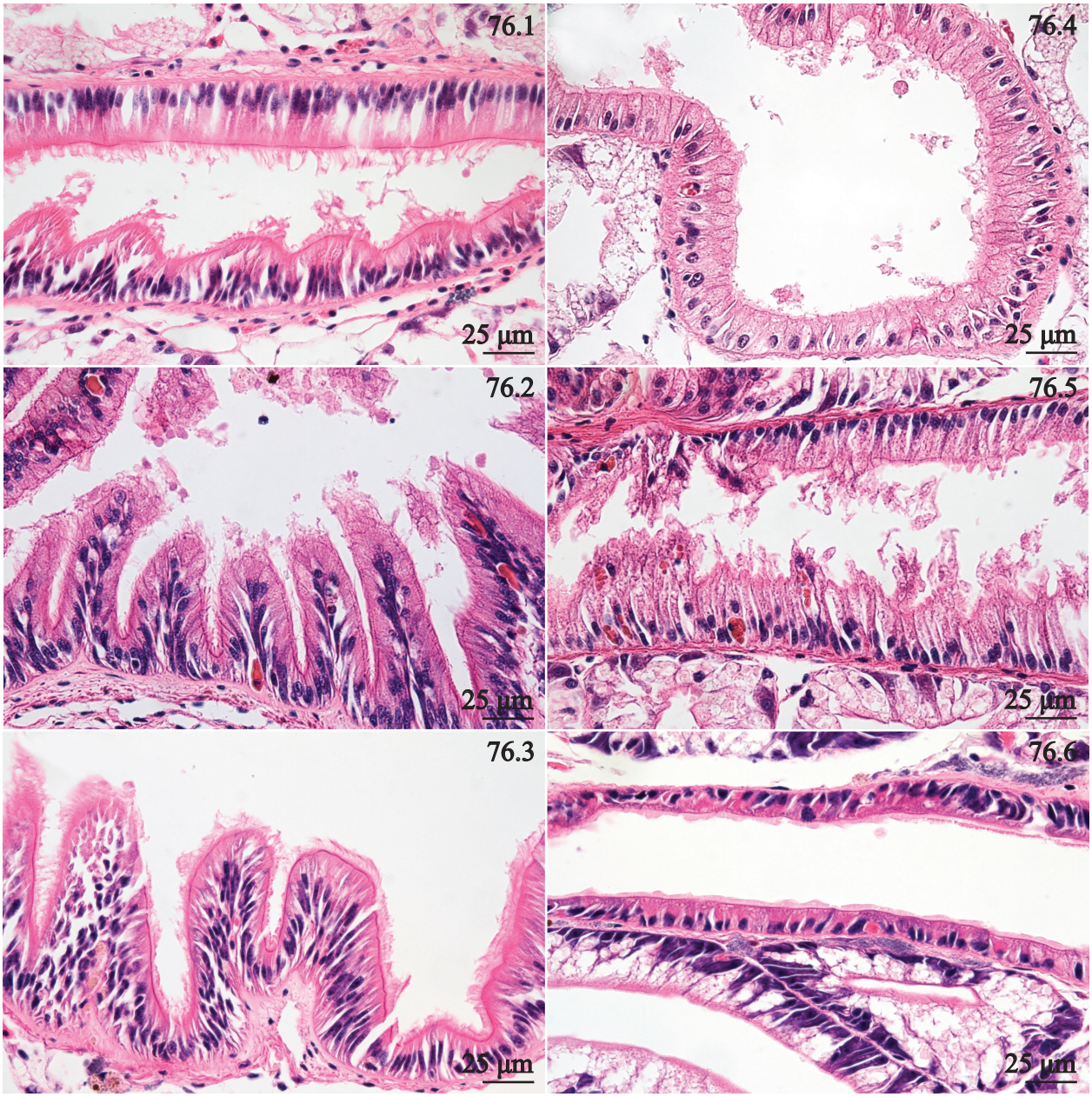
76.1
25 µm
76.4
25 µm
76.2
25 µm
76.5
25 µm
76.3
25 µm
76.6
25 µm

PLATE 77. Blind end of the midgut in the crystalline style sac of *Villosa nebulosa*, *Fusconaia cerina*, and *Strophitus connasaugaensis*. 1. Blind end of the midgut of *Villosa nebulosa*. 2. Blind end of the midgut of *Fusconaia cerina*. 3. Blind end of the midgut of *Strophitus connasaugaensis*.

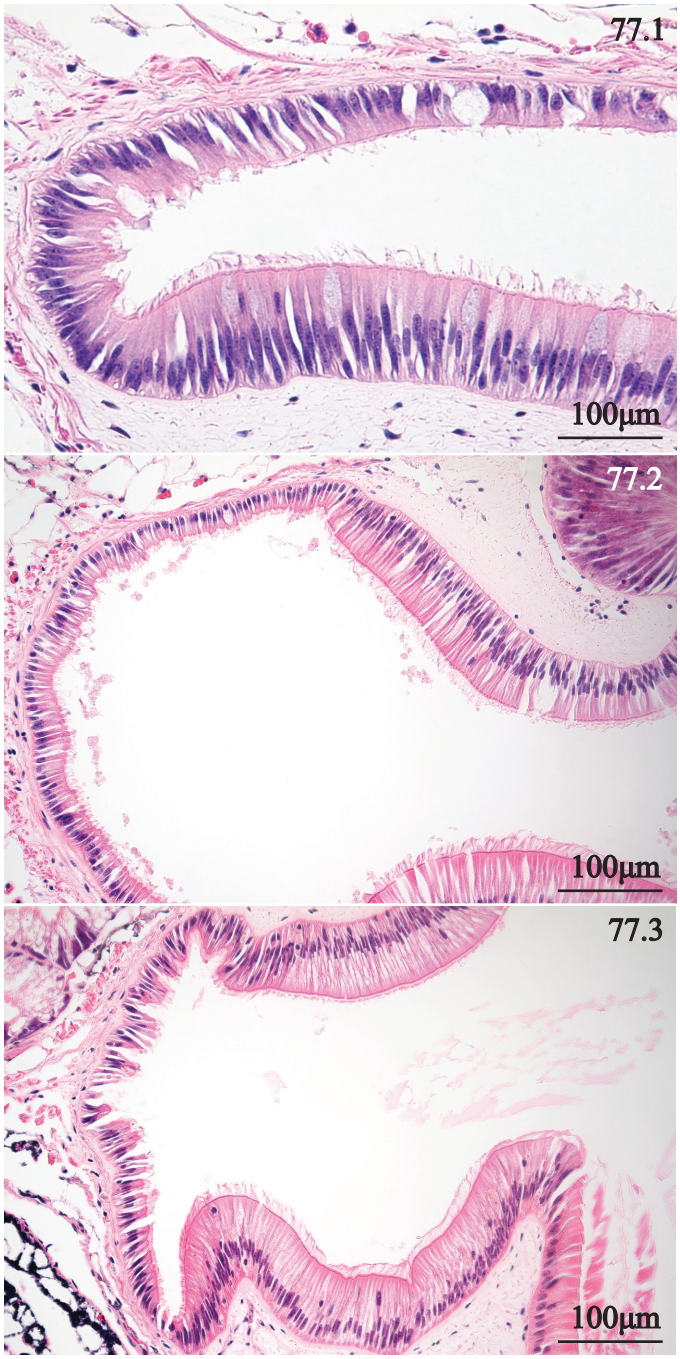
77.1
100µm
77.2
100µm
77.3
100µm

PLATE 78. Second intestinal limb of *Villosa nebulosa*, *Fusconaia cerina*, and *Strophitus connasasaugaensis.* 1. Second intestinal limb of *Villosa nebulosa*. 2. Second intestinal limb of *Fusconaia cerina*. 3. Second intestinal limb of *Strophitus connasaugaensis*.

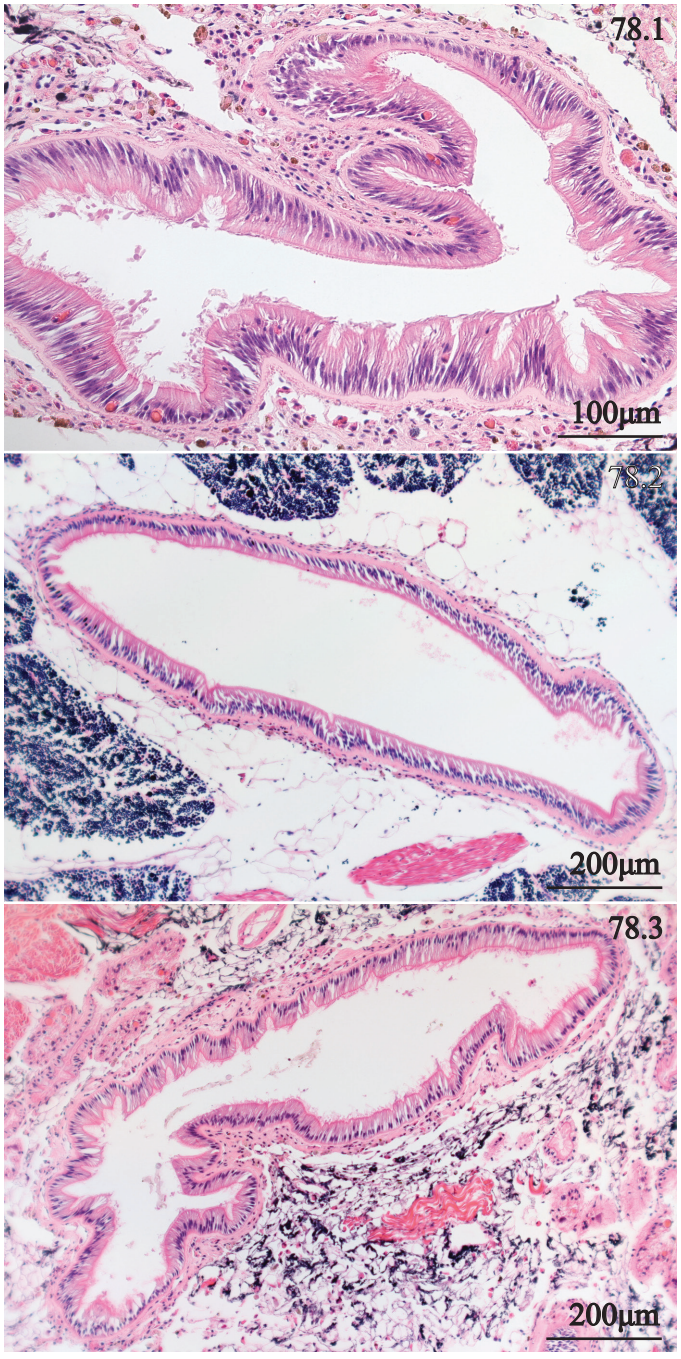
78.1
100μm
78.2
200μm
78.3
200μm

PLATE 79. Median fissure of the pedal ganglion of *Villosa nebulosa*, *Fusconaia cerina*, and *Strophitus connasaugaensis.* 1. Median fissure of the pedal ganglion of *Villosa nebulosa*. 2. Median fissure of the pedal ganglion of *Fusconaia cerina*. 3. Median fissure of the pedal ganglion of *Strophitus connasaugaensis*.

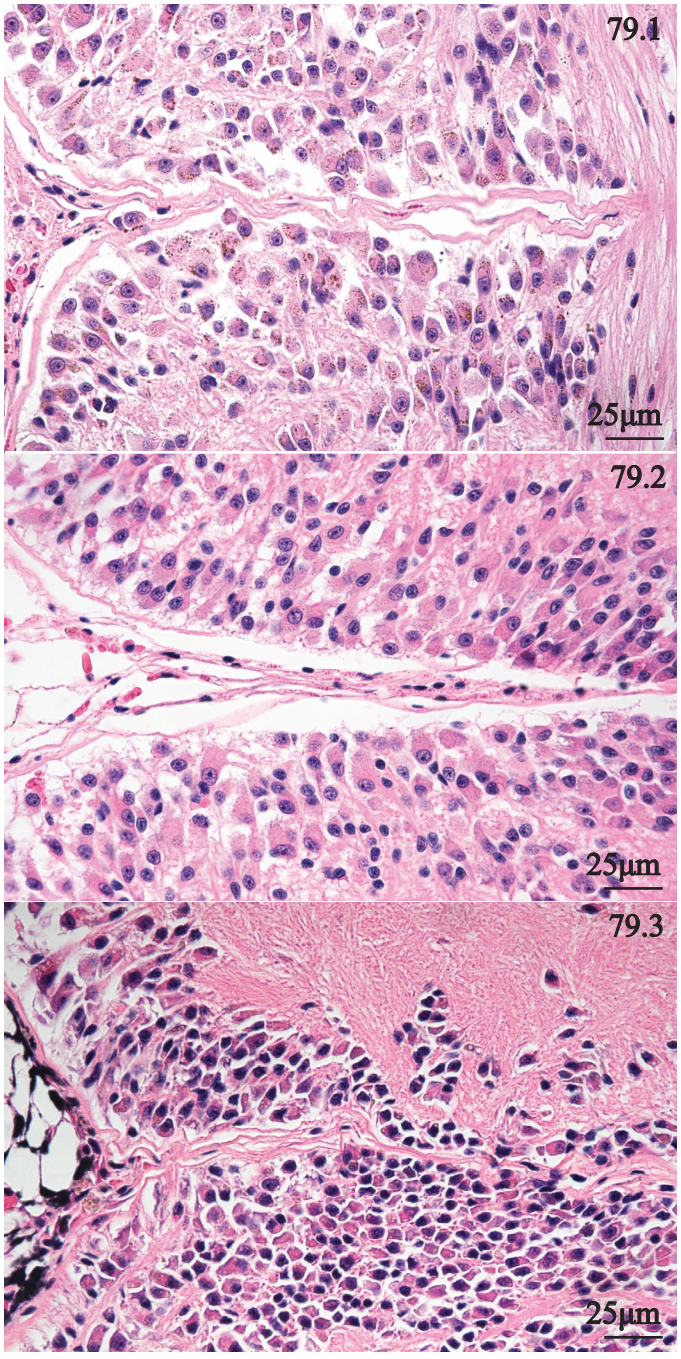
79.1
25µm
79.2
25µm
79.3
25µm

PLATE 80. Mature ovarian acinus of *Villosa nebulosa*, *Fusconaia cerina*, and *Strophitus connasaugaensis.* 1. Mature ovarian acinus of *Villosa nebulosa*. 2. Mature ovarian acinus of *Fusconaia cerina*. 3. Mature ovarian acini of *Strophitus connasaugaensis*.

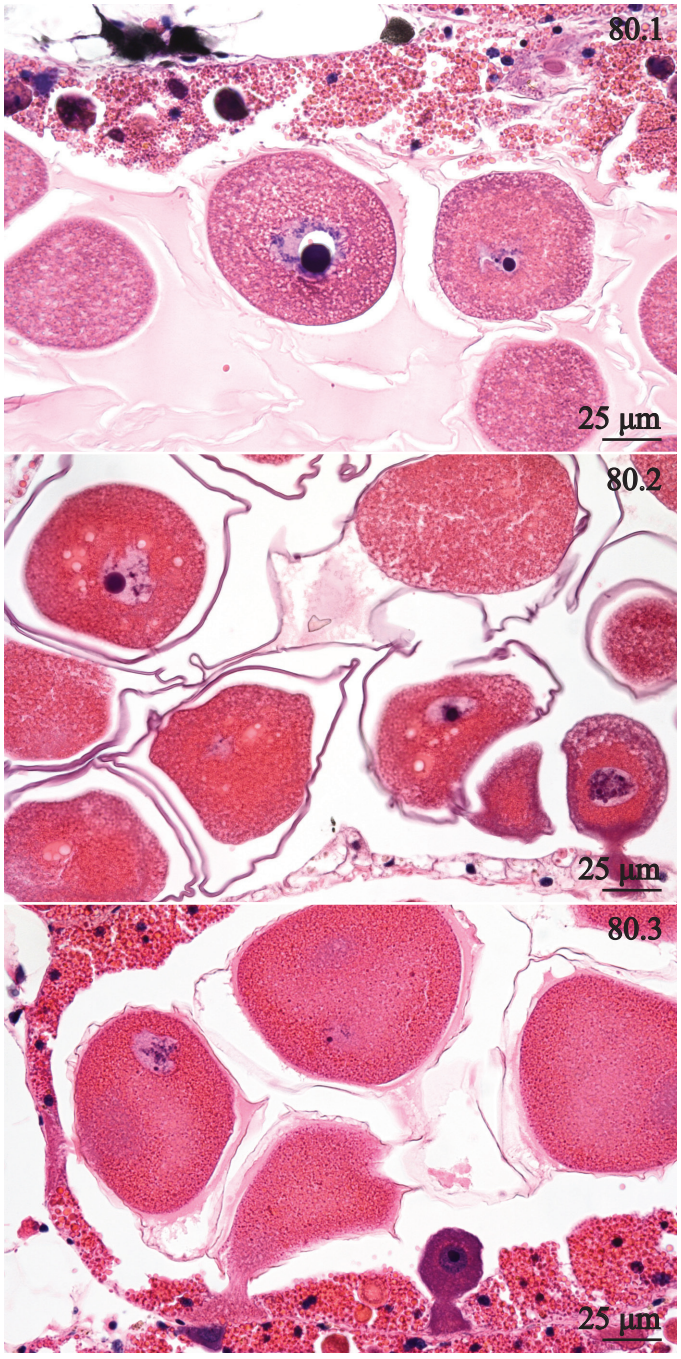
80.1
25 µm
80.2
25 µm
80.3
25 µm

Chapter 8

CONCLUSION AND DISCUSSION OF FUNCTIONAL MORPHOLOGY OF TISSUES OF THE ALABAMA RAINBOW (*Villosa nebulosa*), GULF PIGTOE (*Fusconaia cerina*), AND ALABAMA CREEKMUSSEL (*Strophitus connasaugaensis*)

8.1. Conclusion

Based upon a limited range of histological differences between *Villosa nebulosa*, *Fusconaia cerina,* and *Strophitus connsauagaensis*, I accept the null hypothesis that there are few interspecific differences in the structure of "soft tissues." Considering the highly conserved nature of unionid tissues across species and subfamilies, the use of specific tissues as biomarkers of mussel health and/or stream health are of potential value to state and federal monitoring agencies regardless of the mussel species targeted for study. Workers interested in monitoring mussel health or stream health by studying unionid tissues for histopathological changes that could possibly correspond to infectious agents or contaminants should focus on structurally conserved tissues (Table 5). Workers should not study tissues that exhibit interspecific variation because their observations are less comparable (Table 5).

During the development of this dissertation, I have used histology atlases or synoptical anatomical references regarding marine bivalves to gain familiarity with bivalve anatomy, and physiology (Galtsoff, 1964, Norton and Jones, 1992, Eble 2001, Grizel, 2003). The work in this dissertation is different from marine bivalve atlases considering that a consistent series of high resolution, low magnification, and high magnification images were presented, and tissues were described in detail. The above references on marine bivalves are comprehensive in terms of the organ systems considered. However, the images or illustrations presented typically portray large anatomical structures such as the mantle edge at a low magnification (Galtsoff, 1964, Norton and Jones, 1992, Eble, 2001). Low magnification images or illustrations have utility towards describing overall tissue morphology, but limit ones' understanding of the functional attributes of specific cell types. The histology atlas edited by Grizel (2003), differs from this dissertation, and the works of Galtsoff (1964), Norton and Jones (1992), and Eble (2001) in that bivalve

tissues are described mainly with transmission electron microscopy, and special stains for light microscopy to reveal the presence of specific enzymes. Although many details can be observed from the micrographs, the descriptive information regarding each tissue or cell type is limited to the corresponding figure captions, and each chapter has a short overview of the anatomy and physiology of each organ system. Furthermore, considering that the atlas of Grizel (2003) projects the image that the altas is a comparison between clams, mussels, oysters, and scallops, not all chapters focus on comparative anatomy, and the comparative chapters provide limited information regarding functional differences between each species.

There are also several species descriptions of freshwater mussels based on the morphology of "soft tissues" (Pain and Woodward, 1968, Fuller, 1973, Heard and Dougherty, 1980, Smith, 1888, Mansur and da Silva, 1990, Avelar and Cunha, 2009). However, the resolution of anatomical details reported has been low. Some simply portray the visceral mass, gills, and mantle in a lateral view, to show the positions of the foot, inner and outer gills, labial palps, siphon, and adductors (Pain and Woodward, 1968, Fuller, 1974, Heard and Dougherty, 1980, Mansur and da Silva, 1990). In regard to cellular structure of tissues, the focus is placed on selected tissues such as gill, mantle, stomach or ganglia, but limited information is provided regarding the identity, and orientation of specific cell types, and their staining characteristics, such that we could understand tissue function (Heard and Dougherty, 1980, Smith, 1988, Mansur and da Silva, 1990, Avelar and Cunha, 2009).

Furthermore, there are three contributions by A. E. Ortmann that are pertinent to this dissertation, as the titles of these articles may suggest that the anatomy of representative species of Anodontinae, Unioninae, and Lampsilinae, from Alabama, have been described (Ortmann, 1923a, 1923b, 1924). However, Ortmann emphasized morphological features of the shell such

as coloration, geometry and sculpture. Descriptions of "soft tissues" were limited to the position, coloration, and shape of the labial palps, gill, and siphon papillae. Therefore, Ortmann's descriptions are useful for field identification purposes.

The histological descriptions of unionid tissues presented herein may be useful to a variety of user groups. Two recent phylogenetic analyses have provided evidence that Unionidae contains diverging lineages (Campbell and Lydeard 2012a, 2012b). The histological descriptions presented in this disseration suggest that although unionids appear to be diverging, many of their tissues have changed very little over the course of millions of years. The propagation and release of hatchery-reared mussels is seen as a necessary conservation strategy to maintain populations of stream-dwelling mussels. Hatchery personell could use a histology atlas to monitor the health status of wild, cultured, and released mussels. The atlas would represent a point of comparison for each tissue type and could allow people to methodically address questions about how hatchery-reared and wild mussels are different. Freshwater mussels have utility as biological indicators of toxic releases, and cellular changes to specific tissues such as digestive diverticulum, and gonad, have been described from other bivalves as biomarkers of contamination (Cajaraville et al., 1990, Lehmann et al., 2007). Possibly the digestive ducts and gonad have been evaluated for their potential as histopathological biomarkers because they are soft, and easy to section, and because they are widely distributed throughout the body making them easy to locate. There is an information gap concerning what tissues would give the most information following a toxic release, whether there are specific lesions that characterize different types of contaminants (e.g., metals, and organic compounds), and potential chronic health problems associated with long term contact with low levels of toxins that could be linked to declines in unionid populations (Salazar and Salazar, 2007). Given the limited

histopathological information regarding metazoan parasite infections, aquatic animal health specialists may seek an understanding of how infectious agents such as metazoan parasites interact with mussel hosts. Specifically, they may wish to know during circumstances in which a parasite invades more than one type of tissue (Haobin et al. 2008), if the cells of each infeciton site respond to injury in the same way. Another potential question could be, do metazoan parasites that have the ability to invade tissues of same molluscan host more than once during its lifecycle (Mitchell, 1965, Taskinen et al., 1997) ever illicit a host response? I also feel that there are basic research questions regarding tissue function that could be addressed following the study of histological images of unionid tissues presented in this dissertation. For example, Smith (2000) suggested that anodontines may lack a byssal gland during the juveniles phase of their lifecycle because they typically colonize "low energy" environments. The presence of a byssal gland in adult *V. nebulosa*, *F. cerina*, and *S. connasaugaensis* may be an indication that byssal glands are a necessary adaptation in many other unionid species.

8.2. Mantle

The mantle edge secretes precursory shell material that later hardens. The following is a summary of the events that have been proposed for shell formation. The outer mantle lobe secretes a gelatinous, protein-based ribbon called periostracum. The periostracum ribbon is secreted from a crevice between the outer and middle mantle lobes called the periostracal groove (Figs. 2.2, 23.2, 46.2). The ribbon extends distally towards the mantle cavity, and wraps around the ventral surface of the outer lobe. As periostracum extends from the groove, columnar cells located between the periostracal groove and the tips of the outer and middle lobes secrete filamentous substances (possibly proteins) that become incorporated into the extending ribbon (Petit et al., 1978, 1979). As the periostracum ribbon wraps around the outer lobe it bends

multiple times and begins to receive calcium-based crystals from the columnar epithelium located along the ventral surface of the outer mantle lobe (Petit et al., 1979). Although a mechanism for shell formation has been proposed for Unionidae, it is important to note that shell formation has been studied from a limited range of species. Additionally, the above-mentioned studies of cellular structure of the mantle edge have employed different methods to understand various aspects of shell formation. Members of Unionidae are known for exhibiting a high degree of interspecific variation in shell geometry, height, thickness, and sculpture (knobs, ridges or projections on the exterior surface) (Williams et al., 2008). From a sample of histological literature on mantle lobes of bivavles there is variation in the shape of the lobes, number plicae present, and size of plicae across different orders (see Morton, 1987, Morrison, 1993, Eble, 2001, Colville and Lim, 2003). It seems likely that mantle lobe morphology is related to structural differences in bivalve shells, but this topic needs attention.

Morphological differences in the outer mantle lobe of *Villosa nebulosa*, *Fusconaia cerina*, and *Strophitus connasauagaensis* may explain differences in shell thickness. *Villosa nebulosa* and *S. connasaugaensis* have an ovular shell of a moderate thickness and height (Figs. 1.1-1.4, 45.1-45.4). In contrast, the shell of *F. cerina* is circular to rhomboidal, considerably thicker and higher than the shells of *V. nebulosa* and *S. connasaugaensis* (Figs. 22.1–22.4, Williams et al., 2008). The outer mantle lobe of *F. cerina* is branched and pleated, and the epithelium features numerous basophilic cells (Figs. 23.1–2.3.3). Since basophilic cells occupy a region of such a high surface area, the entire lobe may exhibit a high-level of protein production. In contrast, *V. nebulosa* and *S. connasaugaensis* both have a uniramous outer mantle lobe, and the epithelium features fewer plicae (Figs. 2.1, 2.3, 46.1–46.3). Furthermore, plicae along the surface of the outer mantle lobe of these two species were, shorter. Additionally, the columnar cells around the

outer lobe of *F. cerina* appear to be taller than outer lobe cells of *V. nebulosa* and *S. connasaugaensis* (Figs. 23.2, 23.3, 2.2, 2.3, 46.2, 46.3). Considering the above, *F. cerina* may have a greater capacity to produce precursory shell material than either *V. nebulosa* or *S. connasaugaensis* and this ability might explain why *F. cerina* has a thicker shell.

Electron microscopy of the outer, and middle mantle lobes of *Amblema plicata* indicated additional substrate is added to the periostracum as it travels down the length of the mantle lobes (Petit et al. 1978). Although no secretions were observed between the outer and middle lobes of *V. nebulosa*, *F. cerina*, and *S. connasaugaensis*, the basophilic epithelium of the outer lobe may secrete additional substrate into the periostracum ribbon. The basophilic columnar epithelium located on the ventral surface of the outer mantle lobe is likely the site of nacre production (Figs. 2.1, 2.7, 23.1, 23.7, 46.1, 46.7).

An additional consideration for shell formation should be mantle lobe musculature. The mantle edge is rich is somatic musculature and myofibers extend into the mantle lobes. A recent theory regarding the formation of sculpture patterns on the shells of marine bivalves suggests muscle contractions may cause periostracum to build up unevenly. Extension, retraction, and lateral movements of the mantle edge can cause periostracum to accumulate in such a way as to form shell ribs (Checa, 2002). The outer mantle lobe of *F. cerina* is branched and the flexure of one or more of these branches may allow periostracum to thicken.

It is unclear what the role of the triangular and pleated inner mantle lobe is. It seems the inner lobe can extend and retract given its highly muscular composition (Fig. 2.1, 2.5, 23.1, 23.5, 46.1, 46.5). Possibly the inner mantle lobe plays a role in initial settlement of juveniles considering the highly pleated surface and basophilic, subepithelial cells. Perhaps the mantle is glandular during the juvenile stage and produces an anchoring substance similar to a byssus.

Pediveligers of *Ostrea edulis* have a glandular integument that secretes a cement to allow settlement (Cranfield, 1973a, 1973b). Irregular, basophilic cells with a granular cytoplasm were located in the subepithelial tissue of the middle lobe and inner lobe of *V. nebulosa*, *F. cerina*, and *S. connasauagaensis*. Such cells were also located in the subepithelium of the foot (see below). Possibly, these cells produce an adhesive substance that is needed for attachment to substrate, but ducts leading from the cell body to the apical surface of the mantle lobe epithelium were not observed. Therefore, if the basophilic cells may be connected to ducts during an earlier life history stage. Beedham (1958) refers to the inner mantle lobe as the "sensory lobe," possibly because the inner lobe of scallops (*Pecten* spp.) is manifested as a series of tentacles that have a sensory function. However, axons observed in the lateral aspect of the mantle edge were not observed in the inner mantle lobe of *V. nebulosa*, *F. cerina* and *S. connasaugaensis* (e.g., Fig. 47.2). Furthermore, sensory cells such as ciliated olfactory receptors were not observed in histological sections of the inner lobe.

The base of the mantle edge between the pallial line and mantle lobes consists of adipose tissue and musculature. Adipocytes were observed in the subepithelial tissue of the base of the mantle edge (Figs. 2.6, 2.7, 23.1, 23.7, 46.1), and in the middle mantle and have been referred to as vesicular cells or Leydig cells. Leydig cells are located throughout the visceral mass and they may represent a source of energy in the form of glycogen (Colville and Lim, 2003). The dorsal surface of the mantle edge between the pallial line and the inner mantle lobe consists of a region of glandular plicae (Figs. 2.6, 23.6, 46.6). It is not certain what the true function of these structures is, but it seems likely that the plicae are associated with water currents that run parallel with the mantle cavity. The half-shell photographs of the mantle cavity of *V. nebulosa*, *F. cerina*, and *S. connasaugaensis* show that the mantle edge lines up with the incurrent siphon (Figs. 1.6-

1.8, 22.6-22.8, 45.6-45.8). Therefore, the plicae may be associated with water currents entering the mantle cavity, and the mucus produced by the extensive network of goblet cells may bind particles suspended in local water currents, and allow them to be collected by cilia along the gill filaments.

Papilliae around the siphons were sectioned from *V. nebulosa*, *F. cerina*, and *S. connasaugaensis* with the intent of revealing sensory receptor cells and associated nerves. While divisions of the pallial nerve extended from the base of the mantle edge to the main axis of each papilla, sensory neurons were not observed on epithelium surrounding each papilla (Figs. 3.2, 3.3, 24.2, 24.3, 47.2). Sensory receptor neurons have been described from mantle tentacles of *Lima hians* (Owen and McCrae, 1979) and from siphon papillae of *Tellina lineata* and *Macoma biota* (Vitonis et al., 2012). Owen and McCrae (1979) reported that there are three types of sensory receptors, two multi-ciliated receptors, and a third receptor featuring a single kinocilium surrounded by stereocilia. Ciliated receptors consist of types A, and B. Type A receptors consist of a dense tuft of 35-40 cilia distributed across 4-6 cells. Type B receptors have 17-20 cilia on the apical surface of one cell. Based on transmission, and scanning electron microscopy the authors were not able to determine whether the ciliated receptors respond to chemical or mechanical stimuli (Owen and McCrae, 1979). Vitonis et al. (2012) estimated that siphon papillae may contain as many as 10/100 μm^2 ciliated receptors while the epithelium facing the lumen has more sparsely distributed receptors (20/10,000 μm^2). Furthermore papillae and lumen epithelia have different types of ciliated receptors based on cilia density and cilium height. However, the status of ciliated receptors as either chemosensory or mech

Females of *Villosa* have a papillose mantle edge that functions as a lure to attract potential host fishes (Fig. 1.7, Haag et al., 1999, Williams et al. 2008). Species of *Lampsilis* and *Villosa*

are members of Lampsilinae according to Ortmann (1910) and like *Villosa* spp., *Lampsilis* spp. have modified mantle flaps to attract host fishes (Haag and Warren, 1999, Haag et al., 1999, Williams et al., 2008). Kraemer (1967) observed a ganglion in the mantle edge of *L. ventricosa* and proposed that it may regulate mantle flap movements. However, no ganglia were observed in the mantle edge of gravid female *V. nebulosa*.

The middle mantle is a thin, delicate skin-like tissue and serves to exchange blood between the mantle edge and viscera (Figs. 3.4, 24.4, 47.4). Illustrations of the mantle cavity of freshwater mussels suggest that there are a series of anterior to posterior currents along the surface of the middle mantle (Kellog, 1915). Petit et al. (1978) observed ciliated cells along the inner surface of the middle mantle of *Amblema plicata perplicata*. Herein the presence of ciliated cells along the inner mantle surface can be confirmed from *V. nebulosa*, *F. cerina*, and *S. connasaugaensis*.

The darkened, basophilic columnar cells located at the dorsal margin of the isthmus may secrete periostracum (Figs. 3.5, 3.6, 24.5, 47.5). The ligament is composed of periostracum and represents a combined product from secretions of the isthmus and dorsal aspect of the mantle edge; mantle lobes produce the outer layer of the ligament while the inner layer is secreted by the isthmus (Beedham, 1958). Petit et al. (1978) observed thread-like secretions uniting the isthmus and ligament, and Beedham (1958) reported similar staining characteristics between columnar cells of the isthmus and outer mantle lobe.

8.3. Gill

8.3.1. Non-marsupial gill

Gill structure of *V. nebulosa*, *F. cerina* and *S. connasaugaensis* is similar to what has been reported previously on unionids. There was no apparent difference in the structure of gill

filaments between each species studied hererin (Figs. 4.1-4.4, 48.1-48.4, 25.1-25.4). Galbraith et al. (2009) reported marginally significant differences in the density of cirral plates between four unionid species and intraspecific and interspecific variation in the number of cilia per cirrus. Considering the observations of Galbraith et al. (2009) were derived from SEM preparations of ctenidia, there may be differences in cirral plates and density of cilia between *V. nebulosa*, *F. cerina*, and *S. connasaugaensis* at the ultrastructure level.

The fascicles located at the base of the gill possibly represent supporting structures that allow attachment of gill filaments to abdominal connective tissue. Alternatively, the fascicles may represent musculature that allows movement of the entire gill (Figs. 4.6, 4.7, 25.6, 25.7, 48.6). Longitudinal and transverse muscle groups in gill described may control water circulation by altering the diameter of osti and water tubes. However, the description of musculature was based on myofibers that are incorporated into the water tubes (Gardiner et al., 1991). Given the above, it is uncertain whether transverse musculature located at the base of the gill would play a role in water circulation or if muscular contractions generated by this tissue would facilitate the transport of ova into marsupia.

8.3.2. Marsupial gill

Marsupial structure is a reflection of brooding and dispersal strategy. Members of Lampsilinae, such as *Villosa nebulosa*, brood using the posterior portion of the outer gill. A marsupium of *V. nebulosa* is grossly enlarged region of water tubes that becomes distended when filled with glochidia (Ortmann, 1911a). The walls of the water tubes are strengthened with connective tissue fibers to maintain a strong connection between the outer and inner faces of a marsupium as it expands to accomodate ova. The increasing diameter of the water tubes from dorsal to ventral may be reflective of the mechanism of glochidial release (Fig. 5.1). Glochidia

are released from the ventral margin of a marsupium following the appropriate stimulus from a potential host fish (Fig. 5.2). Host fishes may approach a displaying mussel and bite or come into direct contact with flapping mantle tissue. Following a fish strike, a mussel may rapidly expel the contents of one or both marsupia (Haag et al., 1999).

The interbranchial septa and vertical water tube walls of the marsupia of *V. nebulosa* were lined with ciliated columnar cells (Fig. 5.4). Cilia may occur on the septa or along the walls of water tubes of non-marsupial gills of male and female *V. nebulosa*, *F. cerina*, or S. *connasauagaensis*, but appeared to be located in isolated tufts near the ostia (4.2, 25.2, 48.2). However, water currents through the vertical water tubes of unionid gills may be regulated by the mucular contractions of horizontal and vertical muscle fibers (Gardiner et al., 1991). The function of cilia within the marsupial chambers of *V. nebulosa* could serve to exchange oxygen rich and oxygen poor water currents (Figs. 5.4, 5.5), although Richard et al. (1991) indicated that water does not enter the marsupial chamber of anodontines or lampsilines. Perhaps the cilia deliver or disperse nutrients to glochidia (Schwartz and Dimock, 2001).

Glochidia contained within the marsupial water tubes were loosely organized within the lumen. Histological sections of the ventral margin of filled marsupia revealed the presence of a wispy, fibrous material possibly representing a sac that surrounds the entire mass of glochidia (Fig. 5.2). However, the contents of the gill of *V. nebulosa* were delicate and the glochidia and embryos observed in the lumen of the water tube were often fragmented or displayed separation artifacts making it difficult to study a membrane surrounding the mass of glochidia. Mature glochidia were mixed with early stage embryos judging by the presence of spherical clusters of undifferentiated cells (Fig. 5.6). Considering these observations were made from mussels collected in May and that spawning occurrs during the late summer, these observations may

indicate that not all fertilized ova mature into glochidia. Furthermore, there may be a limit to the total number of glochidia that could form from a set of fertilized ova. Glochidia of *V. nebulosa* have discoid valves that lack hooks along the ventral margin. Hookless glochidia are typically gill parasites that attach to the delicate gill lamellae of fishes. Based on laboratory infections, *Villosa nebulosa* is considered to be host specific and transform on species of *Micropterus* (Neves et al., 1985).

Species of *Fusconaia* incubate their larvae using all four gills and are therefore reffered to as tetragenous brooders (Fuller, 1973). The marsupia of *F. cerina* are uniformly thickened dorsal to ventral, and virtually the entire gill becomes incorporated with glochidia. Like the marsupial gill of *V. nebulosa*, the water tubes are strengthened with fibrous tissue. Hookless glochidia of *Fusconaia* spp. are packaged into cylindrical masses called conglutinates (Fuller, 1973, Bruenderman and Neves, 1993, Haag and Warren, 2003). A single, mature conglutinate consists of layers of ova and each layer contains a linear arrangement of peach-colored glochidia, attached to red, unfertilized ova (Figs. 26.1, 26.3). Glochidia mature in a conglutinate while attached to unfertilized ova, and together, glochidia and unfertilized ova are released dorsally, through the suprabranchial cavity, as masses of conglutinates. Exactly how glochidia of *Fusconaia* spp. are transferred to a host fish is unknown, but possibly mature conglutinates, when released from a female mussel, are perceived as aquatic insect larvae and a fish strike may separate some glochidia from a conglutinate and attach to gill tissue of a potential host (Bruenderman and Neves, 1993, Haag and Warren, 2003). This seems plausible given that conglutinates consist of spherical bodies arranged into a cylindrical unit and appear segmented like insect larvae (see DeWalt et al., 2010). Observations of released conglutinates of *F. cerina* indicated that conglutinates are buoyant and cyprinids will closely approach (Haag and Warren,

2003). Laboratory infections have indicated that members of Cyprinidae may be suitable hosts for species of *Fusconaia* (Bruenderman and Neves, 1993, Haag and Warren, 2003)

The structural features of the marsupia of *Strophitus connasaugaensis* generally resembled marsupia of *F. cerina* (Figs. 26.1, 49.1). *Strophitus connasaugaensis* brood using the outer gills and masses of glochidia may be contained within the entire gill. Species of *Strophitus* are generally believed to disperse glochidia within a matrix of mucus (Ortmann, 1911, Lefevre and Curtis, 1912, Haag and Warren, 1995, Hove, 1995, Watters 2002). *Strophitus undulatus* may produce a gelatinous and cylindrical conglutinate (Ortmann, 1911, Lefevre and Curtis, 1912, Watters, 2002). Haag and Warren (1997) reported that glochidia of *S. subvexus* may be released within a copious mucus matrix that may indiscriminately entangle fish, however no specific details regarding the exact nature of the mucus was described. Furthermore, it may be implied from Haag and Warren (1997) that the mucus matrix of *S. subvexus* conglutinates resembles a web of fibers similar to conglutinate of *Anodonta cygnea* and *Anodontoides ferussacianus*. Herein, I observed a placenta-like sac containing glochidia in gills of *S. connasaugaensis* (Fig. 49.1) and the core of placenta tissue appears to contact following the release of glochidia (Fig. 49.6). This cylindircal mass may represent a mold for the formation of a mucoid conglutinate similar to conglutinates described by Watters (2002). The interbranchial septa of the marsupium of S. connasaugaensis are distinctively basophilic and the spherical cells containing wispy cytoplasmic figures may be responsible for the formation of a gel (Fig. 49.3). According to Watters (2002) the glochidia larva may be attached to the exterior of the conglutinate following its release into stream water and that osmotic pressure may drive internalized glochidia out of this gelatinous rod. Glochidia may become anchored to the exterior of the conglutinate by means of a filament extending from interior of the valves. Following the release of conglutinates from

the gill, the opening and closing of glochidial valves may cause the whole conglutinate to move in a worm-like fashion and mimic a prey item of a host fish (Watters, 2002). Based on photographs of released conglutinates of *S. undulatus* it is possible that a fish might perceive conglutinates to be a worm (Barnhart, 2008). Glochidia of *Strophitus* spp. have hooks (Fig. 49.5), can attach to skin, and have proven to be host generalists capable of transforming off a phylogenetically broad spectrum of fish species in a laboratory setting (Watters, 2002). Glochidia of *Strophitus undulatus* may transform on fish gill in a laboratory setting (Hove et al., 1997), but it is not certain where they typically attach in the wild. Interestingly, Lefevre and Curtis (1912) reported that some *S. edentulous* larvae passed the glochdium stage while remaining within the mucoid concluginate since a small-number of newly transformed juveniles were observed by a student worker and these juveniles clearly exhibited a protrusible foot. Considering the above-mentioned adaptations for parasitism, the possibility that glochidia would forego the parasitic stage of their lifecycle and transform within the water tubes of its parent seems remote.

The conglutinates observed in gills of *S. connasaugaensis* resembled a placenta with inner and outer walls of squamous epithelial cells, and a subepithelium consisting of loose connective tissue and hemolymph (Fig. 49.1). Moreover, the placenta resembled a derivation of tissue from the interbranchial septum and water tube walls (Figs. 49.1, 49.6). Histological sections of the placenta revealed a loosely organized group of spinous glochidia, but it was indeterminant as to whether there was a gelatinous rod surrounding the glochidia and located within the placenta. However, the abundant, basophilic goblet cells along the dorsal and ventral surfaces of gill septa of *S. connasaugaensis* may secret mucus into the lumen of the water tube and create a gelatinous rod prior to the release of a conglutinate (Fig. 49.3).

The possibility that glochidia receive nutrients by means of a placenta-like connection to the surrounding gill tissue has been suggested in Schwartz and Dimock (2001). Herein, I have only observed a placenta-like structure in the marsupial gills of *S. connasaugaensis*. Conglutinates of *F. cerina* did not appear to be attached to the vertical walls of the water tube. Embryos and glochidia of *V. nebulosa* appeared to be enclosed within a sac, but the separation artifacts made it difficult to determine whether such a sac was united with the surrounding gill tissue. However, gill tissue was sectioned in a transverse orientation and if the conglutinates of *F. cerina* or the sac encasing glochidia were attached to interbranchial septa, it may not be apparent from this orientation. Possibly, coronal sections through marsupia could provide insight into whether there is a connection between glochidia and gill tissue. Although no physical attachment of glochidia to gill tissue was observed, the abundance of goblet cells on the interbranchial setpa of *F. cerina*, and *S. connasaugaensis* could support the hypothesis that gill tissue somehow delivers nutrients to developing glochidia. Perhaps these cells secrete sugars derived from glycogen deposites in the septa.

8.4. Foot

The foot of *V. nebulosa*, *F. cerina* and *S. connasauagaensis* consisted of dense, regular chords of muscle fibers that become irregular within the ventral tip (Figs. 6.1, 6.3, 6.4, 27.1, 27.3, 27.4, 50.1, 50.3, 50.4). Pedal musculature forms a median, triangular cavity that is likely filled with hemolymph regulated by blood vessels (Brand, 1972). Freshwater mussels burrow into sediment with the muscular foot, and the foot is a hydrostatic organ capable of great distension. For example, Trueman (1968) revealed that the foot of *Margaritifera margaritifera* can be flattened, and blade-like, and later expand ventrally and laterally, exhibiting a distended, spherical shape. The work of Brand (1972) indicated that distension of the foot is achieved by

the rapid filling of pedal hemolymph sinuses with blood. The irregular array of myofibers in the ventral tip of the foot may enable movement in many directions, and possibly maintains tensile strength when the foot is enlarged.

The pedal epithelium of *V. nebulosa*, *F. cerina*, and *S. connasaugaensis* is rugose with deep, irregular crypts along the surface of the integument around the ventral portion of the foot (types 1-3 epithelium). Considering that the foot may be used as an anchor, it seems that the high surface area created by the folded epithelium surrounding the foot would create a strong frictional force and allow a burrowing bivalve to remain embedded (Figs. 6.1, 27.1, 50.1). The plethora of mucus cells within pedal epithelium may create a lubricant that would minimise cutaneous damage from abrasion when the foot is inserted into fine sand. Based on histological sections of the three-unionid species, it seems that the grooves around the foot were deeper on *F. cerina* (Figs. 28.1, 28.2) than on *V. nebulosa* or *S. connasaugaensis* (7.1, 7.2, 51.1, 51.2). This observation could be an indication of an adaptation that mussels in large rivers, such as the Cahaba River, may have to keep themselves firmly embedded in substrate to prevent themselves from being dislodged by strong water currents. Likewise, plicae around the foot of *V. nebulosa* and *S. connasaugaensis* were shorter, and the small size of plicae may reflect adaptation to headwater streams, such as Terrapin Creek and Shoal Creek, where a smaller channel size would accomodate less water volume than a larger river such as the Cahaba. Since the historic ranges of *V. nebulosa*, *F. cerina*, and *S. connasaugaensis* may have overlapped (Williams et al., 2008), these observations could represent local adaptations.

The ventral-most region of the foot was a highly ciliated surface. Cilia may be present further down the vertical length of the foot and visceral mass, but ciliated cells were indistinct in epithelial regions 2-5. Juvenile uninoids have minute gill buds and may employ pedal feeding

during the weeks following transformation from the glochidium stage (Lasee, 1991, Yeager et al., 1994). During pedal feeding, particulate matter may be collected by a combination of foot scraping and ciliary action. Scanning electron microscopy of the foot of juvenile unionids has revealed a densely ciliated pedal surface (Lasee, 1991, Araujo et al., 2002, Lima et al., 2006).

Basophilic granulocytes were distributed within the subepithelium underlying pedal epithelium types one and two (Figs. 6.1, 7.1, 7.3, 27.1, 28.1, 28.2, 50.1, 51.1, 51.2). The function of the granulocytes is unclear, possibly granulocytes are pigment cells associated with the orange coloration of foot and mantle edge of *V. nebulosa* and *S. connasaugaensis*. However, male and female *F. cerina* are somewhat pallid and females develop a temporary red to orange pigmentation when gravid (Fig. 22.6, Bruenderman and Neves, 1993). *Fusconaia cerina* had a significantly high number of basophilic granulocytes such that histological sections of foot were conspicuously violet. Alternatively, granulocytes may produce mucus or an adhesive that may assist with settlement following the transition from glochidium to juvenile. Pediveligers of *Ostrea edulis* have exocrine cells that produce an adhesive to enables attachment to a hard substrate (Cranfield, 1973a, 1973b). However, granulocytes observed in *V. nebulosa*, *F. cerina*, and *S. connasaugaensis* do not have distinct ducts communicating with the surface of the epithelium. A possible explanation for this may be that adhesive cells are only functional during the juvenile stage and ducts atrophy with age since larger mussels burrow into sediment (Trueman 1966, 1968). Lefevre and Curtis (1912) reported that juvenile mussels crawl by extending the foot, attaching to a substrate, and pulling the body forward while the foot is fully extended. Matteson (1948) observed crawling juvenile *E. complanata* and reported that the foot appears to have an adhesive quality. If the basophilic granulocytes are part of a system of glands that secrete an adhesive substance on the surface of the foot, the preponderance of such cells in

the foot of *F. cerina* may represent an adaptation to resist strong water currents. Since, fewer granulocytes were observed in the foot of *V. nebulosa* and *S. connasaugaensis*, this may reflect adaptation to smaller headwater streams (i.e., Terrapin Creek, and Shoal Creek) that would hold a smaller volume of water and may therefore be more stable than a larger river such as the Cahaba.

8.5. Byssal gland

Juvenile unionids produce a single, translucent filament or byssus that allows small mussels to attach to a hard substrate (Kirtland, 1840, Lea, 1856, Smith, 2000). Spherical byssal glands were observed in adult *V. nebulosa*, *F. cerina*, and *S. connasaugaensis* and ciliated byssal canals were observed only in *V. nebulosa* and *F. cerina*. The histological structure of byssal glands and byssal canals observed herein indicate that the byssal gland becomes detached from the byssal canal with age and the byssal canal has largely disappeared in an adult. The histological differences in byssal gland cell types between *V. nebulosa*, *F. cerina*, and *S. connasauagaensis* may reflect variation in the composition of the byssus (Figs. 6.6, 27.6, 50.6), but such differences are presently indeterminate. Smith (2000) observed a series of ducts leading into the byssal gland of juvenile *Elliptio complanata*, and *Lampsilis radiata*. Such ducts were not observed in *V. nebulosa*, *F. cerina*, and *S. connasaugaensis* and the byssal gland of each species consisted of a spherical chamber with tightly associated columnar cells and a well-defined capsule of fibrous tissue. Therefore, it is uncertain whether byssal gland ducts are present in juveniles and there is a need to understand how a potentially non-glandular byssal gland and a more glandular byssal gland would functionally differ. For example, a glandular byssal gland may produce a stronger or larger filament extending from the foot. Smith (2000) proposed a hypothesis that unionids living in “low energy” environments lack a byssal gland while mussels in “high energy”

environments. Presently, this dissertation shows that a representative species from three unionid lineages has a byssal gland. Secondly, Terrapin Creek and Shoal Creek may constitute low energy environments in comparison to the Cahaba River for reasons stated previously. Considering *V. nebulosa* and *S. connasaugaensis* were collected in small streams, and *F. cerina* was collected in a larger river, the "low energy-high energy" hypothesis, in terms of byssal glands, may be rejected.

8.6. Adductors, pedal protractors, pedal retractors, and mesentery

Musculature of the foot, adductors, pedal retractor and mesentery fascicles all have similar cellular characteristics (e.g. Figs. 7.7, 7.8, 8.5, 8.6, 28.7, 28.8, 29.3, 29.6, 51.7, 51.8, 52.5, 52.6). Each type of fibrous tissue consists of long, filamentous cells with a dark, eosinophilic cytoplasm and a distinct, basophilic nucleus. Transverse sections through a whole mussel provide a longitudinal view of the adductors and pedal musculature. Based on longitudinal views of adductor and pedal musculature, subtle variation in cell structure is evident. Adductors consist of long myofilaments with a compressed, elliptical nucleus while pedal muscles appear to be thicker with a spherical to ovular nucleus (Fig. 8.6, 29.3, 52.6). Adductors control opening and closing of the shell, and may be less active than muscle fibers operating the foot. Pedal muscles are a combination of dorsal muscles encircling the viscera and pedal protractor and retractors (Figs. 8.6, 29.8, 52.6). Adductors, pedal protractors and retractors are somatic muscles and yet striations were not present in hematoxylin and eosin stained tissue sections. According to Morrison (1996) the adductor of *Crassostrea virginica* has translucent and opaque regions with the transluscent portion representing the majority of the tissue volume. Translucent muscle has a fast contractile ability and consists of elongated, ribbons of myofibers approximately 3-4 μm thick. Opaque muscle fibers are round, 10-20 μm in diameter with a slow contractile ability

(Morrison, 1996). However, the adductor muscles studied in this dissertation were sectioned in a longitudinal orientation and possible differences between opaque and translucent muscle were not addressed herein.

Mesentery fascicles were observed throughout the visceral mass of *V. nebulosa*, *F. cerina*, and *S. connasaugaensis*. These bands of fibrous tissue extend medially into the coelom from a layer of vertically oriented fibers along the inner surface of the coelom. The muscle fibers extending ventrally into the foot from the base of (Figs. 7.7, 7.8, 28.7, 28.8, 51.7, 51.8) the visceral mass have similar staining characteristics to the mesentery based on hematoxylin and eosin-stained tissue sections. Considering that the mesentery fibers extend across the coelom, it seems their function is to hold the sinistral and dextral portions of the coelom together. Alternatively, if the mesentery fibers stained positively for muscle proteins using Masson's trichrome tstain (Luna, 1968), possibly the fibrous bands could also served to circulate hemolymph in the coelom.

8.7. Digestive system

8.7.1. Labial palps and oral groove

The digestive system consists of the labial palps, oral groove, esophagus, digestive diverticulum, stomach, crystalline style sac and intestine. Particles gathering in the ventral food groove of the inner gill travel anteriorly by means of ciliary action. The palps are positioned close to the anterior curvature of the inner gill such that food groove particles may be dispelled and captured by the palps. Particulate matter that does not get captured by the palps may fall dorsally and may be transported posteriorly towards the excurrent siphonal aperture by means of cilia. Cilia located on the middle mantle, and lateral portion of the foot may facilitate the departure of rejected particles (Kellog, 1915). Palps are muscular, endowed with large

hemolymph sinuses and connective tissue, which suggests that each lip is contractile and pliable (Figs., 8.1, 29.1, 52.1). Particles captured by the palps may travel anteriorly, perpendicular to the length of the plicae, become incorporated into a mucoid mass traveling to the esophagus (Kellog, 1915). No cellular differences in the cellular structure of labial palps were observed between *V. nebulosa*, *F. cerina*, and *S. connasauagaensis.* However, based on the scanning electron microscopy observations of unionid gills by Galbraith et al. (2009), it seems that there could be interspecific differences in the density of these bristle-like structures. Also, considering the observations of ciliated sensory receptors on mantle tentacles (Owen and McCrae, 1979), and on siphons (Vitonis et al., 2012), there may be ciliated, sensory receptors on the free distal tips of the palps. Given that there are different types of ciliated receptors, the density of receptors, and their specific morphological features (e.g., number of cilia, height of cilia) may provide insights into particle selection at the labial palps. Presently, sensory receptors were not observed on the palps, but perhaps they would be located more readily with scanning electron microscopy and I would expect that there are sensory receptors located at the free distal margin of the palps, and along the surface of the inner palp epithelium, and that sensory receptors would be absent along the outer surface of each palp since the functional component of the labial palps comprises the ridges and troughs of the inner epithelium.

The oral groove represents a continuation of the labial palps and transfers ingested particles to the esophagus. Variation in the size of the oral groove may be reflective of differences in the quantity of matter ingested by each species. The oral groove of *F. cerina* and *S. connasaugaensis* resembled a cavity (Figs. 30.1–30.3, 53.1–53.3) while oral groove of *V. nebulosa* was a more narrow tube (Figs. 9.1–9.3). Seemingly a broad cavity would

accommodate a larger volume of particulate matter than the narrower, tubular oral groove of *V. nebulosa*.

The esophagus connects the oral groove with the digestive diverticulum (Figs. 9.4, 30.5, 53.4). The esophageal lining consists of conical plicae bearing ciliated columnar cells, and the deep grooves between the plicae may allow separation of small and large-sized particles (Yokley, 1968). Given the abundant ciliated cells, and concentric layers of connective tissue surrounding the lumen, it seems that ingested matter is delivered into digestive diverticulum by means of ciliary action, and not peristalsis (e.g., Figs. 9.5, 53.5).

The shape of the oral groove was similar between *S. connasaugaensis*, and *F. cerina*. Additionally, the morphology of the lumen of the digestive diverticulum at the point of merger with the esophagus was similar between *S. connasaugaensis* and *F. cerina*. Such features are suggestive of a closer phylogenetic relationship to each other than to *V. nebulosa*. Additionally, the large oral groove and digestive gland entrace featured by both species possibly indicates that a larger quantity of particulate matter enters the digestive gland than in *V. nebulosa*. An alternative hypothesis could be that the rate at which particles move between the labial palps and the anterior portion of the digestive gland are different. If this hypothesis is correct, perhaps the expansive oral groove chamber, and the anterior digestive gland chamber would cause particles to "bounce" around, and not move efficiently within a more well-defined tube. Observations of flourescent dye-labeled particles traveling across the gill filaments of *Mytilus edulis* and *Arca zebra* for example, suggests that ciliary action may not cause particles to move within a perfectly vertical or horizontal, linear direction (Ward et al., 1998).

8.7.2. Digestive diverticulum

Digestive diverticulum is a large network of blind-ended tubules and constitutes one of the largest organs in a freshwater mussel. The openings of digestive tubules were mainly located between the esophagus and anterio-dorsal stomach chamber (Figs. 9.4, 54.1, 30.5). A smaller subset of tubules communicated with the snistral and dextral portions of the posterio-ventral stomach chamber. Together, there was no obvious histological difference between the anterior digestive diverticulum tubules and both the sinistral and dextral tubules leading into the posterio-ventral stomach chamber. Therefore, it would seem that each region of the digestive diverticulum is functionally identical. However, it is not clear why there is a separation of anterior and posterior digestive gland ducts. Seemingly these ducts take in particulate matter that escapes passage into the initial series of digestive gland ducts. A possible explanation for this could be that the anterior portion of the digestive gland could be filled to capacity and an additional set of digestive ducts could handle excess food matter.

Based upon the tissue structure of *V. nebulosa*, *F. cerina*, and *S. connasaugaensis*, it seems that ciliated primary tubules carry ingested particles down the length of a tubule, but it is not clear whether ingested matter travels into the secondary and tertiary portions of each tubule since mussels were not fixed in the field and therefore, ingested matter that would normally be contained within the tubules was expelled. Some literature regarding ciliated digestive tubules suggests that cilia along the epithelial folds may create incurrent and excurrent pathways for particulate matter (Owen, 1955) but it is unclear whether cilia all around the lumen of primary tubules would create a synchronous ascending current, and then later generate a synchronous descending current following a chemical change in the lumen. In contrast, Owen (1955) also stated that the subepithelium surrounding the digestive tubules contained myofibers that would

create rhythmic contractions or peristalsis. Peristalsis seems unlikely considering the extensively developed ciliated epithelium and although fibrous tissue was observed in the subepithelium of digestive tubules of *V. nebulosa*, *F. cerina*, and *S. connasaugaensis*, it more closely resembled thin, wispy connective tissue. Secondary tubules feature copious cytoplasmic vesicles, microvilli, and the lumen may appear to be bubbling. Possibly secondary tubules produce mucus since tubule secretions were eosinophilic. Tertiary tubules constitute the longest and most conspicuous aspects of the organ. The conspicuously vesiculated cytoplasm and dark, basophilic nuclear regions may be an indication of enzyme synthesis. Based on the above observations it seems that particulate matter may be carried into the digestive diverticulum to be chemically broken down, and subsequently, ciliary action would transport broken down particulate matter posteriorly into the stomach. However, the digestive diverticulum literature presents competing hypotheses regarding possible functions of digestive tubules. Diverticulum cells may be absorptive considering observations India ink, iron, or carmine particles in cytoplasm of tubule cells following experimental feeding trials (Yonge, 1926b, Owen, 1955). Furthermore, wet mounts or frozen sections of digestive tubules of recently collected animals contain green or brown intracellular pigments while tubule cells appear colorless following a period of starvation (Mansour and Zaki, 1946). Alternatively, proteases, lipases, and enzymes capable of digesting carbohydrates have been isolated from digestive tubules of various marine bivalve species (Yonge, 1926b). Eble (1966) revealed the presence of acid phosphatase, alkaline phosphatases, and esterases on the apical surface of digestive tubules of *C. virginica* and reported that enzymes were most abundant during the summer and least abundant during the winter.

The long, finger-like plicae extending into the lumen of primary digestive gland tubules of *F. cerina* may be an indication that it feeds on algae or bacteria of a small size (Figs. 31.3, 31.4).

The larger lumen of the primary tubules of *V. nebulosa* and *S. connasaugaensis* could represent adaptations for feeding on larger-sized particulate matter (Figs. 10.2, 54.3). However, mussels were not fixed in the field, so this hypothesis is speculatory. Additionally, the long, slender plicae in the primary tubules of *F. cerina* may be indicative of foregut efficiency while the foregut of *V. nebulosa* and *S. connasaugaensis* is seemingly less efficient. Possible support for this hypothesis may be derived from examining the morphology of the second and third limbs of the intestine (see below).

8.7.3. Stomach

The stomach is a large chamber located between the digestive diverticulum and crystalline style sac. The walls of the stomach are rugose with ciliated columnar cells (e.g., Figs. 10.5, 10.6, 32.1, 32.3, 55.1, 55.2). Descriptions of the stomach of *Anodonta* have suggested that grooves in the stomach walls may transport particulate matter parallel to the grooves. Additionally, there may be circumferential currents that churn food matter (e.g. Fig. 55.5, Purcheon, 1958, Dinamani, 1967). A cyclic arrangement of eosinophilic masses of fluid was observed in histological sections of the stomach of *V. nebulosa*, *F. cerina*, and *S. connasaugaensis*. In addition to particle sorting, stomach epithelium may produce enzymes. For example, cellulase and dipeptidyl-aminopeptidase activity was detected in *C. gigas*, and N-acetylglycosaminidase was detected in *Pecten maximus* (Boucaurd-Camou and Henry, 2003). The histological sections of freshwater mussel stomachs in this dissertation provide some evidence of secretory activity in the stomach (e.g. Fig. 32.3–32.5). Eosinophilic, spherical vesicles were observed in close proximity to the stomach epithelium of each species. Additionally, a large, dense, mucoid mass was observed in the dextral portion of the anterior stomach chamber of *F. cerina* (Fig. 32.1). Therefore, the stomach of a freshwater mussel has a secretory epithelium, but hematoxylin and eosin stains are

non-specific and since the mussels were given some time to purge, evidence of chemical breakdown in the stomach lumen was not observed. The eosinophilic vesicles observed in the stomach lumen may represent mucus and not enzymes or stomach acid (e.g., Figs. 32.2, 32.3).

Additionally, the stomach epithelium, especially in the postero-ventral chamber possesses an eosinophilic cuticle, referred to as the gastric shield (Figs. 10.7, 10.8, 32.4, 32.5, 33.4, 55.5, 56.3), and it may represent a dense form of mucus (Shaw and Battle, 1957, 1959, Norton and Jones, 1992, Boucaurd-Camou and Henry, 2003). Curiously, the gastric shield has been proposed to function along with the crystalline style as part of a grinding apparatus (Owen, 1955) (see below).

Although no significant morphological differences in stomach structure were observed between *V. nebulosa*, *F. cerina*, and *S. connasaugaensis*, stomach structure is different across the various orders or lineages of Bivalvia (Purcheon, 1958, Dinamani, 1967). However, the authors did not propose any explanation as to what could be driving these differences.

8.7.4. Crystalline style sac

Particulate matter is routed through a long sinuous intestine following passage through the stomach. Histological sections of *V. nebulsoa*, *F. cerina*, and *S. connasaugaensis* reveal that the style sac consists of a sinistral circular chamber and a dextral and more linear duct (Figs. 11.1, 34.1, 34.4, 57.1). Based upon necropsies of freshwater mussels for the purpose of exploring metazoan parasites, the style is a long translucent rod that is soft and flexible. The style appears to be layered and particulate matter may become trapped within the concentric layers. The sectioning and staining characteristics of the gastric shield and style are similar, suggesting both structures have similar chemical composition. The rigid cilia in the style sac (Figs. 11.4, 34.2, 57.2) may cause the gelatinous rod to rotate causing loose food matter in the stomach to condense into a bolus such that is can efficiently travel through the intestine. Therefore, the

elaborate mucosa constituting the gastric shield may work harmoniously with the style rod to coagulate a large, and loosely organized volume of digested food matter coming from the expansive lumen of the stomach.

Given that the mussels were allowed to purge prior to being processed for histology, it is not clear whether condensed food matter traveling through the style sac passes through the spherical portion or the more linear midgut located laterally. However, it is my personal hypothesis that the food matter would be directed into the midgut located laterally to the style. If not, the midgut would probably be non-existant or reduced similar to the morphology of the style sac of *Anadara inflata* described by Kato and Kubomura (1954). The style sac of *A. inflata* is depicted as ovular, and laterally expansive with a compressed or truncated midgut (Kato and Kubomura, 1954). The midgut of *V. nebulosa*, *F. cerina*, and *S. connasaugaensis* features wispy cilia and goblet cells, but it was not clear whether any of the cells secrete enzymes. The narrow, basophilic cells comprising style sac epithelium type three seem specialized for protein synthesis. Kato and Kubomura (1954) suggested that the narrow, basophilic cells in the style sac produce a filamentous secretion, which may be an initial component of the style rod. Owen (1955) suggested that the style releases enzymes into the stomach, but provided no empirical evidence to support this idea. Boucaurd-Camou and Henry (2003) observed enzymes in sections of the style, but it was not clear what cells secrete enzymes or whether enzymes become incorporated into style rod layers from an anterior source.

Although it is recognized that the style creates sufficient suction to draw ingested material from the stomach into the intestine, there are a series of hypotheses regarding the function of the style that seem questionable. In the literature review regarding crystalline style function, Nelson (1918) indicated that several prior anatomical works on bivalves had proposed the hypothesis

that the style extends into the stomach, and rotates in close proximity to the stomach wall such that it would pulverize food matter like a morter and pestle. Yonge (1926a) proposed that the rotation of the style causes cilia located along the stomach wall, to fuse together, and form the gastric shield (Yonge, 1926a). Other anatomical works on the digestive tract of bivalves suggest the style grinds against the gastric shield to pulverise particulate matter (Owen, 1955, Shaw and Battle, 1957, Galtsoff, 1964, Lomte and Jadhay, 1980, Boucaurd-Camou and Henry, 2003). Owen (1955, Fig. 13) showed diagramatically that the esophagus opens near the crystalline style sac such that the rotation of the style would create suction needed to draw particulate matter towards a rigid sorting area. Furthermore, the figure caption states that this mechanism is representative of what occurs in most species of Eulamellibranchia. Considering the above, the idea that the style is a grinding apparatus seems to have gained broad support, and the above information is summarized in books (Brusca and Brusca, 2002, Allaby, 2003).

The idea that the style rod is a grinding apparatus is questionable considering both the style and shield are soft. Nelson (1918) explained that the style, water soluble, and composed of mucus that is rolled up by ciliary action. Several others have pointed out that the style rod is soft and flexible (Owen, 1955, Lomte and Jadhay, 1980). A possible explanation for the grinding hypothesis could be that the style coagulates, and becomes thickened when immersed in alcohol or boiling water (Nelson, 1918), and it would therefore appear to be a dense solid structure in a specimen preserved for anatomical study. Careful examination of figures (11.1, 11.2, 34.1, 34.6) show creasing artefacts to the style that would indicate that the microtome knife had passed through a dense object. Based upon histological sections of *V. nebulosa*, an eosinophilic rod-shaped mass was observed between the style sac and stomach, but it was not possible to determine whether this mass was traveling into the style sac or into the stomach (Fig. 11.2).

Based upon the shape and sectioning characteristics, it appeared to be a soft, gelatinous medium. Concentric, semicircular rays were observed in the stomach of all three species, but it seems likely that they represent a churning fluid (e.g. Fig. 55.5). Additionally, gastric shield covers stomach epithelium in several locations including ventral surfaces where a pestle-like structure would never touch, and may support the hypothesis that it is an elaborate binding agent. Furthermore, if the style grinds particulate matter, it is unclear as to why grinding would occur between the stomach and intestine, especially considering the extensive digestive tubules located anterior to the stomach. It is also critical to point out that the illustration of the position of the crystalline style sac to the intestine and digestive diverticulum as depicted in Owen (1955) was proposed to be representative of many species of Eulamellibranchia. Based on serial sections of the digestive tract of *V. nebulosa*, *F. cerina*, and *S. connasaugaensis*, the esophagus and digestive diverticulum are not located near the style sac and particles would not directly enter this structure from the esophagus. Nevertheless, the illustration in Owen (1955) appears in the more recent work of Boucaurd-Camou and Henry (2003) and appears to have been accepted at face value. Considering the significant morphological differences in the crystalline style sac and stomach across different bivalve orders (Kato and Kubomura, 1954, Purcheon, 1958, Dinamani, 1967)

The morphological differences to the style sac of *V. nebulosa*, *F. cerina*, and *S. connasaugaensis* are different, but the significance of such differences remains unclear given that mussels were allowed to purge prior to being processed for histology. However, given that midgut of *F. cerina* had a different shape in comparison to the shape of the midgut of *S. connasaugaensis* and *V. nebulosa*, possibly this represents a difference in how food matter is

consolidated as it enters the intestine. However, the significance of such a mechanism remains unclear in respect to how nutrients are absorbed in the intestine.

8.7.5. Intestine

The intestine of *V. nebulosa*, *F. cerina*, and *S. connasaugaensis* is a long tubular organ that extends through the medial and posterior portions of the visceral mass. The intestine bends several times to form five regions or limbs. Based upon histological sections of the digestive tract, the direction of the alimentary canal of *V. nebulosa*, *F. cerina*, and *S. connasauagaensis* was generally identical and resembles the layout described from *Anodonta* spp. (Simpson, 1884, Gutheil, 1912).

The crystalline style sac represents the first descending limb of the intestine (Figs. 12.1, 35.2, 58.2). The walls of the style sac feature numerous folds and there was an eosinophilic mass typically associated with the ridges and troughs of the style sac walls. Since epithelial types 1-3 were sometimes seen on both the anterior and posterior walls of this intestinal limb, it seems that the style sac does not maintain its stem-loop configuration as it descends (Figs. 12.1, 35.2, 58.3). Possibly, since style sac epithelium continuous until the base of the visceral mass, circular mixing of food matter may continue to occur until the second intestinal limb. Even though the descending style sac appears to be significantly pleated, I think these folds are associated with mixing rather than absorption.

The absorptive intestine seemingly begins with the second limb considering the bubbling observed in some areas and considering the conspicuous folding of the intestinal wall seen in *V. nebulosa*, and *S. connasaugaensis* (Figs. 11.7, 12.5, 58.1, 58.4). In each species, the second and third intestinal limb featured numerous goblet cells and a dense, eosinophilic mass of chyme (Figs. 12.4, 35.4, 58.5). In many areas, the ciliated cells along the intestinal wall appeared to be

bubbling (Figs. 12.4, 12.5, 58.5), but it was not clear what these secretions might be. The second, and third intestinal limbs appeared to have at least three cell types. The first cell type was ciliated with eosinophilic vesicles while the second cell type, lacked vesicles. Goblet cells represented the third cell type, but these cells were sparsely distributed. Although microvillar cells are typically associated with the intestinal epithelium of a vertebrate (Ross et al. 2003), there was not any indication of such cells in the intestine of each unionid species. This could mean that either the ciliated cells of the intestine have a significant capacity for absorption by themselves or microvilli were obscurred from view.

The second, and third intestinal limbs of *V. nebulosa* and *S. connasaugaensis* consisted of sinuous to deeply folded walls (Figs. 11.7, 58.1), but in *F. cerina*, the walls lacked folds or plicae (Fig. 35.1). A possible explanation for these differences could be that the deeply infolded walls of the ciliated digestive diverticulum tubules are more effective at delivering particles to cells that utilize intracellular digestion. A second explanation could be that *F. cerina* is taking in a greater volume of particulate matter than *V. nebulosa* or *S. connasaugaensis*.

The lumen of the fourth and fifth intestinal limbs was considerably larger than the lumen of the style sac, second and third intestinal limbs. In general fourth and fifth intestinal limbs may have similar functions considering the morphological similarity of the typhlosole and surrounding intestinal wall (Figs. 13.3, 13.8, 36.1, 36.4, 59.1, 59.4). The primary distinction between the fourth and fifth intestinal limbs was the presence of granulocytes located along the ventral wall. Granulocytes reside in flattened plicae, have a teardrop-shape, and contain eosinophilic to basophilic intracellular granules (Figs. 13.4, 36.2, 59.2). However, it is presently uncertain what the function of the granulocytes located within the plicae of the ventral wall of the fourth limb. There are two possible explanations, the strong staining character may be

indicative of an aporcine cell that may produce enzymes or mucins. For example, aminopeptidase activity was detected in sections of the lower intestine of *P. maximus* (Boucaurd-Camou and Henry, 2003). Goblet cells observed in histological sections of *V. nebulosa*, *F. cerina*, and *S. connasauagaensis* mantle and labial palp sometimes have an eosinophilic, and granular appearance (Figs. 8.3, 29.5, 52.3). Alternatively, the granules observed in ventral epithelial cells of the fourth intestinal limb may represent intracellular bacteria. Symbiotic intracellular bacteria are known from species of marine bivalves (Lucinidae, Thyasiridae, Vesicomyidae, Mytilidae) that live in sulfur rich environments. In many cases energy is derived from the oxidation of hydrogen sulfide by intracellular ctenidial bacteria (Cavanaugh et al., 2006). Intracellular bacteria are also known from the digestive tracts of herbivorous insects. Symbiotic bacteria inhabiting the digestive tract of such insects may allow insects to feed on diets that are rich in carbohydrates, but deficient in amino acids (Bauman et al., 2006). Transmission electron microscopy, bacterial stains such as Giemsa, or *in situ* hydribridization using a universal bacterial DNA probe are needed to discern the nature of these granulocytes. Considering that the fourth and fifth intestinal limbs have a large typhlosole restricting the lumen, and a perimeter of repeating plicae, it seems that absorption continues to occur. However, the morphological differences between the second and third, and fourth and fifth limbs may be an indication that the absorptive processes occurring in each region are not identical. Scanning or transmission electron microscopy would provide a higher resolution images of the cell types characterizing each intestinal limb and could shed light on how or if absorption is different.

Histological sections of intestine sometimes revealed wandering hemocytes in the epithelium (e.g. Figs. 12.6, 13.3, 36.3). Yokley (1968) observed wandering cells throughout the digestive tract and indicated that brown to green intracellular pigments may be evidence that these cells

can engulf foreign bodies from digestive epithelium. Owen (1955) reported wandering cells in different places throughout the digestive tract. Owen (1955) suggested that hemocytes move into the digestive tract epithelium to engulf particles and that intracellular digestion by means of hemocytes is one of many ways in which bivalves derive nutrients from ingested matter. However, considering the sparse distribution of hemocytes in the epithelium of the intestine, it seems unlikely that phagocytic wandering cells would play a significant role in digestion. Alternatively, hemocytes may periodically move into the digestive epithelium to engulf invasive pathogens or repair local injuries.

Another curious matter regarding the function of the intestine are the observations of Owen (1955), and Yokley (1968). Both authors reported that there are concentric bands of myofibers surrounding the intestine of bivalves. The supporting images in Owen (1955) are not informative about myofibers and the micrographs appear to show dark-staining, and thin filaments. The micrographs from Yokley (1968) were blacked-out because the dissertation is non-circulating and only photocopies were available. Throughout the digestive tract of *V. nebulosa*, *F. cerina*, and *S. connasaugaensis*, overlapping connective tissue fibers were typically observed supporting folded epithelial tissue (e.g. Figs. 11.4, 13.5, 35.3, 36.3, 57.3, 59.5). In some cases connective tissue appeared to be densely compacted around the intestine similar to a serosa. Owen (1955), and Yokely (1968) suggested that muscle tissue in the digestive tract of a bivalve would create peristalsis. However, this hypothesis seems unlikely given that the epithelium of the alimentary canal of each unionid species has extensively ciliated with numerous folds or grooves along the walls. Secondly, the crystalline style rotates and delivers particulate matter into the intestine and this seems like a logical alternative to peristalsis in a suspension-feeding animal that does not consume a large solid mass of food.

Considering the histological differences in oral groove, digestive diverticulum, style sac, and intestine, it seems that *V. nebulosa*, *F. cerina*, and *S. connasaugaensis* have different feeding strategies. Overall, the digestive tract of *V. nebulosa* and *S. connasaugaensis*, were most similar to each other, but different in comparison to *F. cerina*. It is difficult to speculate about how the feeding habits of each mussel could be different. Although *V. nebulosa* and *S. connasaugaensis* were collected in headwater streams, and *F. cerina* was obtained from a large river, the historic ranges of each species could have overlapped. Terrapin Creek and Shoal Creek may have less plankton biomass than the Cahaba considering that these areas have more shade. However, historically, *V. nebulosa* and *S. connasaugaensis* occurred in large rivers like the Cahaba, so it is likely that there is no relationship between the morphological features of the digestive tract of each species and available plankton. Histology of field fixed mussels could reveal whether quantity of ingested matter, or specific species of algae or bacteria, but this could be problematic considering that routine tissue preparation for paraffin embedding or electron microscopy removes water-soluble liquids (Sims et al., 1991). Therefore, we may end up with an incomplete picture of the dietary composition.

8.8. Cardiovascular system

The heart consists of a pair of laterally positioned auricles and a median muscular ventricle (e.g. Figs. 14.5, 60.1). Overal cardiac structure of *V. nebulosa*, *F. cerina*, and *S. connasaugaensis* was very similar. Auricles and ventricle consisted of an epicardium of squamous cells, and a distinct myocardium of cardiac muscle. However, there was less investment of cardiac myofibers in the auricles than observed in the ventricle, possibly because the auricles are blood receving conduits that need to be distensible (Motley, 1932).

Andrews and Jennings (1993) reported that auricles of *Anodonta* sp. merge with the walls of the pericardium, and that fluid may leak out of the auricles into the surrounding pericardial gland. However auricles of each mussel species studied herein extended freely into the pericardial cavity to merge with the ventricle at an oblique angle. Furthermore, Andrews and Jennings (1993) proposed that fluid may also leak out of the auricles into the surrounding pericardial cavity. Based on histological sections of three unionid species, it was not obvious whether the auricular epicardium would leak (Figs. 14.3, 37.4, 60.4). Examining the surface of the auricles of *V. nebulosa*, *F. cerina*, and *S. connasaugaensis* may provide insight into whether there are gaps between epicardial cells that would be indicative of the passive transport of fluid into the surrounding pericardial cavity. Scanning electron microscopy of the heart of *C. gigas* has indicated that the ventricle and auricles each have a robust composition. Higher magnification images of the surface of the auricle and ventricle do not provide much information concerning the possibility of pores. Although *C. gigas* is a marine bivalve, the morphological features of the auricles and ventricles seem to be morphologically comparable to the heart of a unionid and may be an indication that fluid does not leak out of the heart (Le Pennec and Grizel, 2003).

There is a pair of muscular, auriculoventricular valves separating each sinistral and dextral auricle (Figs. 14.6, 37.5, 60.5), from the ventricle, to maintain proper tidal rhythm (Motley, 1932). Cardiac myofibers in the ventricle are significantly developed, with numerous longitudinal and transversely oriented myofibers. Considering the extensive development of longitudinal and transverse myofibers in the ventricle (Figs. 14.2, 37.3, 60.3), the orientation of myofibers would seemingly cause the ventricle to contract in a circular, and linear (posterior-to-anterior) fashion to drive blood into anterior, and posterior aortic vessels (Brand, 1972). Additionally, as in the heart of a vertebrate (Ross et al., 2003) cardiac myofibers were spaced

apart to facilitate constant expansion and contraction of the organ, and to maintain a supply of oxygen to the myofibers. Additionally, myofibers contained brown, granular inclusions and it is uncertain what this material represents or how it relates to cardiac function (e.g. Fig. 37.3). Furthermore, intracellular inclusions were not observed in any other muscle tissue in *V. nebulosa*, *F. cerina*, or *S. connasaugaensis*.

Arteries, veins and capillaries were located throughout the body, but it was sometimes difficult to distinguish between arteries and veins (e.g. Figs. 15.1–15.4). Arteries in vertebrates have a dense wrapping of smooth muscle with a circular lumen. Veins typically have thinner walls with an irregular somewhat flattened lumen (Ross et al., 2003). The aorta for example, would have a thick muscular wall, but histological sections of the anterior and posterior aorta of mussels revealed a large, ovular lumen with a limited muscular wrapping. Thick musculature enclosed the lumen of arteries near the base of the foot, possibly to rapidly fill pedal hemolymph sinuses with blood in order to facilitate expansion of the tissue (Trueman, 1966, Brand, 1972).

Regarding accessory cardiac structures, there was a large sphincter-like structure located at the base of the visceral mass between the anterior nephridium, and visceral mass (Fig. 15.6). This structure occurs in *V. nebulosa*, *F. cerina*, and *S. connasauagaensis*, but is only shown for *V. nebulosa*. This structure may be the median ventral sinus discussed in Brand (1972). The median ventral sinus is thought to be a regulatory structure that controls the flow of blood through the renal plicae, and through the hemolymph sinus between the nephridium and visceral mass. Possibly this sphincter-like structure helps maintain normal tidal rhthym. Narain (1972) observed a posterior aortic bulb just posterior to the ventricle in *Lamellidens corrianus*. Based on the reduced and low-resolution micrographs, it appears that there is an ovular mass of tissue near the aorta, but it is not possible to determine its composition. During the histological

sectioning for this dissertation, blood vessels were typically not surrounded by concentric layers of smooth muscle, but a posterior aortic vessel in *V. nebulosa* appears to have a loose wrapping of fibers (Fig. 17.4) and possibly supports the observation of Narain (1972). However, the image of the posterior aortic bulb described by Narain (1972) is reduced, and the image resolution is low since my personal copy of this article was a photocopy sent to me through interlibrary loan. Therefore, it is difficult to determine how the posterior aorta of *V. nebulosa* is comparable to that of *L. corrianus*. Also, Andrews and Jennings (1993) suggested that there are a series of well-defined blood vessels that converge at the base of the ctenidia, leading to the auricles. In transverse sections of the heart, a pale, violet, granular mass was observed at the base of the gill (e.g., Fig. 15.7). Additionally, there was a network of loose connective tissue between the aurcles and the gill. Well-defined blood vessels leading from the base of the gills to the auricles were not observed. Possibly this region conveys blood into the auricles in a diffuse manner considering the funnel-shaped configuration of unionid auricles.

Hemolymph consisted of distinct cellular and non-cellular components. Eosinophilic, granular hemocytes were observed throughout the coelom and mantle of *V. nebulosa*, *F. cerina*, and *S. connasaugaensis* (Figs. 8.3, 14.4, 38.4, 48.2, 52.2). Literature regarding hemocytes of unionids and marine bivalves suggests that there are distinct types of blood cells (Dundee, 1953). However, potential differences between hemocytes observed throughout the coelom and mantle are presently indeterminate. Hemolymph fluid was represented by a diffuse, black-pigmented material, throughout the body, typically within interstitial spaces (e.g. Figs. 8.1, 8.4, 38.2, 57.1, 61.1). Considering that black granules were observed in the heart and interstitial spaces, it may represent plasma and interstitial fluid. Black granules may represent hematin, a pigmentation

that occurs in blood-rich tissues when acidic formalin and hemoglobin react (Myers and McGavin, 2007).

The pericardial gland is a diffuse network of adipocyte-like cells located laterally and dorsally to the pericardial cavity (Figs. 15.8, 38.4, 61.4). Clearly this spongy tissue transmits blood through the dorsum, and the high surface area of this tissue would be an indication that blood travels slowly through this region. Although the pericardial gland is thought to play some role in filtration, the exact function of this tissue is indeterminate (Morse, 1987, Andrews and Jennings, 1993). An additional possibility that the bivalve researchers may have overlooked is hemopoiesis. In an effort to understand the host-parasite relationship between the infective larval stages of trematodes (*Fasciola hepatica*), and snails (*Lymnaea truncatula*), Rondelaud and Barthe (1981) observed hemocyte proliferation between the nephridium and pericardium following experimental infection of snails with infective trematode larval stages (miracidium). Possible support of this hypothesis is the presence of emarginated, eosinophilic cells resembling hemocytes, along the surface of the adipocyte-like cells.

8.9. Renal system

Overall histological features of the nephridium of *V. nebulosa*, *F. cerina*, and *S. connasaugaensis* reveal certain insights into renal physiology of bivalves. Overall nephridial structure was different from anterior to posterior (Figs. 16.1, 17.1, 39.1, 40.1, 62.1, 63.1). The ventral nephridial limb is compressed anteriorly because it is located adjacent to the visceral mass. The lumen of the anterior portion of the ventral nephridial limb is restricted by the numerous infoldings (Figs. 16.1, 39.1, 62.1). Given the extensive network of branched plicae, it seems that reabsorption occurs in the anterior portion of the ventral nephridium. Plicae become more widely spaced apart posteriorly between the posterior margin of the visceral mass and

posterior adductor and the overall lumen of the nephridium expands possibly to accommodate a larger volume of fluid. Epithelial folds have a stem-loop structure and the cells have a pale-staining cytoplasm (Figs. 17.1, 40.1, 63.1) . Therefore, the posterior portion of the nephridium may function similar to the thin loop of Henle in a vertebrate (Ross et al., 2003). Dorsal nephridium resembles a sac and contains a small number of short, thin plicae. Considering the absorptive nature of the ventral nephridial limb, the function of dorsal nephridium is thought to be analogous to a bladder (Myers and Franzen, 1970, Andrews and Jennings, 1993). The structure of the nephridium of *V. nebulosa*, *F. cerina* and *S. connasaugaensis* is similar to descriptions of unionid nephridia of *Pleurobema cordatum* and *Quadrula nodulata* (Yokley, 1968, Myers and Franzen, 1970).

Renal filtrate may be derived from blood flowing through the pericardial gland. Podocytes are associated with the pericardial cavity and may be distinguished from other cells by the presence of branched cytoplasmic extensions of the basal part of the cell known as pedicels. Fluid derived from hemolymph may pass out of the pericardial gland and into the pericardial cavity (Meyhöfer et al., 1986, Morse, 1987). A more recent study indicated that podocytes of *A. cygnea* may be located anteriorly to the nephridium may allow passage of fluid into the renal-pericardial canal (Andrews and Jennings, 1993). A competing hypothesis regarding filtration suggests that fluid may pass through the pericardial wall from the pericardial gland (Yokley, 1968). Goblet cells located around the lumen of the renal-pericardial canal possibly secrete mucus into the renal lumen (Figs. 16.8, 39.6, 62.6), but the presence of mucigen has not been confirmed. Since these cells were located along the anterior wall of the pericardial sac, perhaps some of these cells represent podocytes. It is difficult to pinpoint exactly where podocyes occurred because there is no light microscopy reference point. Morse (1987) for example,

illustrated two podocytes in a diagram portraying the path of fluid from the pericardial gland to the nephridium, but there is no information about the appearance of the surrounding tissue. Since podocytes were portrayed as teardrop-shaped columnar cells in Morse (1987), and since Andrews and Jennings (1993) stated that podocytes are located in the anterior region of the pericardial cavity, the columnar epithelium at the anterior portion of the pericardial sac at the entrance to the renopericardial canal may contain podocytes.

Ciliated cells in the renopericardial canal seemingly create the driving force needed to propel renal filtrate posteriorly through the nephridium. Cilia were conspicuous in the renopericardial canal (Figs. 16.8, 39.6, 62.6), and urethra (Figs. 16.7, 39.6, 62.7), but there were no obvious indications of cilia throughout the ventral and dorsal nephridial limbs. Fine, wispy structures were observed on the apical surface of cuboidal cells representing the stem-loop structures of the posterior nephridium (Figs. 17.2, 40.2, 63.2). However, it seemed that these filamentous structures were the remnants of a fluid. Given the limited extend of cilia in the nephridium, and the extensive volume of tissue throughout the entire ventral and dorsal nephridial limbs, and that unionid exhibit low cardiovascular pressure (Brand, 1972), it would seem that passage of filtrate through the nephridium occurs at a slow rate.

The columnar epithelium of the ventral nephridial limb of *V. nebulosa*, *F. cerina*, and *S. connasaugaensis* contained a red to brown intracellular granules. Brown intracellular granules were most conspicuous in *V. nebulosa* (Fig. 16.3), and the red granules were most conspicuous in *S. connasaugaensis* (Fig. 62.2). In most cases, the granular material resembled wandering hemocytes. The brown granules may represent either senescent hemocytes or hemocytes with engulfed material. In either case the eosin dye poorly presented itself and suggests some chemical change occured in the cytoplasm of wandering cells. It is unclear why the epithelium

of *S. connasauagaensis* would have such a strong eosinophilic and granular staining character. An alternative explanation for the intracellular granules in the ventral nephridium could be that the columnar cells are phagocytic or absorb substances from the nephridial lumen via microvilli to form concretements. Concrements may consist of lipofuscin granules, membrane remnants or other substances that would appear to be electron dense when the tissue is studied with transmission electron microscopy. Concrements may later be expelled into the lumen once the intracellular vacuole-lysosome system is filled to capacity (Morse, 1987).

Teardrop cells with an apical, transparent vesicle (Figs. 16.5, 39.3, 62.3) have been observed in unionids such as *Q. nodulata* (Myers and Franzen, 1970) as well as marine bivalves such as *C. virginica* (Galtsoff, 1968). Teardrop cells with apical vesicles located in the bladder and have been previously suggested to pinch off the apical vesicle. The vesicle may contain an anionic substance based on a positive staining reaction with Heidenhein's Azan Stain (Myers and Franzen, 1970). Possibly, this anionic substance is ammonia.

The cuboidal cells of the posterior nephridium (Figs. 17.2, 63.2), and especially dorsal nephridial cells (both, dorsal and ventral) contained brown intracellular granules (Figs. 16.4, 39.5). Possibly this substance represents more accumulations of waste products that have become internalized within renal epithelium. The observation of plicae in the dorsal nephridium is somewhat surprising considering the extensive infoldings of the anterior portion of the ventral limb. The plicae in the dorsal nephriidum would suggest that reabsorption continues to occur at a low level once filtrate enters the dorsal nephridium, which is thought to represent a bladder (Myers and Franzen, 1970, Andrews and Jennings, 1993).

8.10. Nervous system

Freshwater mussels have a decentralized nervous system consisting of a pair of anterior cerebral ganglia (Figs. 19.1, 42.1, 65.1), a bilobed pedal ganglion (Figs. 18.1, 41.1, 64.1) and visceral ganglion located posteriorly (Figs. 19.2, 42.3, 65.3). Each ganglion has a distinct cortex and medulla. Unipolar neurons are typically located in the cortex of a bivalve while bipolar and multipolar neurons tend to be located within the medulla (Tauc, 1966). However, cell bodies of the medulla in *V. nebulosa*, *F. cerina*, and *S. connasaugaensis* were minute, making it difficult to determine whether some are neurons or glial cells. The pedal ganglion of F. cerina had thickened axons and connective tissue surrounding each hemisphere (Fig. 41.1). It is unclear how the function of the pedal ganglion of *F. cerina* may differ from that of *V. nebulosa*, and *S. connasauagaensis* considering the later two species lacked thickened axons and connective tissue fibers (Figs. 18.1, 64.1). Each ganglion is associated with local tissue function and movement of musculature. Based upon experiments in which bodily regions are separated from the cerebral ganglion, it appears that the cerebral ganglion is required for complex motor functions. Moreover, ganglia are linked to each other and can work together to regulate tissue function. For example, the visceral ganglion enables shell closure, but opening requires signals from cerebral ganglia (Tauc, 1966).

The spherical statocysts located laterally to the pedal ganglion are associated with equilibrium. Statocysts are fluid-filled capsules containing a ciliated epithelium (Figs. 20.6, 43.3, 66.3). Sensation of equilibrium is thought to be derived from neural impulses created following contact between the statolyth and ciliated cells. Evidence of statocyst function is derived from experimental investigations in which impaired righting response was observed following mechanical damage to the statocyst or its associated nerve (Cragg and Nott, 1977).

8.11. Reproductive system

Gonadal acini of unionids are typically small throughout most of the year, generally between fall and spring (Yokley, 1972). Unionids breed during the summer and the specific spawning period is different among the various unonid species. The peak spawning period of *V. nebulosa* in Terrapin Creek was between late July and early August similar to the spawning time reported from Big Moccasin Creek, VA (Zale and Neves, 1982b). The spawning period of *F. cerina* in Cahaba River occurs during May, similar to the spawning period of *F. cuneolus* in Clinch River, VA (Bruenderman and Neves, 1993). Male and female *S. connasaugaensis* achieve reproductive maturity between late July and early August. Acini expand to accommodate a large volume of spermatozoa in males (Figs. 21.6, 44.6, 67.6) and a small number of enlarged, mature oocytes in females (Figs. 21.3, 44.3, 67.3). Immature testicular (Figs. 21.5, 44.5, 67.5), and especially ovarian acini (Figs. 21.2, 44.2, 67.2) contained eosinophilic granules. The small granules likely constitute fluid, however the larger granules observed in immature ovarian acini are possibly a combination of polar bodies and degenerative oocytes considering the abundance of pyknotic nuclei within the lumen. Immature testicular acini also contained pyknotic nuclei to a lesser extent. Therefore, it seems that gametogenesis occurs outside of the spawning season and that oocytes and spermatocytes breakdown prematurely. Specific seasonal cellular changes to acini were previously described from *P. cordatum* (Yokley, 1972).

Regarding mature ova, differences were pronounced owing to their great size. The vitelline membrane was the most distinctively different feature of oocytes (Figs. 21.3, 44.3, 67.3). Based upon histological sections of filled marsupia of *F. cerina*, it seems that the structure of vitelline membranes may be important for embryo packing. The vitelline membranes were irregular, filamentous extensions of ova, and ova appeared to be held together within a conglutinate by

vitelline membranes (Figs. 26.1, 26.3). Therefore, the vitelline membranes of *F. cerina* may be adhesive and provide strength to a conglutinate. Histological sections of filled marsupia of *V. nebulosa* and *S. connasaugaensis* were derived from animals collected months after ovarian maturity making it difficult to link structural characteristics of vitelline membranes to embryo packing (Figs. 5.2, 49.4). Differences in the thickness or composition of the vitelline membrane of bivalve ova are typically matched by corresponding adaptations of the spermatozoa. Thickened ova of *Mytilus edulis* for example, may be correspondingly fertilized by spermatozoa that possess a large acrosome, which would be required to penetrate a thickend, and gelatinous membrane (Popham, 1979).

There were no obvious differences in the structure of spermatozoa of each unionid species based upon hematoxylin and eosin stained sections (Figs. 21.6, 44.6, 67.6). However, spermatozoa are diminutive and certain structural details such as the morphology of the acrosome are only evident with transmission electron microscopy (Rocha and Azevedo, 1990). Morphology of spermatozoa of marine bivalves can be highly species specific at the ultrastructure level and variation is associated with fertilization strategies. Differences are associated with external fertilization, fertilization in mantle cavity, and whether sperm are released freely or packaged into spermatophores (Morse and Zardus, 1997). Spermatocytes and sperm morula of immature testicular acini were loosely arranged making it difficult to describe specific details of cellular progression from a spherical, single-celled spermatocyte to a spermatids and spermatozoa. Spermatogenesis in immature and mature acini was different. Immature acini were characterized by “atypical” spermatogenesis consisting of copious sperm morula (Figs. 21.5, 44.5, 67.5) while mature acini were characterized as exhibiting “typical” spermatogenesis (Figs. 21.6, 44.6, 67.6, van der Schalie and Locke, 1941, Heard, 1975).

Atypical and typical spermatogenesis may produce sperm cells that are identical based on light microscopy, but it is unclear whether there is a difference at the ultrastruture level.

LITERATURE CITED

Ahlstedt, S. A., and J. J. Jenkinson. 1986. A mussel die-off in the Powell River, Virginia and Tennessee, in 1983. In: Neves R. J. (ed) Proceedings of the workshop on die-offs of freshwater mussels in the United States, June 23-25, Davenport, IA, United States Fish and Wildlife Service, Upper Mississippi Conservation Committee, p. 21–28.

Alexander, M. K. 2007. Muscatine's pearl button industry. Arcadia Publishing, Charleston, SC, pp 128.

Allaby, M. 2003. A dictionary of zoology, Oxford University Press, 2nd ed, Oxford, pp 597.

Allen, W. R. 1914. The food and feeding habits of freshwater mussels. Biological Bulletin 27: 127–146.

Andrews, E. B., and K. H. Jennings. 1993. The anatomical and ultrastructural basis of primary urine formation in bivalve mollusks. Journal of Molluscan Studies 59: 223–257.

Atkins, D. 1937. On the ciliary mechanisms and interrelationships of lamellibranchs. Part III: Types of lamellibranch gills and their food currents. Quarterly Journal of Microscopical Science 79: 375–421.

Atkinson, C. L., M. R. First, A. P. Covich, S. P. Opsahl, and S. W. Golladay. 2011. Suspended material availability and filtration-biodeposition processes performed by a native and invasive bivalve species in streams. Hydrobiologia 667: 191–204.

Araujo, R., N. Cámara, and M. A. Ramos. 2002. Glochidium metamorphosis in the endangered freshwater mussel *Margaritifera auricularia* (Spengler, 1793): A histological and scanning electron microscopy study. Journal of Morphology 254: 259–265.

Avelar, W., and A. Cunha. 2009. The anatomy and functional morphology of *Diplodon rhombeus fontainianus* (Orbigny, 1835) (Mollusca Bivalvia, Hyriidae). Brazilian Journal of Biology 69: 1153–1163.

Baker, F. C. 1923. The use of molluscan shells by the Cahokia Mound Builders. Contribution from the Museum of Natural History, University of Illinois 34: 328–334.

Baker, F. C. 1930. The use of animal life by the mound-building Indians of Illinois. Contribution from the Museum of Natural History, University of Illinois 54: 41–64.

Baker, R. A. 1976. Tissue damage and leukocytic infiltration following attachment of the mite *Unionicola intermedia* to the gills of the bivalve mollusk *Anodonta anatina*. Journal of Invertebrate Pathology 27: 371–376.

Barnhart, M. C. 2008. Unio gallery: http://unionid.missouristate.edu. Accessed 09/28/2012.

Barnhart, M. C., W. R. Haag, W. N. Roston. 2008. Adaptations to host infection and larval parasitism in Unionoida. Journal of the North American Benthological Society 27: 370–394.

Bakker, K. E., and C. Davids. 1973. Notes on the life history of *Aspidogaster conchicola* Baer, 1826 (Trematoda; Aspidogastridae). Journal of Helminthology 47: 269–276.

Baumann, P., **N. A. Moran, and L. Baumann.** 2006. Bacteriocyte-associated endosymbionts of insects. In: Rosenberg E., Stackebrandt E., Thompson F., DeLong E., Lory S. (eds) The Prokaryotes - A Handbook on the Biology of Bacteria. Volume 1: Symbiotic Associations, Biotechnology, Applied Microbiology, pp 403–438.

Beckett, D. C., B. W. Green, A. C. Miller, and S. A. Thomas. 1996. Epizoic invertebrate communities on upper Mississippi River unionid bivalves. American Midland Naturalist 135: 102–114.

Bedford, J. W., E. W. Roelofs, and M. J. Zabik. 1968. The freshwater mussel as a biological monitor of pesticide concentration in a lotic environment. Limnology and Oceanography 13: 118–126.

Beedham, G. E. 1958. Observations of the mantle of Lamellibranchia. Quarterly Journal of Microscopical Science 99: 181–197.

Bishop, C. D., R. Hudson, and J. L. Farris. 2007. Propagation and culture of freshwater mussels. In: Farris, J. L., and J. H. Van Hassel (eds) Freshwater Bivalve Ecotoxicology, CRC Press, Boca Raton, FL, 65–95.

Blodgett, K. D., and R. E. Sparks. 1986. Documentation of a mussel die-off in pools 14 and 15 of the upper Mississippi River. In: Neves R. J. (ed) Proceedings of the workshop on die-offs of freshwater mussels in the United States, June 23-25, Davenport, IA, pp 76–90.

Boucaurd-Camou, E. and M. Henry. 2003. The digestive system. In: Grizel, H. (ed) Atlas d'histologie et de cytology des mollusques bivalves marins = An atlas of histology and cytology of marine bivalve molluscs. Ifremer Plouzané, France, pp 65–116. (in French and English).

Brand, A. R. 1972. The mechanism of blood circulation in *Anodonta anatina* (L.) (Bivalvia, Unionidae). Journal of Experimental Biology 56: 361–379.

Brooks, W. K. 1882. Handbook of Invertebrate Zoology for Laboratories and Seaside Work. S. E. Cassino, Publisher, Boston, Massachusetts. 392 p.

Brück, A. 1914. Die muskulatur von *Anodonta cellensis* Schröt ein beitrag zur anatomie und histologie der muskelfasern. Zeitschrift für Wissenschaftliche Zoologie 110: 481–619.

Bruenderman, S. A., and R. J. Neves. 1993. Life history of the endangered fine-rayed pigtoe *Fusconaia cuneolus* (Bivalvia: Unionidae) in the Clinch River, Virginia. American Malacological Bulletin 10: 83–91.

Brusca, R. C., and G. J. Brusca. 2002. Invertebrates, 2nd ed. Sinauer Associates, Inc., pp. 936.

Buchanan, A. 1986. Die-off impacts on the mussel fauna of selected reaches of the Bourbeuse and Meramec Rivers, Missouri. In: Neves, R. J. (ed) Proceedings of the workshop on die-offs of freshwater mussels in the United States, June 23-25, Davenport, IA, pp 44–54.

Burkhead, M. J., S. Leavell, R. B. Weiss, K. Kuehnl, H. Valentine, G. T. Watters, and B. A. Wolfe. 2009. Analysis and cytologic characterization of hemocytes from freshwater mussels (*Quadrula* sp.). Veterinary Clinical Pathology 38: 426–436.

Cajaraville, M. P., G. Díetz, I. A. Marigómez, and E. Angulo. 1990. Responses of basophilic cells of the digestive gland of mussels to petroleum hydrocarbon exposure. Diseases of Aquatic Organisms 9: 221–228.

Cavanaugh, C., Z. P. McKiness, I. I. G. Newton, and F. J. Stewart. 2006. Marine chemosynthetic symbioses. In: Rosenberg E., Stackebrandt E., Thompson F., DeLong E., Lory S. (eds) The Prokaryotes - A Handbook on the Biology of Bacteria. Volume 1: Symbiotic Associations, Biotechnology, Applied Microbiology, pp 475–507.

Chaudhry, H. S., and A. S. Narain. 1972. Functional morphology of the heart of the freshwater mussel *Lamellidens corrianus*. Zoologische Beiträge 18: 339–342.

Checa, A. G. 2002. Fabricational morphology of oblique ribs in bivalves. Journal of Morphology 254: 195–209.

Chittick, B., M. Stoskopf, M. Law, R. Overstreet, and J. Levine. 2001. Evaluation of potential health risks to eastern elliptio (*Elliptio complanata*) (Mollusca: Bivalvia: Unionida: Unionidae) and implications for sympatric endangered freshwater mussel species. Journal of Aquatic Ecosystem Stress and Recovery 9: 35–42.

Clark, H. W., and C. B. Wilson. 1912. The mussel fauna of the Maumee River. Bureau of Fisheries Document No. 757., 94 p.

Colville, A. E., and R. P. Lim. 2003. Microscopic structure of the mantle and palps in the freshwater mussels *Velesunio ambiguous* and *Hyridella depressa* (Bivalvia: Hyriida). Molluscan Research 23: 1–20.

Cooke, A. H. 1895. Molluscs. In: Harmer, S. F., and Shipley, A. E. (eds) The Cambridge Natural History. Vol. III. Macmillan and Co., New York. 1–459.

Cosgrove, P., L. Hastie, and I. Sime. 2007. Recorded natural predation of freshwater pearl mussels *Margaritifera margaritifera* (L.) in Scotland. Journal of Conchology 39: 469–472.

Cragg, S. M., and J. A. Nott. 1977. The ultratructure of the statocysts in the pediveliger larvae of *Pecten maximus* (L.) (Bivalvia). Journal of Experimental Marine Biology and Ecology 27: 23–36.

Cranfield, H. J. 1973a. A study of the morphology, ultrastructure, and histochemistry of the foot of the pediveliger of *Ostrea edulis*. Marine Biology 22: 187–202.

Cranfield, H. J. 1973b. Observations on the function of the glands of the foot of the pediveliger of *Ostrea edulis* during settlement. Marine Biology 22: 211–223.

DeWalt, R. E., V. H. Resh, and W. L. Hilsenhoff. 2010. Diversity and classification of insects and Collembola. In: Thorp J. H., and Covich A. P. (eds) Ecology and classification of North American freshwater invertebrates, 3rd ed. Elsevier, Amsterdam pp 587–657.

Dinamani, P. 1967. Variation in the stomach structure of the bivalvia. Malacologia 5: 225–268.

Dundee, D. S. 1953. Formed elements of the blood of certain fresh-water mussels. Transactions of the American Microscopical Society 72: 254–264.

Eble, A. F. 1966. Some observations on the seasonal distribution of selected enzymes in the American Oyster as revealed by enzyme histochemistry. Proceedings of the National Shellfisheries Association 56: 37–42.

Eble, A. F. 2001. Anatomy and histology of *Mercenaria mercenaria*. In: Kraeuter J. N., and Castagna M. (eds) Biology of the hard clam. Elseveir, Amsterdam pp 117–220.

Edgar, A. L. 1965. Observations on the sperm of the pelecypod *Anodontoides ferussacianus.* Transactions of the American Microscopical Society 84: 228–230.

Fredericksen, D. W. 1972. Morphology and taxonomy of *Cotylogaster occidentalis* (Trematoda: Aspidogastridae). Journal of Parasitology 58: 1110–1116.

Fryer, G. 1961. The developmental history of *Mutela bourguignati* (Ancey) Bourguignet (Mollusca: Bivalvia). Philosophical Transactions of the Royal Society of London, Series B, Biological Sciences. 244: 259–298.

Fuller, S. L. H. 1973. *Fusconaia masoni* (Conrad 1834) (Bivalvia: Unionacea) in the Atlantic drainage of the southeastern United States. Malacological Review 6: 105–117.

Fuller, S. L. H. 1974. Clams and mussels (Mollusca: Bivalvia). In: Hart, Jr., C. W., and Fuller S. L. H. (eds), Pollution ecology of freshwater invertebrates. Academic Press, New York, pp 215–273.

Galbraith, H. S., S. E. Frazier, B. Allison, and C. C. Vaughn. 2009. Comparison of gill surface morphology across a guild of suspension-feeding unionid bivalves. Journal of Molluscan Studies 75: 103–107.

Galtsoff, P. S. 1964. The American oyster *Crassostrea virginica* Gmelin. Fishery Bulletin of the Fish and Wildlife Service. 64: 1–480.

Gangloff, M. M., J. D. Williams, and J. W. Feminella. 2006. A new species of freshwater mussel (Bivalvia: Unionidae), *Pleurobema athearni*, from the Coosa River drainage of Alabama, USA. Zootaxa 2006(1118): 43–56.

Gardiner, D. B., H. Silverman, and T. H. Dietz. 1991. Musculature associated with the water canals in freshwater mussels and response to monoamines *in vitro*. Biological Bulletin 180: 453–465.

Garner, J. T., H. Blalock-Herod, A. E. Bogan, R. S. Butler, W. R. Haag, P. D. Hartfield, J. J. Herod, P. D. Johnson, S. W. McGregor. 2004. Mussels and Snails. In: Mirachi, R. E., Garner, J. T., Metee, M. F., and O'Neil, P. E. (eds) Alabama wildlife, Volume 2. Imperiled aquatic mollusks and fishes. The University of Alabama Press, Tuscaloosa, AL., p. 2–125.

Girod, P. 1889. Manipulations de zoologie. Animaux vertebres, animaux invertebres, Guide pour les travaux pratiques de dissection, Tome 1, J. B. Bailliere, Pairs, France, pp 158.

Gordon, M. J., B. K. Swan, and C. G. Paterson. 1979. The biology of *Unionicola formosa* (Dana and Whelpley): a water mite parasitic in the unionid bivalve, *Anodonta cataracta* (Say), in a New Brunswick lake. Canadian Journal of Zoology 57: 1748–1756.

Gordon, M. E., and D. G. Smith. 1990. Autumnal reproduction in *Cumberlandia monodonta* (Unionoidea: Margaritiferidae). Transactions of the American Microscopical Society 109: 407–411.

Graf, D. L., and K. S. Cummings. 2006. Palaeoheterodont diversity (Mollusca: Trigonioida + Unionoida): what we know and what we wish we knew about freshwater mussel evolution. Zoological Journal of the Linnean Society 148: 343–394.

Graf, D. L., and K. S. Cummings. 2007. Review of the systematics and global biodiversity of freshwater mussel species (Bivalvia: Unionoida). Journal of Molluscan Studies 73: 291–314.

Grabarkiewicz, J., and W. Davis. 2008. An introduction to freshwater mussels as biological indicators. EPA-260-R-08-015. U.S. Environmental Protection Agency, Office of Environmental Information, Washington, DC, 108 p.

Grizzle, J. M., and C. J. Brunner. 2009. Infectious diseases of freshwater mussels and other freshwater bivalve mollusks. Reviews in Fisheries Science 17: 425–467.

Grizel, H. 2003. Atlas d'histologie et de cytology des mollusques bivalves marins/An atlas of histology and cytology of marine bivalve molluscs. Ifremer, Plouzané, France 200 p.

Gutiérrez, J. L., C. G. Jones, D. L. Strayer, and O. O. Iribarne. 2003. Mollusks as ecosystem engineers: the role of shell production in aquatic habitats. Oikos 101: 79–90.

Gutheil, F. 1912. Über den darmkanal und die mitteldarmdruse von *Anodonta cellensis* Schröt. Zeitschrift für wissenschaftliche Zoologie 69: 444–538. (in German)

Haag, W. R., and M. L. Warren, Jr. 1997. Host fishes and reproductive biology of 6 freshwater mussel species from the Mobile Basin, USA. Journal of the North American Benthological Society 16: 576–585.

Haag, W. R., and M. L. Warren, Jr. 1999. Mantle displays of freshwater mussels elicit attacks from fish. Freshwater Biology 42: 35–40.

Haag, W. R., M. L. Warren, Jr., and M. Shillingsford. 1999. Host fishes and host-attracting behavior of *Lampsilis altilis* and *Villosa vibex* (Bivalvia: Unionidae). American Midland Naturalist 141: 149–157.

Haag, W. R., and M. L. Warren, Jr. 2003. Host fishes and infections strategies of freshwater mussels in large Mobile Basin streams, USA. Journal of the North American Benthological Society 22: 78–91.

Haag, W. R., and M. L. Warren, Jr. 2010. Diversity, abundance, and size structure of bivalve assemblages in the Sipsey River, Alabama. Aquatic Conservation: Marine and Freshwater Ecosystems 20: 655–667.

Hartfield, P. 1993. Headcuts and their effect on freshwater mussels. In: Cummings, K. S., Buchanan, A. C., and Koch L. M. (eds) Conservation and Management of Freshwater Mussels. Proceedings of a UMRCC Symposium, October 1992, St. Louis, MO, Upper Mississippi River Conservation Committtee, Rock Island IL, p. 131–141.

Haobin, W., X. Yan-han, W. Chun-gen, F. Tao. 2008. Histopathological effect of *Unionicola arcuata* eggs on different tissues in *Cristaria plicata*. Jiangxi Science 26: 544–547. (in Chinese with English abstract)

Healy, J. M. 1989. Spermiogenesis and spermatozoa in the relict bivalve genus *Neotrigonia*: relevance to trigonioid relationships, particularly Unionoidea. Marine Biology 103: 75–85.

Heard, W. H. 1975. Sexuality and other aspects of reproduction in *Anodonta* (Pelecypoda: Unionidae). Malacologia 15: 81–103.

Heard, W. H., and B. J. Dougherty. 1980. Anatomical redescription of *Pleiodon* (*Cameronia*) *spekii* (Pelecypoda: Mutelidae: Pleiodoninae). Malacological Review 13: 45–53.

Heinricher, J. R., and J. B. Layzer. 1999. Reproduction by individuals of a nonreproducing population of *Megalonaias nervosa* (Mollusca: Unionidae) following translocation. American Midland Naturalist 141: 140–148.

Henley, W. F., R. J. Neves, T. Caceci, and R. G. Saacke. 2007. Anatomical descriptions and comparison of the reproductive tracts of *Utterbackia imbecillis* and *Villosa iris* (Bivalvia: Unionidae). Invertebrate Reproduction and Development 50: 1–12.

Hove, M. C., R. A. Engelking, M. E. Peteler, E. M. Peterson, A. R. Kapuscinski, L. A. Sovell, and E. R. Evers. 1997. Suitable fish hosts for glochidia of four freshwater mussels. Conservation and Management of Freshwater Mussels II: Proceedings of a UMRCC Symposium. 21–25.

Howes, G. H. 1885. An atlas of practical elementary biology. Macmillan and Co., London. 116 p., with 24 plates.

Huehner, M. K., and F. J. Etges. 1981. Encapsulation of *Aspidogastr conchicola* (Trematoda: Aspidogastrea) by unionid mussels. Journal of Invertebrate Pathology 37: 123–128.

Jenkinson, J. J., and S. A. Ahlstedt. 1986. Mussel die-off in the Powell River, Virginia and Tennessee, in 1983. In: Neves, R. J. (ed) Proceedings of the workshop on die-offs of freshwater mussels in the United States, June 23-25, Davenport, IA, p. 21–28.

Jones, J. W., and R. J. Neves. 2010. Descriptions of a new subspecies of freshwater mussels, *Epioblasma ahlstedti* and *Epioblasma florentina aureola* (Bivalvia: Unionidae), in the Tennessee River drainage, USA. Nautilus 124: 77–92.

Kat, P. W. 1983. Morphological divergence, genetics, and speciation among *Lampsilis* (Bivalvia: Unionidae). Journal of Molluscan Studies 49: 133–145.

Kato, K., and K. Kubomura. 1954. On the origins of the crystalline style of lamellibranchs. The Science Reports of the Saitama University, Series B, Biology and Earth Sciences. B3: 135–152.

Kays, W. T., H. Silverman, and T. H. Dietz. 1990. Water channels and water canals in the gill of the freshwater mussel, *Ligumia subrostrata*: ultrastructure and histochemistry. The Journal of Experimental Zoology 254: 256–269.

Kellog, J. L. 1915. Ciliary mechanisms of lamellibranchs with descriptions of anatomy. Journal of Morphology 26: 625–701.

Kirtland, J. P. 1840. Fragments of natural history. Number 1. Habits of naiades. American Journal of Science and Arts 39: 164–168.

Kraemer, L. R. 1967. The distribution of the posterior nerves in *Lampsilis ventricosa* (Barnes). Bulletin of the American Malacological Union 1967: 42.

Kraemer, L. R. 1978. Discovery of two kinds of statocysts in freshwater bivalve mollusks: some behavioral implications. Bulletin of the American Malacological Union 1978: 24–28.

Kunz, G. F. 1897. A brief history of the gathering of fresh-water pearls in the United States. Bulletin of the United States Fish Commission 17: 321–330.

Lasee, B. A. 1991. Histological and ultrastructural studies of larval and juvenile *Lampsilis* (Bivalvia) from the upper Mississippi River. Ph.D. Dissertation, University of Iowa, Ames, IA, 146 p.

Lea, I. 1856. Description of the byssus in the genus *Unio*. Proceedings of the Academy of Natural Sciences of Philadelphia 8: 213–214.

Lefevre, G. and W. C. Curtis. 1910. The marsupium of the Unionidae. Biological Bulletin 89: 31–34.

Lefevre, G., and W. C. Curtis. 1912. Studies on the reproduction and artificial propagation of freshwater mussels. Bulletin of the Bureau of Fisheries 30: 107–201, plates 6–17.

Lehmann, D. W., J. F. Levine, and J. M. Law. 2007. Polychlorinated biphenyl exposure causes gonadal atrophy and oxidative stress in *Corbicula fluminea* clams. Toxicology and Pathology 35: 356–365.

Lillie, F. R. 1895. The embryology of Unionidae. Journal of Morphology 10: 1–100.

Lillie, F. R. 1897. On the origin of the centers of the first cleavage spindle in *Unio complanata*. Science 5: 389–390.

Lima, P., U. Kovitvadhi, and J. Machado. 2006. *In vitro* culture of glochidia from the freshwater mussel *Anodonta cygnea*. Invertebrate Biology 125: 34–44.

Lomte, V. S., and M. L. Jadhav. 1980. A study on the crystalline style of the freshwater mussel, *Parreysia corrugata*. Hydrobiologia 69: 175–178.

Luna, L. G. 1968. Manual of histologic staining methods of the Armed Forces Institute of Pathology, Third edition. McGraw-Hill Book Company, NY, 257 p.

Mansour, K., and F. G. Zaki. 1946. The digestive diverticula of *Unio prasidens* as organs of secretion. Proceedings of the Egyptian Academy of Sciences 2: 38–44.

Mansur, M. C. D., and M. d-G. O. da Silva. 1990. Compared morphology and microanatomy of *Bartlettia stefanensis* (Moricand, 1856) with *Anodontites tenebricosus*. (Lea, 1834) (Bivalvia, Unionoida, Muteloidea). Amazonia 11: 147–166.

Margo, T. 1860. Uber die muskelfasern der mollusken. Ein beitrag zur vergleichenden structur- und entwicklungs-lehre des muskelgewebes. Sitzungsberichte der mathem.-naturw. Classe der kaiserlichen Akademie der Wissenschaften besonders abgedruckt 39: 560–582., with two plates. (in German)

Matteson, M. R. 1948. Life history of *Elliptio complanatus* (Dillwyn, 1817). American Midland Naturalist 40: 690–723.

McCall, P. L., G. Matisoff, and M. J. S. Tevesz. 1986. The effects of a unionid bivalve on the physical, chemical, and microbial properties of cohesive sediments from Lake Erie. American Journal of Science 286: 127–159.

McGregor, S. W., and J. T. Garner. 2005. Results of qualitative sampling for protected mussel species at selected stations in the Cahaba River System, Alabama, 2005. Geological Survey of Alabama, Open-file report 0524, 15 p.

Meyhöfer, E., M. P. Morse, and W. E. Robinson. 1985. Podocytes in bivalve molluscs: Morphological evidence for ultrafiltration. Comparative Physiology B 156: 151–161.

Mitchell, R. 1965. Population regulation of a water mite parasitic on unionid mussels. Journal of Parasitology 51: 990–996.

Mitra, S. R. 1901. The crystalline style of Lamellibranchia. Quarterly Journal of Microscopical Science s2-44: 591–602, with one plate.

Morse, M. P. 1987. Comparative functional morphology of the bivalve excretory system. American Zoologist 27: 737–746.

Morse, M. P., and J. D. Zardus. 1997. Bivalvia. In: Harrison F. W. (ed) Microscopic Anatomy of Invertebrates, Volume 6A: Mollusca II, Wiley-Liss, Inc., New York, pp 7–118.

Morton, B. 1987. The functional morphology of *Neotrigonia margaritacea* (Bivalvia: Trigoniacea), with a discussion of phylogenetic affinities. Records of the Australian Museum 39: 339–354.

Morrison, C. M. 1993. Histology and cell ultrastructure of the mantle and mantle lobes of the eastern oyster, *Crassostrea virginica* (Gmelin). American Malacological Bulletin 10: 1–24.

Morrison, C. M. 1996. Adductor and mantle musculature. In: Kennedy V. S., Newell R. I. E., and Eble A. E. (eds) The eastern oyster *Crassostrea virginica*. Maryland Sea Grant College, College Park, MD, pp 169–183.

Motley, H. L. 1932. Histology of the fresh-water mussel heart with reference to its physiological reactions. Journal of Morphology 54: 415–427.

Motley, H. L. 1943. Physiological studies concerning the regulation of heartbeat in freshwater mussels. Physiological Zoology 7: 62–84.

Myers, P. R., D. S. Frazen. 1970. Histological studies of the nephridium and pericardial lining of *Quadrula nodulata*. Nautilus 83: 139–144.

Myers R. K., and M. D. McGavin. 2007. Cellular and tissue responses to injury. In: McGavin, M. D., and Zachary J. F. (eds) Pathologic basis of veterinary disease, Fourth edition. Mosby, Inc., St. Louis, MO. p. 3–63.

Naimo, T. J. 1995. A review of the effects of hevy metals on freshwater mussels. Ecotoxicology 4: 341–362.

Narain, A. S. 1972. On the posterior aortic bulb of the fresh water mussel, *Lamellidens corrianus*. Indian Biologist 4: 81–83.

Narain, A. S. 1973. On the muscular apparatus of the heart of the fresh water mussel, *Lamellidens corrianus*. Zoologische Beiträge 157–161.

Narain, A. S., and M. P. Singh. 1974. Experimental investigations into the traversing of ventricle by gut in the unionid bivalve, *Lamellidens corrianus*. Experientia 30: 1415–1416.

Narain, A. S. 1976. A review of the structure of the heart of mollusks, particularly bivalves, in relation to cardiac function. Journal of Molluscan Studies 42: 46–62.

Nelson, T. C. 1918. On the origin, nature, and function of the crystalline style of lamellibranchs. Journal of Morphology 31: 53–111.

Nelson, T. C. 1925. Recent contributions to the knowledge of the crystalline style of lamellibranchs. Biological Bulletin 49: 86–99.

Neves, R. J. 1987. Proceedings of the workshop on die-offs of freshwater mussels in the United States, June 23-25, Davenport, IA, United States Fish and Wildlife Service, Upper Mississippi Conservation Committee, 166 p.

Neves, R. J., L. R. Weaver, and A. V. Zale. 1985. An evaluation of host suitability for glochidia of *Villosa vanuxemi* and *V. nebulosa* (Pelecypoda: Unionidae). American Midland Naturalist 113: 13–19.

Neves, R. J., and J. C. Widlak. 1987. Habitat ecology of juvenile freshwater mussels (Bivalvia: Unionidae) in a headwater stream in Virginia. American Malacological Bulletin 5: 1–7.

Neves, R. J., A. E. Bogan, J. D. Williams, S. A. Ahlstedt, and P. W. Hartfield. 1997. Status of aquatic mollusks in the southeastern United States: a downward spiral of diversity. In: Benz, G. W., and Collins, D. E. (eds) Aquatic Fauna in Peril: The southeastern perspective. Special publication 1, Southeastern Aquatic Research Institute, Lenz Design and Communications, Decatur, GA, p. 43–85.

Newton, T. J., and W. G. Cope. 2007. Biomarker responses of unionid mussels to environmental contaminants. In: Farris, J. L., and Van Hassel, J. H. (eds) Freshwater bivalve ecotoxicology, Boca Raton, FL, p. 257–284.

Norton, J. H., and G. W. Jones. 1992. The giant clam: An anatomical and histological atlas. Australian Centre for International Agricultural Research, Canberra, Australia, 142 p.

Ortmann, A. E. 1909a. Unionidae from an Indian garbage heap. The Nautilus 23: 11–15.

Ortmann, A. E. 1909b. The destruction of the fresh-water fauna in western Pennsylvania. Proceedings of the American Philosophical Society 48: 90–110.

Ortmann, A. E. 1910a. A new system of the Unionidae. The Nautilus 23:114–120.

Ortmann, A. E. 1910b. The marsupium of Anodontinae. Biological Bulletin 19: 217.

Ortmann, A. E. 1911a. A monograph of the najads of Pennsylvania. Memoirs of the Carnegie Museum 4: 279–347.

Ortmann, A. E. 1911b. The anatomical structure of certain exotic naiades compared with that of the North American forms. The Nautilus 24: 103–108, plates 6–7; 114–120; 127–131.

Ortmann, A. E. 1923a. Notes on the anatomy and taxonomy of certain Unioninae and Anodontinae from the Gulf drainage. The Nautilus 36: 73–84, 129–132.

Ortmann, A. E. 1923b. Notes on the anatomy and taxonomy of certain Lampsilinae from the Gulf drainage. The Nautilus 37: 56–60.

Ortmann, A. E. 1924a. Notes on the anatomy and taxonomy of certain Lampsilinae from the Gulf drainage. The Nautilus 37: 99–105, 137–144.

Österling, M. E., B. L. Arvidsson, and L. A. Greenberg. 2010. Habitat degradation and the decline of the threatened mussel *Margaritifera margaritifera*: influence of turbidity and sedimentation on the mussel and its host. Journal of Applied Ecology 47: 759–768.

Owen, G. 1955. Observations on the stomach and digestive diverticula of the Lamellibranchia. I. The Anisomyaria and Eulamellibranchia. Quarterly Journal of Microscopical Science 96: 517–537.

Owen, G., and J. M. McCrae. 1979. Sensory cell/gland cell complexes associated with the pallial tentacles of the bivalve *Lima hians* (Gmelin), with a note on specialized cilia on the

pallial curtains. Transactions of the Royal Society of London. Series B, Biological Sciences 287: 45–62.

Owen, C. T., M. A., McGregor, G. A. Cobbs, and J. E. Alexander, Jr. 2011. Muskrat predation on a diverse unionid mussel community: impacts of prey species composition, size and shape. Freshwater Biology 56: 554–564.

Pain, T., and F. R. Woodward. 1968. A monograph of the African bivalves of the genera *Brazzaea* Bourguiguat, *Mweruella* Haas, *Prisodontopsis* Tomlin and *Pseudospatha* Simpson. Revue de Zoologie et de Botanique Africaines 77: 190–220.

Parker, R. S., C. T. Hackney, and M. F. Vidrine. 1984. Ecology and reproductive strategy of a South Louisiana freshwater mussel, *Glebula rotundata* (Lamarck) (Unionidae: Lampsilini). Freshwater Invertebrate Biology 3: 53–58.

Parmalee, P. W., and A. E. Bogan. 1998. The freshwater mussels of Tennessee. The University of Tennessee Press, Knoxville, TN, pp 328.

Pauley, G. B. 1968. A disease of the freshwater mussel, *Margaritifera margaritifera*. Journal of Invertebrate Pathology 12: 321–328.

Pauley, G. D., and C. D. Becker. 1968. *Aspidogaster conchicola* in mollusks of the Columbia River System with comments on the host's pathological response. Journal of Parasitology 54: 917–920.

Peck, R. H. 1877. The minute structure of the gills of Lamellibranch Mollusca. Quarterly Journal of Microscopical Science 17: 43–66, plate 7.

Petit, H. 1977. A scanning electron microscopic (SEM) study of the mantle-shell relationship in the freshwater mussel *Amblema plicata perplicata* (Conrad). Anatomical Record 187: 680–681.

Petit, H., W. L. Davis, and R. G. Jones. 1978. Morphological studies on the mantle of the fresh-water mussel *Amblema* (Unionidae): scanning electron microscopy. Tissue & Cell 10: 619–627.

Petit, H., W. L. Davis, and R. G. Jones. 1979. Morphological studies on the periostracum of the fresh-water mussel *Amblema* (Unionidae): light microscopy, transmission electron microscopy, and scanning electron microscopy. Tissue & Cell 11: 633–642.

Posner, C. 1875. Ueber den bau der najadenkieme. Archiv für mikroskopische Anatomie 517–560, plates 31–32. (in German)

Purcheon, R. D. 1958. The stomach in the Eulamellibranchia: Stomach Type IV. Proceedings of the Zoological Society of London 131: 487–525.

Radley, J. D., and M. J. Barker. 1998. Palaeoenvironmental analysis of shell beds in the Wealden Group (Lower Cretaceous) of the Isle of Wight, southern England: an initial account. Cretaceous Research 19: 489–504.

Rafinesque, C. S. 1820. Monograph of the fluviatile bivalve shells of the River Ohio, containing twelve genera and sixty-eight species, 72 p. (Translated from French by J. Dobson, Philadelphia, 1832).

Raβbach, R. 1912. Beiträge zur kenntis der schale und schalenregeneration von *Anodonta cellenss* Schröt. Zeitschrift für wissenschaftliche Zoologie 103: 363–448.

Ravera, O., R. Cenci, G. M. Beone, M. Dantas, and P. Lodigiani. 2003. Trace element concentrations in freshwater mussels and macrophytes as related to those in their environment. Journal of Limnology 62: 61–70.

Reid, R. G. B. 1965. The structure and function of the stomach in bivalve molluscs. Journal of Zoology 147: 156–184.

Richard, P. E., T. H. Dietz, and H. Silverman. 1991. Structure of the gill during reproduction in the unionids *Anodonta grandia*, *Ligumia subrostrata*, and *Carunculina parva texasensis*. Canadian Journal of Zoology 69: 1744–1754.

Ridewood, W. G. 1903. On the structure of gills of Lamellibranchia. Philosophical Transactions of the Royal Society of London 195: 147–284.

Rocha, E., and C. Azevedo. 1990. Ultrastructure study of the spermatogenesis of *Anodonta cygnea* L. (Bivalvia: Unionidae). Invertebrate Reproduction and Development 18: 169–176.

Rondelaud, D., and D. Barthe. 1981. The development of the amoebocyte-producing organ in *Lymnaea truncatula* Müller infected by *Fasciola hepatica* L. Zeitschrift für Parasitenkunde 65: 331–341.

Ross, M. H., H. I. Kaye, and W. Pawlina. 2003. Histology: A text and atlas. 4th Ed. Lippinicott Williams & Wilkins, Baltimore, MD. 864 p.

Salazar, M. H., and S. M. Salazar. 2007. Linking bioaccumulation and biological effects to chemicals in water and sediment: A conceptual framework for freshwater bivalve ecotoxicology. In: Farris, J. L., and Van Hassel, J. H. (eds) Freshwater bivalve ecotoxicology, CRC Press, Boca Raton, FL, p. 215–255.

Schwartz, M. L., and R. V. Dimock, Jr. 2001. Ultrastructural evidence for nutritional exchange between brooding unionid mussels and their glochidia larvae. Invertebrate Biology 120: 227–236.

Shaw, B. L., and H. I. Battle. 1957. The gross and microscopic anatomy of the digestive tract of the oyster *Crassostrea virginica* (Gmelin). Canadian Journal of Zoology 37: 325–347.

Shaw, B. L., and H. I. Battle. 1959. The chemical composition of the gastric shield of the oyster *Crassostrea virginica* (Gmelin). Canadian Journal of Zoology 37: 214–215.

Siebert, W. 1913. Das körperepithel von *Anodonta cellensis*. Zeitschrift für wissenschaftliche Zoologie. 106: 449–525.

Silverman, H., W. L. Stevens, and T. H. Dietz. 1983. Calcium concentrations in the gills of a freshwater mussel serve as a calcium reservoir during periods of hypoxia. Journal of Experimental Zoology 227: 177–189.

Silverman, H., W. L. Steffens, and T. H. Dietz. 1985. Calcium from extracellular concretions in the gills of freshwater unionid mussels is mobilized during reproduction. Journal of Experimental Zoology 236: 137–147.

Silverman, H., W. T. Kays, and T. H. Dietz. 1987. Maternal calcium contribution to glochidial shells in freshwater mussels (Eulamellibranchia: Unionidae). Journal of Experimental Zoology 242:137–146.

Silverman, H., P. E. Richard, R. H. Goddard, and T. H. Dietz. 1989. Intracellular formation of calcium concretions by phagocytic cells in freshwater mussels. Canadian Journal of Zoology 67: 198–207.

Simpson, C. T. 1884. Anatomy and physiology of *Anodonta fluviatilis*. New York State Museum, Annual report 35: 22–191.

Simpson, C. T. 1898. The pearly fresh-water mussels of the United States; their habits, enemies, and diseases, with suggestions for their protection. Bulletin of the United States Fish Commission 18: 279–288, plate 65.

Simpson, C. T. 1900. Synopsis of the Naiades, or peraly freshwater mussels. Proceedings of the United States National Museum 22: 501–1044.

Sims, D. E., J. A. Wesfall, A. L. Kiorpes, and M. M. Horne. 1991. Preservation of tracheal mucus by nonaqueous fixative. Biotechnic and Histochemistry 66: 173–180.

Smith, H. M. 1898. The mussel fishery and pearl-button industry of the Mississippi River. Bulletin of the United States Fish Commission 18: 289–314, plates 77–85.

Smith, D. G. 1988. Notes on the biology and morphology of *Margaritifera hembeli* (Conrad, 1838) (Unionacea: Margaritiferidae). Nautilus 102: 159–163.

Smith, D. G. 2000. Investigations of the byssal gland in juvenile unionids. In: Tankersley, R. A. (ed) Proceedings of the Conservation, Care, and Propagation of Freshwater Mussels Symposium, Columbus OH, 1998, Part 1, Ohio Biological Survey, Ohio State University, Columbus, OH pp 103–107.

Smith, D. G., B. K. Lang, and M. E. Gordon. 2003. Gametogentic cycle, reproductive anatomy, and larval morphology of *Popenaias popeii* (Unionoida) from the Black River, New Mexico. Southeastern Naturalist 48: 333–340.

Splittstoβer, P. 1913. Zur morphologie des nervensystems von *Anodonta cellensis* Schröt. Zeitschrift fur Wissenschaftliche Zoologie 104: 388–470.

Stasek, C. R. 1963. Synopsis and discussion of the associated of ctenidia and labial palps in the bivalve Mollusca. The Veliger 6: 91–97.

Stevens, A. 1982. The haematoxylins. *In* Theory and practice of histological techniques, 2nd ed., J. D. Bancroft, and A. Stevens (eds.). Churchill Livingstone, Edinburgh, Scotland, p. 109–121.

Tankersley, R. A., and R. V. Dimock, Jr. 1992a. Quantitative analysis of the structure and function of the marsupial gills of the freshwater mussel *Anodonta cataracta*. Biological Bulletin 182: 145–154.

Tankersley, R. A., and R. V. Dimock. 1992b. Endoscopic visualization of the functional morphology of the unionid mussel *Pyganodon cataracta*. Canadian Journal of Zoology 71: 811–819.

Taskinen, J., T. Mäkelä, and E. T. Valtonen. 1997. Exploitation of *Anodonta piscinalis* (Bivalvia) by trematodes: parasite tactics and host longevity. Annales Zoologici Fennici 34: 37–46.

Tauc, L. 1966. Physiology of the nervous system. In: K. M. Wilbur, and C. M. Yonge (eds), Physiology of Mollusca, Volume II, Academic Press, New York, p. 387-454.

Trueman, E. R. 1966. Bivalve mollusks: Fluid dynamics of burrowing. Science 152: 523–525.

Trueman, E. R. 1968. The locomotion of the freshwater clam *Margaritifera margaritifera* (Unionacea: Margaritiferidae). Malacologia 6: 401–420.

van Appledorn M., and C. E. Bach. 2007. Effects of zebra mussels (*Dreissena polymorpha*) on mobility of three native mollusk species. American Midland Naturalist 158: 329–337.

van der Schalie, H. 1938. Contributing factors in the depletion of naiads in the eastern United States. Basteria 3: 51–57.

van der Schalie, H., and F. Locke. 1941. Hermaphroditism in *Anodonta grandis*, a fresh-water mussel. Occasional Papers of the Museum of Zoology 432: 1–7. plates 1–3.

Van Snik Gray, E., W. A. Lellis, J. C. Cole, and C. S. Johnson. 2002. Host identification for *Strophitus undulatus* (Bivalvia: Unionidae), the Creeper, in the Upper Susquehanna River Basin, Pennsylvania. American Midland Naturalist 147: 153–161.

Vaughn, C. C., and C. C. Hakenkamp. 2001. The functional role of burrowing bivalves in freshwater ecosystems. Freshwater Biology 46: 1431–1446.

Vinyard, W. C. 1955. Epizoophytic algae from mollusks, turtles, and fish in Oklahoma. Proceedings of the Oklahoma Academy of Science 34: 63–65.

Vitonis, J. E. V. V., C. P. Zaniratto, F. M. Machado, and F. D. Passos. 2012. Comparative studies on the histology and ultrastructure of the siphons of two species of Tellinidae (Mollusca: Bivalvia) from Brasil. Zoologia 29: 219–226.

Waller, D. L., and and B. A. Lasee. 1997. External morphology of spermatozoa and spermatozeugmata of the freshwater mussel *Truncilla truncata* (Mollusca: Bivalvia: Unionidae). American Midland Naturalist 138: 220–223.

Watters, G. T. 2002. The kinetic conglutinate of the creeper freshwater mussel, *Strophitus undulatus* (Say, 1817). Journal of Molluscan Studies 68: 155–158.

Ward, J. E., L. P. Sanford, R. I. E. Newell, and B. A. MacDonald. 1998. A new explanation of particle capture in suspension-feeding molluscs. Limnology and Oceanography 43: 741–752.

White, R. M. 1942. The pericardial cavity and the pericardial gland of the Lamellibranchia. Proceedings of the Malacological Society of London 25: 4–88

Williams, J. D., A. E. Bogan, and J. T. Garner. 2008. Freshwater mussels of Alabama and the Mobile Basin in Georgia, Mississippi, and Tennessee. University of Alabama Press, Tuscaloosa, AL, 908 p.

Williams, J. D., A. E. Bogan, and J. T. Garner. 2009. A new species of freshwater mussel, *Anodonta hartfieldorum* (Bivalvia: Unionidae), from the Gulf Coastal Plain drainages of Alabama, Florida, Louisiana, and Mississippi, USA. Nautilus 123: 25–33.

Wilson, C. B., and H. W. Clark. 1912a. The mussel fauna of the Muamee River. Bureau of Fisheries Document No. 757. U.S. Department of Commerce and Labor, Bueareau of Fisheries, Washington, DC, 72 p.

Woody, C. A., and L. Holland-Bartels. 1993. Reproductive characteristics of a population of the washboard mussel *Megalonaias nervosa* (Rafinesque 1820) in the upper Mississippi River. Journal of Freshwater Ecology 8: 57–66.

Yeager, M. M., D. S. Cherry, and R. J. Neves. 1994. Feeding and burrowing behaviors of juvenile rainbow mussels, *Villosa iris* (Bivalvia: Unionidae). Journal of the North American Benthological Society 13: 217–222.

Yokley, P., Jr. 1968. A study of the anatomy of the naiad *Pleurobema cordatum* (Rafinesque, 1820) (Mollusca: Bivalvia: Unionoida). Ph.D. Dissertation, Ohio State University, 139 p.

Yokley, P., Jr. 1972. The life history of *Pleurobema cordatum* (Rafinesque 1820) (Bivalvia: Unionacea). Malacologia 11: 351–364.

Yonge, C. M. 1926a. Structure and physiology of the organs of feeding and digestion in *Ostrea edulis*. Journal of the Marine Biological Association of the United Kingdom 14: 295–396. plates 1–2

Yonge, C. M. 1926b. The digestive diverticula in the lamellibranchs. Transactions of the Royal Society 54: 703–717. With two plates.

Zale, A. V., and R. J. Neves. 1982. Reproductive biology of four freshwater mussel species (Mollusca: Unionidae) in Virginia. Freshwater Invertebrate Biology 1: 17–28.

Zale, A. V., and R. Suttles. 1986. Mussel mortalities in the Neosho River system, Oklahoma. In: Neves R. J. (ed) Proceedings of the workshop on die-offs of freshwater mussels in the United States, June 23-25, Davenport, IA, p. 39–43.

Zhong, L., T.-Y. Xiao, J. Huang, L.-Y. Dai, X.-Y. Liu. 2011. Histopathological examination of bivalve mussel *Hyriopsis cumingii* Lea artificially infected by virus. Acta Hydrobiologica Sinica 35: 666–671.

Appendix 1

Figure A1. Longitudinal view of *Anodonta cellensis* showing the position the anterior adductor (AA), foot (FO), digestive diverticulum (DD), stomach (ST), crystalline style sac (CS), intestine (IN), mantle (MA), gill (GI), posterior adductor (PA), and heart (HE), and nephridium (NE). Redrawn from Gutheil (1912).

A.1